AMMRC CR 71-14

CRACK PROPAGATION STUDIES IN GLASSY POLYMERS

September 1971

Final Report

by

LAWRENCE J. BROUTMAN

and

TAKAO KOBAYASHI

Illinois Institute of Technology
Chicago, Illinois 60616

Contract Number DAAG 46-69-C-0075

Prepared for

ARMY MATERIALS AND MECHANICS RESEARCH CENTER
Watertown, Massachusetts 02172

R

282

UNCLASSIFIED

Security Classification

DOCUMENT CONTROL DATA - R & D

(Security classification of title, body of abstract and indexing annotation must be entered when the overall report is classified)

1. ORIGINATING ACTIVITY (Corporate author)	2a. REPORT SECURITY CLASSIFICATION
Illinois Institute of Technology Chicago, Illinois 60616	Unclassified
	2b. GROUP

3. REPORT TITLE

CRACK PROPAGATION STUDIES IN GLASS POLYMERS

4. DESCRIPTIVE NOTES (Type of report and inclusive dates)

Final Report 16 June 1969 to 15 October 1970

5. AUTHOR(S) (First name, middle initial, last name)

Broutman, Lawrence J., and
Kobayashi, Takao

6. REPORT DATE	7a. TOTAL NO. OF PAGES	7b. NO. OF REFS
September 1971	294	86

8a. CONTRACT OR GRANT NO.	9a. ORIGINATOR'S REPORT NUMBER(S)
DAAG46-69-C-0075	
b. PROJECT NO. DA IF 162203A150	AMMRC CR 71-14
c. AMCMS Code 5122.11.195	9b. OTHER REPORT NO(S) (Any other numbers that may be assigned this report)
d.	

10. DISTRIBUTION STATEMENT

Approved for public release; distribution unlimited

11. SUPPLEMENTARY NOTES	12. SPONSORING MILITARY ACTIVITY
	Army Materials & Mechanics Research Center Watertown, Mass. 02172

13. ABSTRACT

The object of this study was to determine the influence of crack velocity on the fracture surface work of glassy polymers. Poly(methyl methacrylate) and polystyrene were studied and it was hypothesized that the fracture surface work as a function of crack velocity could be explained by molecular relaxation behavior. Activation energies were determined for the fracture process at various temperatures and crack velocities.

The fracture surface work of rubber modified acrylics has been studied as a function of crack velocity and rubber concentration. The fracture surface work is greatly dependent upon both rubber concentration and crack velocity and more than one maximum in the curve of fracture surface work versus crack velocity can occur depending upon the rubber concentration.

A method of crystallizing thick polycarbonate sheets by acetone vapor was developed. The mechanical properties of these sheets were studied as a function of residual acetone content. Cold rolling of these sheets as well as amorphous thermoplastics was accomplished and the impact strength can be greatly increased by cold rolling.

A micromechanics analysis using finite element methods was performed on rubber modified polymers and the internal stresses were calculated as well as the modulus of elasticity and critical stress for stress whitening as a function of rubber concentration.

DD FORM 1 NOV 68 1473 REPLACES DD FORM 1473, 1 JAN 64, WHICH IS OBSOLETE FOR ARMY USE.

UNCLASSIFIED

Security Classification

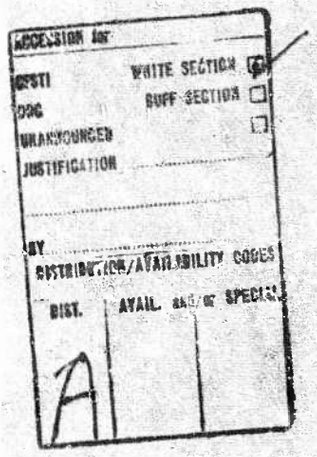

The findings in this report are not to be construed as an official Department of the Army position, unless so designated by other authorized documents.

Mention of any trade names or manufacturers in this report shall not be construed as advertising nor as an official indorsement or approval of such products or companies by the United States Government.

DISPOSITION INSTRUCTIONS

Destroy this report when it is no longer needed.
Do not return it to the originator.

14 KEY WORDS	LINK A		LINK B		LINK C	
	ROLE	WT	ROLE	WT	ROLE	WT
Organic polymers						
Crack propagation						
Fracture surface work						
Cold rolling						
Impact strength						
Crystallinity						
Strain rate						

CRACK PROPAGATION STUDIES IN GLASSY POLYMERS

AMMRC CR 71-14

Final Report

by

Lawrence J. Broutman

and

Takao Kobayashi

September 1971

Illinois Institute of Technology
Chicago, Illinois

Contract Number DAAG 46-69-C-0075

D/A Project IF 162203A150
AMCMS Code 5122.11.195
Reduction of Vulnerability of Army Aircraft

Prepared for

ARMY MATERIALS AND MECHANICS RESEARCH CENTER
Watertown, Massachusetts 02172

FORWARD

There has been in recent years a growing interest in the use of organic palymers for lightweight armor applications because of the relatively low density and pramising performance of these materials. To improve further the degree of ballistic protection afforded by polymeric materials, it is necessary to examine in detail the nature of the failure processes. For example, the occurrence of fracture causes the absorption of much energy and is, therefore, an important mechanism involved in defeating the projectile. Hence there is great interest in developing more knowledge concerning the detailed energetics of fracture processes and their dependences upon polymer structural features.

The work described in this report was performed at the Illinois Institute of Technology under Contract No. DAAG 46-69-C-0075. This research was sponsored by the Army Materials and Mechanics Research Center, Watertown, Massachusetts with Dr. Anthony F. Wilde as Technical Supervisor.

Chapters 1 thru 7 of this report have been also submitted as the Ph.D. thesis of Mr. Takao Kobayashi. Chapters 8 and 9 are a portion of the Ph.D. thesis which will be submitted by Mr. S. Krishnakumar.

TABLE OF CONTENTS

CHAPTER CONTINUED Page

LIST OF TABLES

LIST OF FIGURES

SUMMARY

In order to increase the understanding of polymer fracture phenomena and to establish correlations between polymer molecular structure and fracture behavior, studies of the effects of velocity and temperature on fracture surface work of the most commonly used glassy amorphous homopolymers —— poly(methyl methacrylate) and polystyrene —— have been carried out. In addition, the effects of crack velocity and rubber content on fracture surface work of rubber modified acrylic polymers have been studied in order to characterize the influence of rubber particle inclusions on fracture behavior of these materials. The ultimate goal of this effort is to help develop more fracture resistant materials on a rational basis.

The experimental results of fracture surface work as a function of crack velocity in poly(methyl methacrylate), polystyrene, and rubber modified acrylic polymers indicate that crack velocity has a strong influence on fracture surface work. The fracture surface work versus crack velocity curves of these materials obtained at room temperature show that fracture surface work increases as crack velocity increases up to certain levels. When the crack velocity exceeds this specific point, the fracture surface work of poly(methyl methacrylate) and polystyrene abruptly drops. It appears that the fracture surface work versus crack velocity curves have discontinuities at this critical crack velocity. Rubber modified acrylic polymers also exhibit decreases in fracture surface work above certain crack velocities; however, the rates of decrease are not abrupt. The magnitudes and locations of the peaks of fracture surface work in rubber modified acrylic polymers depend on rubber concentration. Furthermore, materials containing ten, thirteen and sixteen percent of rubber exhibit two peaks.

These discontinuities and decreases in the curves of fracture surface work versus crack velocity cause unstable propagation and lead to catastrophic failure; therefore, it is important to know what material parameters cause an abrupt drop or moderate decrease in fracture surface work. In order to investigate this point the fracture surface work of poly(methyl methacrylate) as a function of crack velocity at different temperatures has been studied. Considering the fracture process as a rate process, the apparent activation energies have been obtained by applying an Arrhenius equation to the results of crack velocity and temperature corresponding to certain iso-(fracture surface work) values. It was found that two distinct values of apparent activation energies exist: one corresponding to the α -process, and the other to the β -process of the molecular relaxation processes. The α -process is the molecular relaxation process related to the main glass transition temperature, and flow of molecules may be possible in this process. The β-process is the molecular relaxation process related to the β -(glass-glass) transition temperature, and crazing may be related to this β -process. On the basis of this analysis, it has been postulated that the molecular relaxation processes (α -, β -, and γ -processes) govern the crack propagation phenomena. The crack propagation in poly(methyl methacrylate) at room temperature can be explained by this hypothesis: when crack velocity is low, the fracture process is dominated by the α-process; when crack velocity increases the β -process related to crazing starts to mix with the dominant α -process. This causes a sharp increase in fracture surface work. As the crack velocity further increases it reaches a critical crack velocity above which the α -process no longer takes place. At this point the fracture process changes from the α -process to the β -process. The value of fracture surface work corresponding to the β -process at this crack velocity is very small and appears as

a discontinuity in the curve of fracture surface work versus crack velocity. The ratio of these critical crack velocities at which α - to β -process changes occur in poly(methyl methacrylate) and polystyrene shows good agreement with the ratio of β -relaxation peak frequencies of poly(methyl methacrylate) and polystyrene.

Rubber modified acrylic polymers are frequently known to exhibit an additional molecular relaxation phenomenon due to the presence of rubber particles. According to the above hypothesis, another type of process should be considered in addition to the α - and β -processes based on the matrix polymer. This may be demonstrated by the existence of two peaks in the fracture surface work versus crack velocity curve for rubber modified acrylic polymers. With this hypothesis it is therefore possible to lay a foundation for the explanation of diversified fracture phenomena.

The mechanical properties of crystallized and cold rolled crystallized polycarbonates have been studied. Thermal and acetone vapor crystallization were attempted and it was determined that the acetone vapor technique was superior, particularly for thick sheets. It has been demonstrated that a cold rolled crystalline polycarbonate possesses superior strength combined with toughness.

The influence of cold rolling on the impact properties of amorphous polymers has been studied. It has been demonstrated that rolling greatly increases the impact strength of almost all the polymers which have been studied. The results of impact strength determined as a function of roll reduction are presented in Chapter 8.

Finally, the internal stresses in rubber modified polymers have been studied using a finite element numerical analysis. The internal stresses in the matrix and at the interface between the rubber particle and matrix are studied as a function of rubber properties and concentration. In addition the modulus of elasticity and critical stress for stress whitening have been calculated as a function of rubber concentration.

CHAPTER I

INTRODUCTION

A. Objective of Research

Extensive efforts have been made to characterize the properties of polymeric materials in order to determine their optimum uses on a rational basis; however, the performace of these materials against fracture cannot be predicted by conventional mechanical properties. Griffith (1) showed that the tensile strength of a brittle or glassy material was related to material parameters such as elastic modulus, fracture surface energy, and flaw size, and Berry (2) demonstrated that this concept was also applicable to polymeric materials. As a result of these studies, fracture studies of polymeric materials have seen extensive new developments. Particular interests in this development are studies of the influence of molecular parameters on the fracture process. Providing one understands the influence of material structure as well as viscoelastic properties on the fracture process, the development and the evaluation of new or existing materials can be rationally performed for better impact and fracture resistance. An important parameter to be studied is the fracture surface work which represents the energy required to create a unit area of new fracture surface. In this study the term fracture surface work is used instead of fracture surface energy in order to indicate that the irreversible work which takes place at the crack tip is included. Polymer molecular parameters which have been widely studied are molecular weight (3,4,5), crosslinking (5,6,7,8), pre-orientation (9), tacticity and crystallinity (5), and polymer molecular structures (5). The effects of temperatures (3,4,5,6,10,11) and crack velocities (11,12,13,14,15,16) have been also studied, although studies of the influence of crack propagation rates on fracture mechanism or fracture surface work are not as common as studies on temperature effects. From the results of these studies, which are reviewed in the next section of this chapter, it can be concluded that a relation exists between fracture surface work and molecular parameters such as molecular weight and its distribution, cross-linking, crystallinity, and pre-orientation. However, a more detailed understanding of molecular parameter effects remains unclear. For example, through the work by Broutman and Kobayashi (5) it has been learned that the fracture surface work of polystyrene is almost twice as great as that of poly(methyl methacrylate), and yet the molecular weight is considerably less than that of cast poly(methyl methacrylate) polymer. The glass transition temperatures are quite near each other, and the molar cohesion or cohesive energy density is not more than 10 percent different for these two polymers. In these studies the fracture surface work of the polymeric materials has been treated as an inherent property; however, the studies of temperature and crack velocity effects have revealed that the fracture surface work is greatly influenced by temperature and crack velocities (or strain rate) as are the viscoelastic parameters. Thus, the fracture surface work of polymeric materials is not an inherent property but should be treated as a viscoelastic parameter. If the fracture surface work is a viscoelastic parameter, the special insight needed to understand the fracture mechanisms of polymeric materials may be obtained by studying the effects of crack velocity and temperature. Some attempts have already been made to explain the dependence of the fracture surface work on the rate of crack propagation. Mueller and Knauss (11) have demonstrated that for constant crack velocity the rate-dependent

fracture energy (fracture surface work) of elastomers above the glass transition temperature can be calculated from a knowledge of intrinsic fracture energy and creep compliance of the material, based on the assumption that the material behavior follows linear viscoelasticity laws. Thus, they consider the rate-dependent fracture energy as a deduced property instead of a fundamental property of the material. The intrinsic fracture energy was used to represent half of the energy required for rupture under the condition that no energy dissipation occurs through viscous forces around the advancing crack tip.

At the present stage of development, experimental data is needed to further establish the relations between fracture surface work and the various molecular parameters, and to better understand the fracture mechanisms occurring at the crack tip. One of the objectives, therefore, of this research was to understand the effect of crack velocity on the fracture surface work and to attempt to find the relations between the fracture process and molecular and viscoelastic parameters by considering both the effects of crack velocity and temperature.

B. Review of Fracture Studies of Polymeric Materials

In this section only those results of fracture studies which are pertinent to this research will be reviewed. The development of theories and experimental methods, the influence of molecular parameters, temperature and crack velocities on fracture surface work, and fracture surface characteristics will be discussed.

1. Fracture Surface Work Theories and Measurement Methods.

Griffith (1), realizing the discrepancy between the theoretically estimated and the experimentally observed values of tensile strength of brittle materials, first proposed a satisfactory explanation of brittle fracture strength partly based on the work of Inglis (17). Griffith assumed the presence of very small cracks in the material and made use of Inglis' calculation of stresses by regarding the cracks as very flat elliptical holes. Griffith made a further assumption that crack propagation will occur when the increase in surface energy due to the crack extension is balanced by the elastic strain energy release due to crack extension. In other words, the energy released in forming a crack is the difference between the elastic strain energy that can be stored in the specimen without a crack and the elastic strain energy stored in the cracked specimen, and this released energy will become the gain in the surface energy. In the case of a thin elastic plate (plane stress) with a very flat elliptic crack of length 2c under uniaxial tension, Griffith's assumptions lead to the famous Griffith equation:

$$\sigma_{ult} = \sqrt{\frac{2\gamma E}{\pi c}} \qquad (1)$$

where σ_{ult} = ultimate tensile strength, γ = surface energy, and E = Young's modulus.

Orowan (18,19) later modified Griffith's equation to account for irreversible work such as plastic deformation and viscous deformation which take place at the highly stressed crack tip. The modified Griffith equation is then represented by

$$\sigma_{ult} = \sqrt{\frac{2E(\gamma + P)}{\pi c}} \qquad (2)$$

where P represents the irreversible work.

Irwin (20) defined a parameter, G, the elastic strain energy release rate with crack extension, and referred to it as a crack extension force. When the crack extension force, G, becomes equal to a critical value G_c, the critical strain-energy release rate of the material, crack propagation occurs. The critical crack extension force, G_c, is equal to twice the fracture surface energy γ in Griffith's equation. Irwin further showed that the crack extension force G is given by the equation (21):

$$G = \frac{f^2}{2\omega} \cdot \frac{dC}{da} \qquad (3)$$

where f is the applied load,

ω is the crack width,

C is the compliance of the system,

and a is the crack length.

The application of Griffith's equation to polymeric materials was first shown by Berry (2). He demonstrated that σ_{ult} was proportional to $1/\sqrt{c}$; however, the experimental value of γ for the material tested was nearly 10^3 times as great as the calculated fracture surface energy because of the irreversible work occurring. It appears that even the most macroscopically brittle materials such as inorganic glasses exhibit some irreversible work at a crack tip or other contribution which increases the value of γ.

Recent studies of the fracture surface work of polymeric materials show that fracture surface work is not an inherent property of polymers but a viscoelastic parameter; however, it is a valuable quantity which can be measured experimentally and used to relate changes in a material's molecular structure to the fracture resistance of the material. The first method used to determine experimentally the fracture surface work quantity was the measurement of the tensile strength of a material using an edge or centrally notched and cracked tensile specimen. The tensile strength is measured for several artificially induced crack lengths so that a sufficient relation between the ultimate tensile strength and the crack length is established, and from the equation (2) the fracture surface work is determined.

A more accurate measurement of fracture sufrace work can be obtained by using a cleavage technique to propagate a crack. Broutman (6,9) and Berry (2,7, 22,23) developed the uniform height double cantilever beam cleavage specimen which has side grooves along the center line to control the crack propagation path, and studied the effects of molecular parameters and temperature on the fracture surface work. In order to determine the fracture surface work with this type of

cleavage technique it is necessary to measure the force of separation at the specimen ends, the resulting end deflection, and the crack length. The procedure is described by Broutman (6). Mostovoy, Crosley and Ripling (24) have developed another type of cleavage specimen with constant compliance change in terms of crack length which results in a tapered double cantilever beam specimen. The purpose of this tapered specimen, as one can see from the equation (3) in which dC/da (a function of crack length) is constant by designed specimen geometry, is to eliminate the need for measuring the crack length as a function of the applied force and deflection; thus it simplifies measurement and calculation of fracture surface work. Another benefit of this specimen is that the crack will propagate with a constant velocity for a constant rate of separation of the specimen ends, provided that the crack width remains constant and the rate-sensitivity of the material fracture surface work does not change from positive to negative. The rate-sensitivity of fracture surface work will be discussed in detail in Chapter VI. The tapered cleavage specimen is therefore very useful for studying the effects of crack velocity on fracture surface work. The design of this specimen and the newly developed sandwich tapered specimen for ductile materials will be discussed in Chapter III.

2. Fracture Surface Characteristics.

The appearance of a polymer fracture surface has been a valuable tool in understanding and interpreting fracture mechanisms; therefore, careful inspection of a fracture surface is a necessary part of an investigation and cannot be divorced from other more quantitative measurements such as fracture surface work. To be correct, any fracture process theory should predict or be able to explain fracture surface appearance. Main features observed and investigated on the fracture surfaces are as follows: color, surfoce roughness, and crazing. Detailed discussion of these features can be found in an article entitled "Fracture Topography" by Wolock and Newman (25); therefore, the following review of these features will be brief.

It was the observation of colors on fresh fracture surfaces of poly(methyl methacrylate) that led investigators (26,27) to conclude that a thin layer of oriented material existed at the fracture surfaces. This conclusion was further justified by the fact that the experimental fracture surface work was much greater than the theoretical value which implied a great amount of viscous or plastic flow had to occur. Figure 1 shows Berry's model of the proposed viscous flow mechanism in polymer fracture (2).

The roughness of the fracture surface is also a valuable asset in evaluating the energy absorbing capability of the material in front of the crack. Broutman (6,9) and Wolock and Newman (25) have discovered that the surface roughness is proportional to the fracture surface work exhibited by the polymer. Increasing surface roughness corresponds to increasing fracture toughness or fracture surface work. A recent study of crack propagation in polystyrene by Hull (28) suggests a possible relation between crazing and surface roughness. Cotterell (15,29) has studied the fracture surfaces of poly(methyl methacrylate) in terms of crack velocities. He observed three distinct features of surface appearance with respect to crack velocities. When the crack velocities are low (0-700 feet/second), the fracture surface is glassy smooth and shows a distinctive color. In the crack velocity range between 700 and 1,700 feet/second, hyperbolic markings are observed on the fracture surface. The density of hyperbolic markings increases with velocity; furthermore, the density is

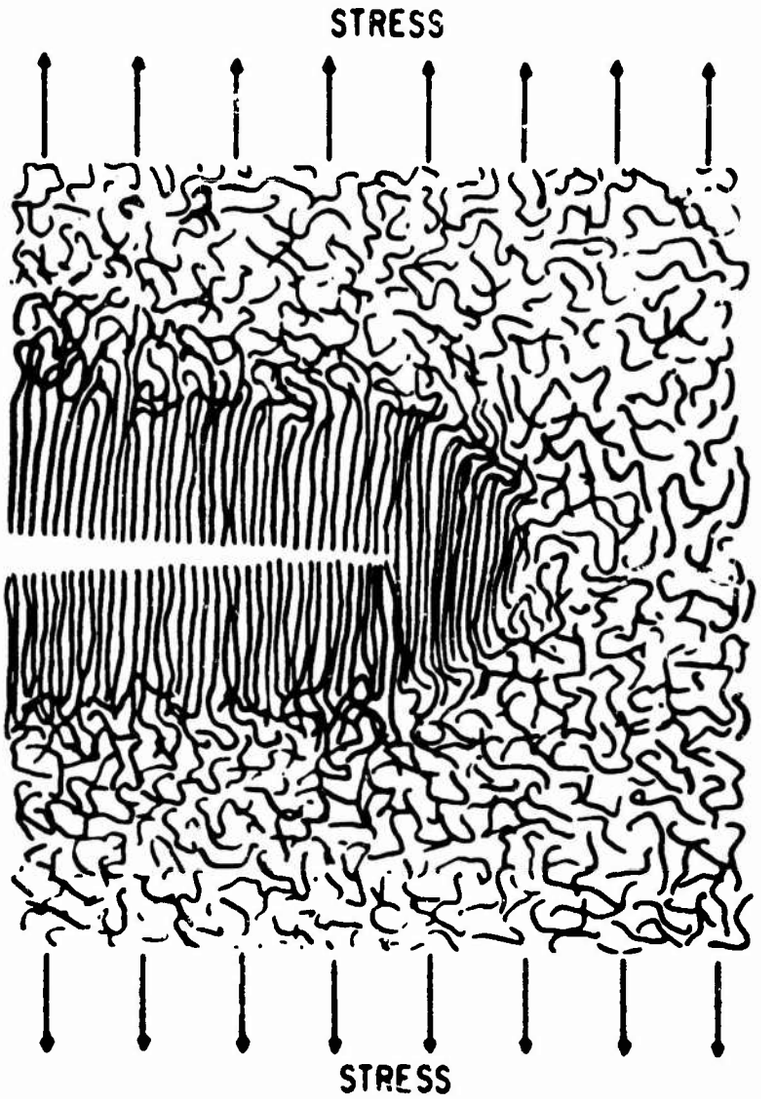

FIGURE 1. PROPOSED VISCOUS FLOW MECHANISM IN POLYMER FRACTURE (BERRY, REF. 2).

proportional to the fracture toughness. When the crack velocity exceeds 1,700 feet/second, the fracture surface is very rough.

It has been established that crazing plays an important role in the fracture process. Kambour has observed for several polymers such as poly(methyl methacrylate) and polystyrene that brittle fracture involves a crazing response ahead of the crack tip. He stated that the extent and complexity of crazing response varies from material to material and also with temperature and crack velocity; nevertheless, crack propagation in glassy polymers may be more exactly termed the formation and breaking of crazes. In another work Kambour (31) measured the thickness of the colored layer on the fracture surface of poly(methyl methacrylate) which was cleaved at temperatures 0, 25, 45, 60, and 67°C with near zero crack velocity. He found that the layer thickness appears constant up to 60°C, but at 67°C thermal collapse of the layer prevented accurate measurement. In addition to the simple colored layer on the fracture surface of poly(methyl methacrylate) he found surface complexity which might be interpreted as subsurface crazing. This feature was found to be a function of temperature, fracture velocity, and the stress state. For example, at 40°C and above, complexity is not seen on cleavage surfaces. At 25°C it is apparent on 5-30% of the surface, and below this temperature it increases markedly. At -80°C the fracture surface is so complicated no color exists at all. It is unfortunate that the crack velocity was not available. The polymers investigated by Kambour are shown in Table 1.

Van den Boogaart studied the behavorial differences in rapidly and slowly formed crazes (32). He found that the quickly formed crazes were completely healed by the annealing treatment, while the slowly formed crazes did not recover so well, this clearly demonstrating their more crack-like character.

Murray and Hull (33) studied the fracture surface of polystyrene and observed that at low crack velocities the crack propagates by tearing through the center of the craze; however, when the crack is propagating at a high velocity, splitting of the material along the interface between the craze and the uncrazed material occurs. This is schematically illustrated in Figure 2. As the crack velocities increase, the craze layer becomes thinner since the crack tip approaches the tip of the craze.

Hull stated in another paper on the effect of crazes on crack propagation in polystyrene (28) that cracks propagate preferentially along crazes and that the formation of crazes in the stress field of a propogating crack results in the "hackle" surface. This "hackle" surface is normally associated with bifurcation and branching of the crack; thus it is usually assumed that these processes are due to the crack propagation at speeds close to the limiting velocities. However, Hull speculated that as the crack propagates rapidly along the craze the stress is relaxed locally and the crack slows down. This allows time for new craze formation at the new position of the crack tip. As the stress builds up again the crack will jump along one of the new crazes. Therefore, spacing of hackle bands on the fracture surface will depend on those parameters related to the kinetics of craze growth in a polymer and on the nature of the applied stress. The crack velocities in the hackle marks seem slower than those in planar crack surfaces, contrary to the general belief associating hackle marks with branching of cracks.

Table 1. Summary of Evidence of Craze Formation in Crack Propagation in Glassy Polymers*

Polymer	T_g(°C)	Fracture Temp. Range Where Positive Evidence Found (°C)	Method of Fracture	Type of Evidence
Poly(methyl methacrylate)	105	0-60	Tensile, Cleavage	Color, X-ray
Poly(ethyl methacrylate)	50-60	0-25	Cleavage	Color
Polystyrene	78	25-89	Cleavage	Color
Polymethylstyrene	108	100-119	Cleavage	Color
Acrylonitrile-styrene Copolymer	96	90-100	Cleavage	Color
Poly(vinylacetate)	30	0-25	Cleavage	Color
Polyhydroxy ether	105	25-104	Cleavage	Color
Polycarbonate	140	-195 to +25	Cleavage impact	Color, X-ray
Poly(vinyl chloride)	-80	--	Tensile, Cleavage	None

*Extracted from Kambour, R. P., Mechanism of Fracture in Glassy Polymers," Part I, J. Polymer Sci., 3, 1713 (1965); Part II, J. Polymer Sci., 4, 17 (1966); Part III, J. Polymer Sci., 4, 349 (1966).

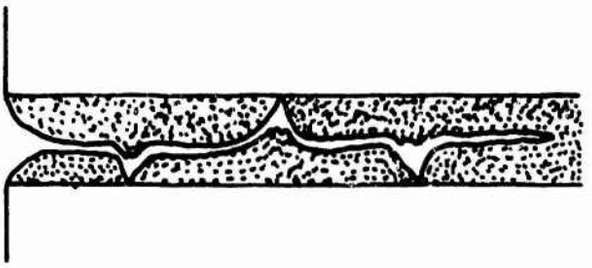

i) CAVITATION OF THE CRAZE AND FINAL SEPARATION BY TEARING OF THE MATERIAL IN THE CRAZE LAYER

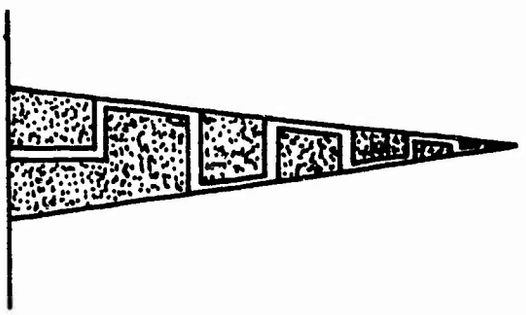

ii) SPLITTING OF THE MATERIAL ALONG THE INTERFACE BETWEEN THE CRAZE AND UNCRAZED MATERIAL

FIGURE 2. SCHEMATIC REPRESENTATION OF CRACK PROPAGATION MECHANISMS IN A CRAZE (MURRAY AND HULL, REF.33).

Crazing thus contributes to various features of the crack propagation process. Furthermore, the induction of crazing in the material is an important energy dissipating mechanism during the fracture process. This point will be further discussed in Chapter VI.

3. Molecular Parameters Influencing Fracture and the Fracture Surface Work.

Those polymer molecular parameters whose influence on the fracture process have been studied include molecular weight (3,4,5), crosslinking (5,6,7,8), preorientation (9), tacticity and crystallinity (5), and polymer molecular structures (5). The effects of temperature and crack velocities have also been studied, but these effects will be discussed separately in the next section of this chapter.

It was observed for poly(methyl methacrylate) that increasing the molecular weight (viscosity average molecular weight) caused an increase in fracture surface work, but for molecular weights greater than 400,000 there was not a strong dependence upon molecular weight. The appearance of the fracture surface and the mode of crack propagation is also dependent upon molecular weight. At low molecular weights the crack propagation changes from a continuous propagation to a stick-slip discontinuous propagation. The results for the above studies are presented in Table 2. Irregularities in the data may have been caused by differences in molecular weight distribution but, unfortunately, this data was not provided. Table 2 also shows the results obtained by Benbow (4) who studied the effect of number average molecular weight on the fracture surface work of polystyrene and observed an increase in the fracture surface work with increasing molecular weight. The fracture work was measured in two different regions of the specimen since the crack propagation changed from fast to slow in the same specimen and for all molecular weight except the lowest studied, 60,000. At 60,000 the crack propagation was of a continuous nature similar to high molecular weight poly(methyl methacrylate). Molecular weight distributions were not reported for the materials sutdied by Benbow.

Broutman has also studied the influence of molecular weight and molecular weight distribution on specially prepared polystyrenes. The materials were obtained through the Dow Chemical Co., and narrow distribution polymers were prepared by anionic polymerization while broad distribution polymers were prepared by isothermal polymerization. The fracture surface work measurements were made by uniform cleavage specimens. The results are shown in Table 3. These results further reinforce previous observations that increasing molecular weight increases the fracture surface work; however, if a wide distribution of molecular weight occurs ($\overline{M}_w/\overline{M}_n = 2.47$) the fracture surface work of the polymer with $\overline{M}_w = 279{,}000$ is less than the fracture surface work of the polymer with $\overline{M}_w = 125{,}000$. This demonstrates the importance of studying molecular weight distribution and of carefully characterizing the polymer in order to properly interpret the results.

Broutman and Kobayashi (5) further studied the influence of molecular weight and molecular weight distribution on the fracture surface work of polystyrenes. The results of molecular weight and the fracture surface work are shown in Tables 4 and 5. It is of interest to note that commercial polystyrene sheets exhibited two entirely different appearances at the fracture surface and quite different fracture surface work values in the same specimen. This is also demonstrated in Figure 3 which shows the

Table 2. Effect of Molecular Weight on Fracture Surface Work of Polystyrene and Poly(methyl methacrylate) (Ref. 3 and 4)

Polymer	Molecular Weight	Nature of Surface	Fracture Surface Work 10^5 erg/cm^2
Poly(methyl methacrylate)	$\overline{M}_v$=0.98x10^5	-	1.14
	1.1x10^5	-	1.24
	1.8x10^5	-	1.33
	4.2x10^5	-	1.45
	12.5x10^5	-	1.50
	30x10^5	-	1.35
	60x10^5	-	1.56
Polystyrene	$\overline{M}_n$=260,000**	Rough	3.00
		Laminated	19
	130,000	Rough	1.5
		Laminated	6.1
	80,000	Rough	1.5
		Laminated	1.7
	60,000	Smooth, Mirror-like	0.3

*viscosity average molecular weights

**molecular weights determined by osmometry

Table 3. Fracture Surface Work of Various Molecular Weight Polystyrenes (Ref. 5)

Material*	Polymerization Method	$\overline{M}_w$	$\overline{M}_w/\overline{M}_n$	Fracture Surface Work 10^5 erg/cm^2
S103	Anionic	124,700	1.05	3.15
S109	"	193,000	1.06	5.73
S108	"	201,000	1.08	7.69
B8	Isothermal	279,000	2.47	2.71

*Dow Chemical Co. designation

Table 4. Molecular Weight Determination by Gel Permeation Chromatography for Polystyrenes (Ref.5)

Sample	$\overline{A}_n$ Angstroms	$\overline{A}_w$ Angstroms	$\overline{M}_n^*$	$\overline{M}_w^*$	MWD**
Polystyrene A (Borden Monomer-Polymer Lab)	1167.5	5594.3	48,217	231,045	4.79
Polystyrene C (Borden Monomer Polymer Lab)	185.1	1288.4	7,644	53,211	6.96
Polystyrene B (commercial sheet	511.5	5960	21,125	246,148	11.6
Polystyrene -25***	739.6	7066.3	30,545	291,838	9.55
Polystyrene B-10	1004.9	5623.9	41,502	232,267	5.60
Polystyrene B-50	790.4	8892.8	32,643	367,272	11.25

*Assuming Q=41.3 (molecular weight units per angstrom)

**MWD $= \frac{\overline{A}_w}{\overline{A}_n} = \frac{\overline{M}_w}{\overline{M}_n}$ = molecular weight distribution

***25 megarads

Table 5. Fracture Surface Work of Various Molecular Weight Polystyrenes (Ref.5)

Molecular Weight	Sample Number	Crack Propagation Mode	Fracture Surface Work ($ergs/cm^2$)	Fracture Surface
$\overline{M}_w$ = 53,211**	1	Stick-slip	3.34×10^3	Mirror smooth, no color
	2	Stick-slip	3.70×10^3	
$\overline{M}_w$ = 231,000**	3	Stick-slip	4.20×10^5	Very rough
	4	Stick-slip	4.38×10^5	
$\overline{M}_w$ = 246,148***	5	Stick-slip	3.60×10^5	Very rough
	6	Stick-slip	3.61×10^5	
	7	Stick-slip	3.92×10^5	
	8	Stick-slip	4.62×10^5	
	9	Stick-slip	5.15×10^5	Very rough
		Continuous	2.97×10^5	Smooth, coloration
	10	Stick-slip	4.49×10^5	Very rough
		Continuous	2.84×10^5	Smooth, coloration
	11	Stick-slip	6.10×10^5	Very rough

**Borden Monomer-Polymer Labs ***Commercial source

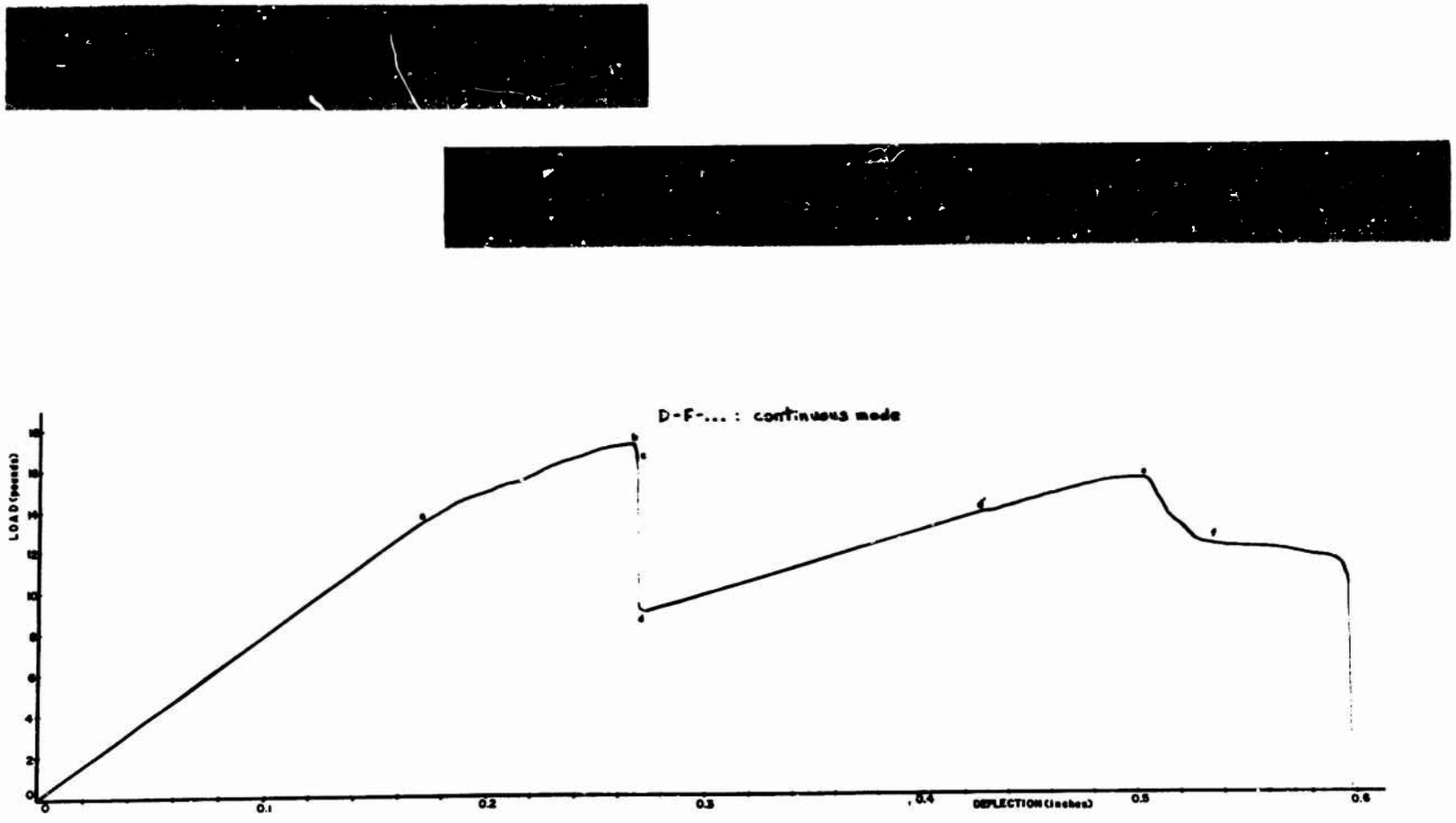

FIGURE 3. LOAD-DEFLECTION CURVE AND FRACTURE SURFACE PHOTOGRAPH OF COMMERCIAL POLYSTYRENE AT 22 °C.

fracture surface appearance and the load-deflection curve, clearly demonstrating the influence of crazing in crack propagation.

Berry (3) has proposed an explanation for the influence of molecular weight on fracture surface work. This work, from the way in which it is defined, is directly proportional to the amount of yield or crazed region that lies immediately ahead of the crack tip. Consequently, the contribution which any particular molecule makes to the surface work will be determined by the length that is contained within this region. A sufficiently long molecule will start in the unyielded region, pass through the yielded region, and terminate once again in the unyielded region. Under these conditions, the contribution made by the molecule will be independent of its length. Thus, as indicated by the results, the fracture work will tend to reach a limiting value at high molecular weights. If one or both ends of a polymer molecule are found within the yielded or crazed region, that molecule will not make a full contribution to the fracture surface work. The polymer chains are believed to be in an extended conformation within the yielded region, and hence the smallest molecule that can contribute fully to the surface work will have its ends on the boundaries of the yielded region, on opposite sides of the fracture plane, and will be fully extended between these points. Assuming that the total thickness of the yielded region is 6 to 7 x 10^3 Å, a fully extended molecule of poly(methyl methacrylate) would have a molecular weight of 2.5 - 3 x 10^5; consequently the fracture surface work must decrease for polymers of lower molecular weight. This is in agreement with Berry's results, considering that it is unlikely for the molecule to become full extended and that there is really a distribution of molecular lengths in the polymer.

Berry's explanation for the influence of molecular weight on fracture surface work is very useful in interpreting the results of the fracture process for one polymer made with different molecular weights; however, the results of recent studies show that the fracture process – and thus the fracture surface work – are greatly influenced by craze formation which is subsequently influenced by temperature and crack velocities. For example, the previously mentioned case of the difference in fracture surface work between poly(methyl methacrylate) and polystyrene cannot be explained by a simple consideration of molecular weight. The fracture surface work of polystyrene is almost twice as great as that of poly(methyl methacrylate), and yet the molecular weight of polystyrene is considerably less than that of the cast poly(methyl methacrylate) polymer.

The influence of crazing at the crack tip on the fracture surface work of linear polymers will be best studied by investigation of the influence of crosslinking on the fracture surface work since it is considered that crosslinking should restrict the viscous flow of molecules and thus restrict crazing at the crack tip. Crosslinking in polystyrene can be induced chemically or through gamma irradiation. In the studies on the effect of crosslinking in poly(methyl methacrylate) by Berry (7) and Broutman (6) crosslinking was induced chemically. Their results show a decrease in fracture surface work. Broutman's results are shown in Figure 4. The results obtained from the chemically crosslinked linear polymers such as poly(methyl methacrylate), however, show disagreement with the results obtained from the network polymers (8) such as the epoxies and unsaturated polyesters shown in Figure 5. Broutman and Kobayashi (5) studied the effect of crosslinking on the fracture surface work of polystyrene which was crosslinked through gamma irradiation. Although polystyrene can be chemically crosslinked by adding various concentrations of

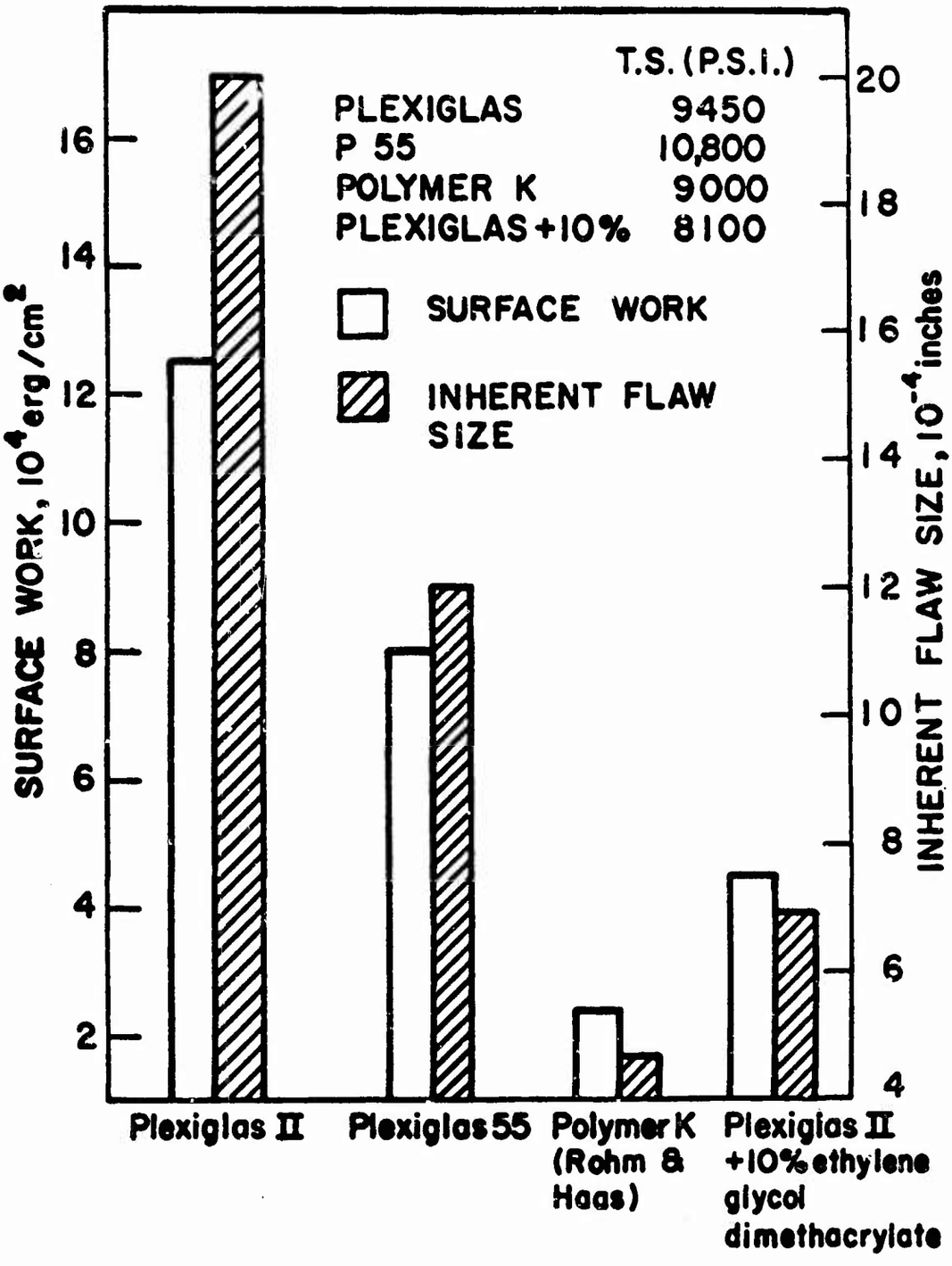

FIGURE 4. EFFECT OF CROSSLINKING ON FRACTURE SURFACE WORK AND INHERENT FLAW SIZE OF PLEXIGLAS (BROUTMAN, REF. 6).

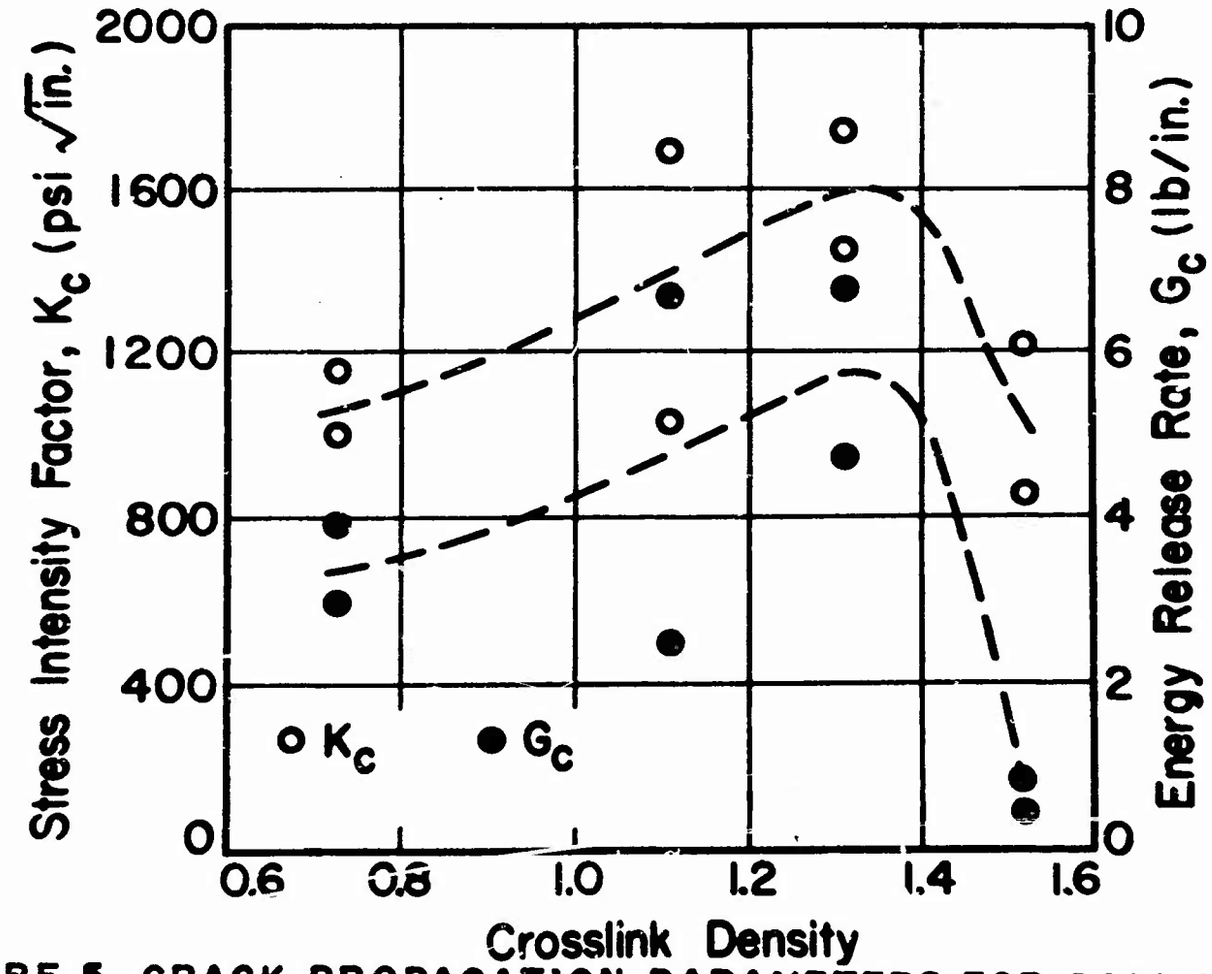

FIGURE 5. CRACK PROPAGATION PARAMETERS FOR POLYSTYRENE–STYRENE COPOLYMERS AS A FUNCTION OF CROSSLINK DENSITY (REF. 8).

divinyl benzene, it was thought that this might make interpretation more difficult because of the addition of a second chemical structure which by itself might change the fracture surface work. These results are shown in Figure 6 together with the measurements of intrinsic viscosity. It was also reported that there is a mirror smooth region at the crack initiation area which demonstrates that crosslinking will reduce the amount of crazing and thus also reduce the fracture surface work of polystyrene.

Since local molecular orientation is believed to occur at the crack tip, it is of great interest to see the effects of molecular pre-orientation on the fracture surface work of thermoplastic polymers. Broutman (9) has investigated the fracture surface work relations for oriented Plexiglas* [poly(methyl methacrylate)] and polystyrene sheets. A commercial multiaxially stretched Plexiglas sheet illustrated in Figure 7 was used to determine the fracture surface work by a cleavage test in various directions. The fracture surface work parallel to the oriented molecules, as shown, is almost two orders of magnitude less than the work normal to the direction of orientation. Uniaxially hot stretched sheets of polystyrene and poly(methyl methacrylate) were also investigated and the fracture surface work was measured parallel to the orientation. In Figure 8 the large reductions in surface work can be seen as the percentage of hot stretch was increased. The temperatures shown in the figure represent the stretching temperatures. Broutman stated that the fracture surface work of polystyrene, stretched 150% at 240°F is only 7,000 ergs/cm^2 and is only a factor of 10 greater than the theoretical value of surface work for a polymer. Broutman stated that the fracture surface work value of 7,000 ergs/cm^2 indicates a small degree of molecular flow at the tip of the crack. This result reinforces the theory that orientation occurs in the vicinity of a crack tip moving through a glassy amorphous polymer.

Broutman and Kobayashi (5) studied the influence of tacticity and crystallinity on fracture surface work of isotactic polystyrene. The results are shown in Table 6. The isotactic amorphous polystyrene in all cases appears to craze considerably during the initiation of the crack, which accounts for the high value of fracture surface work. The crystalline materials were produced by annealing under pressure at 180°C for time periods from 2 to 6 hours. The densities were measured in a linear density gradient column prepared with demineralized water and a solution of calcium nitrate in demineralized water. The presence of crystals produces a rapid decrease in the fracture surface work of the polymer. This indicates that the crystals apparently act to prevent realignment or orientation of the amorphous molecular chains, and thus orientation and crazing at the fracture surface are inhibited relative to the wholly amorphous specimens.

In order to determine the relationship between polymer molecular structure, transition temperatures, and fracture surface work, Broutman and Kobayashi (5) have selected a series of acrylate and methacrylate polymers since systematic changes in molecular structure can be achieved. The molecular structures and transition temperatures are shown in Table 7. The glass transition temperatures in Table 7 have been studied by Rogers and Mandelkern (34). Halden and Simha (35) have also

---

* Trade name Rohm and Haas Co.

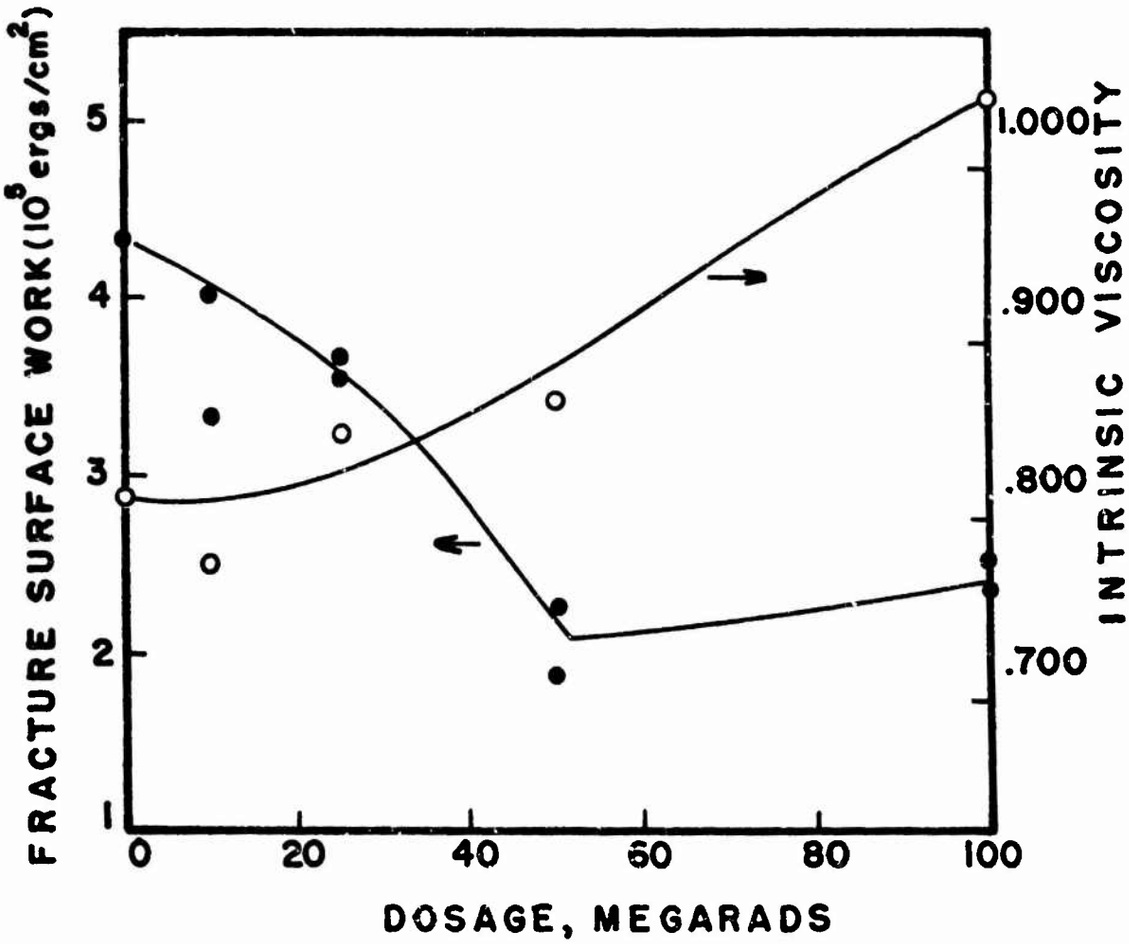

FIGURE 6. INTRINSIC VISCOSITY AND FRACTURE SURFACE WORK MEASUREMENTS FOR IRRADIATED POLYSTYRENE (COMMERCIALLY AVAILABLE SHEET) (REF. 5).

STRETCHED P55	SURFACE WORK (erg/cm^2)
0°	6.5×10^5
45°	5.8×10^5
90°	7.8×10^5
11	1.65×10^4

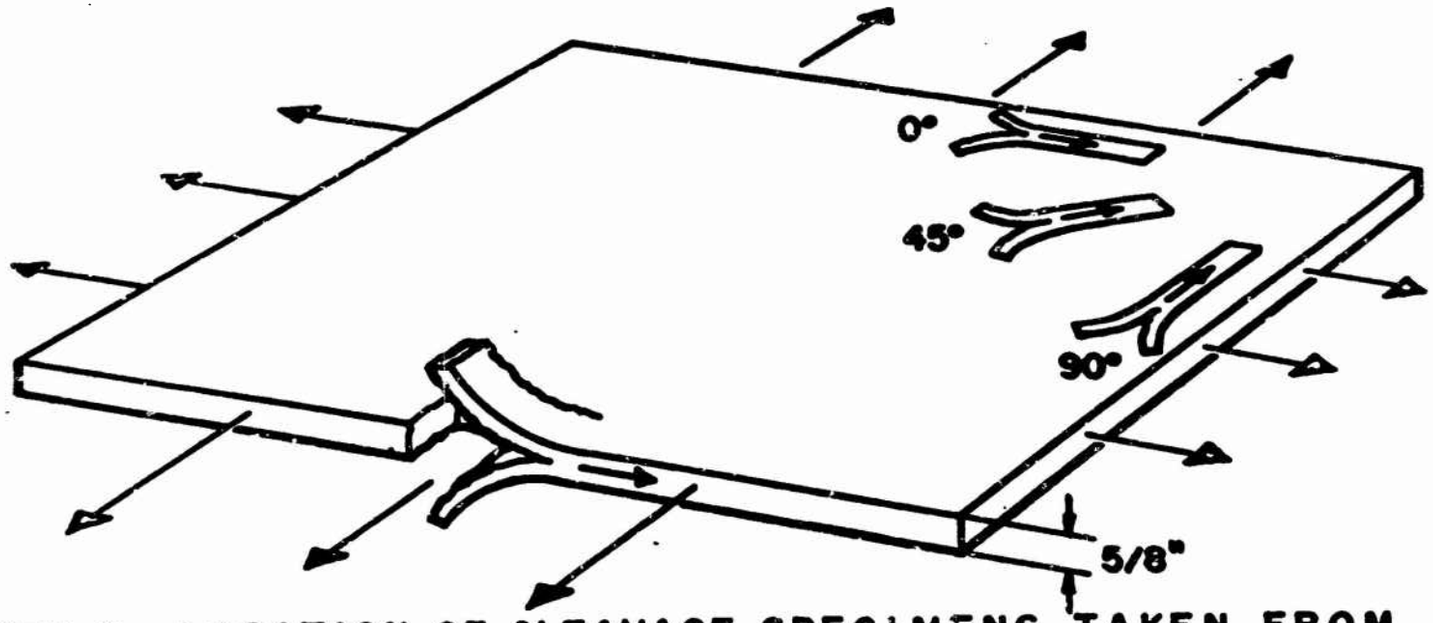

FIGURE 7. LOCATION OF CLEAVAGE SPECIMENS TAKEN FROM MULTIAXIALLY STRETCHED (65%) PLEXIGLAS 55 SHEET (BROUTMAN, REF.9).

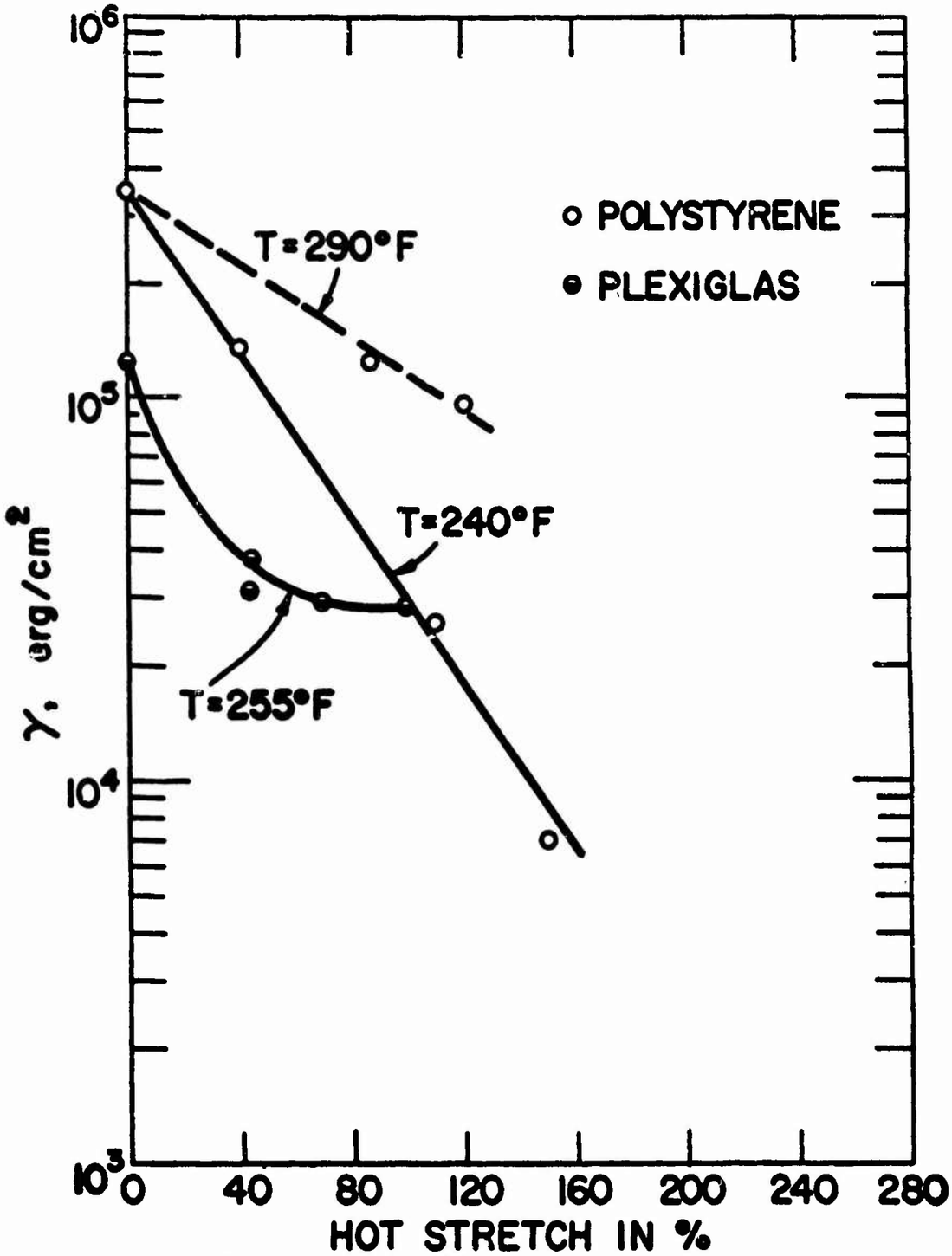

FIGURE 8. FRACTURE SURFACE WORK FOR ORIENTED POLYMERS (BROUTMAN, REF. 9).

Table 6. Fracture Surface Work and Densities of Amorphous and Crystalline Isotactic Polystyrenes (Ref. 5)

Material	Density (grams/cc)	Percent Crystalline Volume	Fracture Surface Work (10^5 ergs/cm^2)	Fracture Surface
Amorphous	1.052	0	9.85	Very rough, crazed
			11.9	Very rough, crazed
Annealed	1.064	20.3	3.16	
			3.52	
	1.067	25.4	2.07	
			2.69	
			2.24	
	1.0738	37	.912	
			.734	
	1.074	37.4	.671	
			.850	

Table 7. Glass Transition Temperatures for Acrylate and Methacrylate Polymers (Ref. 34)

Acrylates 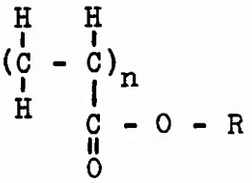 Methacrylates 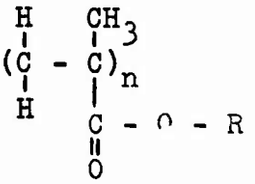

R -	Tg (°C) of Acrylate	Tg (°C) of Methacrylate
methyl ($-CH_3$)	+3	+105
ethyl ($-CH_2-CH_3$)	-22	+65
n-propyl ($-CH_2-CH_2-CH_3$)	-44	+35
n-butyl ($-CH_2-CH_2-CH_2-CH_3$)	-56	+21
iso-butyl ($-CH_2-\underset{\displaystyle CH_3}{\underset{|}{CH}}-CH_3$)		+54
n-hexyl $-(CH_2)_5-CH_3$		-5
n-octyl $-(CH_2)_7-CH_3$		-20

determined glass-glass transition temperatures due to the segmental motion of the pendant groups and their results are reported in Table 8. The results of fracture surface work are summarized in Table 9 together with the corresponding temperature $(T_g - T_{exp})^{\circ}C$. If one considers only methacrylate polymers and compares them with respect to their glass transition temperatures, very little significance can be associated with glass transition temperatures. Even those polymers which are from 260°C to 300°C below their glass transition temperatures have significant differences in fracture surface work. In order to fully understand the influence of polymer molecular structure on fracture surface work it is necessary to have more complete information on the fracture surface work behavior with respect to parameters such as temperature and crack velocities. The properties of polymeric materials are influenced by different molecular relaxation mechanisms at different temperatures; therefore, it is natural to consider that at a crack tip different molecular relaxation mechanisms may be working at different testing temperatures. At this stage a good correlation between polymer molecular structure or glass transition temperature and fracture surface work could not be established; however, by studying the effects of temperature and crack velocities simultaneously, new insight into the relations between molecular structure and fracture surface work may be obtained. In the next section the studies on the effects of temperature and crack velocities on the fracture surface work will be reviewed.

4. Effects of Temperature and Crack Velocity on the Fracture Surface Work.

The effects of temperature on the fracture surface work have been studied by several investigators (4,5,6,7,8,10,22,36). The effect most commonly observed for the thermoplastic polymers is shown in Figure 9 (6). Decreasing the temperature from the glass transition temperature of the polymer causes an increase in the fracture surface work; however, this generalization is not fully applicable since iso-butyl methacrylate decreases fracture surface work with decreasing temperature, and ethyl methacrylate has only a very small change in fracture surface work from room temperature to -196°C. DiBenedetto and Trachte also found that the effect of temperature on the fracture surface work differs from polymer to polymer (36). They studied the brittle fracture properties of polyphenylene oxide, polysulfone, polycarbonate and poly(methyl methacrylate) thermoplastic polymers over a wide range of temperatures. They stated that a maximum in the fracture surface work was observed for polyphenylene oxide and polysulfone at about 85°C below the main glass transition temperatures, while poly(methyl methacrylate) exhibited a continuing increase in the fracture surface work with decreasing temperature.

The fracture surface work is influenced not only by temperature, but also by the crack propagation rate. Studies of the influence of crack velocities on fracture mechanisms or fracture surface work are not as common as studies on temperature effects, but nevertheless, there is some information on this subject (11,12,13,14,15, 16,37,38,39). Measurements by Cotterell (15) on poly(methyl methacrylate) indicate that the fracture toughness increases with increasing crack velocity from 0 to 2,500 feet per second. Increases in surface roughness are also observed. Vincent and Gotham (14) also have reported an increase in fracture surface work with increases in crack propagation velocity for a high molecular weight poly(methyl methacrylate) sheet. However, the measurement methods used to obtain various crack propagation rates varied from tensile methods to cleavage methods to Charpy impact tests, and the results are difficult to interpret. Mostovoy and Ripling (16) have studied the effect of the crack propagation rate on fracture surface work for an epoxy adhesive.

Table 8. Transition Temperatures for Acrylate and Methacrylate Polymers (Ref. 35)

R	Length-Temperature Measurements (°C)				Torsion Pendulum (°C)	
	T_g	$T_{gg}^{(1)}$	$T_{gg}^{(2)}$	$T_{gg}^{(3)}$	T_g	T_{gg}
methyl methacrylate	103	--	15	-130	116	25
ethyl methylacrylate	64	25	-15	-115	73	15
n-Butyl methacrylate	18	-25	-51	-95	2[illegible]	--
iso-Butyl methacrylate	54	25	-25	-88	65	--
methyl acrylate	10	-40	-135	--	--	--

Table 9. Relation between T_g and Fracture Surface Work (Ref. 5)

Corresponding Temperature $(T_g - T_{exp})^{\circ}C$	Fracture Surface Work 10^5 erg/cm^2	Polymer
40	.6 to 9	iso-butyl methacrylate
48	4 (11)	ethyl methacrylate
80	2.57	PMMA
220	1.75	n-butyl methacrylate
261	.30	iso-butyl methacrylate
269	5.3 to 8.00 (12.5)	ethyl methacrylate
301	12 to 15	PMMA
199	60 to 100	methyl acrylate
283	17 to 22	vinyl chloride
225	45 to 60	vinyl acetate
75	4.5	polystyrene

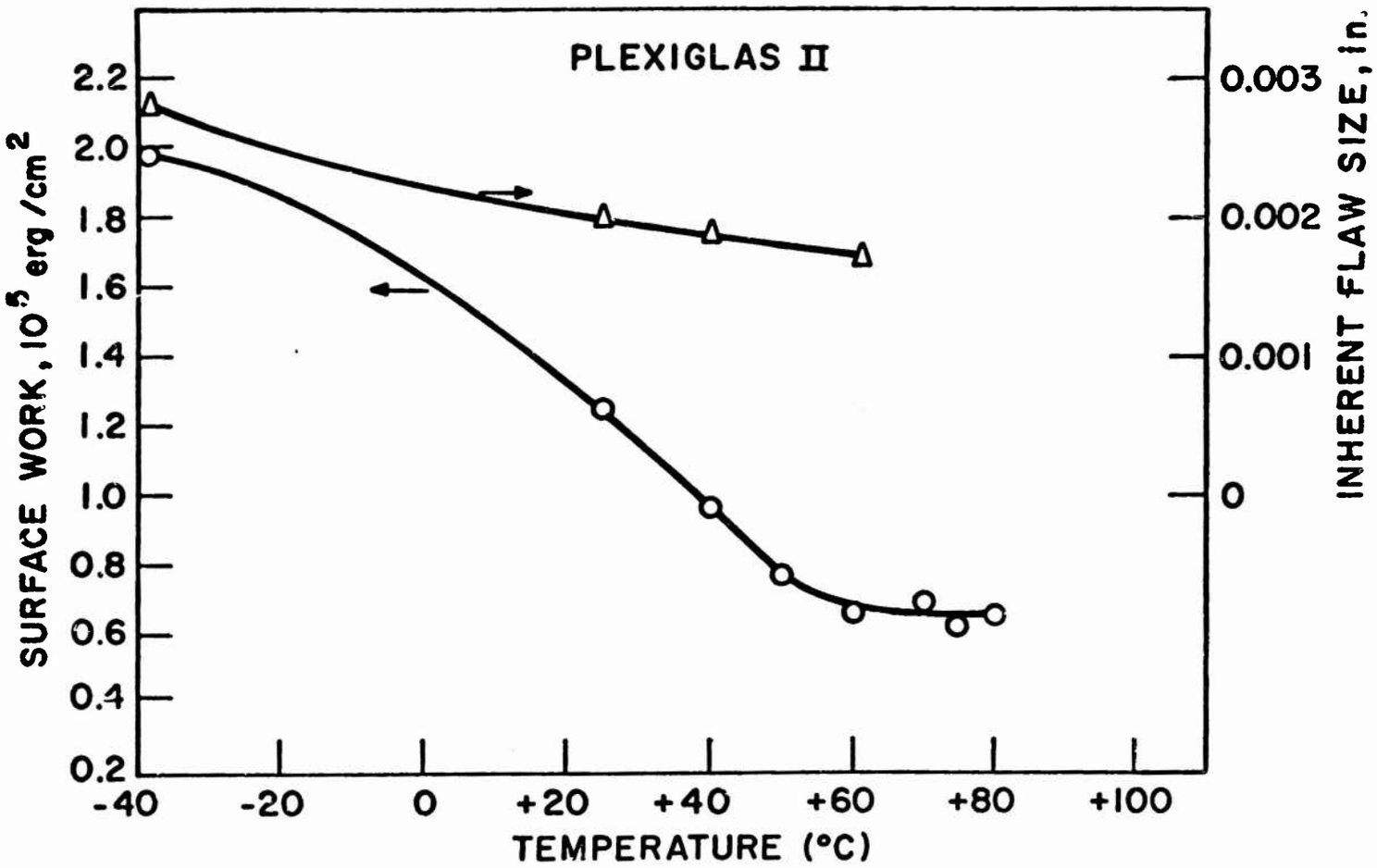

FIGURE 9. FRACTURE SURFACE WORK FOR POLY(METHL METHACRYLATE) AS A FUNCTION OF TEMPERATURE.

A cleavage specimen is used, and the crack is propagated through the thin adhesive layer which bonds aluminum adherends in the shape of the cleavage specimen. Their results also indicate an increase in fracture surface work as the crack propagation rate increases. Investigators from the U.S. Naval Research Laboratory have also studied crack propagation velocity effects in poly(methyl methacrylate) (13). They designed servo-actuated loading equipment controlled by an analog computer to maintain a constant crack velocity in a uniform cleavage bar. They observed an increase in fracture surface work from 2×10^5 to 4.5×10^5 erg/cm^2 while the crack velocity increased from 0.01 to 4 in/sec. Further increases in the crack velocity result in a decrease in the fracture surface work. At the crack velocity of 15 in/sec. the fracture surface work reaches the minimum value of 2.8×10^5 erg/cm^2. After this crack velocity of 15 in/sec., the fracture surface work starts to increase again as the crack velocity increases.

From these accumulated results it is evident that the fracture surface work is influenced by temperature and crack velocity just as are viscoelastic parameters. Decreasing temperature and increasing crack velocity (strain rate) cause increases in fracture surface work. If the fracture surface work is to be considered as a viscoelastic parameter, a complete understanding of the fracture surface work has to come from the careful investigations of the simultaneous effects of temperature and crack velocity.

With respect to the simultaneous effects of temperature and crack velocity on the fracture surface work, tearing behavior of rubber has been extensively studied (37,38). In a rubbery state the previously described experimental techniques for measuring fracture surface work are not valid; however, techniques have been developed for measurement of the tearing energy for rubbery materials, and this quantity has the same significance as the fracture surface work for glassy polymers. Figures 10 and 11 show the dependence of tearing energy on the rate of propagation at different temperatures (37). Veith (37) stated that a Ferry-type transform could be performed on the tearing energy data over the range of temperatures and rates of propagation used in the experiments. This type of treatment for the data was suggested by the general pattern in regard to temperature-rate variations, and the pattern noted is one to be expected for a viscous type process. Particular interest should be paid to Mullins' work on the role of hysteresis in the tearing of rubber (40). Veith summarized the results of Mullins' work in two statements (37):

1) The internal viscosity or damping coefficient of the rubber controls the tearing energy of the rubber. The less mobile the molecular chains, the greater the tearing energy.

2) The development of special structural changes at or near the tips of growing tears affect tearing behavior. These may be the results of anisotropic conditions in the rubber prior to the act of tearing, or they may be formed during the tearing process. When these structure-forming tendencies are intense, knotty or stick-slip tearing is the result. The dependence of tearing energy on internal viscosity which is responsible for hysteresis losses in rubbers is well demonstrated in Figure 12. It can be said from this result that internal viscosity or damping plays a dominant role in determining the energy requirement for the tearing of rubber.

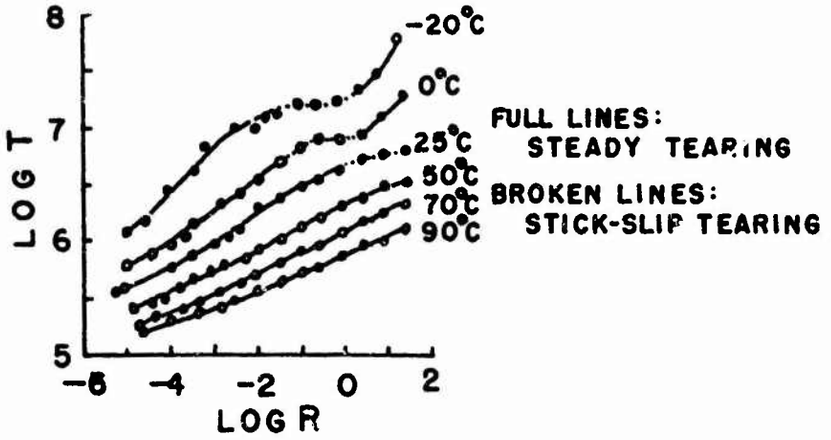

FIGURE 10. DEPENDENCE OF TEARING ENERGY T (ergs/cm^2) ON RATE OF PROPAGATION R (cm/sec) FOR SB-RUBBER (REF. 37).

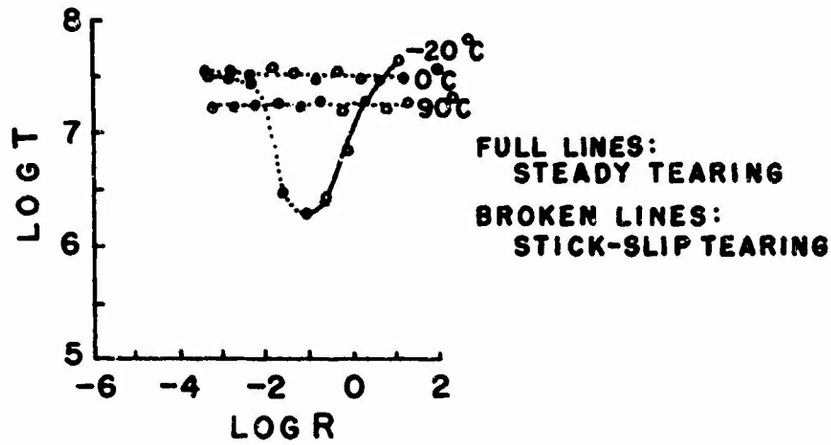

FIGURE 11. DEPENDENCE OF TEARING ENERGY T (ergs/cm^2) ON RATE OF PROPAGATION R (cm/sec) FOR NATURAL RUBBER (REF. 37).

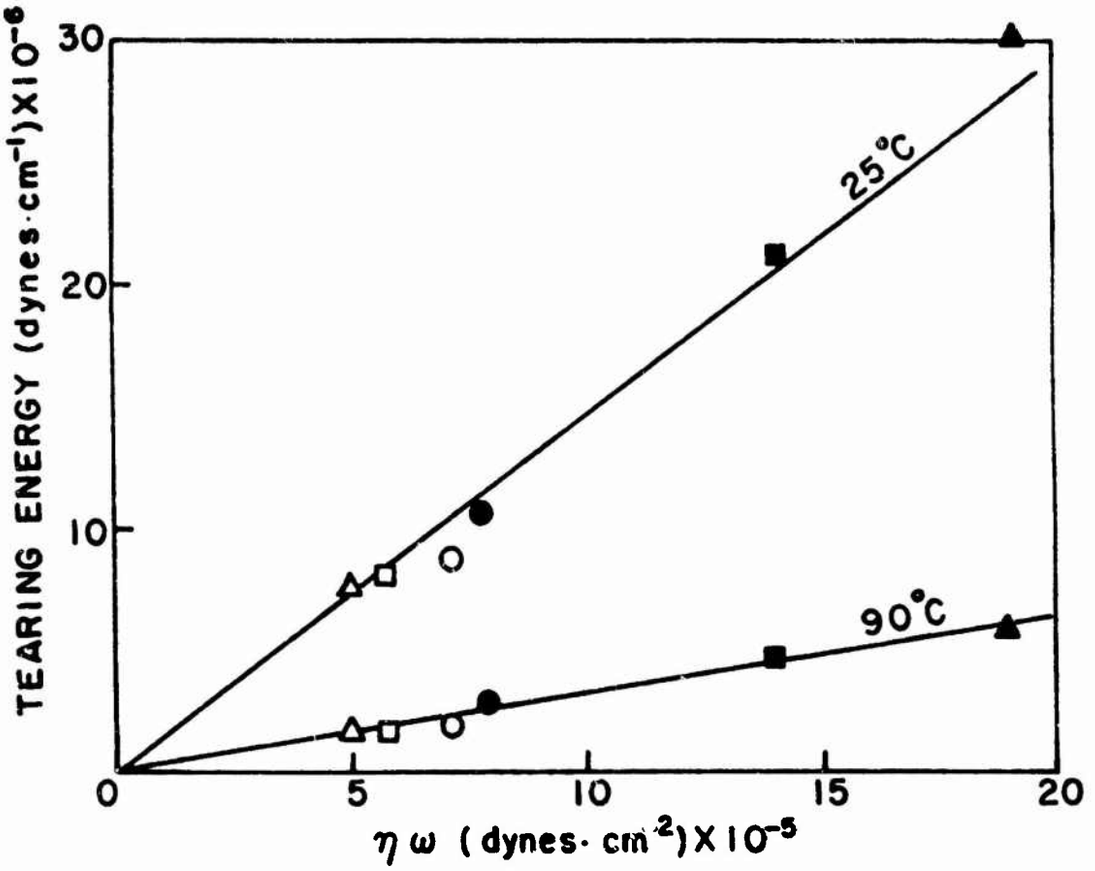

BUTADIENE–STYRENE COPOLYMERS

△	B/S	96/4
□	B/S	87/13
○	B/S	72/28

BUTADIENE–ACRYLONITRILE COPOLYMERS

▲	B/A	82/18
■	B/A	70/30
●	B/A	62/38

FIGURE 12. DEPENDENCE OF TEARING ENERGY T ON DAMPING $\eta\omega$ (MULLINS, REF. 40).

Since the fracture surface work or tearing energy includes the contribution of the irreversible work or the energy dissipation caused by the viscoelasticity of the material, it is of interest to study how much of the fracture surface work or tearing energy is due to the viscous energy dissipation around the crack tip and what is the lower bound of the fracture energy. In an effort to establish a lower bound on the fracture energy of a polyurethane elastomer Mueller and Knauss developed an experimental method to minimize or eliminate the energy dissipation at a crack tip caused by viscosity (11). They tried to remove the internal viscosity sufficiently by swelling the material in a suitable solvent and then performing fracture tests in this state. After obtaining the fracture energy value in the swollen state, this value was related to its counterpart in fracture of the unswollen material. The value thus obtained was termed intrinsic fracture energy. The intrinsic fracture energy is equal to half the energy necessary to create fracture without any energy dissipation through viscous forces around the tip of the advancing crack. Mueller and Knauss further derived the equation which gives the fracture energy as a function of crack velocity and temperature in terms of a rate independent intrinsic fracture energy and a function of the creep compliance of the material.

It seems that the Mueller and Knauss approach explains adequately the basic process defined by Veith (37) as one associated with a continuous increase in fracture energy with increase in the crack propagation rate; however, there are one or more secondary processes. One secondary process produces a decrease in fracture energy with increase in crack velocity which could not be explained.

Definitive work on the study of the simultaneous temperature and crack velocity effects on fracture surface work for glassy polymers has not been reported. In order to fully understand fracture behavior of glassy polymers, carefully designed experiments investigating simultaneous effects of temperature and crack velocity are needed.

CHAPTER II

EXPERIMENTAL EQUIPMENT DEVELOPED FOR FRACTURE STUDIES

A. Side-Groove Cutting Machine for Double Cantilever Beam Cleavage Specimens

A side-groove cutting machine was designed to increase efficiency and accuracy in machining side grooves on the cleavage specimens (Figure 13). Two 1/2 inch diameter spindles are mounted on bearing cases with three precision radial bearings (NICE 1616-DC) for each spindle. These two bearing cases are interconnected by a threaded rod (one half is 1/2-20 left-hand thread and the other half is 1/20-20 right-hand thread) and slide between the horizontal keys of the bearing case housing. Thus the distance between the two spindles is freely adjusted by rotating the threaded rod. On one end of the threaded rod a dial (50 divisions) is set so that the distance between the two spindles is controlled with an accuracy of $\pm$ 0.002 inches. The other end of the threaded rod is connected to the bearing case housing with two lock nuts and a spring. By adjusting the position of these lock nuts on the threaded rod, the two spindles are moved equal distances in the same direction. The bearing case housing slides between the vertical keys mounted on the vertical frame. Thus the vertical position of the spindles can be adjusted. The vertical frame is attached to three rods (1 inch diameter, 36 inches long) which are fixed by two end plates. The same end plates also support three fixed rods on which the specimen carriage moves. The apparatus described above is mounted on a suitable frame with a drive system to feed the specimen carriage. This drive system has feed speeds of 1, 2, 12 and 20 inches per minute.

In order to drive the two spindles with the saw blades a separate motor is mounted on a stand attached to the side of the base frame. A special pulley system was designed so that the spindles rotate clockwise and counterclockwise at a constant speed of about 1,000 r.p.m.

A specimen is vertically clamped on the carriage and passes between two cutters mounted on the spindles whose positions are set symmetrically with respect to the neutral plane of the specimen by the previously described threaded rod.

In order to prevent heating up of the cutters and specimens in machining, compressed air (200 psi) is directed towards the cutting points through copper tubing attached to the vertical frame.

With this groove cutter it takes an average of 7 minutes to machine the side grooves and the initial crack on the 12-inch long specimens. The maximum length specimen which can be machined is about 17 inches.

B. A Servo-Controlled Hydraulically Actuated High-Speed Loading System

In order to investigate the effect of crack velocity on the fracture surface work of polymeric materials and the effect of strain-rate on the mechanical properties of polymers, a servo-controlled hydraulically actuated high speed testing machine was

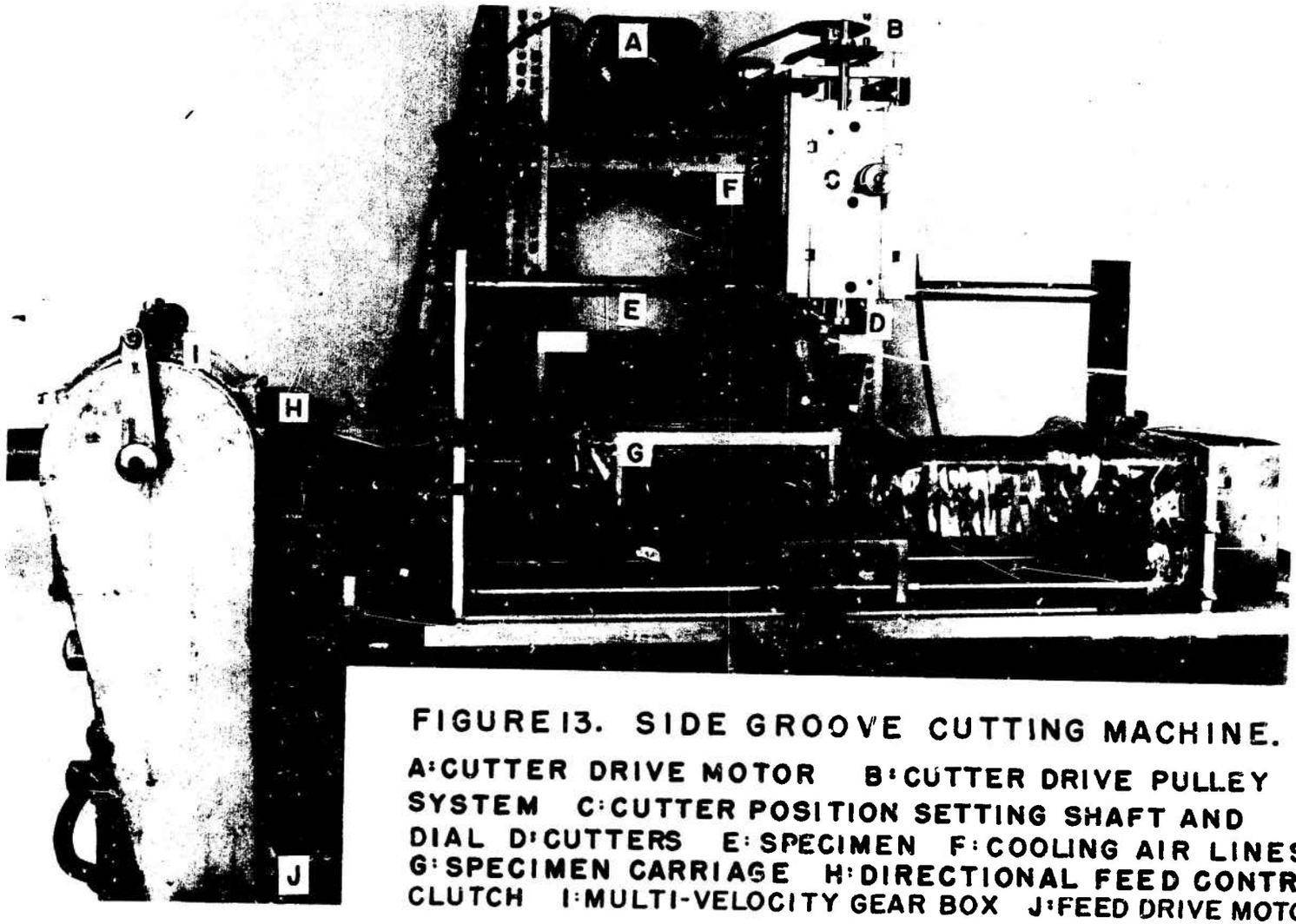

FIGURE 13. SIDE GROOVE CUTTING MACHINE.

A: CUTTER DRIVE MOTOR B: CUTTER DRIVE PULLEY SYSTEM C: CUTTER POSITION SETTING SHAFT AND DIAL D: CUTTERS E: SPECIMEN F: COOLING AIR LINES G: SPECIMEN CARRIAGE H: DIRECTIONAL FEED CONTROL CLUTCH I: MULTI-VELOCITY GEAR BOX J: FEED DRIVE MOTOR

designed and constructed.* It is capable of applying constant cross-head rates of up to 18,000 inches per minute and can develop 2000 pounds of load at the maximum rate in tension or compression. The maximum range of the displacement of the cross-head is ± 6 inches. Controll of the system is provided by an MTS Systems Corporation electronic system controller which is used to drive two servo-valves. These servo-valves regulate the flow of hydraulic fluid to the hydraulic cylinder. This machine can be operated either with displacement control or with load control as a function of time. Each section of the testing machine system is explained in detail in the following sections.

1. The Hydraulic Power System

a) The Power Supply

The hydraulic power supply is a Denison JIC-60 gallon power unit rated at 3000 psi and 20 GPM flow rate which was developed by J. W. Dally and B. R. Beadle at Illinois Institute of Technology in 1966. The drive for the main pump is provided by a 40 H.P. 200 V-3 phase electric motor with a nominal speed of 1200 r.p.m.

The pump is a Denison variable volume axial piston pump capable of a maximum flow of 20 gallons per minute at 1200 r.p.m. It is directed to a high pressure 10-micron filter and then through a check valve to the high pressure header.

The high pressure header is equipped with two adjustable pressure relief valves, a pressure gage, a manual relief valve, and an accumulator. The accumulator is a 2-1/2 gallon 6000 psi bladder type. This accumulator is precharged with dry nitrogen to a pressure of about 500 psi.

The unit is also equipped with a low pressure filtering and temperature regulating circuit which draws fluid from the sump, filters it with a 5-micron low-pressure filter, and cools it with a heat exchanger--the water for which is regulated thermostatically--and returns it to the sump.

b) Hydraulic Lines and Connectors

The lines used on this system are 1" O.D. x 0.110" wall thickness carbon steel tubing rated at 3000 psi with a safety factor of 4. The fittings are of the "Ferulok" variety and have a burst pressure of 16,000 psi at normal temperature. From these lines the flow goes to the loading machine through a 4-way double solenoid spring centered directional control valve.

c) The High Speed Loading Machine Hydraulic System

The fluid from the 4-way solenoid operated directional valve goes to a "Ferulok" cross fitting. To one end is attached a Greer Floating Piston Accumulator

---

* This machine was developed and constructed through a National Science Foundation grant (GK-15361) and has been used extensively in this study.

(rated to 1 gallon 3000 psi Model APA-30-232) pre-charged with dry nitrogen to a pressure of approximately 1000 psi (see Figure 14). Two ends of the cross fittings are connected to the manifolds on which the Moog servo-valves are attached. Each servo-valve is a Moog Model 72-102 and has a rated flow of 40 GPM. The direction and the flow rate of the fluid are controlled by the servo-valves. The controlled flow of the fluid goes to the hydraulic actuator through the abovementioned manifolds. The hydraulic actuator used here is a Miller Fluid Power Co. Model DH-65R double acting cylinder having double rod ends. It has a 1-1/2 inch bore, 12 inch stroke, and a 1 inch diameter rod with 1"-14 x 1-1/8" male thread on each end and 7/16"-20 x 1-1/8" female thread on one end. The cylinder is cushioned on both ends, and it is rated to 3000 psi operating pressure. It is capable of exerting up to a 3000 pound force at the rated pressure of 3000 psi.

The fluid from the hydraulic actuator goes back to the lines through the manifolds, the servo-valves, and the 4-way double solenoid spring centered directional control valve. Between the manifolds and the 4-way directional control valve, a 1/2 gallon Greer Floating Piston Accumulator rated 3000 psi is attached to absorb temporarily the high pressure oil outflow from the hydraulic actuator and to prevent the propagation of water-hammering effects throughout the system.

2. The Electrical System

The electrical system was designed by MTS Systems Corporation to be compatible with our design of the servo-controlled hydraulically actuated high speed loading system. It consists of

(a) a Servo-Controller Model 440.11A

(b) an AC Transducer Conditioner Model 440.22

(c) a DC Transducer Conditioner Model 440.21

(d) a Feedback Selector Model 440.31

(e) a Controller Model 442.11 and

(f) a Function Generator Model 410.21

These components are placed in a console panel (Figure 15). The whole system is designated as MTS Model 906.33 Control Console. The functions of each component will be discussed below.

(a) The Servo-Controller Model 440.11A has dual valve amplifiers for driving two servo-valves simultaneously, and it performs three functions in the electro-hydraulic loading system: control of the hydraulic actuator servo-valves, program pacing, and error detection.

The Servo-Controller is capable of controlling one hydraulic loading "channel" which is often called a "closed loop". A closed loop usually consists of one Servo-Controller, one or two servo-valves, one hydraulic actuator, and one or more Transducer Conditioners, each working in conjunction with a transducer and the Servo-Controller. The term "closed loop" is derived from the fact that the above-mentioned components make a continuous path of interacting elements as shown in

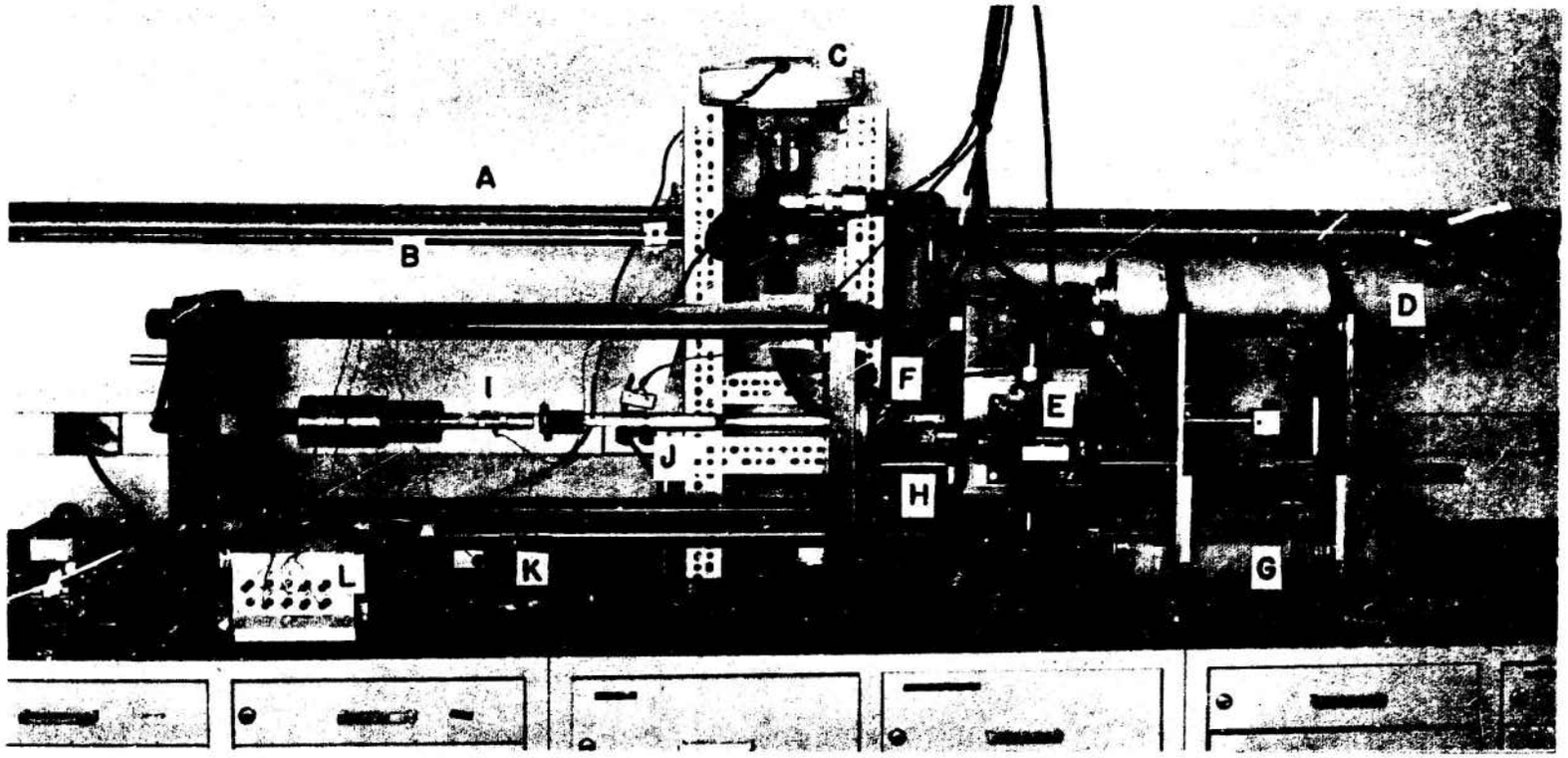

FIGURE 14. SERVO-CONTROLLED HYDRAULICALLY ACTUATED HIGH-SPEED LOADING SYSTEM.

A: PRESSURE LINE B: RETURN LINE C: 4-WAY DIRECTIONAL VALVE
D: PRESSURE LINE ACCUMULATOR E: 40 GPM SERVO-VALVE
F: HYDRAULIC ACTUATOR G: RETURN LINE ACCUMULATOR
H: LVDT I: QUARTZ LOAD-CELL J: SLACK GRIP K: SPECIMEN
L: VELOCITY GAGE

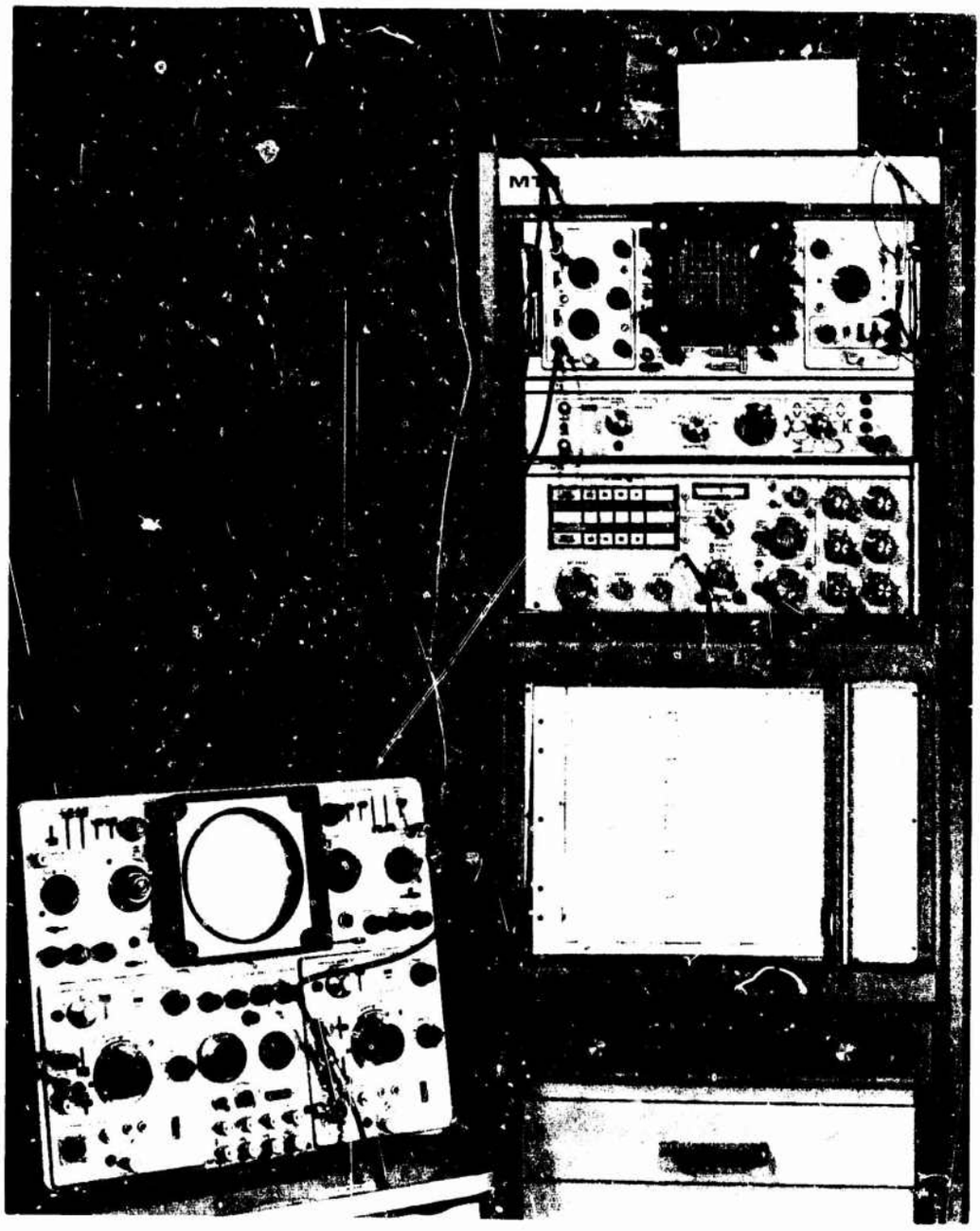

FIGURE 15-1. MTS CONTROL CONSOLE AND SIGNAL RECORDING SYSTEMS.

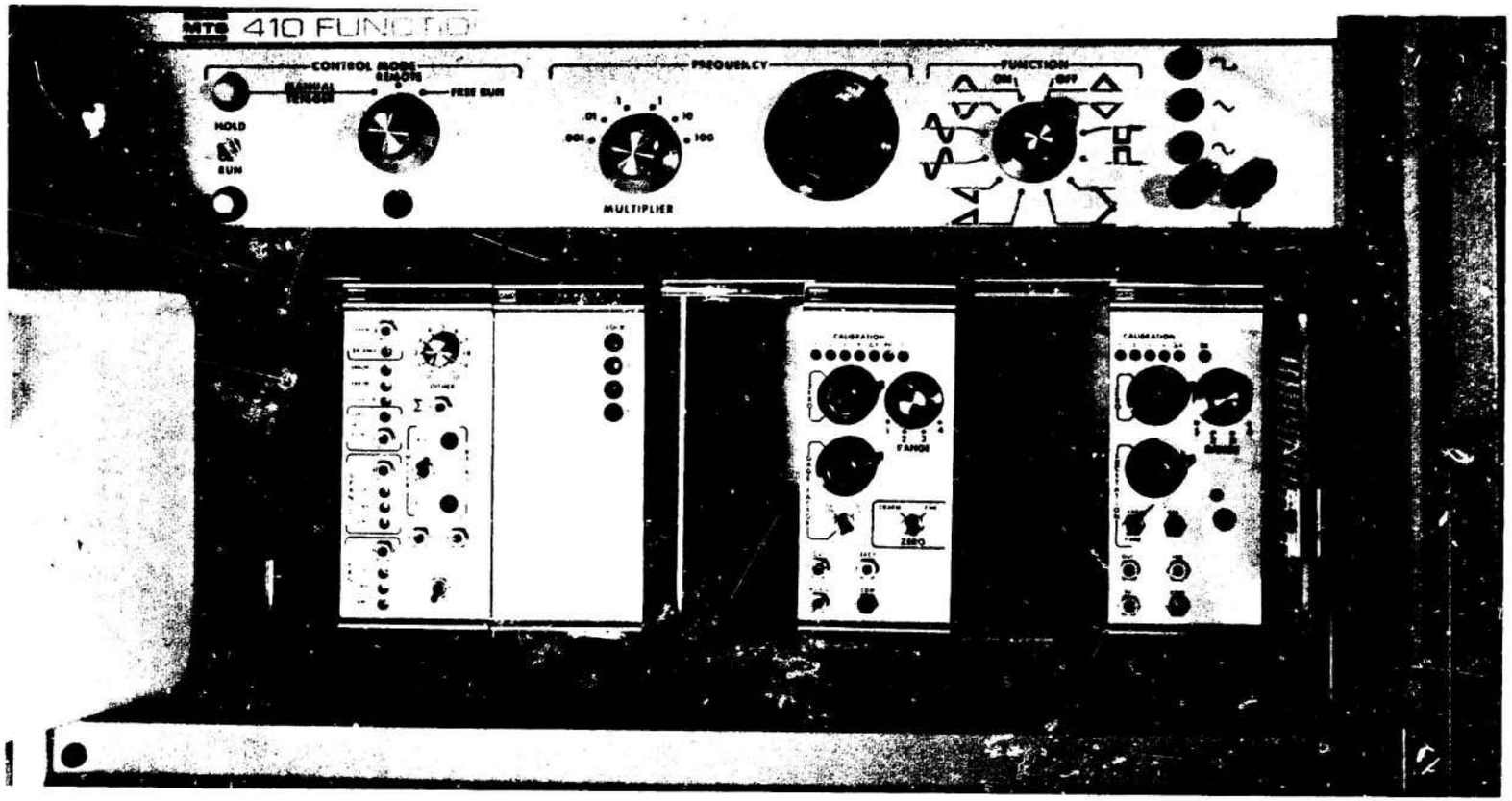

FIGURE 15-2. MTS CONTROL CONSOLE SHOWING SERVO-CONTROLLER, FEEDBACK SELECTOR, AC CONDITIONER, AND DC CONDITIONER.

Figure 16. Anything which affects the behavior of a single component in the loop affects the entire loop. When a specimen is placed within the control loop, it acts as a component in the loop. It, therefore, possesses several unique features. First, the characteristics of the specimen directly affect the gain and frequency response of the loop. Second, by choice of the proper transducer, it is possible to closely control the parameter of interest within the specimen itself. Third, the range of the system is established by the minimum capacity component in the control loop. For example, given adequate force and frequency response in the electro-hydraulic actuator, if a load transducer exhibits full electrical output at 100,000 lbs., the control loop becomes a 100,000 lb. system.

Two inputs to the Servo-Controller are the command and feedback signals. The command signal represents the amount and the direction of some desired mechanical quantity, for example, a certain amount of force or displacement. The transducer accepts a mechanical input from the actuator and produces an electrical output signal (feedback) which represents the amount and the direction of this mechanical input. If command and feedback are not equal (or if an error exists), the Servo-Controller provides an output control signal that has a magnitude proportional to the amount of error and a direction or polarity determined by the direction of error (feedback is either positive or negative with respect to the command).

The control signal causes the servo-valve(s) to open in the direction required to decrease the error and by an amount proportional to the magnitude of the error. The servo-valve opens the hydraulic pressure and return lines between the actuator and the hydraulic supply. This causes the actuator to stroke in the direction that reduces the error. When the error is reduced to zero, the control signal is reduced to zero, and the servo-valve closes.

(b) The AC Transducer Conditioner Model 440.22 is used in the closed-loop electro-hydraulic testing system in conjunction with a Collins Model LMT-711S17 (Stroke $\pm$ 6.00 inches) LVDT (linear variable differential transformer) which is connected to one end of the piston rod of the hydraulic actuator for readout of its stroke.

The Conditioner uses an amplitude-regulated 10 Khz voltage to excite the transducer. It also amplifies and demodulates the output of the transducer, providing a feedback signal which is the DC analog of the quantity sensed by the transducer. The feedback signal is fed to the Servo-Controller, which compares it with the command signal and acts to maintain the controlled variable at the command level.

The Model 440.22 AC Transducer Conditioner has a range selector switch which determines the operating range of the system in the following manner: 100 percent of the transducer's rating (for example, $\pm$ 6 inches stroke), 50 percent of the transducer rating ($\pm$ 3 inches stroke), 25 percent ($\pm$ 1.5 inches stroke) and 10 percent ($\pm$ 0.6 inches stroke) at each level, and the readout output signal is adjusted to give $\pm$ 10 volts at full scale.

(c) The Model 440.21 DC Transducer Conditioner is used in the closed-loop electro-hydraulic testing system, with a resistive strain gage bridge type load cell (Rated 3000 lb. capacity, Excitation 10.0 volts) which was designed and constructed by Mr. Kobayashi. The Transducer Conditioner is primarily associated with the feedback function in the control loop. Its output may also be used for readout purposes.

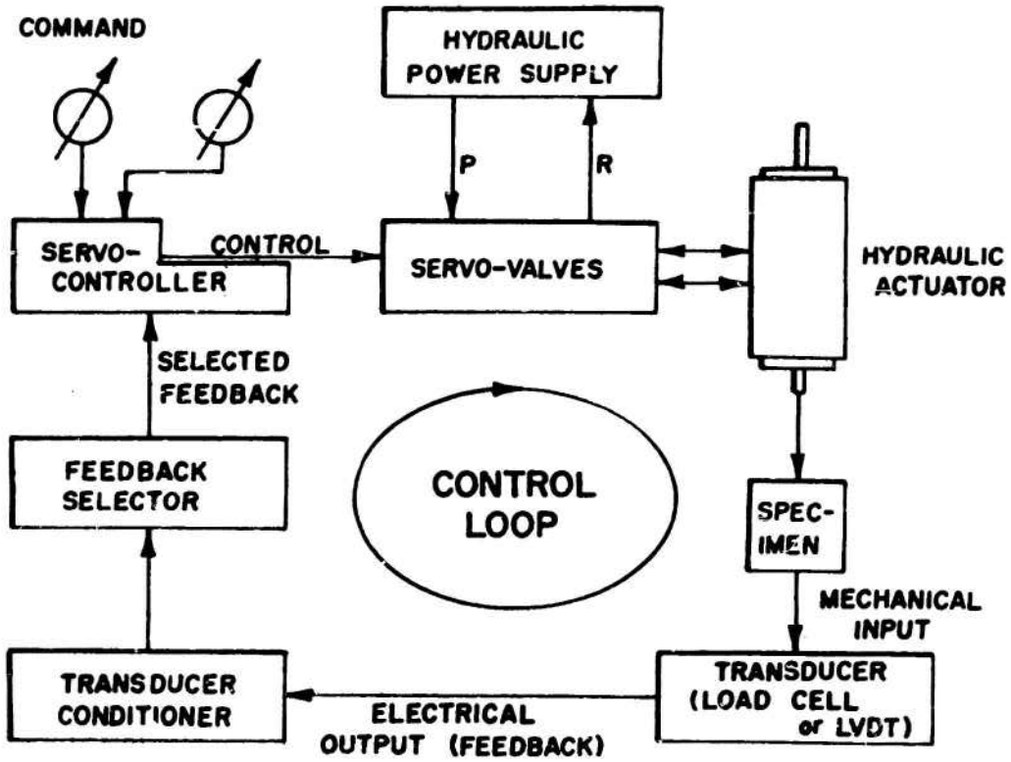

FIGURE 16. BLOCK DIAGRAM OF ELECTRO-HYDRAULIC SERVO-CONTROL LOOP.

The Conditioner uses a precision DC power supply to excite a resistive strain gage bridge type load cell. It also amplifies the output of the transducer, providing a feedback signal which is the DC analog of the quantity sensed by the transducer. The feedback signal is fed to the Servo-Controller, which compares it with the command signal and acts to maintain the controlled variable at the command level.

The Model 440.21 DC Transducer Conditioner has a range selector switch which determines the operating range of the system in the following manner:

100 percent of the load cell rating (3000 pounds capacity, for example)

50 percent of the load cell rating (1500 pounds)

25 percent of the load cell rating (750 pounds)

10 percent of the load cell rating (300 pounds).

At each level, the readout output signal is adjusted to give ± 10 volts at full scale.

(d) The Model 440.31 Feedback Selector is used to allow selection of the controlled variable, load or stroke, in the closed-loop testing system by pressing the appropriate feedback switch. Logic circuiting in the Feedback Selector prevents the simultaneous selection of more than one controlled variable. Additional system logic prevents the application of hydraulic pressure without the selection of a controlled variable. If a power failure should occur during a test, latching relays will hold the last controlled variable selected and automatically select this variable when the system is turned on.

(e) The Model 442.11 Controller is an electronic sub-system containing the principal control, failsafe, and readout selection units in an MTS electro-hydraulic testing system. The Controller consists of a hinged front panel containing operating controls and, behind the front panel, four individual modules, each with a specific function in the system. The functions of the four individual modules have already been explained in the previous sections. All electrical power for the Controller and its modules comes from a common power supply located on a swing-out door at the rear of the Controller. The Model 442.11 has three sets of controls not associated with an individual module: recorder input selectors, oscilloscope input selectors, and calibration controls (for use with either a recorder or oscilloscope).

(f) The Model 410.21 Function Generator (Exact Electronics, Inc.) provides variable frequency sine, half-sine, square, saw tooth, ramp, hold ramp, and triangle functions for dynamic test programs. Output frequency range is 0.001 cps to 1 kcps in six decades. Operating modes are free-running, triggered, control panel (gated), and hold-interrup (Hold Ramp Only). The Model 410.21 Function Generator has no front panel amplitude control. To adjust the amplitude of dynamic commands, the operator uses a SPAN control on an external unit.

3. The Loading System

The loading frame is a 4 column frame as shown in Figure 14. It will accept test specimens up to 12 inches in length and 10 inches in diameter. Several types

of pin loading fixtures were designed for double cantilever beam cleavage type specimens and simple tensile type specimens. A slack grip device was also designed (Figure 17) so that the actuator is accelerated to full speed before it contacts the specimen. This slack grip is used with the pin loading fixtures.

4. Monitoring System

a) The Transducers

A 3000 pound load cell has been designed and constructed with a complete four arm gage bridge. The main element is made from 2024 Aluminum and is shown in Figure 18. The bridge is made of Type EA-13-250MQ-350 gages (Micro-Measurements) and gives a full scale output of 20 mV excited at 10.0 volts. The bridge circuit is shown in Figure 19.

The natural frequency of this load cell with a light weight grip is about 10 Khz, but this frequency is not high enough for high speed testing. For high speed testing, therefore, a quartz force link (Kistler Model 932 A) together with a charge amplifier (Model 504A, Kistler Instrument Corporation) is used to measure load independently from the servo-controlled closed loop system. The quartz force link has the following features:

Range tension	2000 pounds
Range compression	4000 pounds
Resolution	0.01 pounds
Resonant frequency unmounted	55 Khz
Rigidity	12×10^{-8} in/lb.
Rise time	20μ seconds
Linearity	1 percent

With a light weight grip for a double cantilever cleavage type specimen, the natural frequency of the load measuring system is 35 Khz.

(b) The Oscilloscope

The Oscilloscope used is a Tektronix R564B storage oscilloscope equipped with a Type 3A72 Dual-Trace Differential Amplifier plug-in unit and a Type 2B67 Time Base plug-in unit. This unit can read and record signals from any of the transducers and plot them against time. Type 3A72 Dual-Trace Differential Amplifier is a two channel amplifier and can be used in five modes of operation: Channel 1 only, Channel 2 only, algebraic addition or subtraction, and chopped and alternate dual-trace operation. Sensitivity of each channel is variable in 11 calibrated (within 3%) steps from 10mV/Division to 20V/Division and can be continuously variable (uncalibrated) from 10mV to at least 50V/Division.

The time base can sweep from 1 microsecond to 5 seconds per division in 21 calibrated steps. An uncalibrated control provides continuously variable sweep rates

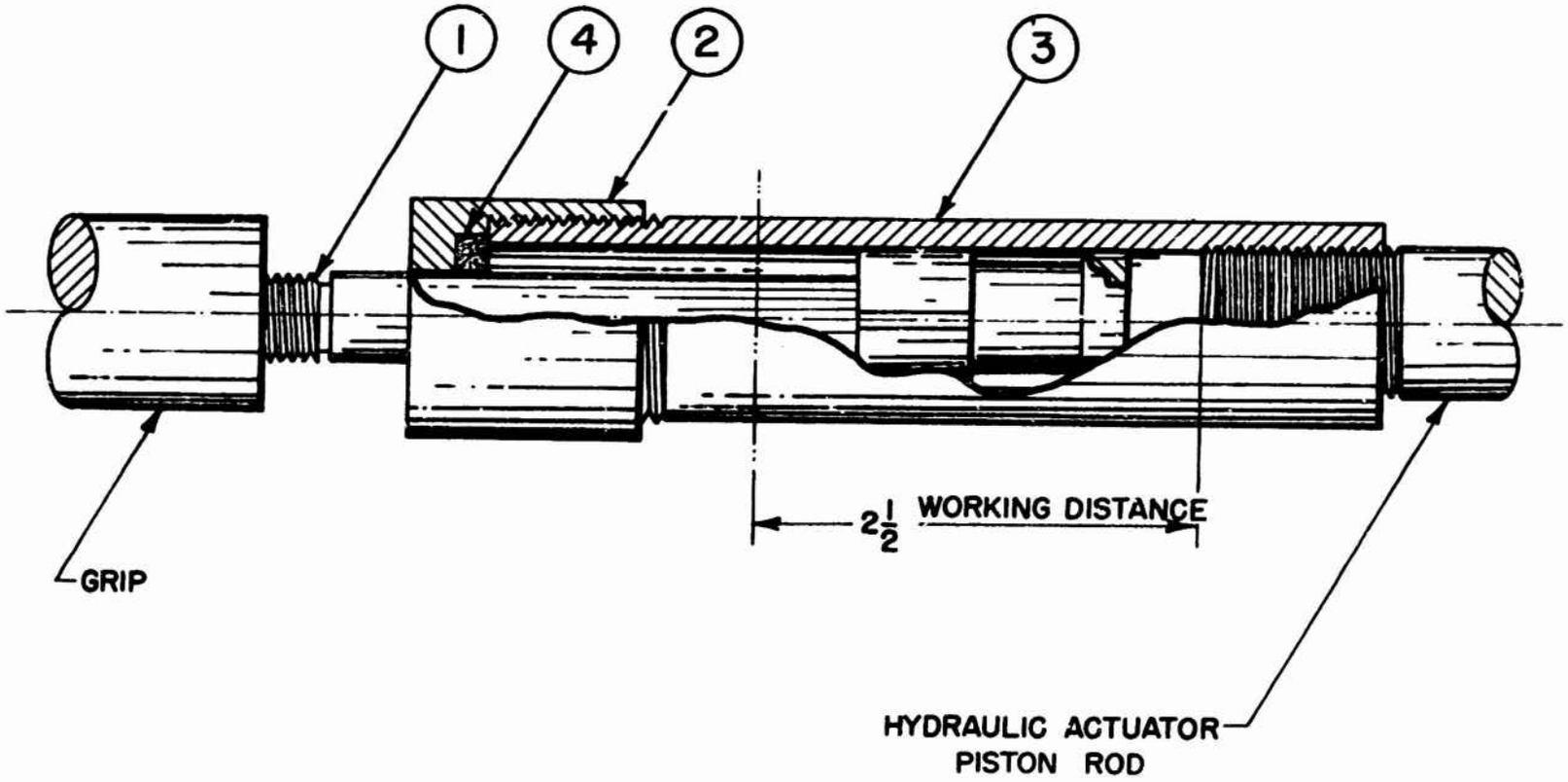

FIGURE 17-1. SLACK GRIP DEVICE (ASSEMBLY DRAWING).

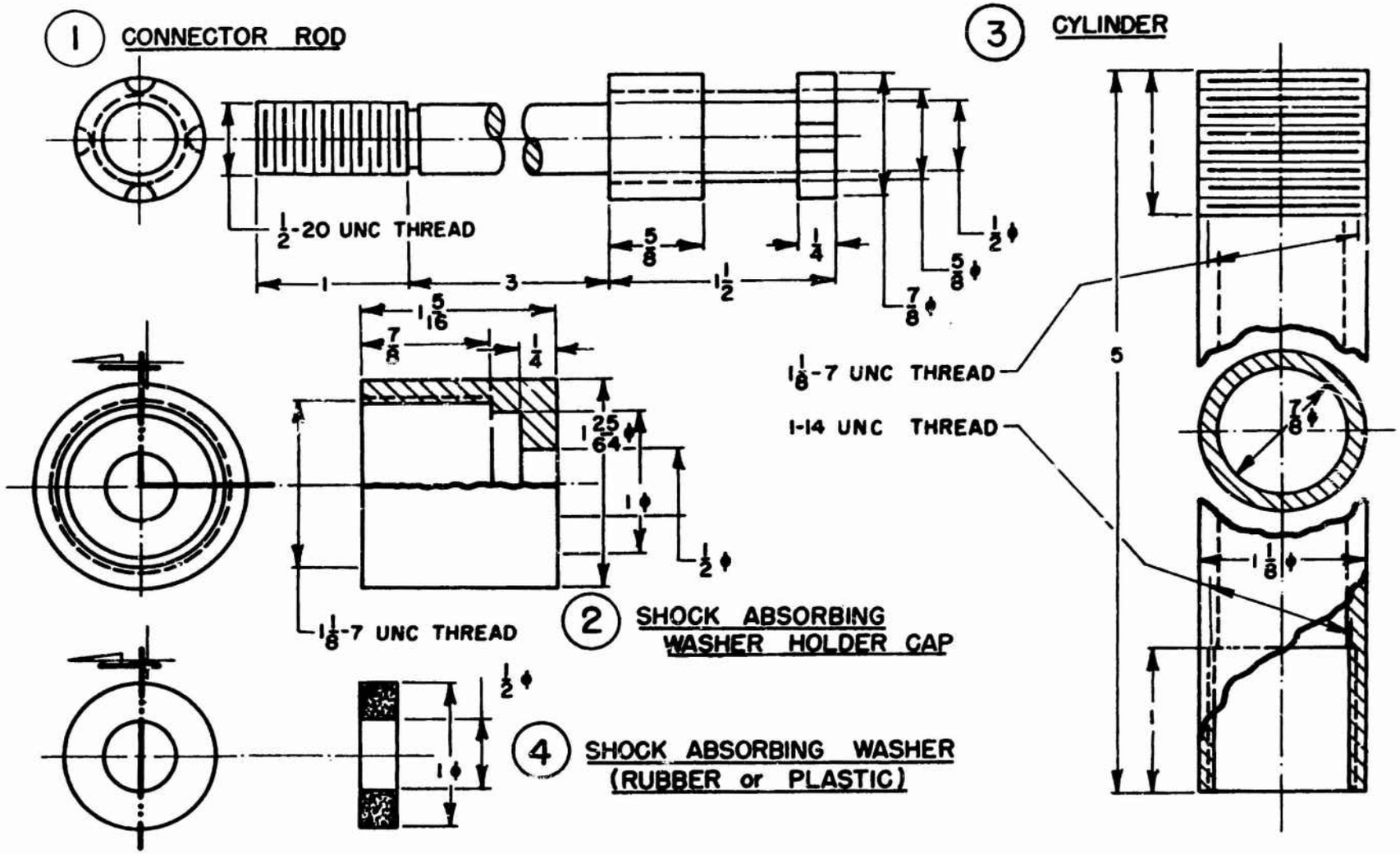

FIGURE 17-2. SLACK GRIP DEVICE (COMPONENTS DRAWING).

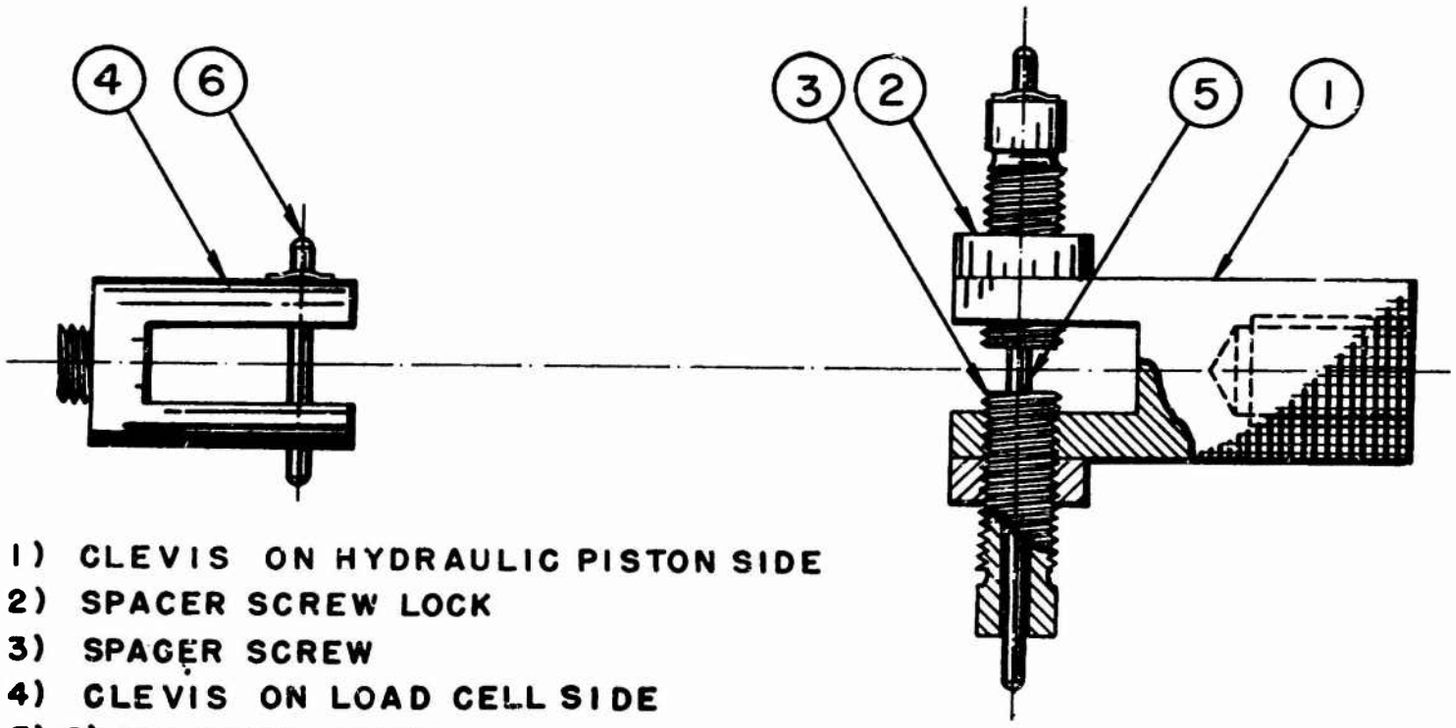

1) CLEVIS ON HYDRAULIC PISTON SIDE
2) SPACER SCREW LOCK
3) SPACER SCREW
4) CLEVIS ON LOAD CELL SIDE
5),6) LOADING PINS

FIGURE 17-3. SLACK GRIP DEVICE (CLEVIS GRIPS FOR CLEAVAGE SPECIMENS).

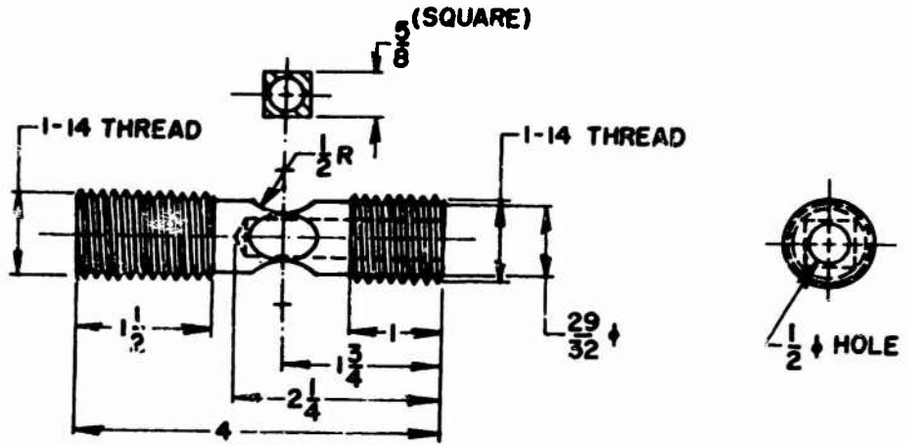

FIGURE 18. MAIN ELEMENT OF STRAIN GAGE TYPE LOAD CELL.

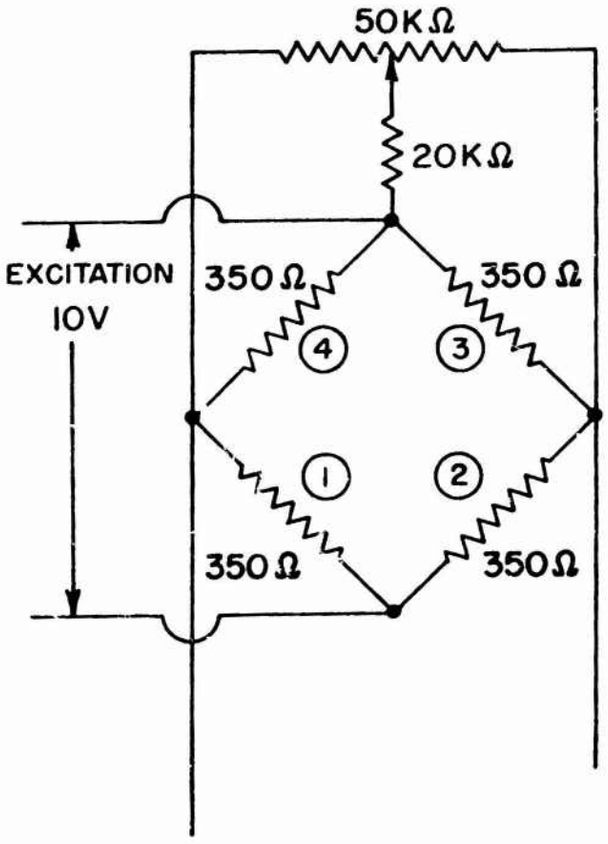

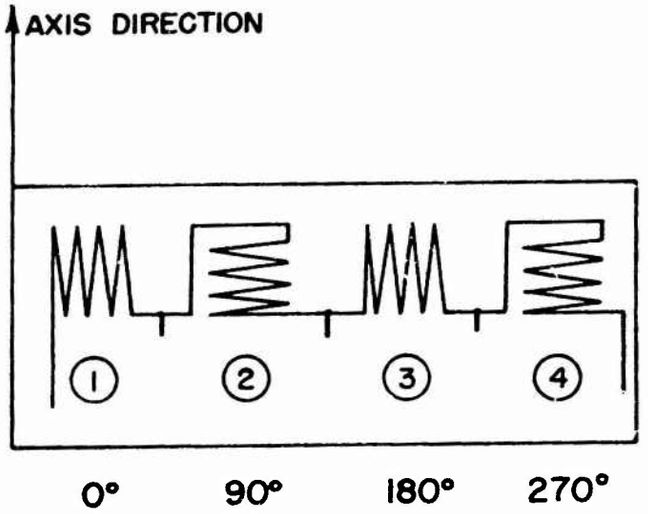

FIGURE 19. BRIDGE CIRCUIT FOR STRAIN GAGE TYPE LOAD CELL.

to about 3 times the step-switch setting. It has a magnifier which provides a 5-times expansion of the center 2 divisions of display. Triggering modes are internal, external, and line. Trigger coupling may be selected from AC slow, AC fast, and DC, and the triggering level and polarity are continuously adjustable. A single sweep may be selected, allowing operation only after manual reset for either triggered or free-running operation.

(c) The X-Y Recorder

The X-Y recorder used is a Varian Aerograph Model F-80 A X-Y Recorder. It, like the oscilloscope, is used to record transducer outputs as a function of time or other transducer outputs. The size of the platen for recording paper is 11-3/4" x 16-7/8". Time base ranges are 50, 20, 10, 5, 2, 1, 0.5 sec/inch, and slew velocity is 17 in/sec. on each axis. Since its slew speed is 17 in/sec., it is used only for low speed tests. Calibrated DC ranges are 0.5, 1, 2, 5, 10, 20, 100, 200, 500 mV/inch, 1, 10, 20, 50 V/inch for each axis, and a continuous adjustable vernier between calibrated ranges is also possible for each axis.

CHAPTER III

SPECIMEN DESIGN AND MEASUREMENT TECHNIQUE

A. Review of Technique

In 1920 Griffith (1) established a fracture criterion for brittle materials; namely, a system would become unstable and a crack would increase in size if

$$-\frac{dU}{d\ell} = \frac{dS}{d\ell} \tag{4}$$

where U is equal to the strain energy and S is equal to the surface free energy. He showed that the solution of this equation for a uniformly loaded bar in uniaxial tension resulted in the equation

$$\sigma_{ult} = \sqrt{\frac{2E\gamma}{\pi c}} \tag{5}$$

where σ_{ult} = ultimate tensile strength
E = Young's modulus of elasticity
γ = fracture surface energy
and c = critical flaw size in material.

Griffith was able to demonstrate that σ_{ult} was proportional to $(1/c)^{\frac{1}{2}}$ for inorganic glasses. Orowan (18) later modified this expression to account for irreversible work which also may occur during the fracture process at the tip of the propagating crack. This irreversible work is primarily attributed to local plastic deformation or viscous deformation of the material at the highly stressed crack tip. The modified Griffith equation is then represented by

$$\sigma_{ult} = \sqrt{\frac{2E(\gamma + P)}{\pi c}} \tag{6}$$

where P represents the irreversible work.

Berry (2) was one of the first to apply this criterion to polymers and he showed that polystyrene and PMMA obeyed the criterion $\sigma_{ult} = k\, c^{-\frac{1}{2}}$. This was accomplished by measuring the tensile strength of bars which had cracks of various lengths introduced into their edges. Berry also determined that the experimental value of the surface energy was much greater than the theoretically predicted value. Thus irreversible work also occurs at the crack tip, and the surface energy is best termed fracture surface work.

Gilman modified the technique used by Obreimov for cleaving mica and established the technique of employing the double cantilever beam cleavage

specimen. He used this method for measuring the fracture surface energy of crystals along particular cleavage planes (41). The cleavage technique has some advantages over using tensile stress fields for crack initiation and propagation. For example, the value of the fracture surface work can be obtained from a few experiments on one specimen. The crack propagation rate can be better controlled and the calculation of the surface work is based on simple beam theory. However, the cleavage technique has theoretical and experimental shortcomings. For example, the cleavage technique cannot be simply applied to isotropic materials, such as polymers in the glassy state, since the gradient of the maximum tensile stress in the vicinity of the crack tip is such that the crack tends to run out of its plane of propagation towards the edge of the specimen. In calculating the value of surface work, it cannot be assumed that the cantilever beams forming the specimen are built into the uncracked region with perfect rigidity so that the elastic strain energy is stored only in the cantilever beams whose lengths are that of the central crack. This is not satisfied because the uncracked region also is deformed and stores part of the elastic strain energy.

Berry modified the configuration of the cleavage specimens formerly used for single crystals with definite cleavage planes by machining fine slots along each face of the specimen, so that the thickness in the median plane is reduced and the crack is directed in the median plane (23). Broutman developed a similar specimen (Figure 20) and with it did extensive studies on the effect of temperature, of cross-linking, of pre-orientation, and of molecular weight and molecular weight distribution on the fracture surface work of various glassy amorphous polymers (6,9). Mostovoy, Crossley, and Ripling have developed another type of cleavage specimen which is a tapered double cantilever cleavage specimen (24). The purpose of this tapered cleavage specimen is to produce a linear compliance change with increasing crack length. This specimen has some advantages over other cleavage specimens: it eliminates the necessity of measuring crack length as a function of the applied load and deflection, and the crack can propagate with a constant velocity for a constant rate of separation of the specimen ends. For a uniform height double cantilever beam cleavage specimen (Figure 20) the crack propagation rate decreases as the crack is driven or as its length increases. Thus, the tapered cleavage specimen simplifies the calculations and the experiment but is more difficult to machine. The design of this specimen will be discussed in the next section.

In many of the studies of polymer fracture, basic theories are developed or applied assuming the polymers are ideal brittle materials and the fracture surface work is treated as an inherent material property. However, it should be recognized that the fracture surface work of polymeric materials is not an inherent material property, but is influenced by temperature and crack velocity (i.e., strain rate). In order to fully understand the fracture behavior of strain rate and temperature sensitive polymeric materials, it is necessary to characterize the fracture surface work in terms of crack velocity and temperature. For the purpose of characterizing the crack velocity effect on the fracture surface work, the conventional fracture specimens such as edge notched tensile specimens and 3 point notched bending specimens are not suitable since for these specimens it is not possible to easily control the crack propagation rate. The double cantilever beam cleavage specimens, on the contrary, are stable against fracture propagation because the crack extension force, G, decreases with increasing crack length for fixed displacement. Thus, the

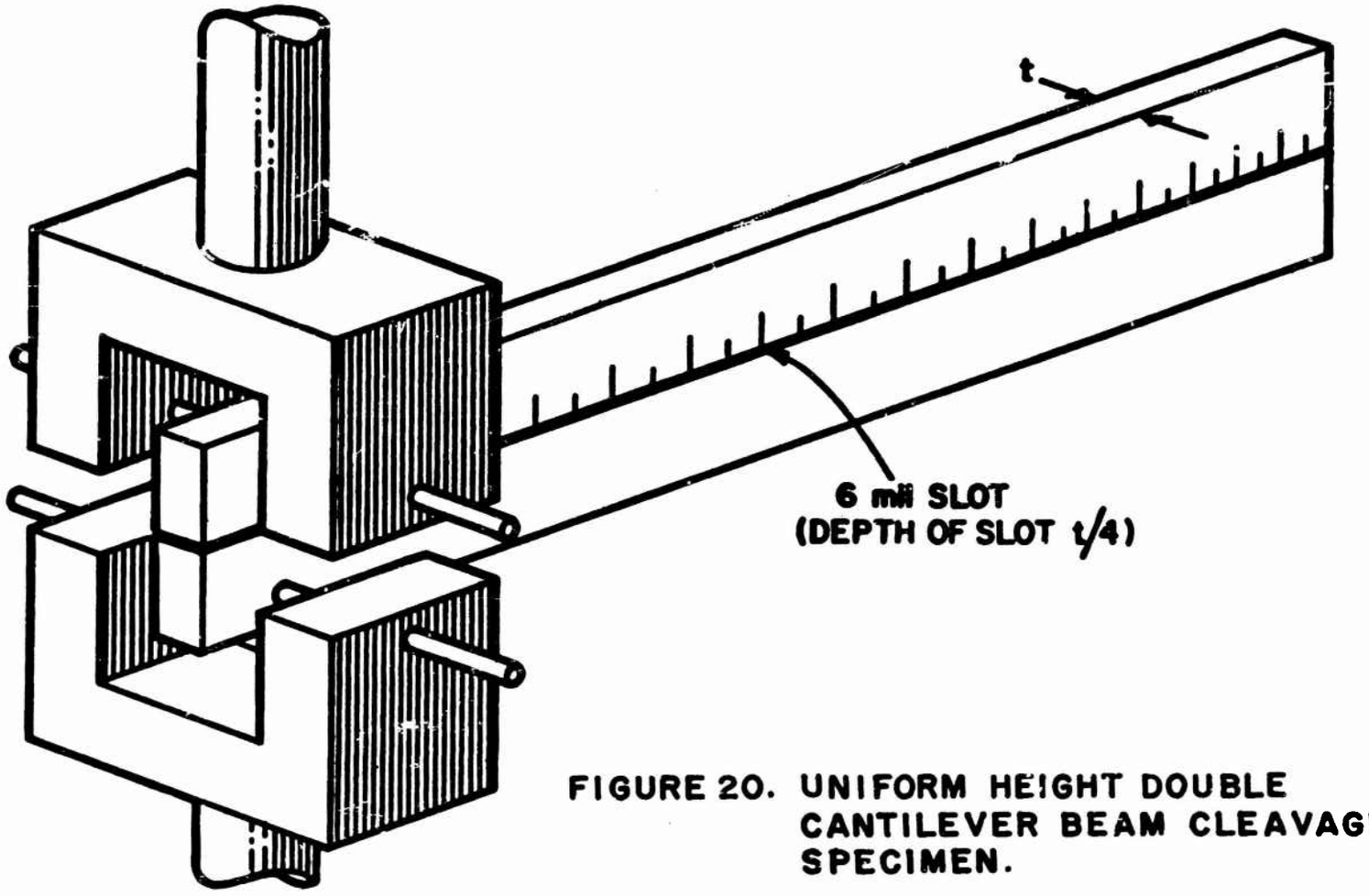

FIGURE 20. UNIFORM HEIGHT DOUBLE CANTILEVER BEAM CLEAVAGE SPECIMEN.

double cantilever beam cleavage specimens (especially tapered double cantilever beam cleavage specimens) are the most suitable type of specimens for studying the crack velocity effect on fracture surface work. In the next sections, the design of a tapered cleavage specimen and a sandwich tapered cleavage specimen for studying tough and ductile polymeric materials is discussed.

B. Specimen Design

(1) Tapered Double Cantilever Beam Cleavage Specimen

In order to investigate the effect of crack velocity on fracture toughness, it is necessary to have a specimen which, due to its geometry, produces stable crack propagation and also makes data analysis simple. D. P. Clausing studied crack stability problems assuming linear elastic fracture mechanics for different specimen configurations (42). His results indicate that double cantilever beam cleavage specimens are quite stable and are therefore suitable for the investigation of crack velocity effects on fracture surface work. In determination of fracture surface work from a uniform height double cantilever beam cleavage specimen, one has to measure force, deflection, and crack width at each crack length since the specimen compliance changes non-linearly with respect to crack length. By designing a proper contour for a tapered double cantilever beam cleavage specimen, one can obtain a constant compliance change with respect to crack length.

The use of this type of specimen has been reported by Mostovoy, Crossley, and Ripling (24), and stress intensity factors have been calculated by Shrawley and Gross (43). The authors of the present report also used this type of specimen in a previous study (5). The crack extension force or critical strain energy release rate, G_c, which is twice the value of fracture surface work and is frequently referred to in fracture toughness investigations, is defined as

$$G_c = 2\gamma = \frac{f_c^2}{2w} \frac{\partial C}{\partial \ell} \qquad (7)$$

where γ = fracture surface work

f_c = applied load at fracture

w = crack width

ℓ = crack length

C = total specimen compliance at crack length ℓ.

The derivation of this equation can be found elsewhere (21).

If the specimen is designed so that the compliance changes linearly with crack length, i.e., $\partial C/\partial \ell$ = constant, then G_c or γ depends only upon the failure load (f_c), providing that the crack width remains constant.

Since the cleavage specimen is treated as a pair of identical cantilver beams, design of a tapered cleavage specimen is determined through the terms representing

bending, sheor, and end rotation deflections. The compliance of the specimen, C, con be expressed os $C = 2\delta/f$; where 2δ = total separation of cantilever beoms ot the point of loading ond f = force opplied to the specimen ends. Therefore

$$C = \frac{24}{Eb} \int_o^{\ell} \frac{X^2}{h^3} \, dX + \frac{6(1+\nu)}{Eb} \int_o^{\ell} \frac{1}{h} \, dX \tag{8}$$

where E = Young's modulus

ν = Poisson's ratio

b = specimen width

X = distance along the crack plane measured from the looding point

h = beom height ot the distonce X.

The first term on the right hond side of the equotion represents the bending components while the second term is the shear component.

By differentioting Eq. (8) in terms of ℓ, one has

$$\frac{dC}{d\ell} = \frac{6}{Eb} \left[\frac{4\ell^2}{h^3} + \frac{1+\nu}{h} \right] \tag{9}$$

and setting $\frac{dC}{d\ell}$ = constont, K, one obtoins

$$\frac{6}{Eb} \left[\frac{4\ell^2}{h^3} + \frac{1+\nu}{h} \right] = K \tag{10}$$

$$\therefore \frac{4\ell}{h^3} + \frac{1+\nu}{h} = K \frac{Eb}{6} = M \tag{11}$$

Therefore

$$Mh^3 - (1+\nu)h^2 - 4\ell^2 = 0 \tag{12}$$

The specimen used by Mostovoy et ol. was designed using Eq. (9) by selecting o volue of M ond then determining h os o function of beam length ℓ. Therefore

$$G_c = 2\gamma = \frac{f_c^2}{2w} K = \frac{f_c^2}{2w} \frac{6}{Eb} M \tag{13}$$

The specimen designed by the authors not only included the compliance components of bending and shear but also the end rotation effect. The end rotation results from elastic distortions in the support, allowing the cantilever to rotate at the assumed built-in end of the beams. Mostovoy et al. have shown empirically that the end rotation effects can be included in the compliance equation by using an effective crack length $\ell + \ell o$ where $\ell o = 0.6h$ in the bending term of compliance. The factor 0.6 was determined experimentally by use of calibration bars. The compliance is therefore modified so that

$$C = \frac{6}{Eb}\left[\frac{4(\ell + \ell o)^3}{3h^3} + \frac{(1+\nu)}{h}\ell\right] \tag{14}$$

Eq. (14) can then be modified so that

$$Mh^3 - (1+\nu)h^2 - 4(\ell + 0.6h)^2 = 0 \tag{15}$$

or

$$\ell = \left[\sqrt{Mh - (1+\nu)} - 1.2\right]\frac{h}{2} \tag{16}$$

From Eq. (16), for any given value of the constant M a relation between h and ℓ can be established. The specimens used in this study have been designed for an M of 400/3 ond 40/3 assuming $\nu = 0.35$. Figure 21 shows the plots of Eq. (16), that is, one half of the symmetric specimens for M equal 400/3 and 40/3. In order to estimate the relation between crack velocity and crosshead rate the following calculation is carried out (16).

Compliance is given by

$$C = \frac{\delta}{f} = K\ell + a \tag{17}$$

where $K = \frac{\partial C}{\partial \ell} = \frac{6M}{Eb}$ = constant and a = constant.

By differentiating Eq. (17) with respect to time one has

$$\frac{1}{f}\frac{d\delta}{dt} - \frac{\delta}{f^2}\frac{df}{dt} = K\frac{d\ell}{dt} \tag{18}$$

where $\frac{d\delta}{dt}$ is the crosshead rate

$\frac{df}{dt}$ is the load variation in time

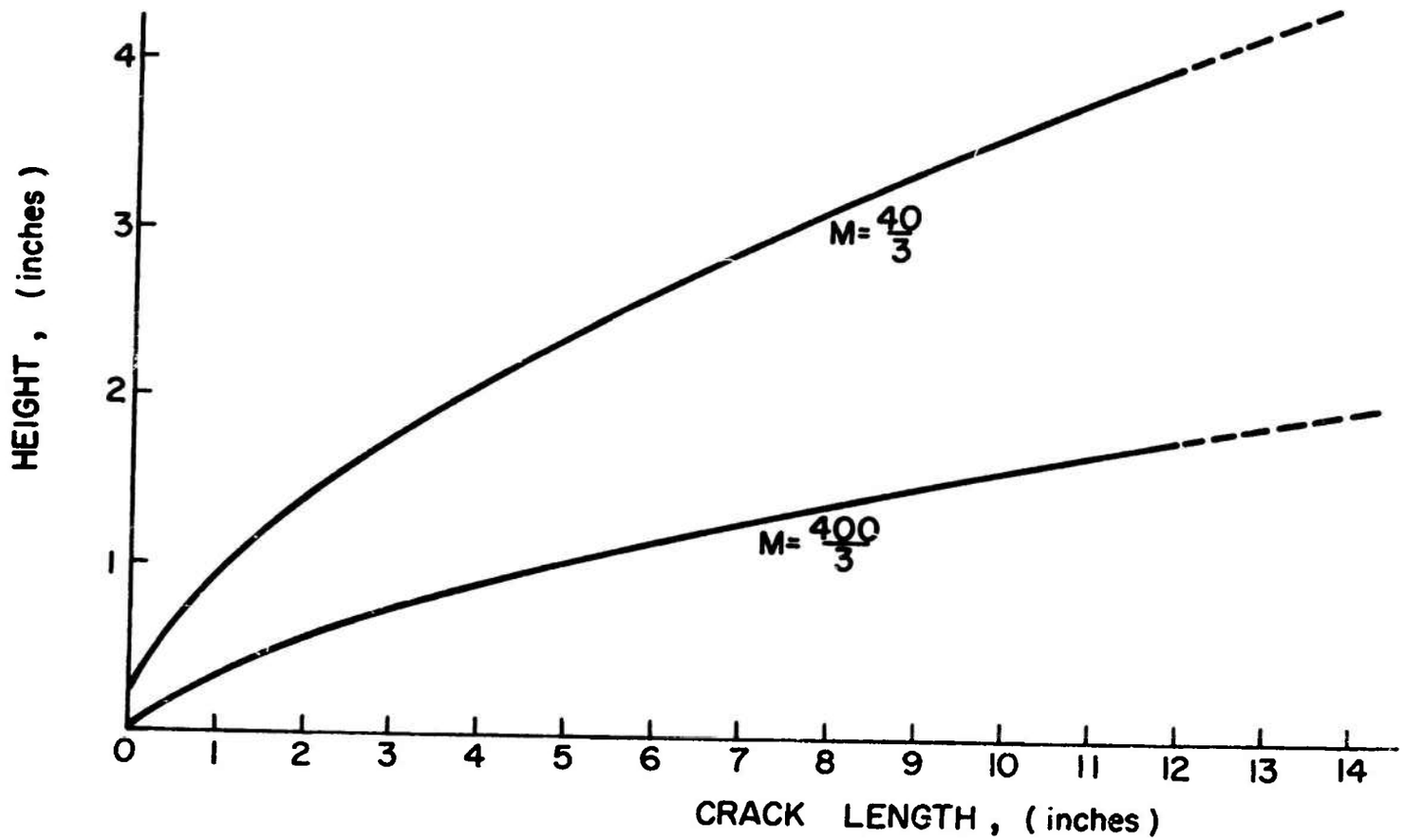

FIGURE 21. CALCULATED TAPERED SPECIMEN CONTOURS FOR CONSTANTS OF M=400/3 AND 40/3.

and $\frac{d\ell}{dt}$ is the crack velocity.

For a tapered specimen $\frac{df}{dt} = 0$; therefore

$$\frac{d\ell}{dt} = \frac{1}{Kf} \frac{d\delta}{dt} = \frac{1}{f\frac{dC}{d\ell}} \frac{d\delta}{dt} = \frac{1}{\frac{6Mf}{Eb}} \frac{d\delta}{dt} = \left(\frac{b}{6M}\right)\left(\frac{E}{f}\right)\frac{d\delta}{dt} \qquad (19)$$

Eq. (19) shows the relation between the crack velocity and the crosshead rate (specimen end separation rate). In this equation the factor $f\ \partial C/\partial \ell$ shows a moderate increase as the crosshead rate increases. However, as shown in Figure 22 a linear relationship exists between displacement rate and crack velocity.

(2) Design of a Sandwich Tapered Double Cantilever Beam Cleavage Specimen

A tapered cleavage cantilever specimen is very useful for isotropic homogeneous brittle and semi-brittle materials, but until this time it has not been usable with ductile, tough and/or anisotropic materials because of excessive bending or breakage of the specimen arms. In order to make it possible to measure the fracture surface work of these materials a new modified sandwich tapered double cantilever beam cleavage specimen was developed. Construction of this specimen is as follows:

(1) Rigid reinforcement plates are bonded to both sides of the specimen sheet by proper adhesives.

(2) After curing these adhesives the side grooves and initial crack are machined through the reinforcement plates into the test specimen by a specially designed side-groove cutting machine.

(3) Then the specimen is affixed to the template with double coated tape, and the countour of the tapered cleavage specimen is machined by router.

These steps are shown in Figure 23.

The advantages of this specimen construction are revealed by the following calculation.

The compliance, C_i, of the test material made up in the form of a double cantilever beam specimen with crack length ℓ, specimen thickness b_i, and Young's modulus E_i, is given by

$$C_i = \frac{\delta_i}{f_i} = \frac{6}{E_i b_i}\left[\frac{4(\ell + \ell_o)^3}{3h^3} + \frac{(1+\nu_i)}{h}\ell\right] \qquad (20)$$

where δ_i is the total deflection of the specimen end under the load f_i

ν_i is Poisson's ratio of test material

h is the height of the specimen at crack length ℓ.

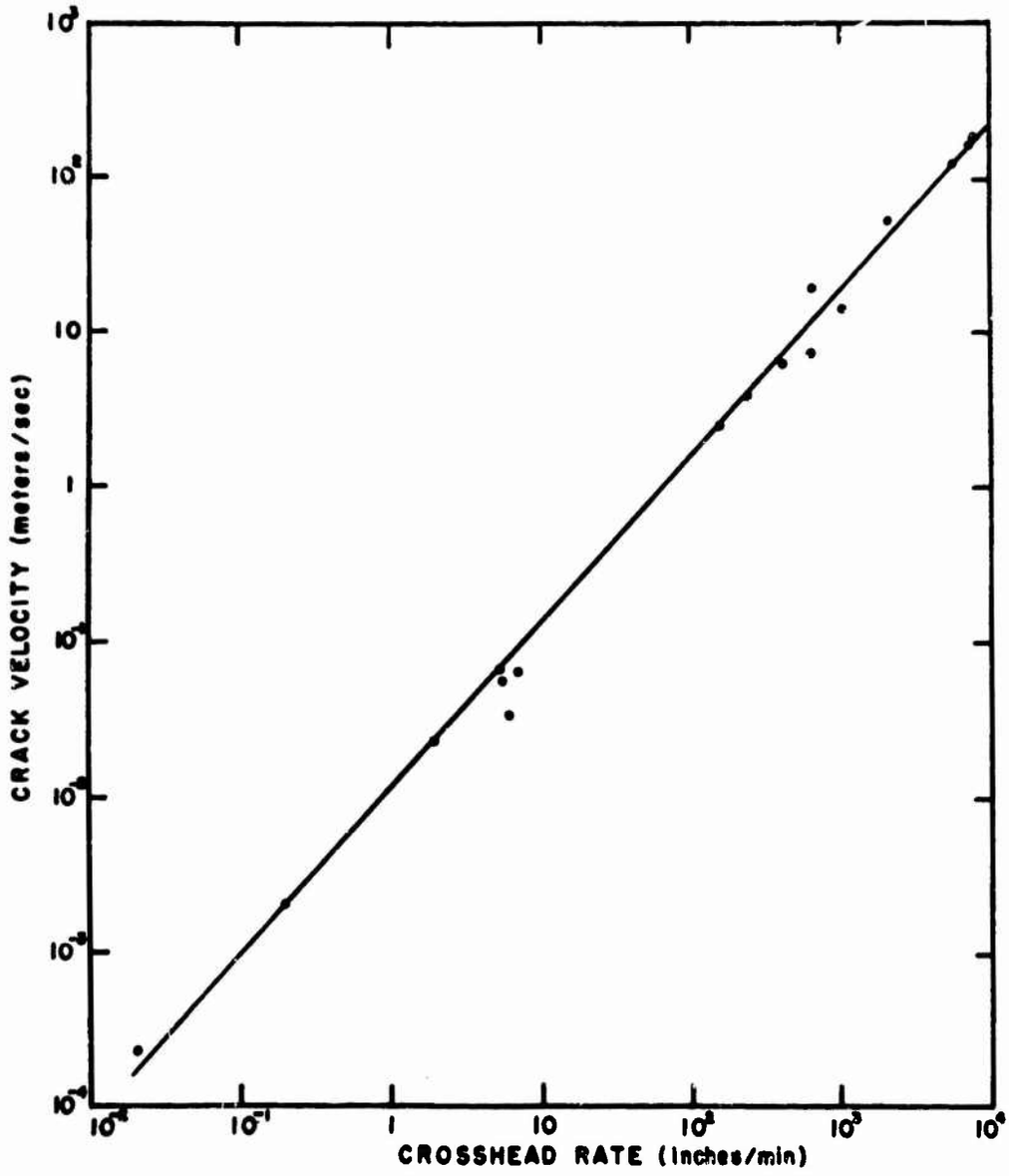

FIGURE 22. EXPERIMENTAL RELATION BETWEEN CRACK VELOCITY AND CROSSHEAD RATE.

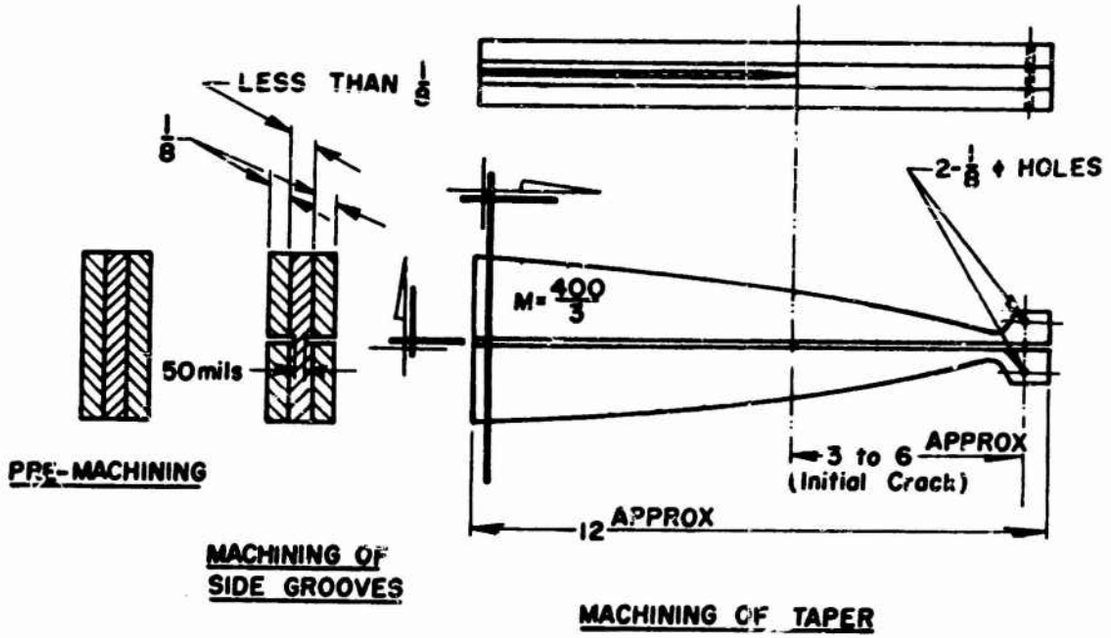

FIGURE 23. SANDWICH TAPERED CLEAVAGE SPECIMEN CONSTRUCTION STEPS.

The compliance, C_o, of the reinforcement material made up in the form of a double cantilever beam specimen with crack length ℓ, specimen thickness b_o, and Young's modulus E_o is given by

$$C_o = \frac{\delta_o}{f_o} = \frac{6}{E_o b_o} \left[\frac{4(\ell + \ell_o)^3}{3h^3} + \frac{(1 + \nu_o)}{h} \ell \right] \tag{21}$$

where δ_o is the total deflection of the specimen end under the load f_o

ν_o is the Poisson's ratio of reinforcement material.

If the reinforcement plates in the shape of a double cantilever beam specimen are bonded to both sides of a test material plate of the same shape, then the deflection of the three plates becomes the same. That is,

$$\delta_i = \delta_o = \delta \tag{22}$$

The total load f applied on the sandwich specimen end to produce deflection δ is

$$f = f_i + 2f_o \tag{23}$$

Therefore the compliance of the sandwich specimen is

$$C = \frac{\delta}{f} = \frac{\delta}{f_i + 2f_o} = \frac{1}{\frac{1}{C_i} + \frac{2}{C_o}} \tag{24}$$

From Eq. (20) and (21) we have

$$\frac{1}{C_i} + \frac{2}{C_o} = \frac{E_i b_i}{6} \left[\frac{1}{\frac{4(\ell + \ell_o)^3}{3h^3} + \frac{(1 + \nu_i)}{h} \ell} \right] + \frac{2E_o b_o}{6} \left[\frac{1}{\frac{4(\ell + \ell_o)^3}{3h^3} + \frac{(1 + \nu_o)}{h} \ell} \right] \tag{25}$$

If one neglects the difference between the Poisson's ratios of the test material and the reinforcement material, the following can be obtained:

$$\frac{1}{C_i} + \frac{2}{C_o} = \frac{E_i b_i + 2E_o b_o}{6} \left[\frac{1}{\frac{4(\ell + \ell_o)^3}{3h^3} + \frac{(1 + \nu)}{h} \ell} \right] \tag{26}$$

Substituting Eq. (26) into Eq. (24), one obtains

$$C = \frac{\delta}{f} = \frac{6}{E_i b_i + 2E_o b_o} \left[\frac{4(\ell + \ell_o)^3}{3h^3} + \frac{(1+\nu)\,\ell}{h} \right]$$

$$= \frac{6N}{E_i b_i + 2E_o b_o} \text{ where } N = \left[\frac{4(\ell + \ell_o)^3}{3h^3} + \frac{(1+\nu)\ell}{h} \right] \qquad (27)$$

By differentiating Eq. (27) with respect to ℓ, the compliance change of the sandwich specimen, $\partial C/\partial \ell$, is obtained in the following form:

$$\frac{\partial C}{\partial \ell} = \frac{6}{E_i b_i + 2E_o b_o} \left[\frac{4(\ell + \ell_o)^2}{h^3} + \frac{(1+\nu)}{h} \right] = \frac{6M}{E_i b_i + 2E_o b_o} \qquad (28)$$

where $M = \dfrac{4(\ell + \ell_o)^2}{h^3} + \dfrac{(1+\nu)}{h}$ = constant by design.

Eq. (28) indicates that the compliance is independent of crack length. The crack extension force, G, is given by the same equation as Eq. (7).

$$G = \frac{f^2}{2w} \frac{\partial C}{\partial \ell} \qquad (29)$$

From Eqs. (27), (28) and (29) one now can calculate the crack extension force G for the case of the sandwich specimen with crack length ℓ and given deflection δ_g: The resulting load f is

$$f = \frac{\delta_g (E_i b_i + 2E_o b_o)}{6N} \quad \text{from Eq. (27)}$$

where N = a function of crack length and Poisson's ratio by design.

The compliance change in terms of a crack length is

$$\frac{\partial C}{\partial \ell} = \frac{6M}{E_i b_i + 2E_o b_o} \quad \text{from Eq. (28)}$$

where M = constant by design.

Therefore $$G = \frac{1}{2w} \left[\frac{\delta_g (E_i b_i + 2E_o b_o)}{6N} \right]^2 \frac{6M}{E_i b_i + 2E_o b_o}$$

Thus

$$G = \frac{M(\delta_g)^2 (E_i b_i + 2E_o b_o)}{12N^2 w} \qquad (30)$$

From Eq. (30) one can see that for the given deflection δ_g the crack extension force can be increased extensively by bonding rigid reinforcement side plates to the test material, that is, by adding a large value of $2E_o b_o$ to $E_i b_i$. If the crack extension force is increased by the sandwiching, then the deflection required to reach the critical extension force ($G_c = 2\gamma$) is decreased. The same effect can be achieved by increasing the groove depth or increasing the specimen thickness for the cleavage specimen but the change is not as great. We can thereby create conditions under which controlled crack propagation through tough ductile materials and measurement of the fracture surface work - two previously unobtainable factors - are readily obtainable. Other advantages of this sandwich tapered cleavage specimen include:

(1) It is particularly suitable for long term environmental fracture tests because errors due to creep or stress relaxation of the cantilever beams are minimized by selecting metal reinforcement side plates.

(2) In determining the crack velocity effect on the fracture surface work this specimen is useful since, by changing the side reinforcement material, one can obtain a wide range of compliance changes and crack velocities.

C. Test Procedure

After machining, specimens are carefully annealed in an oven to eliminate the residual stress induced by machining. In order to examine the side groove depth effect and the seriousness of the residual stress effect on the fracture surface work, two sets of Plexiglas specimens were prepared. One set consisted of several specimens of different side groove depths and was carefully annealed in an oven at about 100°C temperature for about 10 hours, then slowly cooled to room temperature at a cooling rate of 0.6°C per minute. The other set also consisted of several specimens of different side groove depths but was not annealed. The measured results of fracture surface work are shown in Figure 24 as a function of the ratio between crack width and plate thickness. Crack velocities are also recorded and shown in the figure to compare data of annealed and unannealed specimens under similar conditions. The results show that the annealed specimens produce consistent fracture surface work values over a wide range of ratios between crack width and plate thickness, while the fracture surface work from the unannealed specimens increases rapidly as the ratio between crack width and plate thickness decreases. This increase is considered to be the effect of residual stress since the increased depth of the side grooves means increased work at the cutting edge, thus resulting in increased heat generation at the cutting edge. A slight increase in the fracture surface work of annealed specimens at a low ratio between crack width and plate width is considered to be a velocity effect which will be discussed in detail in Chapters IV and VI.

After annealing, thin lines of conductive paint are drawn across the grooved crack path in order to determine the crack tip position and to calculate the average

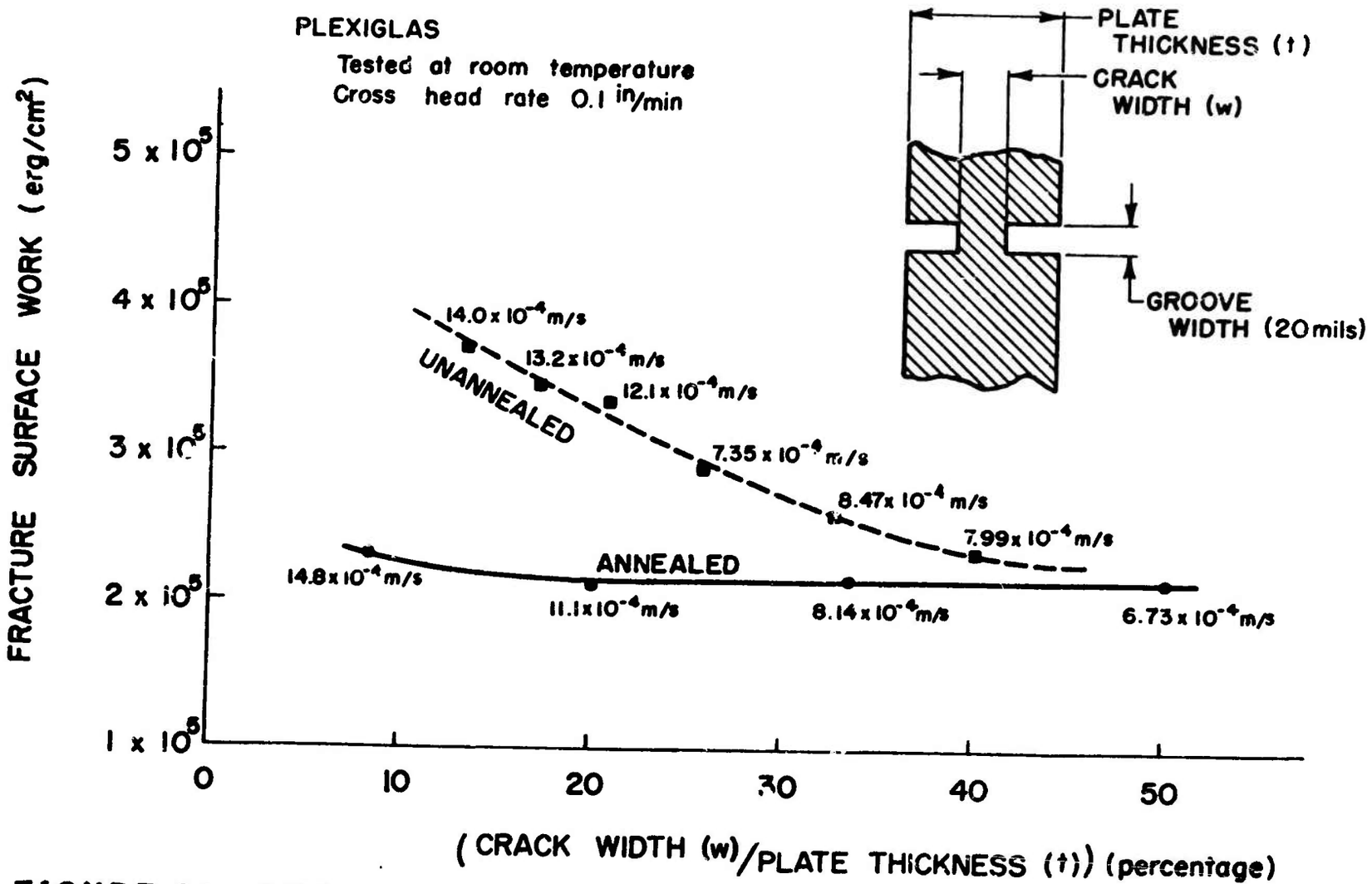

FIGURE 24. RESIDUAL STRESS EFFECTS ON FRACTURE SURFACE WORK OF PLEXIGLAS.

crack velocity as shown in Figure 25. Terminals of these conductive paint lines are then connected to an electrical circuit which produces a 20 mV voltage drop as each line is broken by the advancing crack (Figure 26).

Testing of specimens was carried out in a servo-controlled electro-hydraulically actuated high-speed testing machine and in an Instron testing machine. In the high-speed testing machine the specimen is held in grips with two pins as shown in Figure 14. A constant crosshead rate in the range of 2 to 18,000 in/min is used to cleave the specimen. Recording of load, displacement, and crack tip position signals is done by two oscilloscopes (Tektronix R564B with a Type 3A72 Dual-Trace Differential Amplifier plug-in unit and a Type 2B67 Time Base plug-in unit, and Tektronix Type 556 Dual Beam Oscilloscope) and oscilloscope trace images are photographed with oscilloscope cameras and Polaroid film. In the Instron testing machine the specimen is held in grips with two pins at the head and at the other end one pin which is attached to a pulley mechanism in order to allow the specimen center line to shift in the direction of crosshead movement at half of the crosshead rate (Figure 27).

D. Data Analysis

The calculation of G_c or γ is accomplished by using the equation given in a previous section

$$G_c = 2\gamma = \frac{f_c^2}{2w} \frac{dC}{d\ell} = \frac{f_c^2}{2w} \frac{6M}{Eb} \qquad (13)$$

In this study the experimental value of $dC/d\ell$ is used to calculate G_c or γ since by doing so one automatically accounts for the influence of variation in the rate-sensitive Young's modulus. In order to demonstrate the method of calculation of fracture surface work, the data for an acrylic multipolymer (AMP16) will be reviewed here.

A sandwich double cantilever beam cleavage specimen technique is used. The load versus deflection curve for the specimen is shown in Figure 28. The measurement was made on an Instron testing machine using a separation rate of 0.05 inches per minute. Since the crack propagates in a continuous fashion, a continuous crack growth results with a nearly constant crack propagation load of 34 pounds. Any local variations of load are due to changes in crack width or area. Points are also shown on this graph representing various crack lengths determined visually from calibration lines on the sample. It can be observed that the crack propagated at nearly constant velocity. In order to determine the experimental value of $\partial C/\partial \ell$, the compliance $C = \delta/f$ is calculated at marked crack lengths in Figure 28 and the results are plotted in Figure 29. Figure 29 indicates that the compliance of this sandwich specimen is a linear function of crack length. The slope of the line in Figure 29 is the experimental value of $dC/d\ell = 5.14 \times 10^{-3}$. The measured crack width was an average of 0.0524 inches. By substituting these values in Eq. (7), one can obtain the value of fracture surface work $\gamma = 28.4$ lb/in $= 49.6 \times 10^5$ erg/cm^2.

The crack velocity is obtained by calculating the time between the marked points on the load-deflection curve indicating crack length and then dividing the

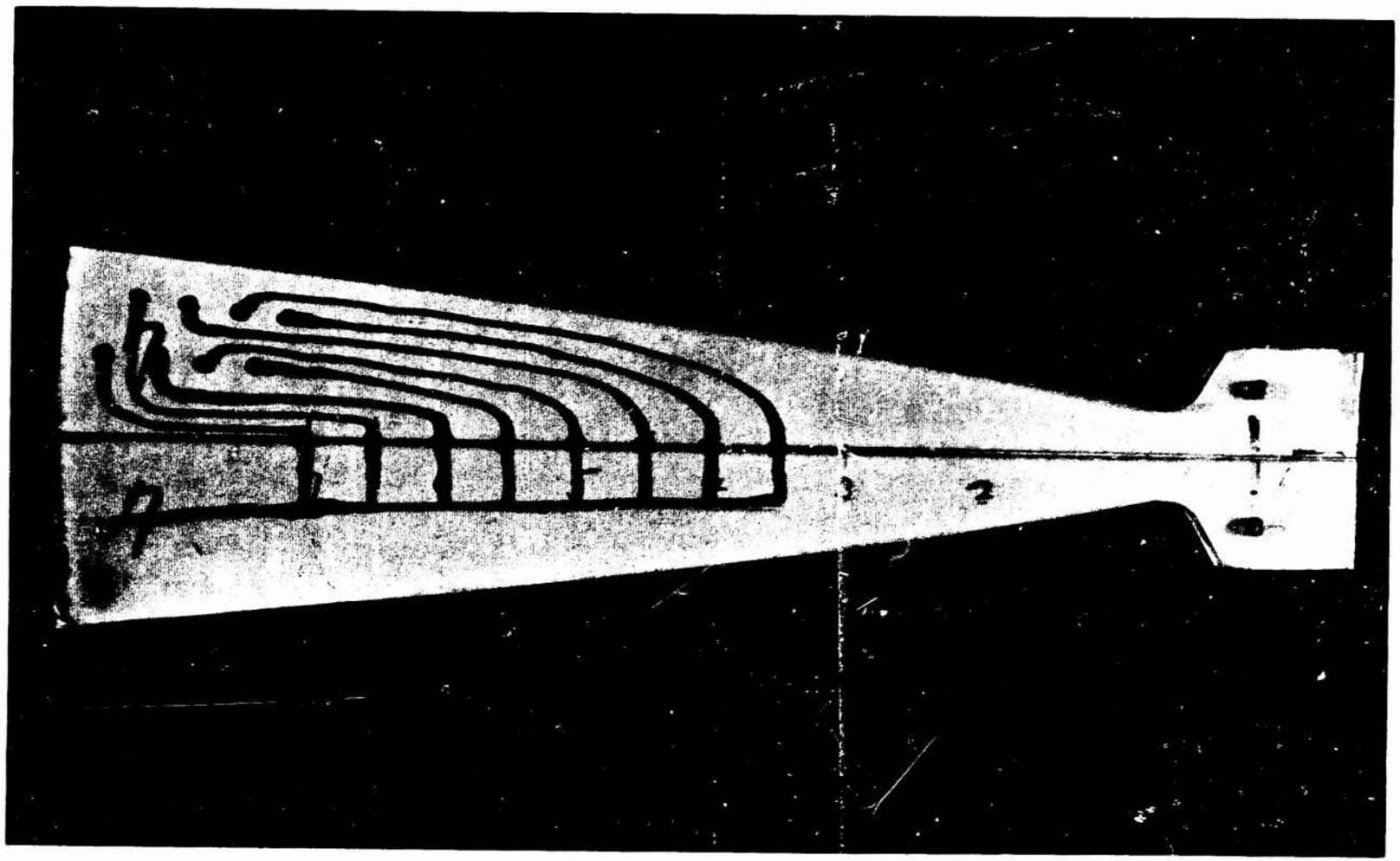

FIGURE 25. SPECIMEN WITH CONDUCTIVE PAINT LINES.

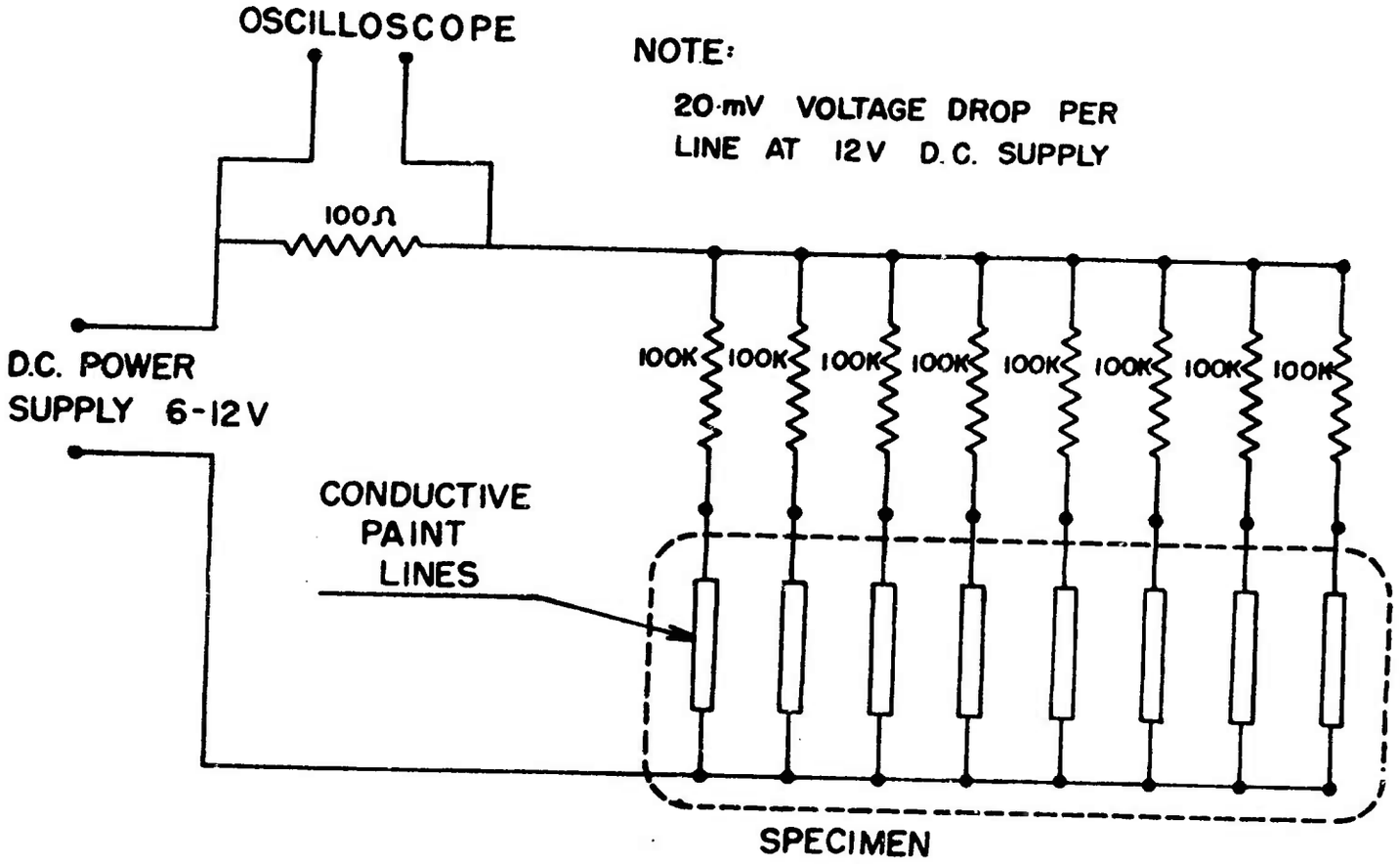

FIGURE 26. VELOCITY GAGE ELECTRICAL CIRCUIT.

FIGURE 27. PULLEY SYSTEM AND INSTRON TESTING MACHINE.
A: PULLEY SYSTEM B: SPECIMEN C: CLEVIS GRIPS

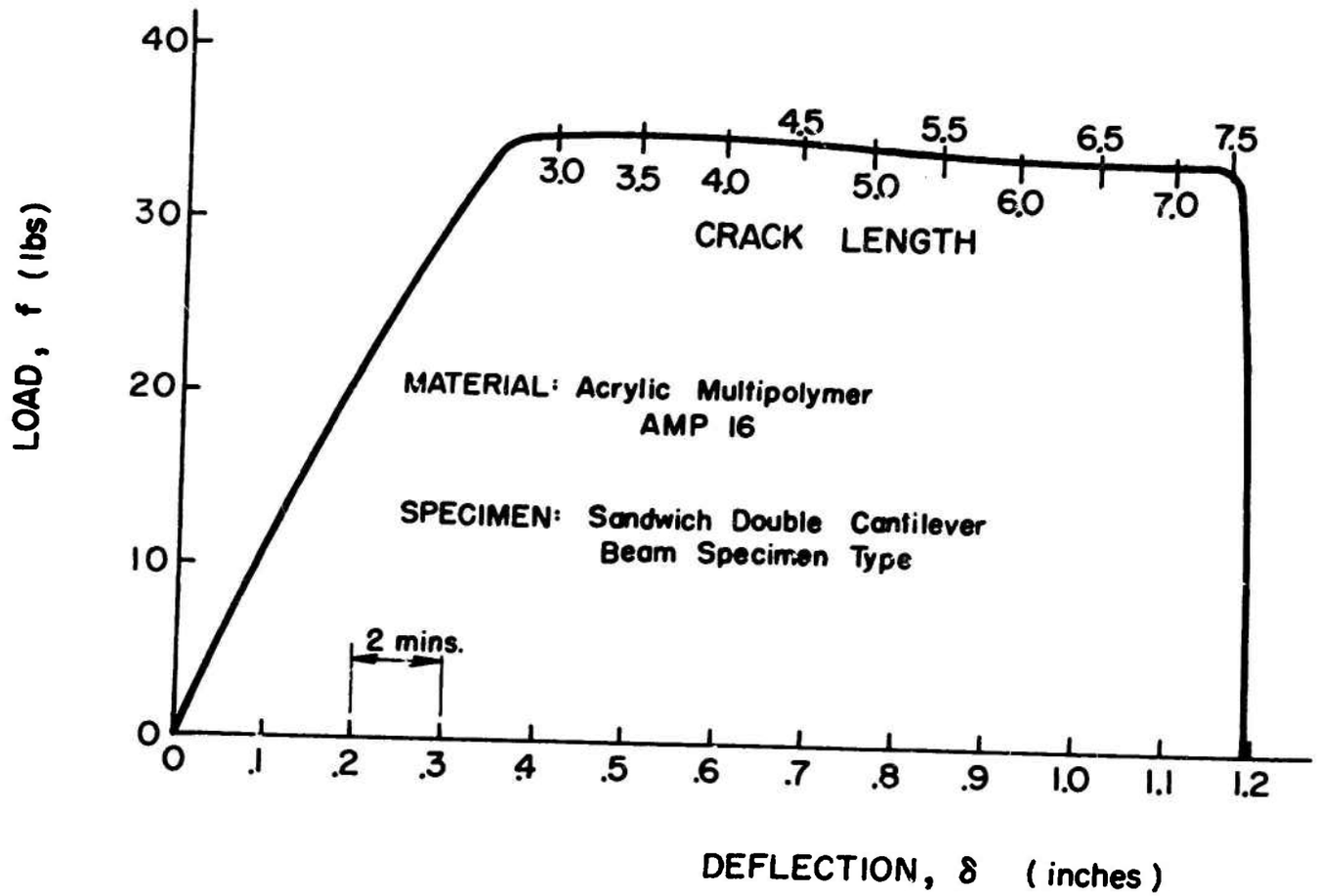

FIGURE 28. LOAD-DEFLECTION CURVE FROM A SANDWICH DOUBLE CANTILEVER BEAM CLEAVAGE SPECIMEN.

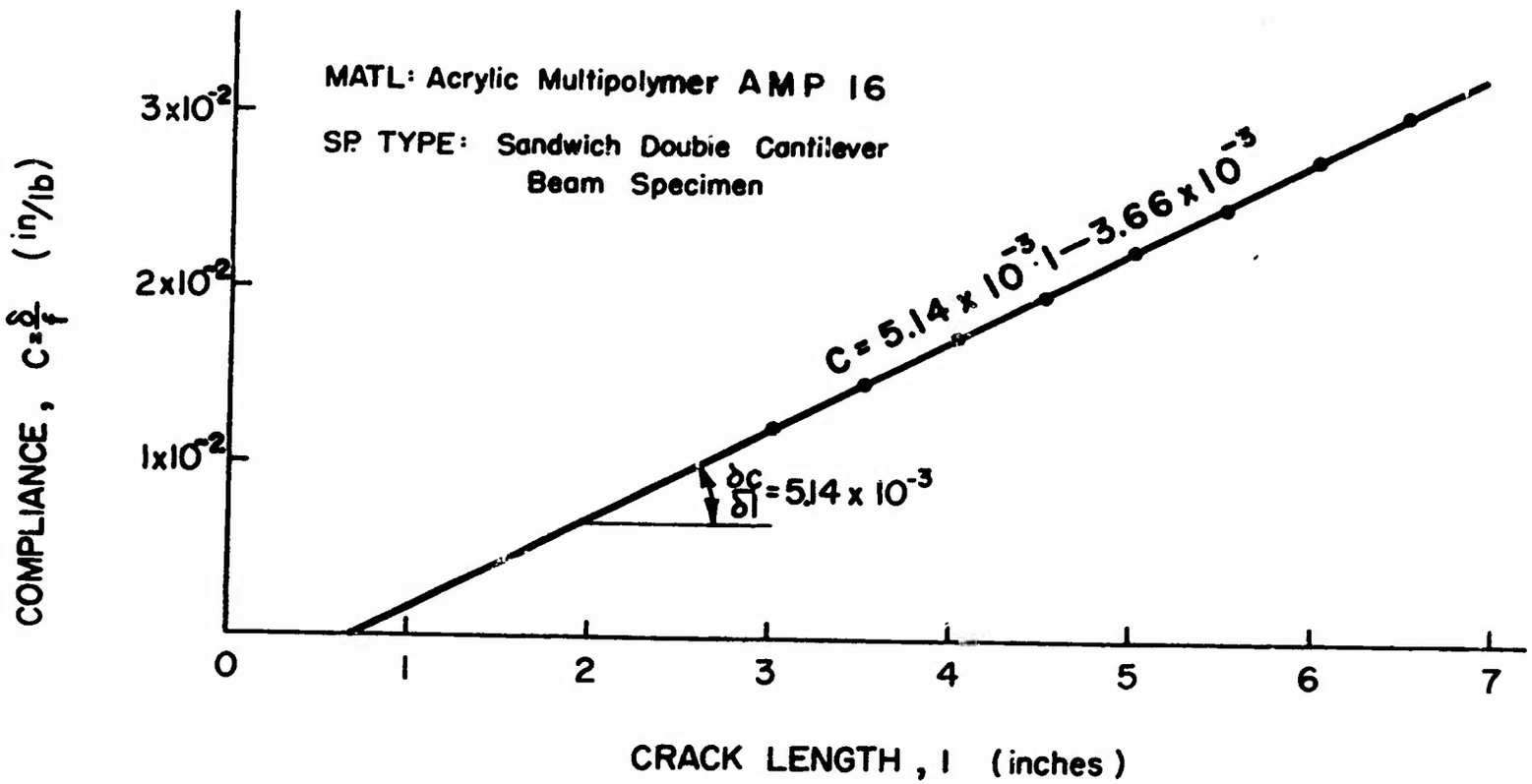

FIGURE 29. COMPLIANCE VERSUS CRACK LENGTH PLOT FOR DETERMINATION OF EXPERIMENTAL COMPLIANCE CHANGE IN TERMS OF CRACK LENGTH.

crack length difference between the points by the calculated time. For example, a crack propagated between $\ell = 6$ in. and $\ell = 7$ in. in 3.50 minutes; therefore, the crack velocity is 1.0 inches/3.50 minutes = 0.286 in/min.

The critical strain energy release rate (G_c) or fracture surface work (γ) can be calculated directly from the force-deflection curve of Figure 28. This is accomplished by measuring the energy released as the crack changes length or

$$U = \frac{f(\delta_2 - \delta_1)}{2} \tag{31}$$

and equating this to the work done

$$W = 2(\ell_2 - \ell_1) w\gamma \tag{32}$$

as the crack increases in length ℓ_1 to ℓ_2.

Thus

$$\gamma = \frac{f(\delta_2 - \delta_1)}{4w(\delta_2 - \delta_1)} \tag{33}$$

and choosing a crack length increase from 6.0 inches to 7.0 inches the energy release is

$$U = \frac{34}{2}(1.100 - 0.925)$$

The work done is

$$W = 2x(7.0 - 6.0) \times 0.0524 \times \gamma$$

so that

$$\gamma = \frac{34}{4 \times 0.0524} \quad \frac{(1.100 - 0.925)}{(7.0 - 6.0)} = 28.4 \text{ lb/in}$$

$$= 49.6 \times 10^5 \text{ erg/in}^2$$

This value agrees well with the one obtained by using Eq. (13).

CHAPTER IV

CRACK PROPAGATION IN AMORPHOUS HOMOPOLYMERS: POLY(METHYL METHACRYLATE) AND POLYSTYRENE

A. Review of Properties of Poly(methyl methacrylate) and Polystyrene

Poly(methyl methacrylate) and polystyrene have great commercial importance and have therefore been extensively studied. However, the understanding of the fracture process for these materials has not yet been fully developed. In reviewing fracture studies of viscoelastic polymers, particularly in the energy approach to the fracture problem, one realizes that the fracture surface work is treated as an inherent property of the material, but as data increases concerning the fracture surface work, it becomes clear that we are not dealing with an inherent property of the material. The fracture surface work like other viscoelastic parameters is greatly influenced by temperature and strain rate (i.e., crack velocity). Considering the applications of these materials, although the fracture surface work is not an inherent property, it is a very important quantity in evaluating the material performance against fracture.

In this section existing data which characterize mechanical behavior of these two materials are reveiwed with special reference to fracture behavior. In the following section of this chapter the crack propagation problem in poly(methyl methacrylate) and polystyrene will be discussed in terms of the fracture surface work and crack velocity. Furthermore, the relationships between the fracture surface work and viscoelastic parameters will also be considered.

Turley and Keskkula (44) measured the mechcnical damping behavior of poly-(methyl methacrylate) and polystyrene utilizing a torsion pendulum which cycled at about 1 cycle per second in the temperature range between -150°C and 150°C. Their results are shown in Figure 30. Poly(methyl methacrylate) exhibits glass transition at about 99°C and the secondary transition at about 20°C for a frequency range of about 1 cycle per second. They also reported that the secondary transition had been associated with motion of the carbomethoxy side chains through the work of Deutsch, Hoff, and Reddish, which was confirmed in experiments performed by Heijboer using a copolymerization approach and a study of molecular models. They further reported that Sinnott suggested and confirmed the occurrence of a third transition in the vicinity of -269°C due to the relaxation of the ester methyl group.

The mechanical damping curve for polystyrene (Figure 30) indicates that at about 0°C there is an indication of a secondary transition in addition to the glass transition in the vicinity of 100°C. Turley and Keskkula (44) reported that Illers and Jenckel suggested that the motion of some phenyl groups which possess less steric hindrance causes this secondary transition. Concerning the third peak appearing at -110°C, they reported that Illers and Jenckel had attributed this peak to torsional motions of a number of $-CH_2 - CH_2 -$ units in the main chain formed by head-to-head coupling. Turley and Keskkula further reported that Sinnot observed still another transition at about -255°C at a frequency of 5.6 cycles per second. For the mechanical damping curves of poly(methyl methacrylate) and polystyrene shown in Figure 30, one can see a marked difference in the damping magnitude of the two materials

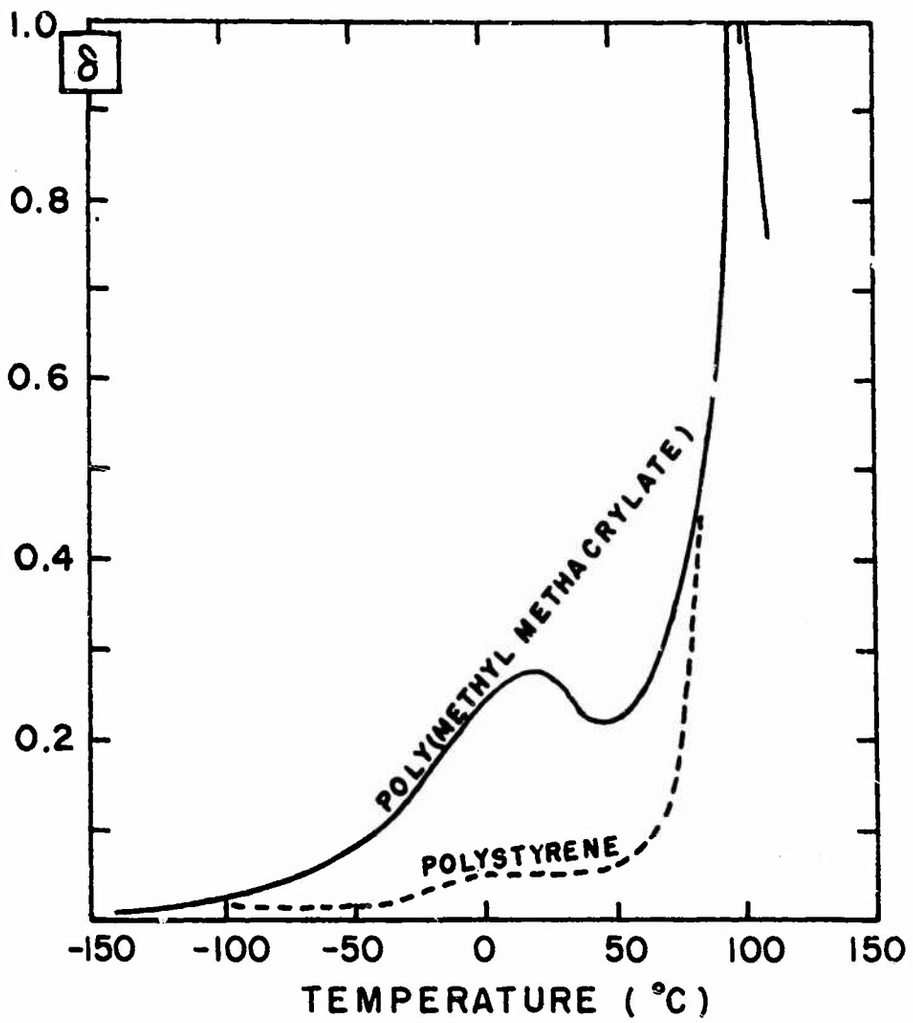

FIGURE 30. MECHANICAL DAMPING OF POLY(METHYL METHACRYLATE) AND POLYSTYRENE VERSUS TEMPERATURE.

in the temperature range betwee.. the glass transition temperature and -100°C. The strength of the β peak in the mechanical damping curve of polystyrene is very small compared with that of poly(methyl methacrylate). These transition temperatures are generally influenced by a measuring frequency. In Ref. 44 Turley and Keskkula state that the general rule of thumb is that a decade increase in frequency will displace the transition region about 7°C.

Boyer surveyed some of the progress made in the area of relating mechanical properties to molecular structure in the past 10 years in his paper titled, "Dependence of Mechanical Properties on Molecular Motion in Polymers" (45). He reported that Roetling observed the yield stress behavior of poly(methyl methacrylate) for 30°C to 90°C over six decades of rate and in analyzing the yield stress behavior he had to use a Ree-Eyring equation with two activation energies, 24 and 81 kcal/mol. The value of 24 kcal/mol is the apparent activation energy associated with the β peak as obtained from dynamic data and the higher value of 81 kcal/mol is the apparent activation energy associated with the glass transition temperature. Roetling's results are shown in Figure 31 (46). The equation used by Roetling is given by

$$\left(\frac{\sigma}{T}\right) = \sum_i \left(\frac{1}{A_i}\right) \sinh^{-1} \left[\left(\frac{C_i \dot{\epsilon}}{T}\right) \exp\left\{\frac{\Delta H_i}{RT}\right\}\right] \tag{34}$$

where the constants used by Roetling are

Process	$\Delta H_i \times 10^{-3}$	$A_i \times 10^{6}$	$\ell n\ C_i$
β	24.0	7.2	-25.0
α	81.0	15.0	-90.0

Zitek and Zelinger (47) simplified the Eyring equation and obtained the following form:

$$\sigma_Y = A - BT + CT \log \dot{\epsilon} \tag{35}$$

where σ_Y = yield stress

T = absolute temperature

$\dot{\epsilon}$ = deformation rate

and A, B, C = equation parameters.

They applied this equation to the experimental data on poly(methyl methacrylate) and obtained the results shown in Figure 32. On the curve for higher deformation speed in Figure 32, Zitek and Zelinger noted that the disappearing of the β-process of poly(methyl methacrylate) due to its lower activation energy could be seen, as is well known from dynamic measurements. Concerning each process, they formulated the following conclusions:

(1) The α-process first appears at approximately glass transition temperature. Kinetic unit, however, does not change during transition from β- to the α- process,

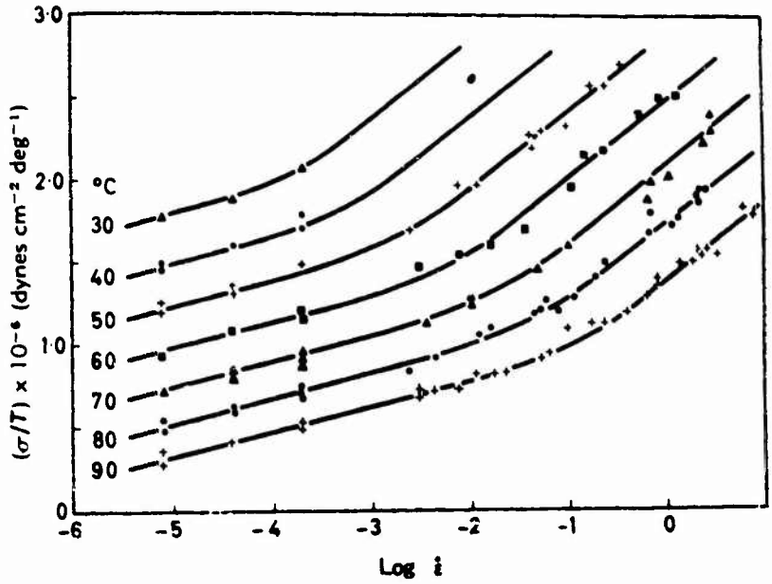

FIGURE 31. YIELD STRESS BEHAVIOR OF POLY(METHYL METHACRYLATE) (REF. 46).

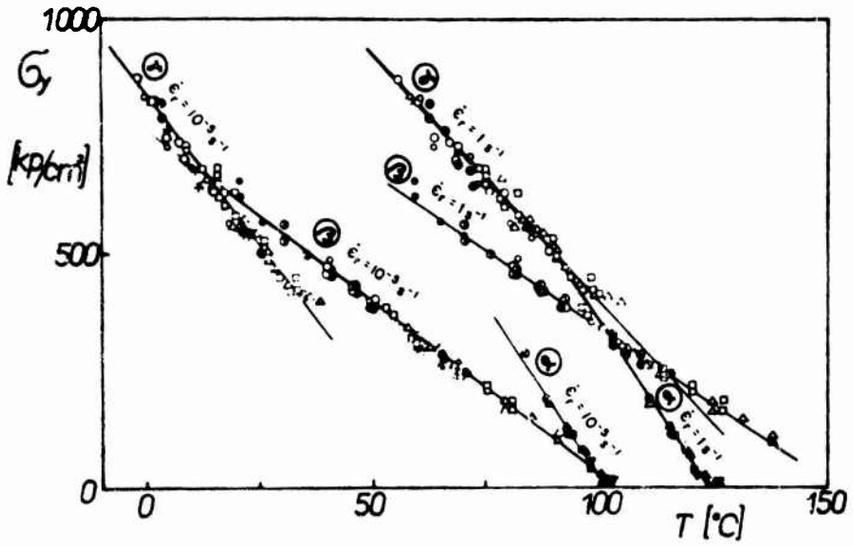

FIGURE 32. GENERALIZED YIELD STRESS DEPENDECE ON TEMPERATURE FOR POLY(METHYL METHACRYLATE) (REF. 47).

since it is inversely proportional to the parameter C in the equation (35). The β- to α-transition occurs below the glass transition temperature and is rate-independent.

(2) The β-process is initiated in the vicinity of the β-transition temperature of polymers. In this process the kinetic unit remains the same as that in the α-process. Unlike the α-β transition temperature, the γ-β-transition temperature is strongly influenced by strain rate.

(3) The γ-process begins in the region where neither α- nor β-processes occur, and the kinetic unit in this case is substantially smaller than in the two former cases. Boyer further reported (45) the study of Maxwell and Harrington in which they measured the energy required to break the poly(methyl methacrylate) tensile specimens at velocities from 0.001 inches per second to 185 inches per second at temperatures 30, 50, 70 and 90°C. Their results are shown in Figure 33. In analyzing the data of Maxwell and Harrington, for 30°C, 50°C and 90°C, Boyer assumed that in the 30°C curve the abrupt drop in energy at A-B implies a merging of the α and β transitions. Another possibility is that the β transition is outside the left margin of Figure 33. For the 50°C curve he assumed that a sharp drop in energy at C-D represents the α transition while that at D-E indicates the β transition or a strong influence of the α transition on the β process. In the case of the 90°C curve the drop at F-G is considered to be the α or glass transition while H-I would be the β transition. In order to calculate apparent activation energies for both the α and β processes, Boyer selected two iso-energy levels (3 and 5.5 foot-pounds) and read the rate of straining for each curve (Figure 33). These data are shown in Table 10 (Ref. 45). From this table he constructed Figure 34 to obtain the apparent activation energy for the α and β processes.

TABLE 10.

CALCULATION OF APPARENT ACTIVATION ENERGIES FROM DATA IN FIGURE 33 FOR PMMA

Temp (°C)	Strain Rate (in/s) (at 5.5 ft-lb)	β-Process (at 3 ft-lb)	Ratio of Strain Rate β:α
30	0.005	0.025	1
50	0.011	0.11	10
70	0.032	3.2	100
90	0.063	50.0	800

From Figure 34 he obtained the apparent activation energies of 34 kcal/mol for the β process and 8.5 kcal/mol for the α process.

Boyer replotted the data in Table 10 into Figure 35 and commented that Figure 35 suggests that at temperatures below 30°C and strain rate less than 0.01 in/sec a double break in the impact energy versus strain rate curve might be still observed.

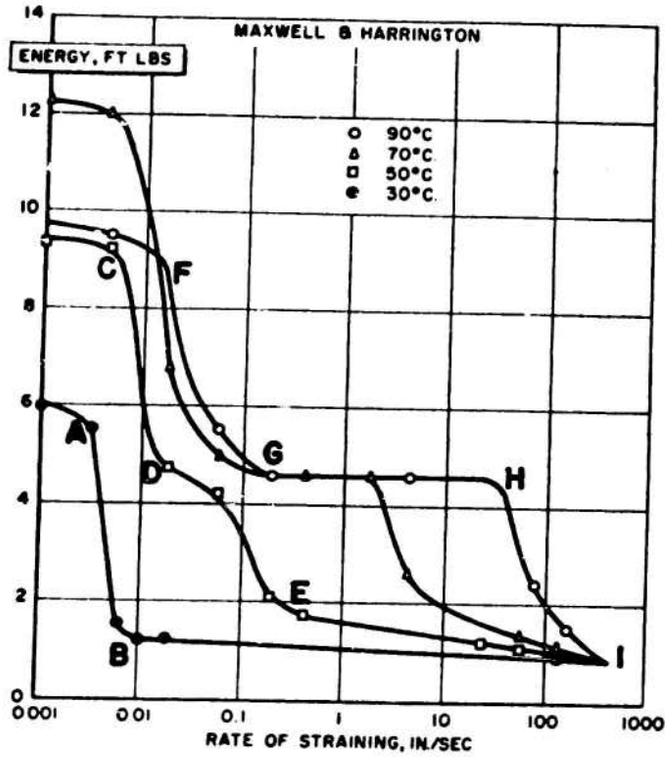

FIGURE 33. ENERGY OF TENSILE FAILURE FOR POLY-(METHYL METHACRYLATE) AS A FUNCTION OF STRAIN RATE AND TEMPERATURE (REF. 45).

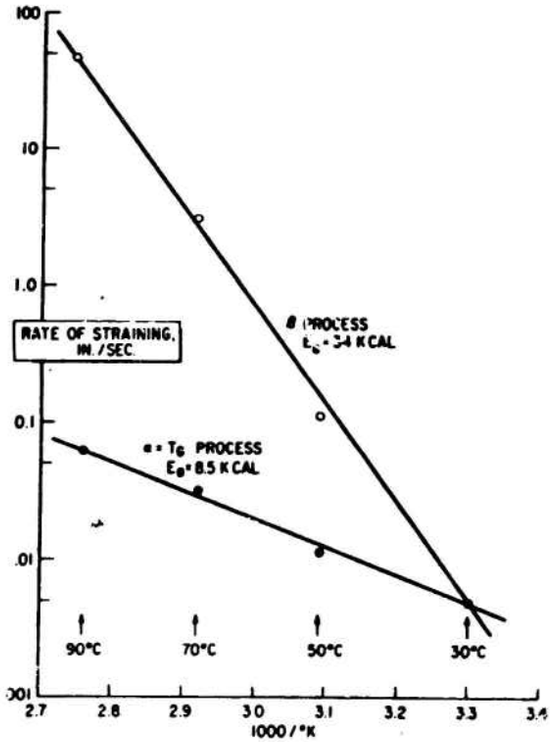

FIGURE 34. ARRHENIUS PLOT OF RATE OF STRAINING AT CONSTANT IMPACT ENERGY AGAINST RECIPROCAL TEMPERATURE (REF. 45).

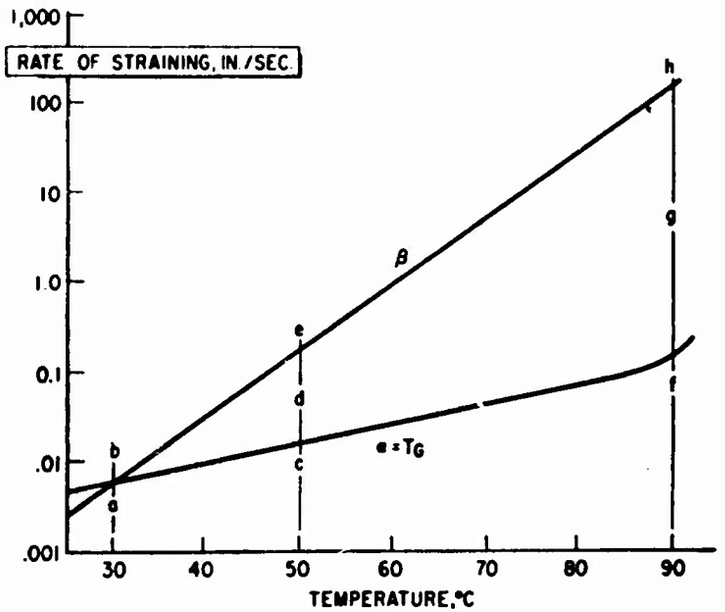

FIGURE 35. ALTERNATE FORM OF ACTIVATION ENERGY PLOT USING A LINEAR TEMPERATURE SCALE (REF. 45).

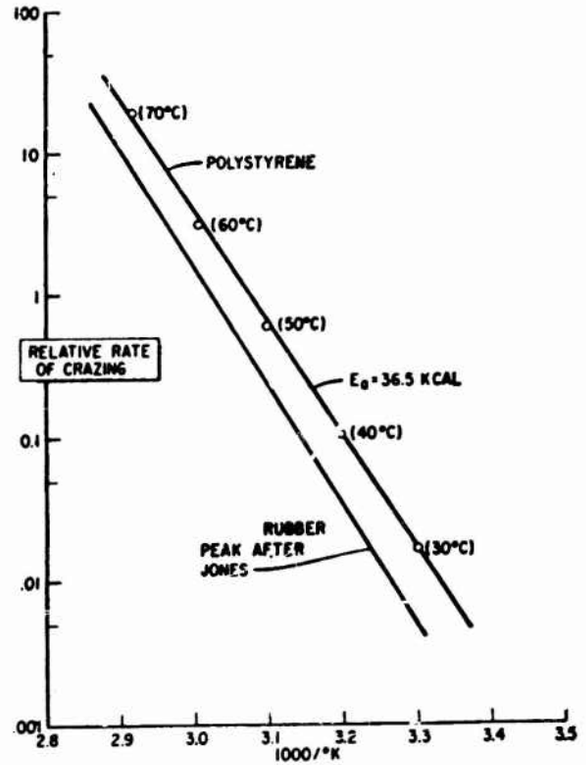

FIGURE 36. ARRHENIUS PLOT OF RELATIVE RATE OF CRAZING AS A FUNCTION OF TEMPERATURE (REF. 45).

Boyer and Andrews (45) examined data on crack growth rate as a function of temperature for poly(methyl methacrylate) at only two temperatures (20°C and 40°C) and obtained an apparent activation energy of 26 kcal/mol. Concerning the β peak of polystyrene Boyer reported the investigation of Illers who found that the β peak appeared in the region of 25-60°C as the frequency changed from 0.05 to 40 Hz with an apparent activation energy of 35-40 kcal/mol. Andrews and Boyer examined the temperature coefficient of crazing for polystyrene, utilizing the Maxwell and Rahm data, and found that values of the relative rate of crazing from 30 to 70°C gave a perfect linear plot of log rate versus 1/T with an apparent activation energy of 36.5 kcal/mol (45). Their plot is shown in Figure 36. McCrum, Read, and Williams plotted the frequency-temperature locations of the mechanical α and β relaxation and the dielectric α relaxation (48). Their results are shown in Figure 37.

In this section the basic viscoelastic properties of poly(methyl methacrylate) and polystyrene are reviewed with respect to the transition temperatures and related α- and β-processes. In the next section crack propagation phenomena in poly(methyl methacrylate) and polystyrene are studied over a wide range of crack velocities in terms of the fracture surface work. Existing data concerning the fracture studies of both materials are also reviewed in the light of this study. In Chapter VI the dynamic crack propagation phenomena in polymers will be discussed with respect to the basic viscoelastic parameters.

B. Experimental Studies of Crack Propagation in Poly(methyl methacrylate) and Polystyrene

Poly(methyl methacrylate) is generally classified as a brittle material; however, it is known to exhibit slow stable crack propagation with some particular fracture surface features. For example, colors and river pattern markings appear on the surface prior to catastrophic rapid crack propagation if it is tested at room temperature using a tensile fracture specimen. If a cleavage type specimen is fractured at low crosshead rates, poly(methyl methacrylate) fractures in a very stable and continuous crack propagation mode. Polystyrene, on the other hand, exhibits a discontinuous and unstable crack propagation mode with crazed and rough fracture surfaces at room temperature. In order to characterize crack propagation phenomena in poly(methyl methacrylate) and polystyrene, the fracture surface work was measured over a wide range of crack velocities at room temperature. In addition, the fracture surface work was studied at different temperatures in a limited range of crack velocities. The type of specimen used in this experiment is a tapered double cantilever beam cleavage specimen with a contour design constant of $M = 400/3$. A detailed discussion of specimen design may be found in Chapter III. For high crack velocity testing a slightly modified specimen, which will be explained later in this section, was used. For low crack velocity tests, side grooves are machined along each face of the specimen in a specially designed side groove cutting machine (Chapter II), so that the thickness in the median plane is reduced to 0.050 inches. An initial crack is made by closing the distance between two spindles of the cutter. After machining, the specimen is carefully annealed in an oven to eliminate the residual stresses induced by machining. The effects of residual stresses are demonstrated in Figure 24 in Chapter III. Reference lines indicating crack length are next drawn at half-inch intervals on one side of the annealed specimen. These reference lines are used to

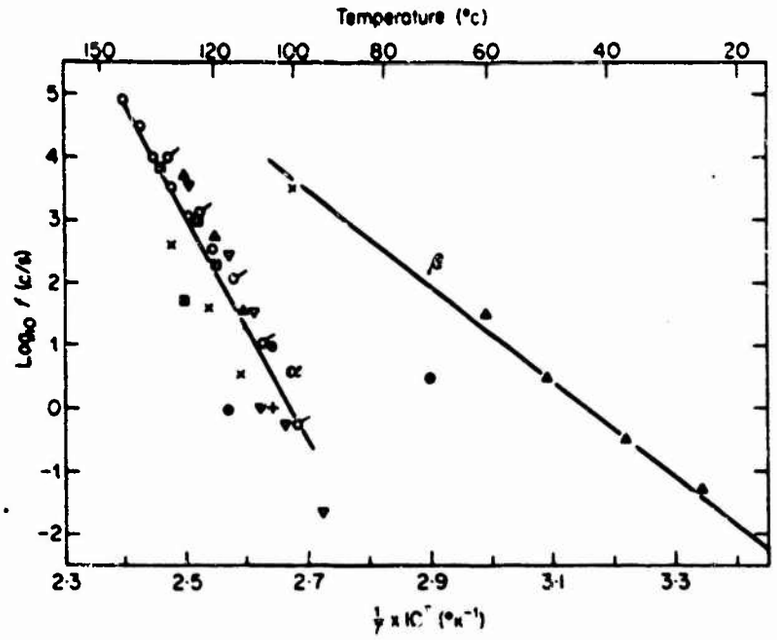

Mechanical

- ● $\tan\delta_G$ vs. T Atactic (Schmieder and Wolf, 1953)
- ▲ G'' vs. T Atactic, β process (Illers, 1961)
- ■ Q^{-1} vs. T Atactic (Wall, Sauer and Woodward, 1959)
- ▼ $\tan\delta_G$ vs. T Atactic (Illers and Jenckel, 1958)
- × $\tan\delta_E$ vs. T (Becker, 1955)
- + $\tan\delta_G$ vs. T Isotactic, amorphous and crystalline (Newman and Cox, 1960)
- ◑ E'' vs. T Isotactic, atactic and blends (Takayanagi, 1963)

Dielectric

- ○ $\tan\delta$ vs. $\log f$ Atactic (Broens and Müller, 1955)
- ⊡ $\tan\delta$ vs. T Atactic (Broens and Müller, 1955)
- △ ε'' vs. T Atactic (Baker and others, 1953)
- ◌ ε'' data Atactic (Kästner, and Schlosser and Pohl, 1963)
- ▽ ε'' vs. f Atactic (Saito and Nakajima, 1959b)

FIGURE 37. FREQUENCY-TEMPERATURE LOCATIONS OF α AND β RELAXTIONS IN POLYSTYRENE (REF. 48).

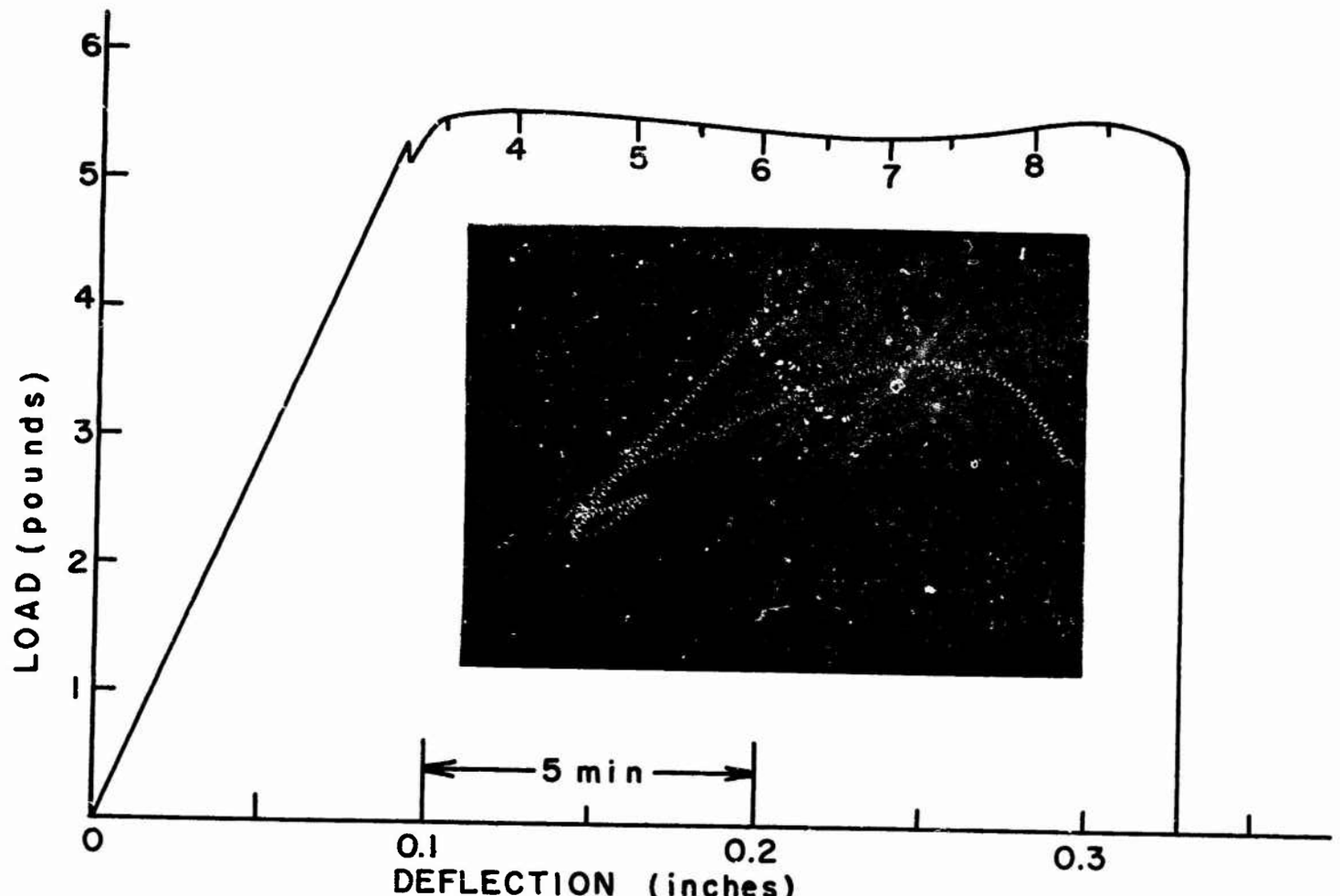

FIGURE 38. LOAD-DEFLECTION CURVE AND FRACTURE SURFACE OF POLY-(METHYL METHACRYLATE) TESTED AT 22°C AND CROSSHEAD RATE OF 0.02 in/min.

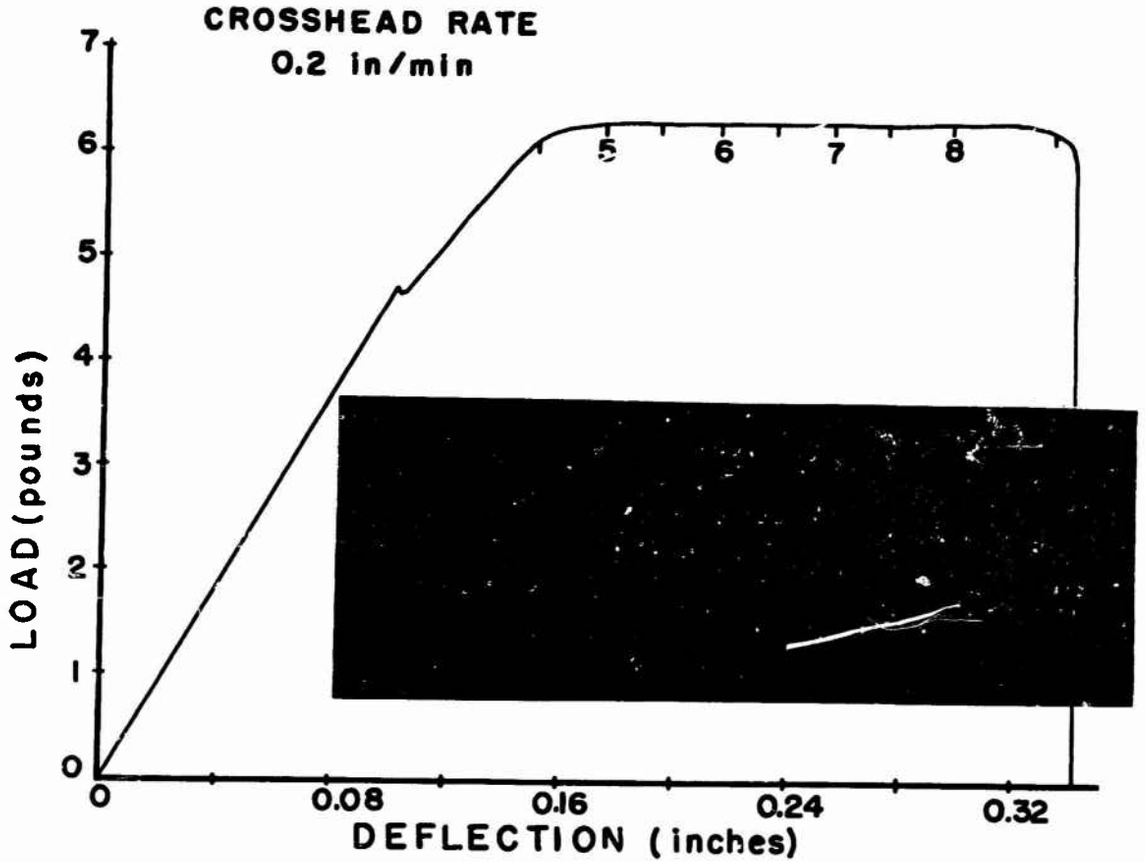

FIGURE 39. LOAD--DEFLECTION CURVE AND FRACTURE SURFACE OF POLY(METHYL METHACRYLATE) TESTED AT 22 °C AND CROSSHEAD RATE OF 0.2 in/min.

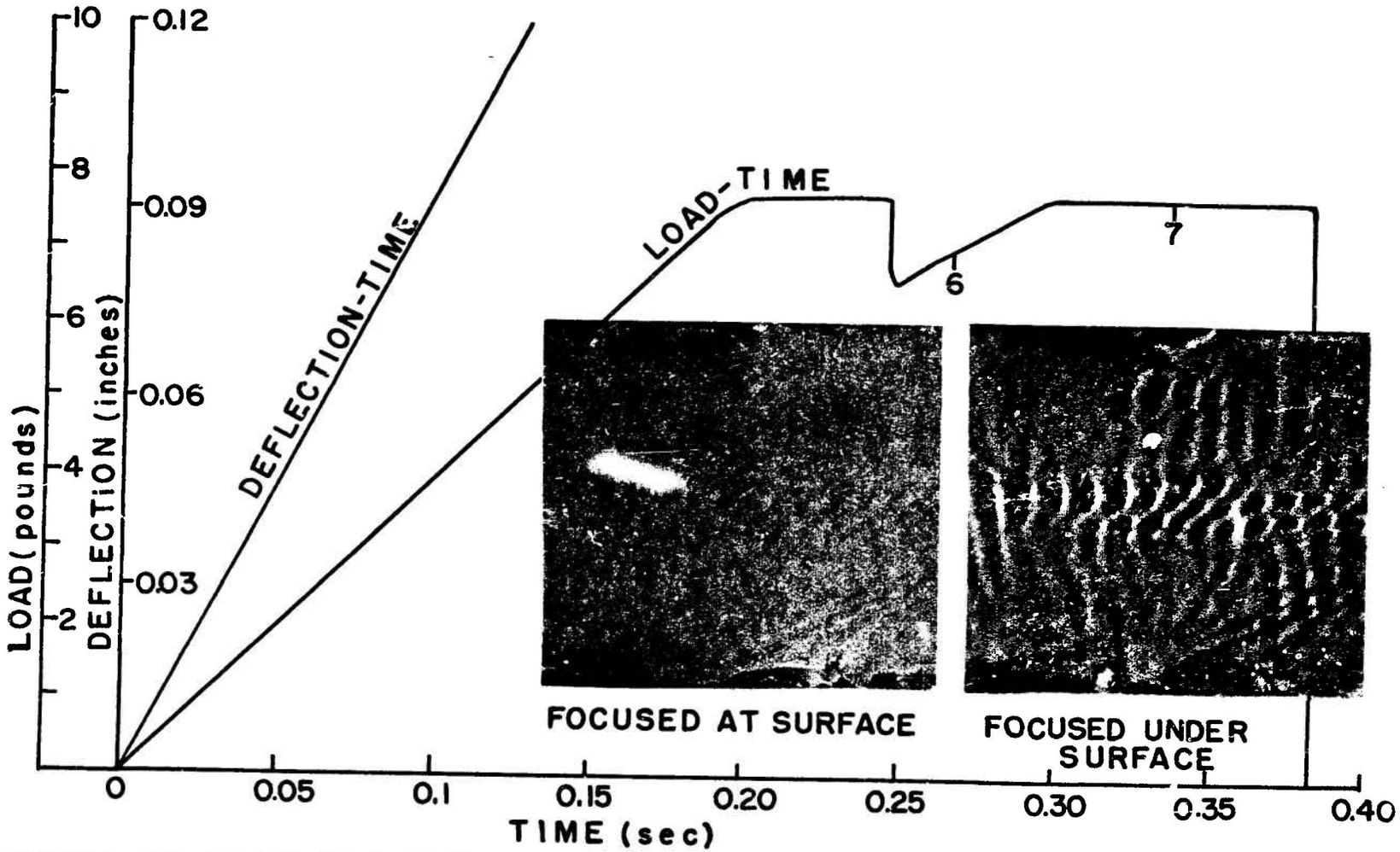

FIGURE 40. LOAD AND DEFLECTION VERSUS TIME CURVES AND FRACTURE SURFACE OF POLY(METHYL METHACRYLATE) TESTED AT 22°C AND CROSSHEAD RATE OF 5.5 in/min.

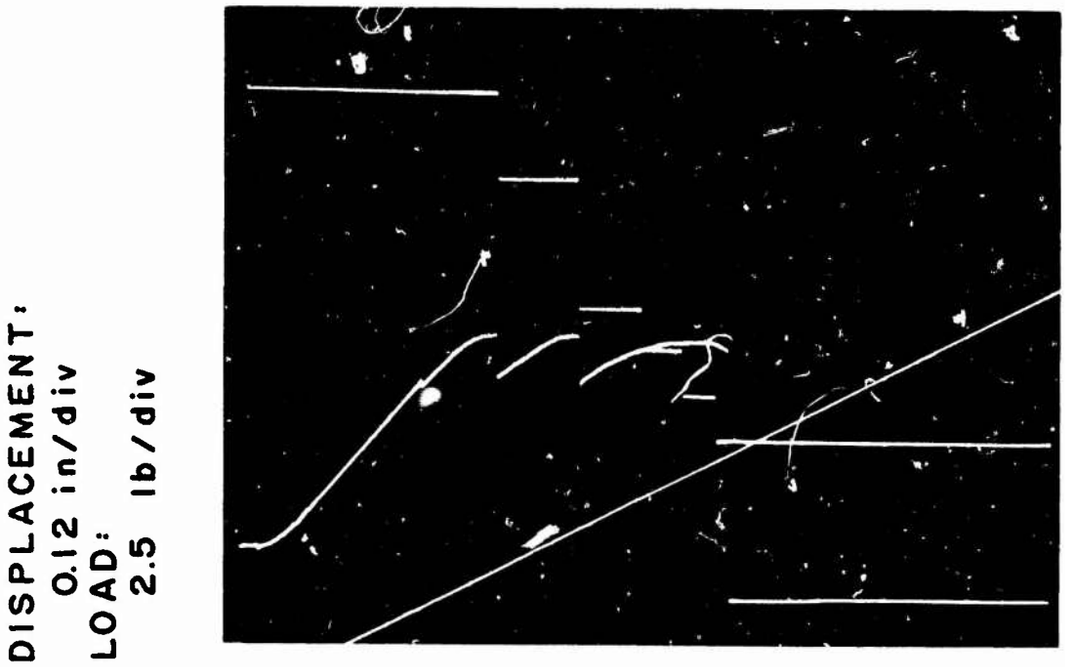

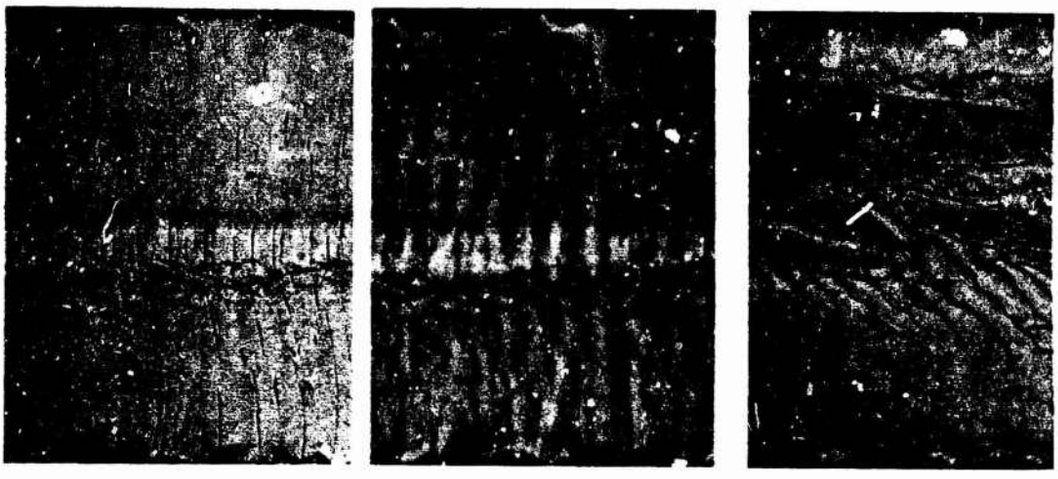

FOCUSED AT SURFACE | FOCUSED UNDER SURFACE | DIFFERENT REGION OF SURFACE

FIGURE 41. LOAD, DEFLECTION, CRACK TIP POSITION RECORD AND FRACTURE SURFACE OF POLY(METHYL METHACRYLATE) TESTED AT 22°C AND CROSSHEAD RATE OF 7in/min.

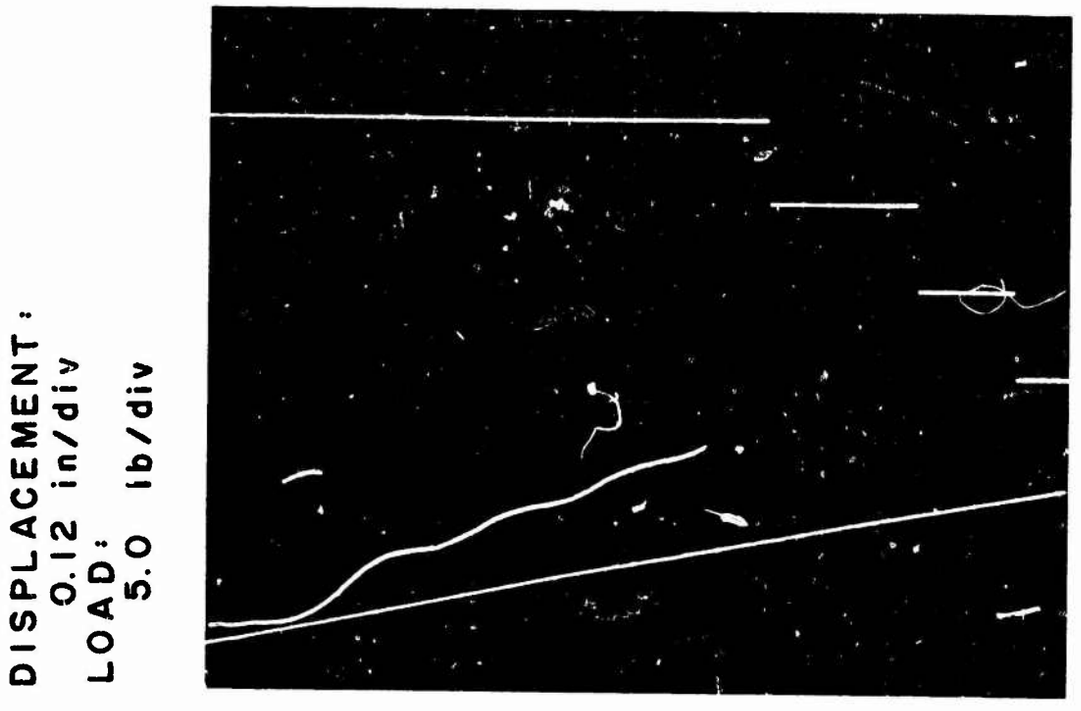

AVERAGE CRACK VELOCITY : 2.54 meters/sec

FIGURE 42. LOAD, DEFLECTION, CRACK TIP POSITION RECORD AND FRACTURE SURFACE OF POLY(METHYL METHACRYLATE) TESTED AT 22 °C AND CROSSHEAD RATE OF 156 in/min.

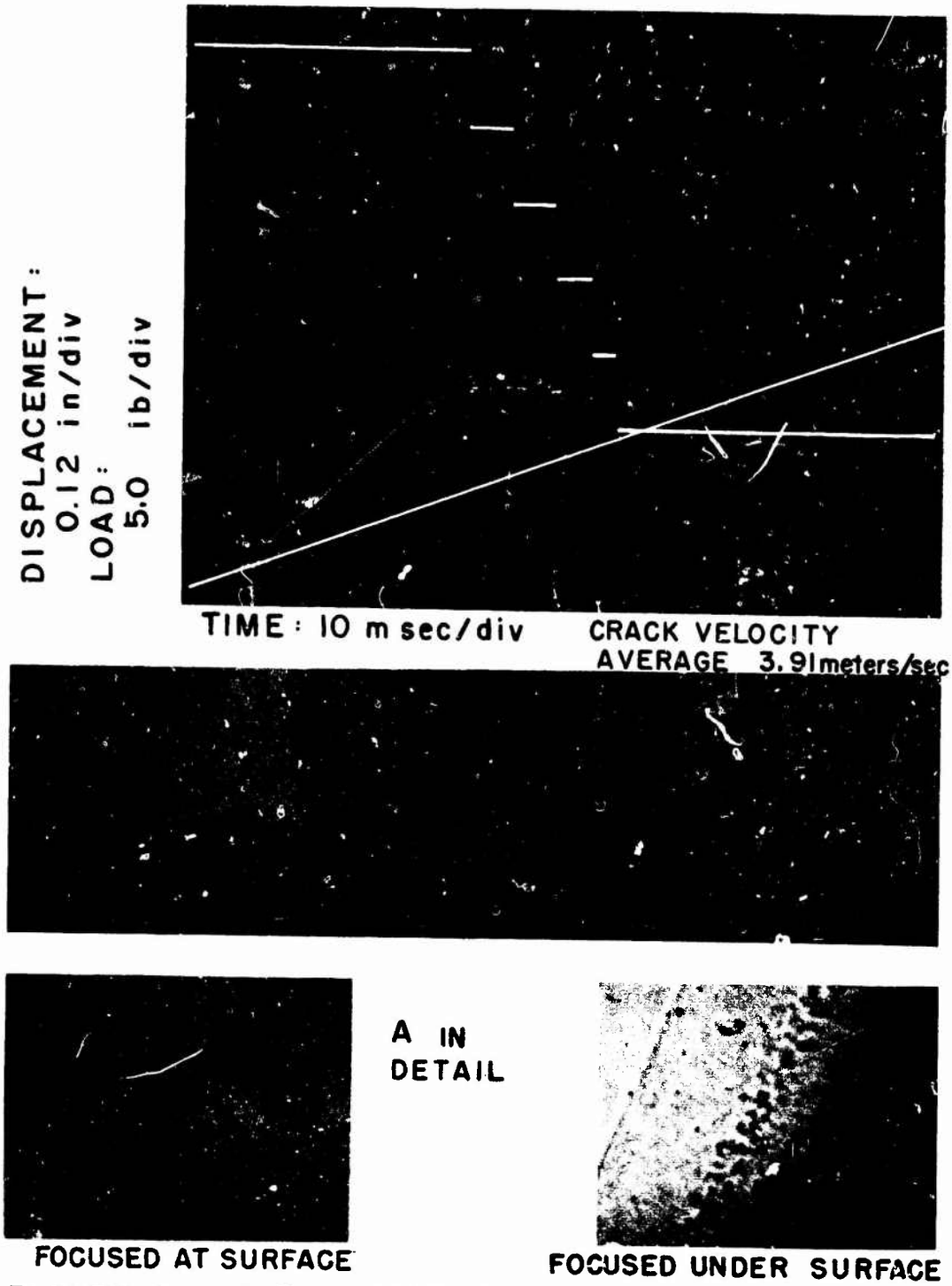

FIGURE 43. LOAD, DEFLECTION, CRACK TIP POSITION RECORD AND FRACTURE SURFACE OF POLY(METHYL METHACRYLATE) TESTED AT 22°C AND CROSSHEAD RATE OF 245 in/min.

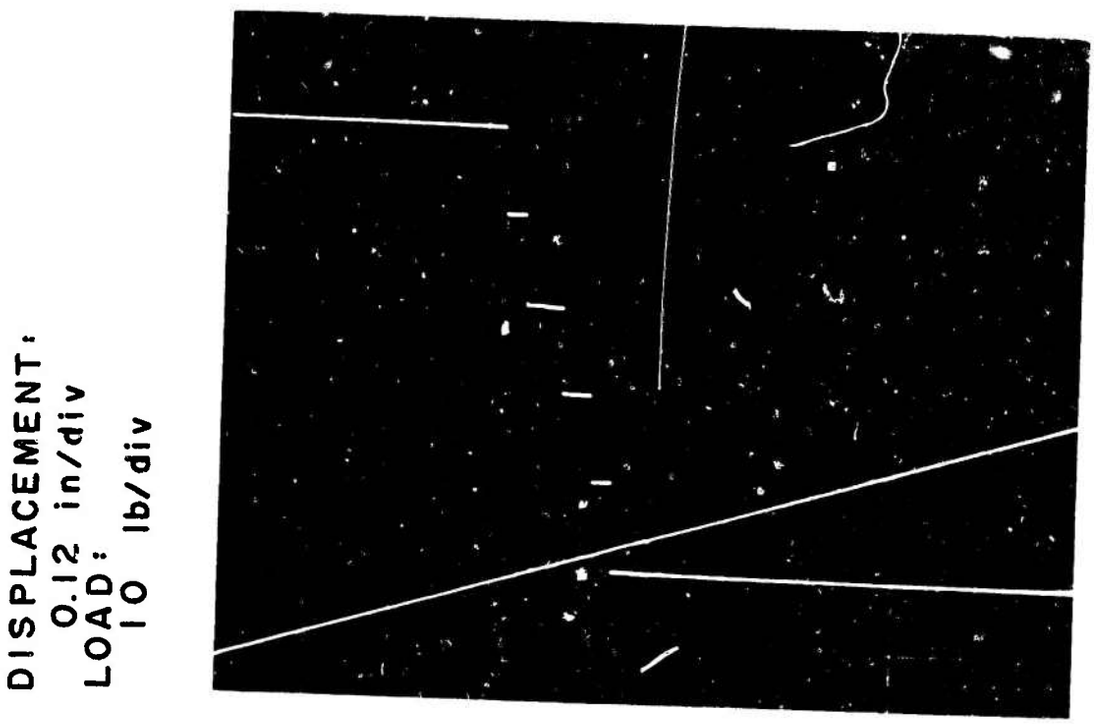

AVERAGE CRACK VELOCITY : 53 meters / sec

FIGURE 44. LOAD, DEFLECTION, CRACK TIP POSITION RECORD AND FRACTURE SURFACE OF POLY(METHYL METHACRYLATE) TESTED AT 22 °C AND CROSSHEAD RATE OF 2088 in/min.

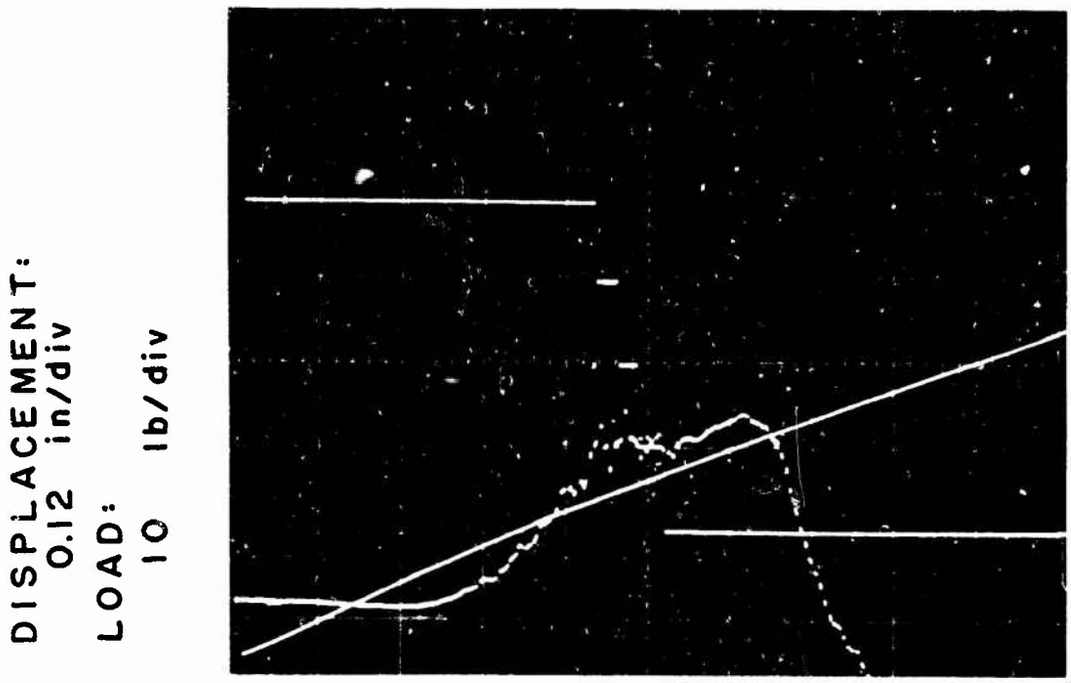

AVERAGE CRACK VELOCITY: 127 meters/sec

FIGURE 45. LOAD, DEFLECTION, CRACK TIP POSITION RECORD AND FRACTURE SURFACE OF POLY(METHYL METHACRYLATE) TESTED AT 22 °C AND CROSSHEAD RATE OF 5760 in/min.

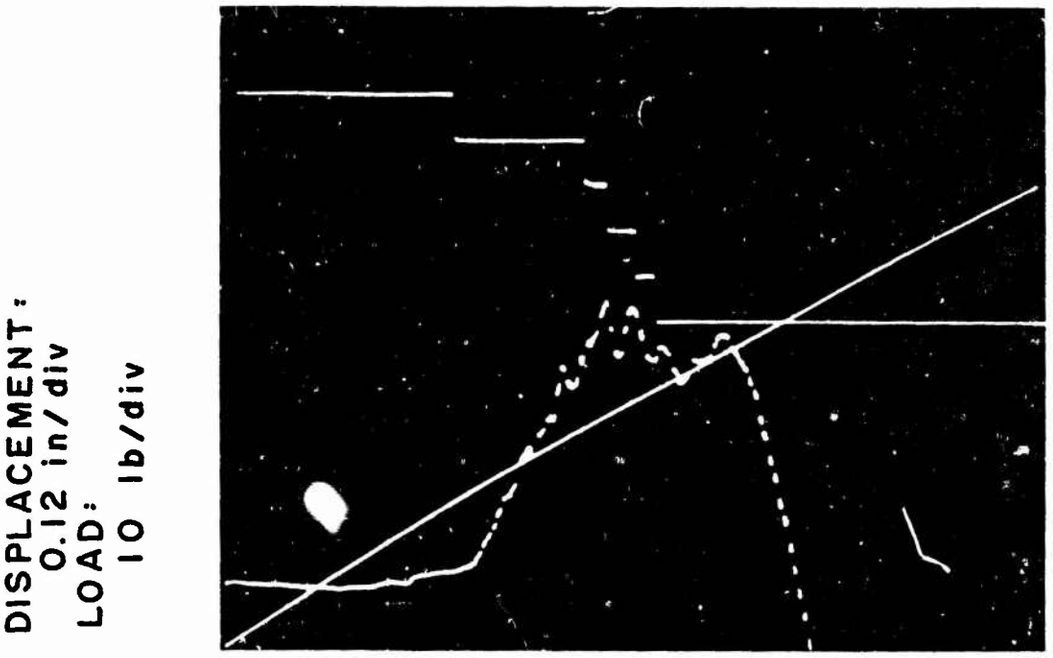

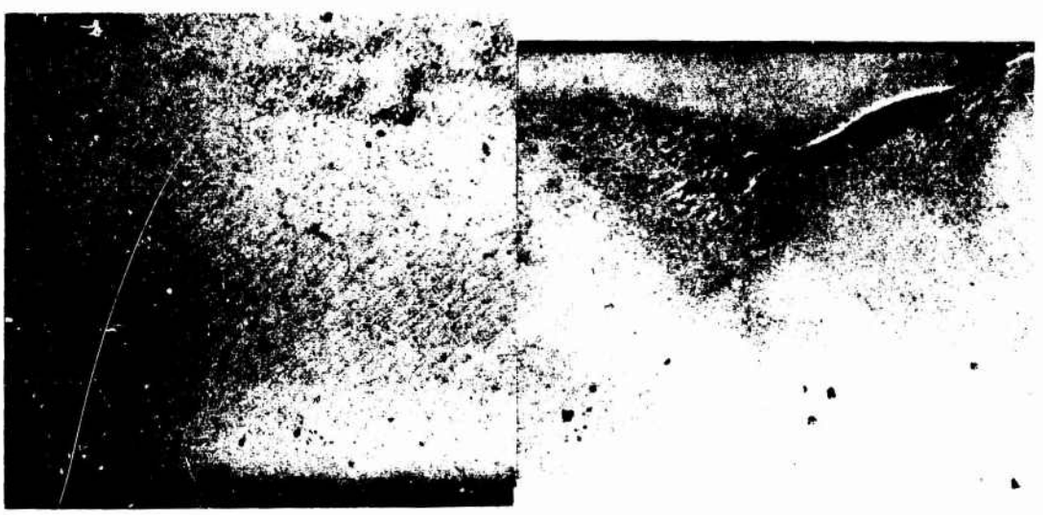

AVERAGE CRACK
VELOCITY: 186 meters/sec

FIGURE 46. LOAD, DEFLECTION, CRACK TIP POSITION RECORD AND FRACTURE SURFACE OF POLY(METHYL METHACRYLATE) TESTED AT 22°C AND CROSSHEAD RATE OF 7632 in/min.

Table 11. Experimental Results of Crack Velocities and Fracture Surface Work for Poly(methyl methacrylate) at 22°C.

Cross Head Rate (in/min)	Crack Velocity (meters/sec)	Fracture Surface Work ($ergs/cm^2$)
0.02	2.29×10^{-4}	1.80×10^{5}
0.2	2.09×10^{-3}	2.15×10^{5}
2.0	2.31×10^{-2}	2.58×10^{5}
6.05	3.36×10^{-2}	2.60×10^{5}
5.5	5.43×10^{-2}	2.76×10^{5}
7.0	6.40×10^{-2}	3.51×10^{5}
5.25	6.55×10^{-2}	3.10×10^{5}
156	2.54	2.15×10^{5}
245	3.91	2.17×10^{5}
416	6.35	2.22×10^{5}
642	7.25	2.32×10^{5}
1030	14.3	2.44×10^{5}
642	19.3	2.54×10^{5}
2088	53.0	1.49×10^{5}
5760	127.0	2.69×10^{5}
7200	162.0	5.25×10^{5}
7632	185.5	5.14×10^{5}

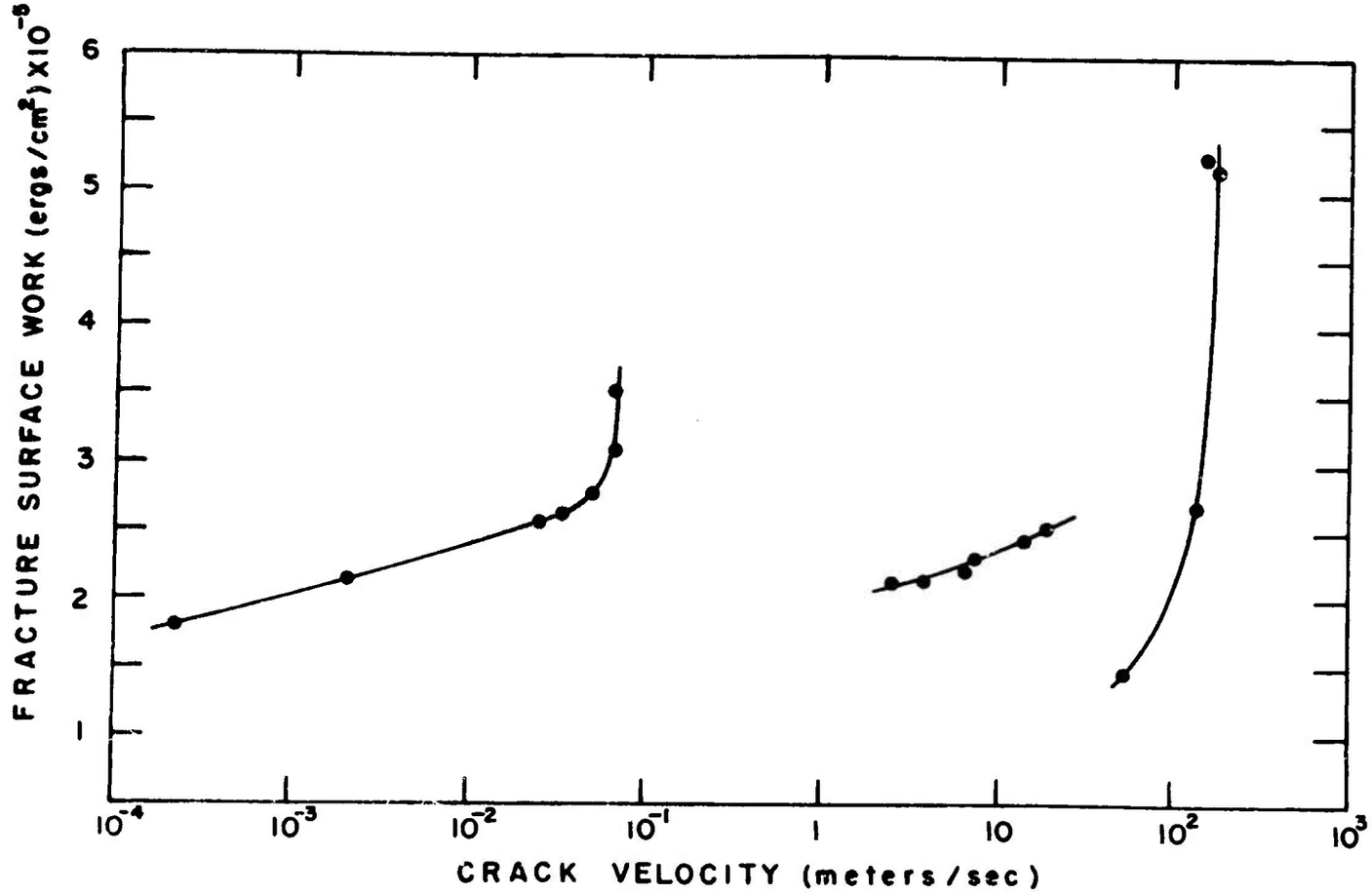

FIGURE 47. FRACTURE SURFACE WORK VERSUS CRACK VELOCITY AT 22°C FOR POLY (METHL METHACRYLATE).

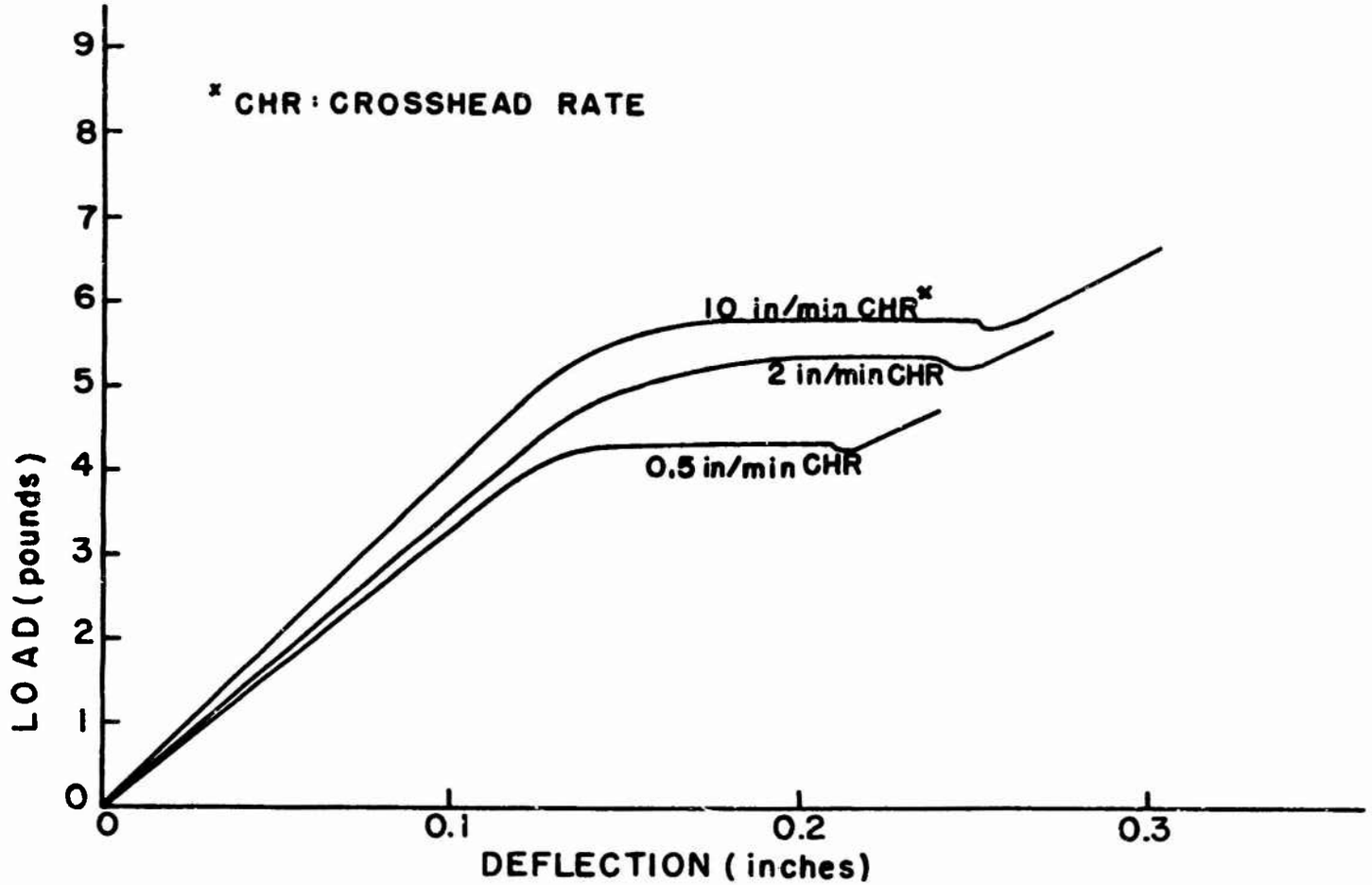

FIGURE 48-1. LOAD-DEFLECTION CURVES OF POLY(METHYL METHACRYLATE) TESTED AT 62°C.

CROSSHEAD RATE
0.5 in/min

CRACK VELOCITY
5.47×10^{-3}
meters/sec

CROSSHEAD RATE
2.0 in/min

CRACK VELOCITY
1.86×10^{-2}
meters/sec

CROSSHEAD RATE
10 in/min

CRACK VELOCITY
8.63×10^{-2}
meters/sec

FIGURE 48-2. FRACTURE SURFACES OF POLY-(METHYL METHACRYLATE) TESTED AT 62 °C.

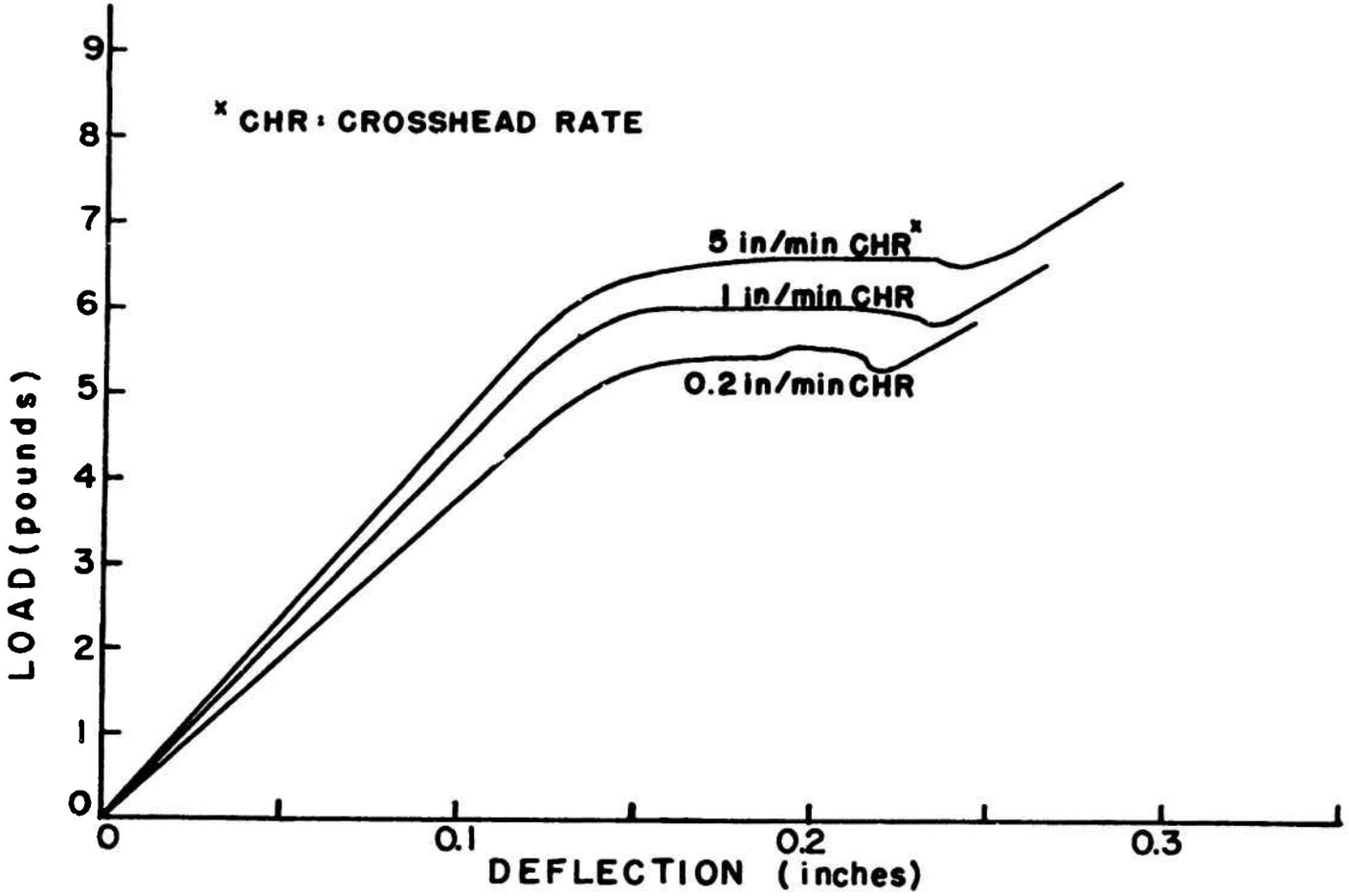

FIGURE 49-1. LOAD-DEFLECTION CURVES OF POLY (METHYL METHACRYLATE) TESTED AT 40 °C.

CROSSHEAD RATE
0.2 in/min

CRACK VELOCITY
1.91×10^{-3}
meters/sec

CROSSHEAD RATE
1.0 in/min

CRACK VELOCITY
1.00×10^{-2}
meters/sec

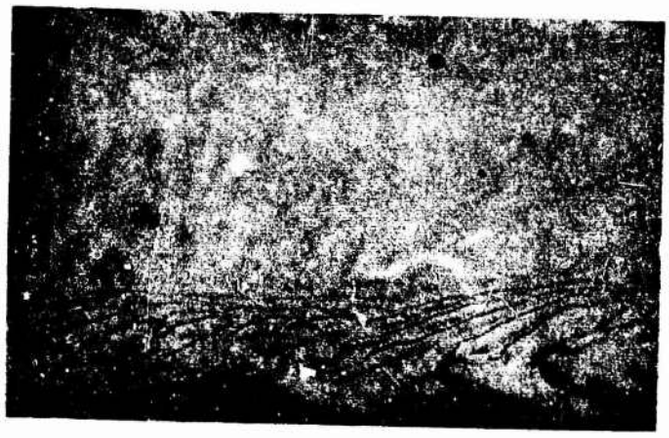

CROSSHEAD RATE
5.0 in/min

CRACK VELOCITY
4.81×10^{-2}
meters/sec

FIGURE 49-2. FRACTURE SURFACES OF POLY-(METHL METHACRYLATE) TESTED AT 40°C.

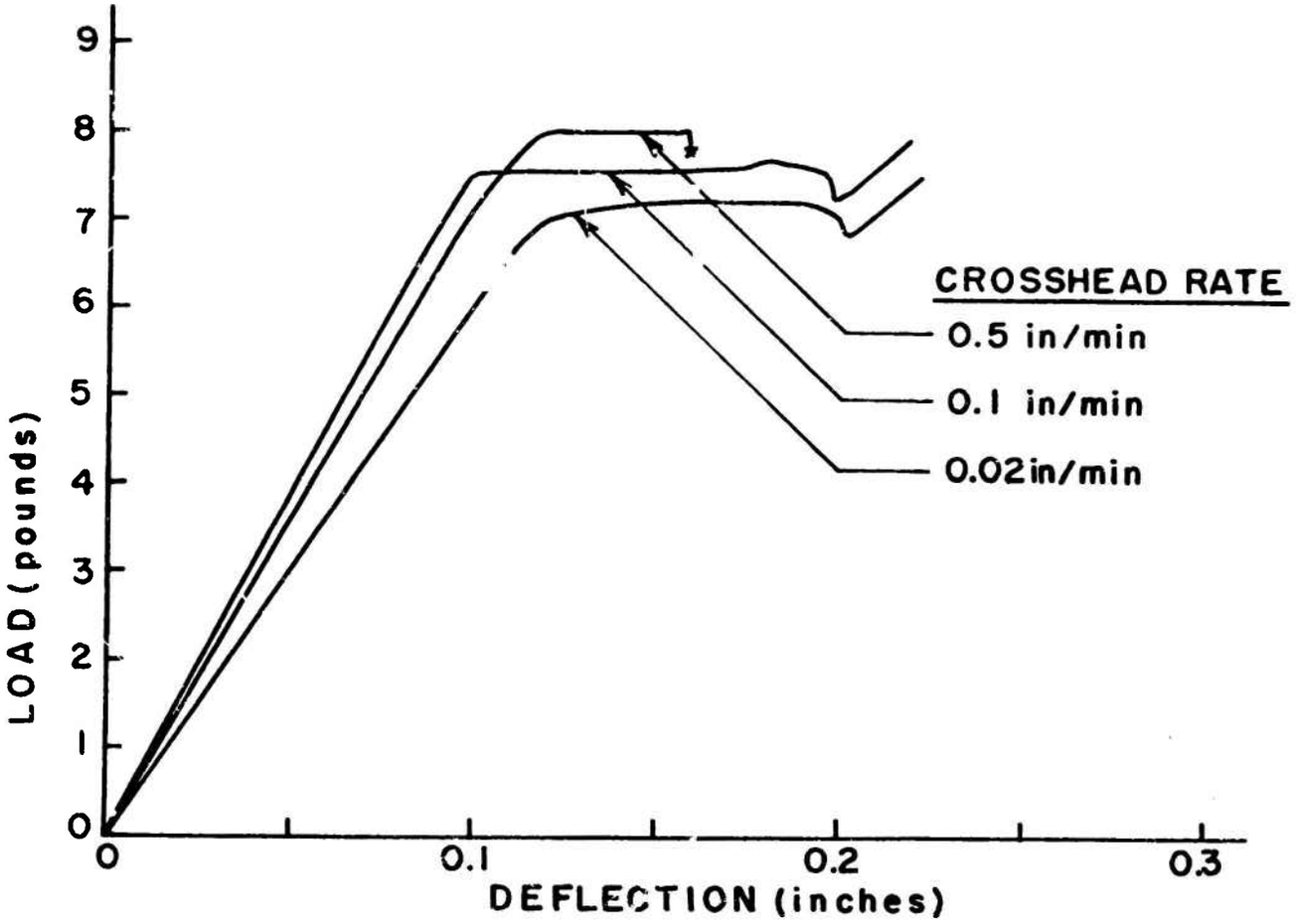

FIGURE 50-1. LOAD-DEFLECTION CURVES OF POLY(METHYL METHACRYLATE) TESTED AT −20 °C.

CROSSHEAD RATE
0.02 in/min

CRACK VELOCITY

2.31×10^{-4}
meters/sec

CROSSHEAD RATE
0.1 in/min

CRACK VELOCITY
1.70×10^{-3}
meters/sec

CROSSHEAD RATE
0.5 in/min

CRACK VELOCITY
5.70×10
meters/sec

FIGURE 50-2. FRACTURE SURFACES OF POLY-(METHYL METHACRYLATE) TESTED AT -20 °C.

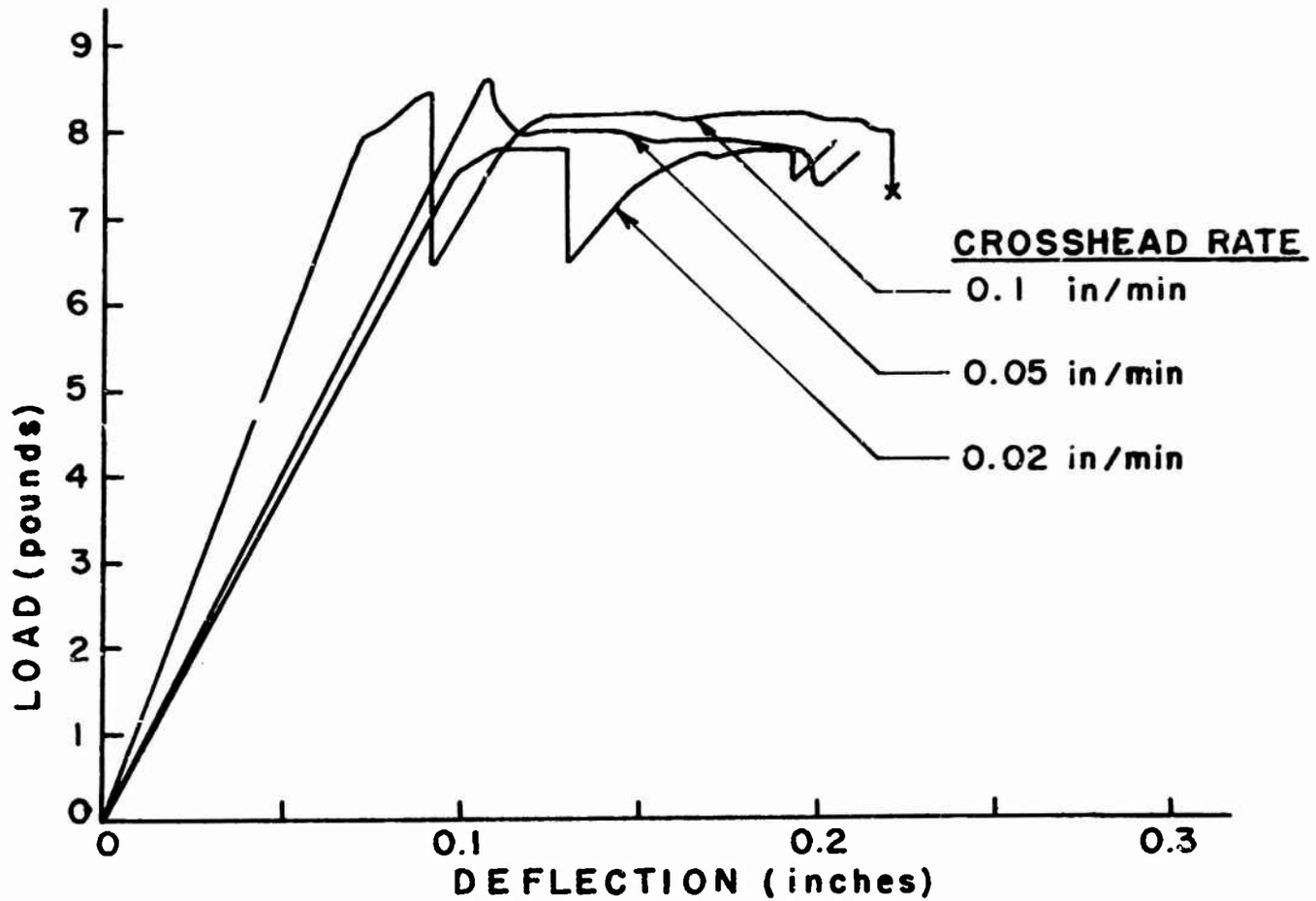

FIGURE 51-1. LOAD-DEFLECTION CURVES OF POLY(METHYL METHACRYLATE) TESTED AT -30 °C.

CROSSHEAD RATE
0.02 in/min

CRACK VELOCITY
2.38×10^{-4}
meters/sec

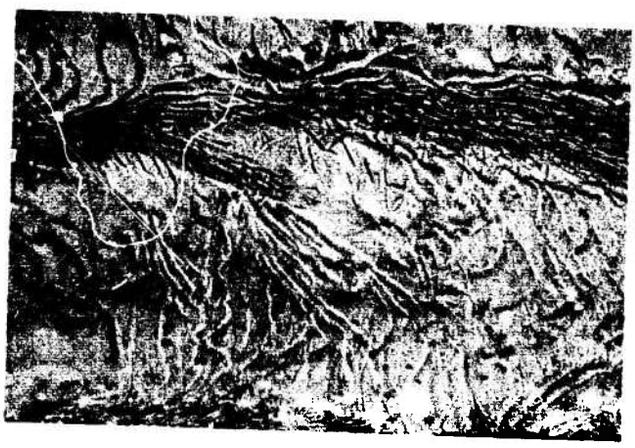

CROSSHEAD RATE
0.05 in/min

CRACK VELOCITY
5.99×10^{-4}
meters/sec

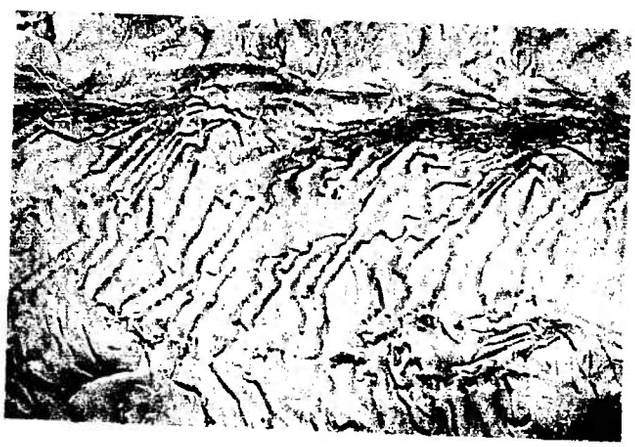

CROSSHEAD RATE
0.1 in/min

CRACK VELOCITY
1.18×10
meters/sec

FIGURE 51-2. FRACTURE SURFACES OF POLY-(METHYL METHACRYLATE) TESTED AT -30°C.

Table 12. Experimental Results of Crack Velocities and Fracture Surface Work for Poly(methyl methacrylate) at Different Temperatures

Temp. (°C)	Cross Head Rate (in/min)	Crack Velocity (meters/sec)	Fracture Surface Work (ergs/cm^2)
-30	0.02	2.38×10^{-4}	2.52×10^{5}
	0.05	5.99×10^{-4}	2.52×10^{5}
	0.10	1.18×10^{-3}	2.57×10^{5}
-20	0.02	2.31×10^{-4}	2.28×10^{5}
	0.10	1.17×10^{-3}	2.39×10^{5}
	0.50	5.70×10^{-3}	2.60×10^{5}
40	0.20	1.91×10^{-3}	1.96×10^{5}
	1.00	1.00×10^{-2}	2.25×10^{5}
	5.00	4.81×10^{-2}	2.54×10^{5}
62	0.50	5.47×10^{-3}	1.40×10^{5}
	2.00	1.86×10^{-2}	2.13×10^{5}
	10.0	8.63×10^{-2}	2.49×10^{5}

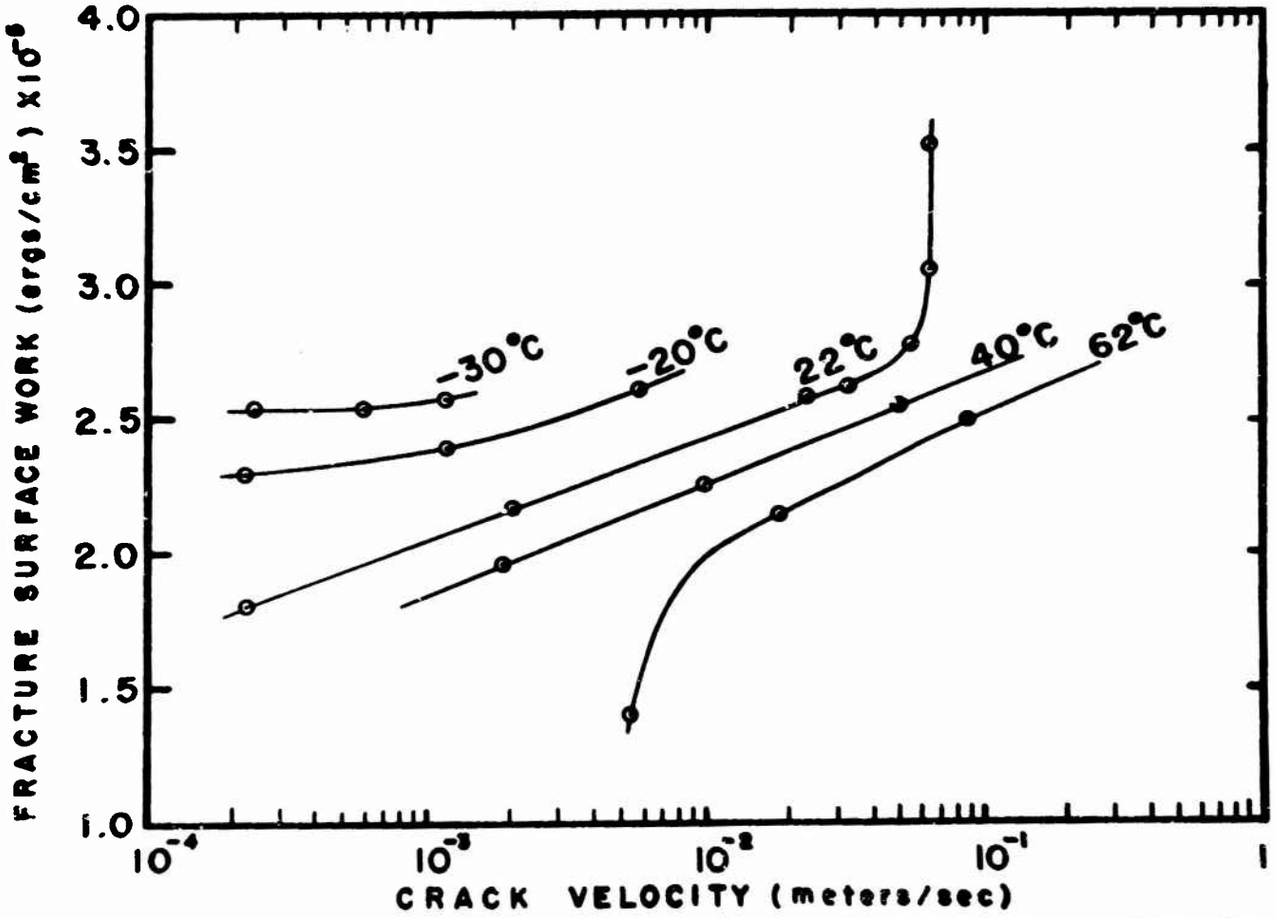

FIGURE 52. FRACTURE SURFACE WORK VERSUS CRACK VELOCITY AT DIFFERENT TEMPERATURES FOR POLY(METHYL METHACRYLATE).

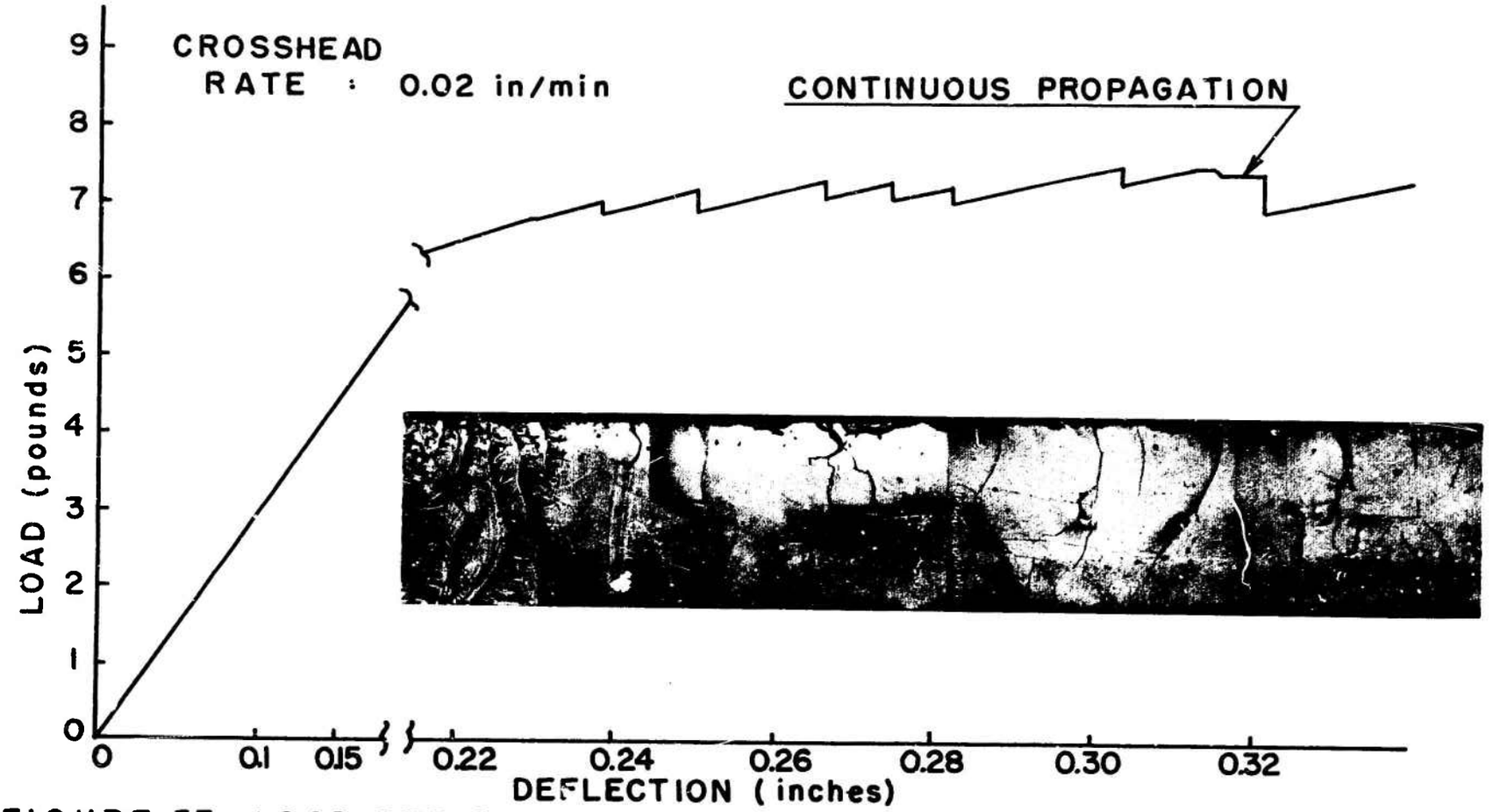

FIGURE 53. LOAD-DEFLECTION CURVE AND FRACTURE SURFACE OF POLYSTYRENE TESTED AT 22 °C SHOWING CONTINUOUS CRACK PROPAGATION.

Table 13. Fracture Surface Work and Crack Velocities of Polystyrene at Room Temperature

Crack Velocity (meters/sec)	Fracture Surface Work ($ergs/cm^2$)
2.89×10^{-4}	3.12×10^{5}
2.71×10^{-4}	2.55×10^{5}
2.54×10^{-4}	2.47×10^{5}
1.95×10^{-4}	2.17×10^{5}
8.1×10^{-5}	1.76×10^{5}*

*constant load

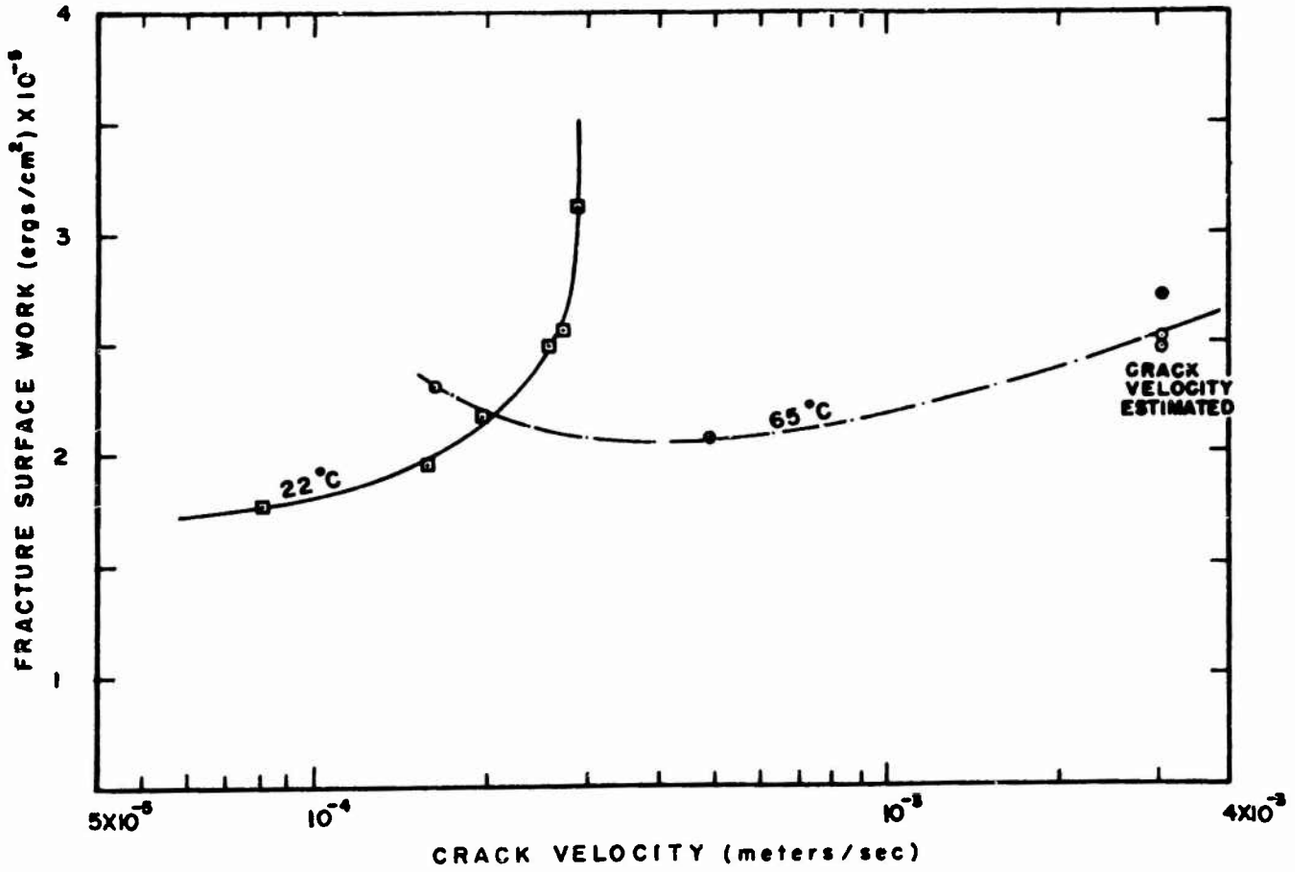

FIGURE 54. FRACTURE SURFACE WORK VERSUS CRACK VELOCITY AT 22°C AND 65°C FOR POLYSTYRENE.

determine the crack tip position during crack propagation so that after the test the crack velocities and the experimental compliance change in terms of crack length can be calculated from the crack tip position. After marking the reference lines, the specimen is affixed to the template with double coated tape and the contour of the tapered cleavage specimen is machined by the router. Three pin holes (two for loading and one for supporting the specimen end in the testing machine) are drilled. For specimens to be tested at high crack velocities a side groove is machined on only one side of the specimen in such a way that the thickness of the median plane is reduced to 0.050 inches. An initial crack is made by deepening the side groove so that the cutter extends to the other side of the specimen. The initial crack length is extended to half of the total specimen length so that the rate of crack extension force increase is reduced to ensure stable crack initiation under a high loading rate. After the annealing procedure reference lines are drawn on the flat side of the specimen. Then the tapered contour is machined by a router. Conductive paint lines are drawn on the reference lines so that an electrical signal is created when the advancing crack passes and breaks through these conductive paint lines. After drying the conductive paint two reinforcing bars, each shaped as half a tapered cleavage specimen, are bonded with double coated tape on the flat side of the specimen. This specimen construction gives more rigidity to the specimen beams and reduces the rate of sudden crack width increase if the crack deviates from the grooved plane into the beam. Thus crack propagation becomes more stable. The fracture surface work results obtained from the ordinary tapered cleavage specimen and this slightly modified specimen shows no influence of specimen construction in the same crack velocity range. The data analysis procedure has been discussed in Chapter III.

Some of the load-deflection curves together with photographs of the fracture surface appearance for poly(methyl methacrylate) are shown in Figures 38 to 46. The calculated results of fracture surface work and the crack velocity are tabulated in Table 11. The relation between fracture surface work and crack velocity is plotted in Figure 47.

In order to study the effects of temperature and crack velocity, poly(methyl methacrylate) specimens were tested at temperatures of -30, -20, 40 and 60°C. in the Instron environmental chamber mounted on the Instron testing machine. The load-deflection curves and the fracture surface appearances are shown in Figures 48 to 51. The calculated results of fracture surface work and the crack velocity are tabulated in Table 12. The fracture surface work values versus the crack velocities are also plotted in Figure 52.

In the case of polystyrene it was very difficult to obtain slow continuous crack propagation at room temperature in the experiments which use constant specimen end separation rates; however, it was found that under conditions of low rate of crack extension force increase (low crosshead rate and long crack length) slow continuous crack propagation occurs. In these slow continuous crack propagation regions the fracture surface shows a distinct green or pink color, and is mirror smooth. The crack velocities and the fracture surface work were calculated from the data obtained in these slow crack propagation regions. One example of the load-deflection curve and a fracture surface photograph are shown in Figure 53. It was also found that under constant load conditions the crack propagates smoothly at very low crack velocities at room temperature. The results of fracture surface work measurements in terms of crack velocities at room temperature are tabulated in Table 13 and plotted in Figure 54.

An attempt has been made to obtain fracture surface work at high crack velocities, but at this stage it was not successful. One example of a load-time record and a fracture surface picture at high crack velocity (375m/s) are shown in Figure 55. The crosshead rate used was 9540 in/min.

In addition to room temperature tests, the polystyrene specimens were also tested at 65°C and 67°C. The results are tabulated in Table 14 and plotted in Figure 54.

At 65° and 67°C the crack propagated in a continuous and stable manner at low crosshead rates of 0.02 and 0.05 inches per minute. The load-deflection curve and fracture surface appearance in the region of continuous crack propagation from one of the specimens are shown in Figure 56. Figure 57 shows a photograph of the initiation of hackle marks and the load-deflection curve.

As indicated in Figures 47, 52 and 54, the fracture surface work of poly(methyl methacrylate) and polystyrene is greatly influenced by crack velocity and temperature. For poly(methyl methacrylate) at room temperature, Figure 47 indicates that the fracture surface work increases as the crack velocity increases up to about 6.5 cm/sec. At the crack velocity of about 6.5 cm/sec the crack propagation becomes very unstable and the crack starts to jump. The next experimentally obtained points appear above the crack velocity of 2.5 m/sec, and the fracture surface work values are lower than the values at the crack velocity of 6.5 cm/sec. Further research to establish the fracture surface work in the crack velocity range between 6.5 cm/sec to 2.5 m/sec is now in progress. The question to be answered by further investigation in this crack velocity region concerns the exact location and the magnitude of the peak of fracture surface work in poly(methyl methacrylate). In the crack velocity range between 2.5 m/sec and 20 m/sec, the fracture surface work increases slightly from 2.15×10^5 to 2.54×10^5 ergs/cm^2. The crack propagation in this region is not smooth and continuous, but consists of short jumps. Above the crack velocity of 20 m/sec, the fracture surface work further drops to 1.49×10^5 ergs/cm^2 at 53 m/sec. Above the crack velocity of 53 m/sec the fracture surface work rapidly increases as the crack velocity increases.

In a similar experiment carried out at the Naval Research Laboratory (13), results were obtained indicating that the peak in fracture surface work exists at the crack velocity of approximately 10 centimeters per second (Figure 58). Between the crack velocities of 2.5×10^{-4} and 6.5×10^{-2} m/sec, the fracture surface work values obtained in the Naval Research Laboratory and in this study are similar; however, the values obtained differ sharply above the crack velocity of 2.5 m/sec. Clark and Irwin studied the crack propagation behavior of Plexiglas utilizing ultrasonic-ripple markings to measure crack speed (49). They stated that the crack velocity of 157 ft/sec (48 m/sec) is the minimum stable crack speed for Plexiglas. They also quote from unpublished studies at Naval Research Laboratory stating that a crack in Plexiglas can be moved ahead in a smooth stable manner from a speed below 1 mm/sec to a speed of nearly 0.254 m/sec and that between 0.254 and 46 m/sec a variety of behaviors are possible at nearly the same driving force; furthermore, the crack extension is inherently unstable and the dominant response in this region consists in short run-arrest segments. The value 157 ft/sec (48 m/sec) as the minimum stable crack velocity closely matches the value obtained in this study at the onset of the rapid increase in

FIGURE 55. LOAD AND CRACK TIP POSITION VERSUS TIME RECORD AND FRACTURE SURFACE OF POLYSTYRENE TESTED AT 22°C AND CROSSHEAD RATE OF 9540 in/min.

Table 14. Fracture Surface Work and Crack Velocities of Polystyrene at 65 and 67°C

Temperature (°C)	Crosshead Rate (in/min)	Crack Velocity (meters/sec)	Fracture Surface Work (ergs/cm^2)
	0.02	1.63×10^{-4}	2.30×10^5
65	0.05	4.96×10^{-4}	2.05×10^5
	0.1	3.0×10^{-3} (estimated)	2.70×10^5
67	0.02	1.81×10^{-4}	2.29×10^5

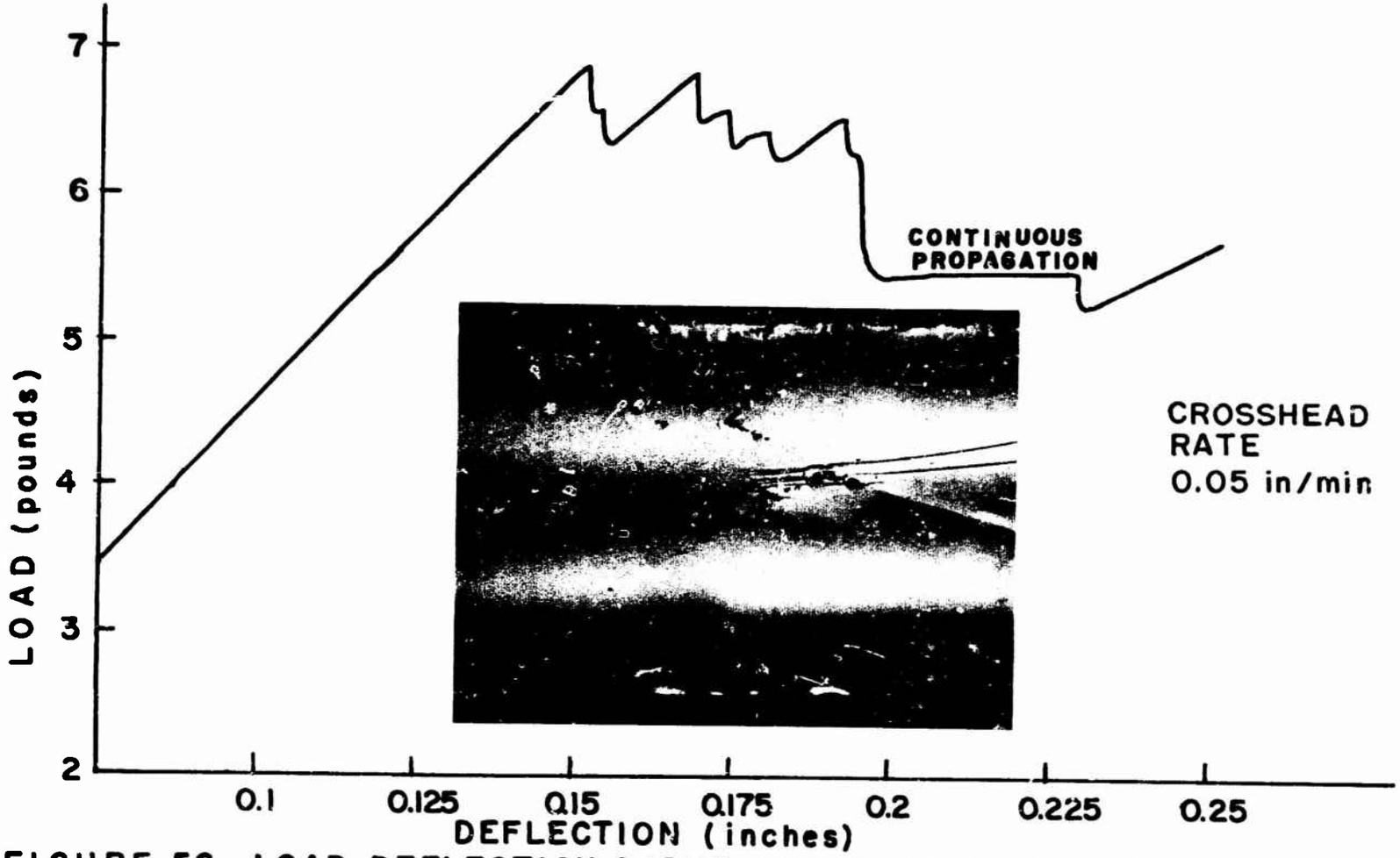

FIGURE 56. LOAD-DEFLECTION CURVE AND FRACTURE SURFACE OF POLYSTYRENE TESTED AT 65 °C SHOWING STABLE CONTINUOUS CRACK PROPAGATION REGION.

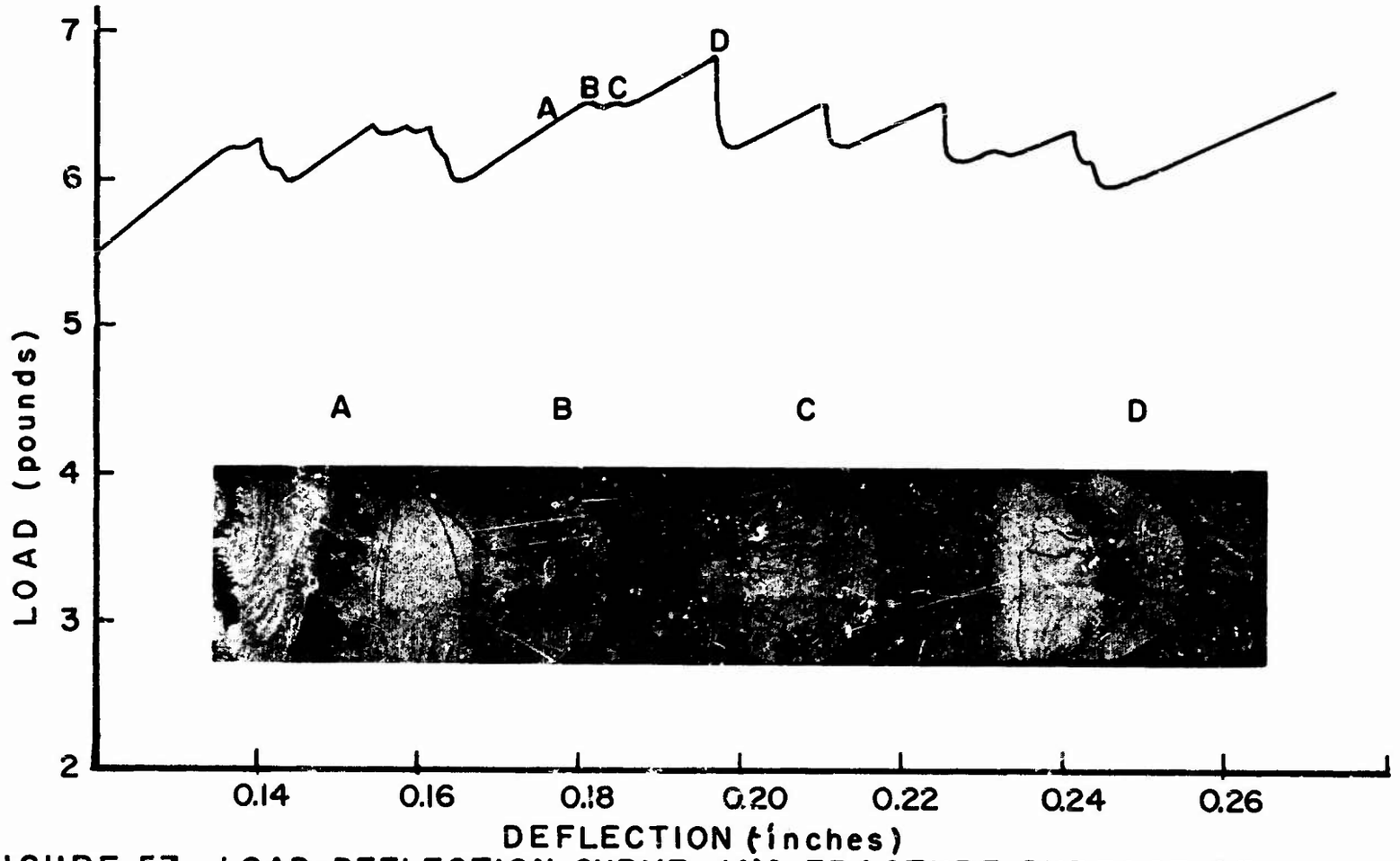

FIGURE 57. LOAD-DEFLECTION CURVE AND FRACTURE SURFACE OF POLYSTYRENE TESTED AT 65 °C.

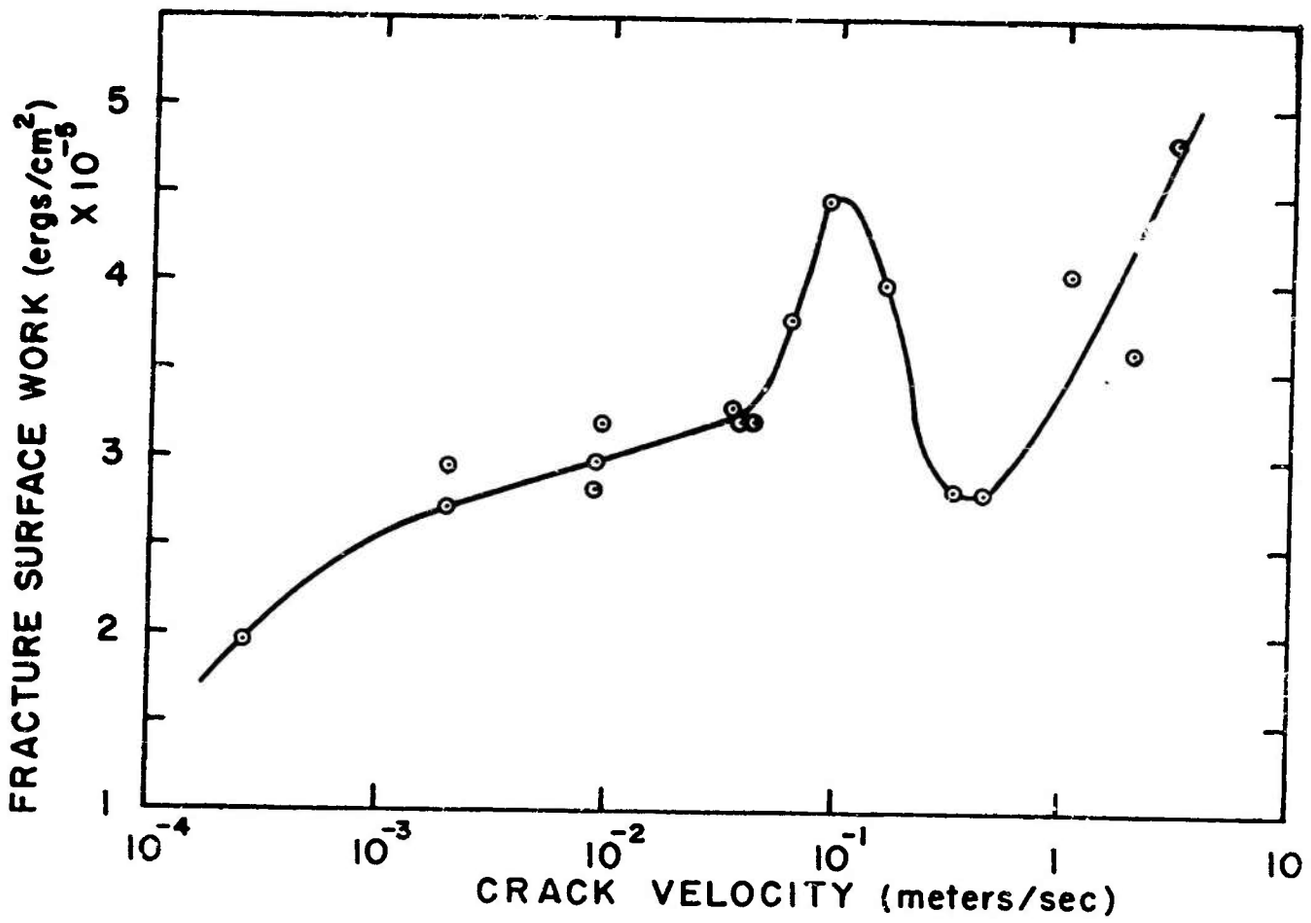

FIGURE 58. FRACTURE SURFACE WORK VERSUS CRACK VELOCITY FOR POLY(METHYL METHACRYLATE) (REF. 13).

fracture surface work shown in Figure 47. B. Cotterell has also studied velocity effects on fracture propagation in poly(methyl methacrylate) sheets (15). He stated that the fracture surface can be classified by appearance into four types which identify the velocity ranges (a) 0-700 ft/sec (0-213 m/sec), (b) 700-1700 ft/sec (213-520 m/sec), (c) 1700-2200 ft/sec (520-670 m/sec), and (d) greater than 2200 ft/sec. He observed that in the range (a) the fracture surface is glassy, smooth, and shows a distinctive color effect; in the range (b) the fracture surface shows hyperbolic markings which increases in density with increasing velocity; in the range (c) the fracture surface is very rough and at the lower end of this velocity range there are distinct periodic markings caused by discontinuous propagation similar to the chevron markings observed in steel at high crack propagation velocities. Fractures normally do not propagate in the range (d) at velocities over 2,200 ft/sec, but when they reach this velocity in poly(methyl methacrylate) they branch to two or three paths. At the present time the velocities obtained in this study are in the range (a), and there are some differences in the observed fracture surface appearance. When the crack velocity is below about 4 cm/sec, the fracture surface is generally smooth and sometimes a surface feature which can be described as a river pattern appears (Figures 38 and 39). In the crack velocity range between 4 and 6.5 cm/sec the fracture surface is flat, but some craze-like markings appear on the surface. By changing the focal point of the microscope one could observe that subsurface deformation took place. As the crack velocity approaches 6.5 cm/sec, the density of craze-like markings and subsurface deformation increases (Figures 40 and 41). In the crack velocity range between 6.5 cm/sec and 53 m/sec fingernail marks perpendicular to the direction of crack propagation appear on the mirror-smooth fracture surface at increasingly larger intervals as velocity increases (Figures 42, 43 and 44). We observed that these fingernail marks disappear above the crack velocity of 53 m/sec, and the fracture surface then has a uniformly mirror-smooth, colored appearance (Figure 45 and 46). Careful observations of these Figures 42, 43, 44, 45 and 46 further reveal that in the crack velocity range between 2.5 and 53 m/sec there exist two kinds of surface appearance corresponding to fast and slow crack propagation. In the slow crack propagation region one can see some subsurface deformation (for example, Figure 43). In the faster crack propagation region one can see parabolic markings (Figure 44). When the crack velocity is above 100 m/sec the fracture surface is covered uniformly by parabolic markings. When the crack velocity approaches 200 m/sec, complex fracture features start to appear regularly (Figure 46).

The effects of temperature and crack velocities were studied in the range of low crack velocities (less than 10 cm/sec). The fracture surface photographs (Figures 48, 49, 50, and 51) reveal that they can be classified into two groups: one group with flat surfaces and negligible subsurface deformation (Figures 48 and 49), and the other flat but with a lot of subsurface deformation (Figures 50 and 51). The fracture surfaces shown in Figures 50 and 51 look very rough, but these features are a result of optical diffraction due to subsurface deformation. These figures suggest that the mechanism of the fracture process at 40°C and 60°C, and the mechanism of the fracture process at -30°C and -20°C may be different. The fracture surface appearance of the specimens tested at room temperature shows that when the crack velocity is low (less than 4 cm/sec) the fracture surface features are similar to the group tested at 40°C and 60°C, and when the crack velocity is between 4 and 6.5 cm/sec, the fracture surface appearance becomes similar to the group tested at -30°C and -20°C. (See Figures 41, 50 and 51).

In the case of polystyrene the fracture surface work increases very rapidly as the crack velocity increases up to about 2.9×10^{-4} m/sec (Figure 54). At about 2.9×10^{-4} m/sec the crack propagation becomes very unstable and the crack starts to propagate discontinuously. This suggests that the fracture surface work in the crack velocity range above 2.9×10^{-4} m/sec is lower than that below 2.9×10^{-4} m/sec. It is very interesting to note that at room temperature the crack velocity at this instability point in polystyrene is a factor of 224 lower than that in poly(methyl methacrylate) (6.5×10^{-2} m/sec). It is clear from Figures 47 and 54 that in order to study the stable continuous crack propagation in polystyrene at room temperature it is necessary to select a testing speed more than 224 times lower than that for continuous crack propagation in poly(methyl methacrylate). In the stable continuous crack propagation region in polystyrene the fracture surface is mirror-smooth and distinctive colors are observed (Figure 56). The fracture surface work of polystyrene in this region is quite comparable to that of poly(methyl methacrylate). At 65°C the crack velocity range in which the crack propagation is continuous expands and a smooth colored surface becomes dominant despite the possibility of discontinuous crack propagation as shown in Figure 57.

CHAPTER V

CRACK PROPAGATION IN RUBBER MODIFIED ACRYLIC COPOLYMERS

A. Review of Properties of Rubber Modified Polymers

In addition to high dimensional stability, outstanding weatherability, and good mechanical strength —— a quality indicated by tensile strength of 8,000 - 11,000 psi and tensile modulus of $3.5 - 4.5 \times 10^5$ psi —— poly(methyl methacrylate) has excellent light transmittance properties. Total white light transmittance is 92 percent and haze measurements average only 1 percent (50). These properties make it highly useful in applications such as windows, display cases, modern furniture, wind screen, and face shields. Poly(methyl methacrylate) is, however, classified as a brittle material, and it exhibits brittle failure. When ballistically impacted, it fails in a complex manner with great amounts of internal crack initiation and propagation, which result in creation of numerous fragments. In such cases, persons near windows or structures made of poly(methyl methacrylate) may be injured by shattered plate fragments even though they are not in line with the trajectory of the object which hits the plate.

In order to improve impact and spallation resistance of brittle polymers such as polystyrene, epoxy, and poly(methyl methacrylate), modifications have been developed by inclusion of rubber particles in the polymeric matrix. Acrylic multipolymers thus obtained (called XT polymers by the developer) are reported to have a light transmission of 87% and a haze transmission ranging from 6 to 9 percent (51).

The modification with rubber particles has other advantages and disadvantages mentioned in Ref. 51 as follows:

1) XT-polymer* is said to have impact strength up to 15 times greater than canventional acrylics.
2) Stress cracking is reportedly no problem.
3) Stiffness is said to be four to five times that of high density polyethylene.
4) XT-polymer claims exceptional chemical properties, many of which are also found in acrylics.

However,

5) Weatherability, which is the outstanding property of acrylic, is not so good, and the new material is not recommended for any outdoor applications.

In this chapter fracture studies on commercial acrylic multipolymers (XT-500 and XT-375) and acrylic multipolymers with seven different rubber content levels are reported. The purpose of this research is to understand the influence of the rubber particle inclusion on the fracture toughness of the modified materials. Furthermore, it is the aim of this research to try to establish the relationships between different testing methods, and the viscoelastic parameters which are most

* Tradename, American Cyanamid Co.

influential on the fracture surface work. In this section existing data on mechanical and viscoelastic properties of plastic-rubber two-phase polymer systems, in addition to those of acrylic multipolymers, are reviewed.

Matsuo, Ueda and Kondo have studied the notched Charpy impact strengths of a series of plastic-rubber two-phase polymer systems —— blends of polyvinylchloride and rubbers with varying chemical structures and ABS palymers —— with respect to the results of dynamic viscoelastic measurement over a wide range of temperatures (52). First, in order to study the effects of the glass transition temperature of the rubber component they prepared four kinds of ABS plastics, each of which contained a rubber phase with a different glass transition temperature. Their composition of ABS polymers is shown in Table 15. The results of notched Charpy impact strength and dynamic loss modulus for these four materials versus temperatures are shown in Figure 59.

TABLE 15

COMPOSITION OF ABS POLYMERS (BY WEIGHT) (REF. 52)

Sample No.	Composition of Rubber Component		Composition of Plastic Component		T_g of Rubber Component
	Butadiene	Styrene	Acrylonitrile	Styrene	
GT-1	35	65	100	300	40°C
GT-2	55	45	100	300	-20°C
GT-3	65	35	100	300	-35°C
GT-4	100	0	100	300	-85°C

Secondly, in order to study the effects of adhesive forces between components they prepared two types of ABS polymers: the graft ABS and the blend ABS. They stated that the graft ABS exhibits stronger adhesive forces due to grafting or entanglement of the molecules at the boundaries. Their results are shown in Figure 60. Thirdly, they studied the effects of compatability between components with polyvinylchloride/rubber blends: incompatible system of polyvinlychloride/polybutadiene blend, semi-compatible system of polyvinylchloride/nitrile-butadiene rubber (acrylonitriie 20%) blend, and polyvinylchloride/nitrile-butadiene rubber (acrylonitile 40%) blend. For these three levels of blend compatibility their results are shown in Figure 61.

Imasawa and Matsuo studied the yield stress (σ_y) and elongation to break (ε_b) for a series of polyvinylchloride-rubber blends, ABS polymer and high-impact polystyrenes over a wide range of temperatures under three different rates ($\dot{\varepsilon}$) (53). The materials used in Ref. 53 are the same as in Ref. 52.

Their results of yield stress and elongation to break for three levels of blend compatibility are shown in Figure 62. To these yield stress results they applied the time and temperature superposition principle and obtained composite curves of yield stress reduced to 20°C. These curves are shown in Figure 63. They also obtained similar curves for the graft and the blend-ABS, and the high-impact

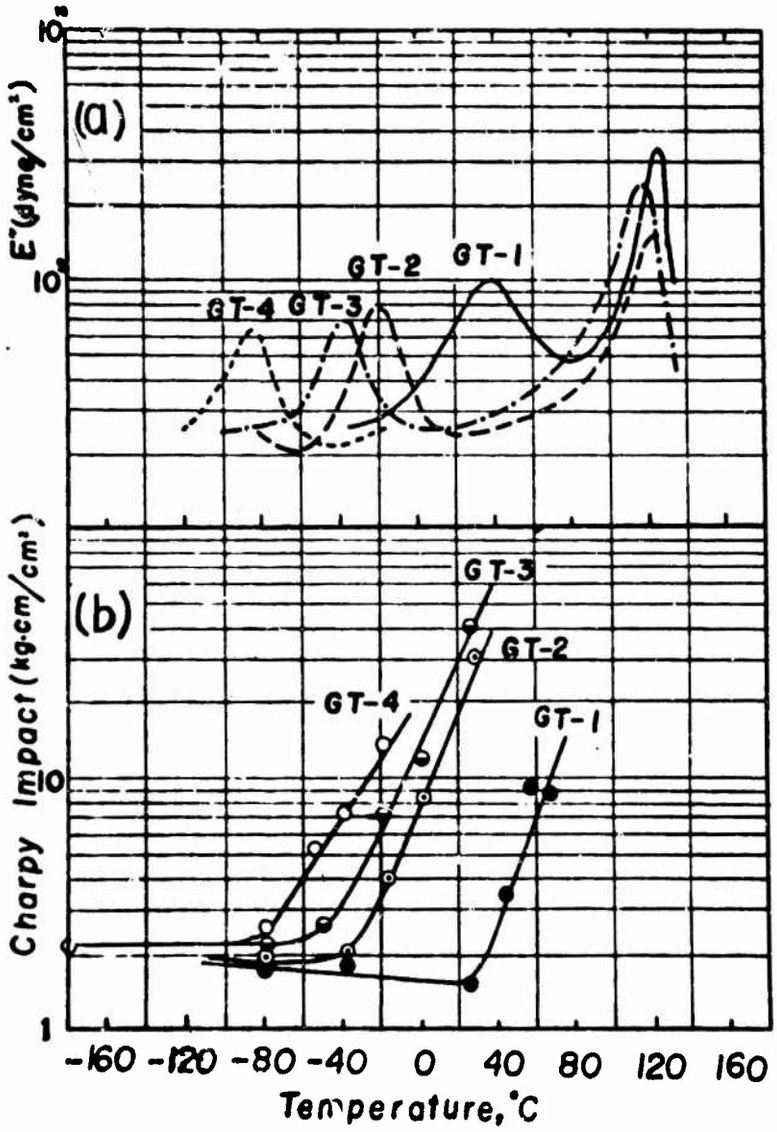

FIGURE 59. TEMPERATURE DEPENDENCES OF DYNAMIC LOSS MODULUS (E") AND CHARPY IMPACT STRENGTH FOR ABS PLASTICS (MATSUO, UEDA, AND KONDO, REF. 52).

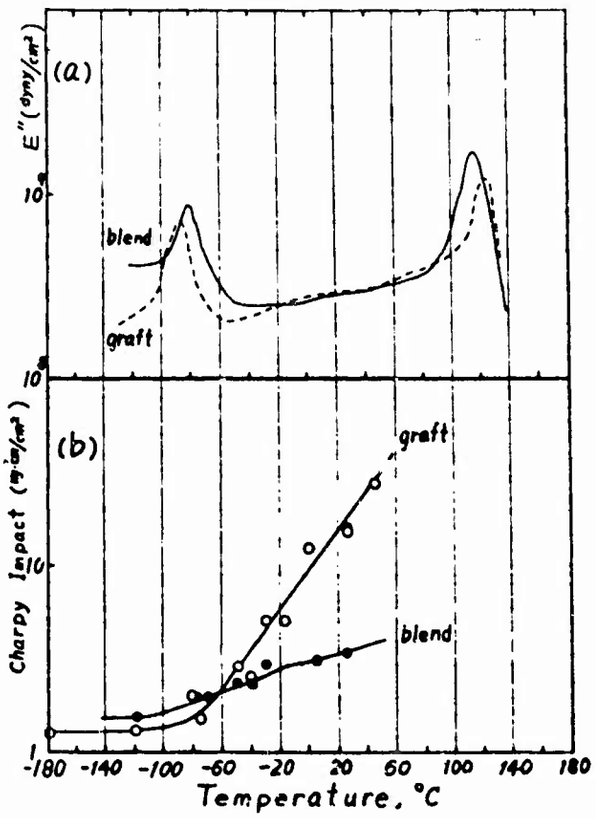

FIGURE 60. TEMPERATURE DEPENDENCES OF E" AND CHARPY IMPACT STRENGTH FOR GRAFT- AND BLEND-ABS (MATSUO, UEDA, AND KONDO REF. 52).

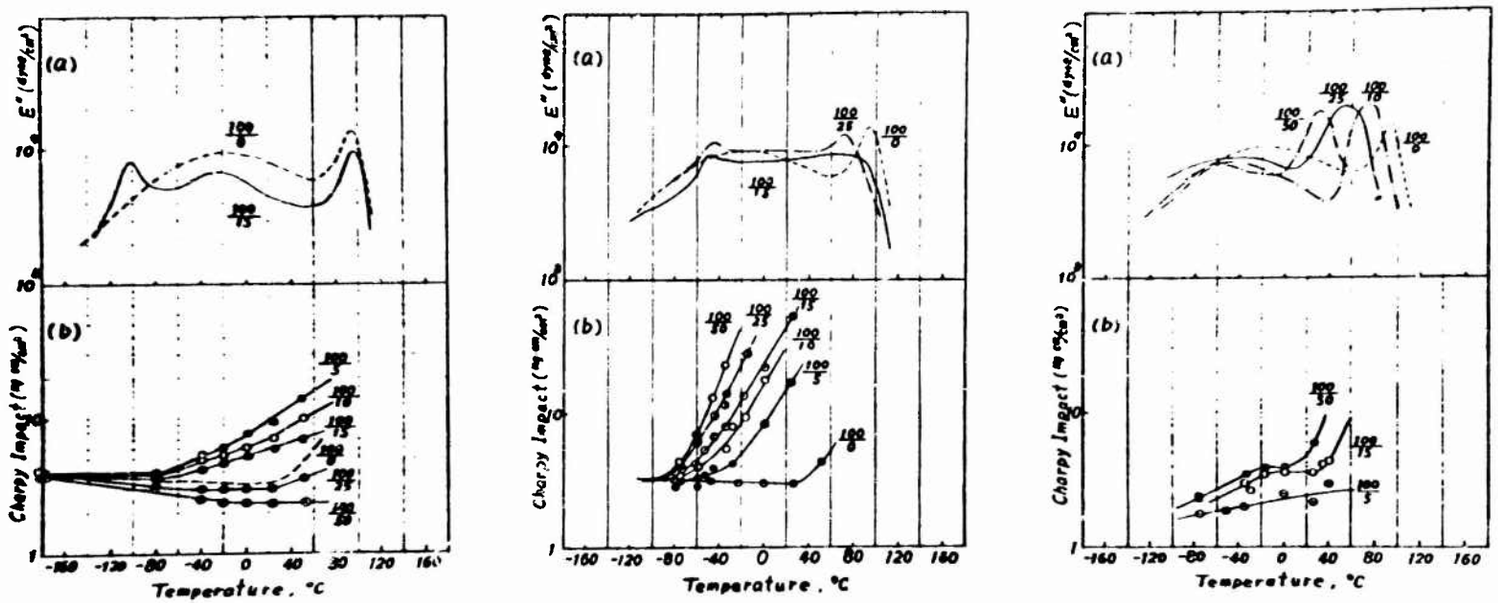

a) PVC/PBD BLENDS (INCOMPATIBLE SYSTEM)

b) PVC/NBR-20 BLENDS (SEMI-COMPATIBLE SYSTEM)

c) PVC/NBR-40 BLENDS (COMPATIBLE SYSTEM)

FIGURE 61. TEMPERATURE DEPENDENCES OF DYNAMIC LOSS MODULUS (E") AND CHARPY IMPACT STRENGTH FOR THREE LEVELS OF COMPATIBILITY SYSTEMS (MATSUO, UEDA, AND KONDO, REF. 52).

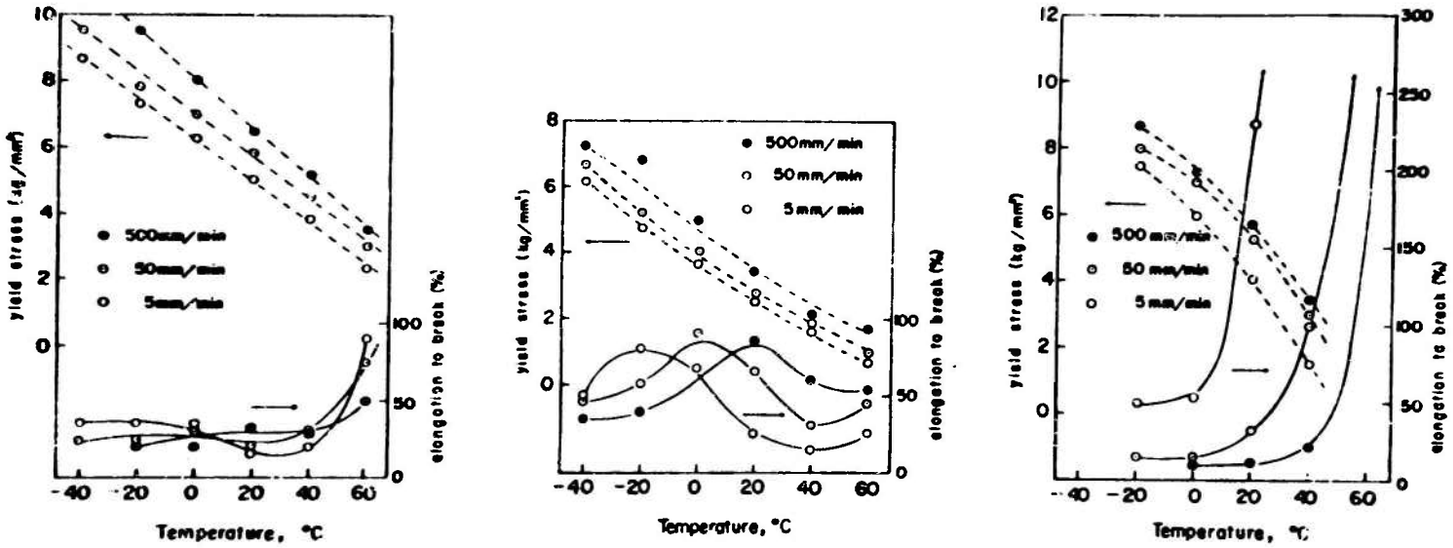

a) PVC/PBD (100/5) BLEND (INCOMPATIBLE SYSTEM)

b) PVC/NBR-20(100/15) BLEND (SEMI-COMPATIBLE SYSTEM)

c) PVC/NBR-40(100/10) BLEND (COMPATIBLE SYSTEM)

FIGURE 62. TEMPERATURE DEPENDENCES OF YIELD STRESS AND ELONGATION-TO-BREAK FOR THREE LEVELS OF COMPATIBILITY SYSTEMS (IMASAWA AND MATSUO, REF. 53).

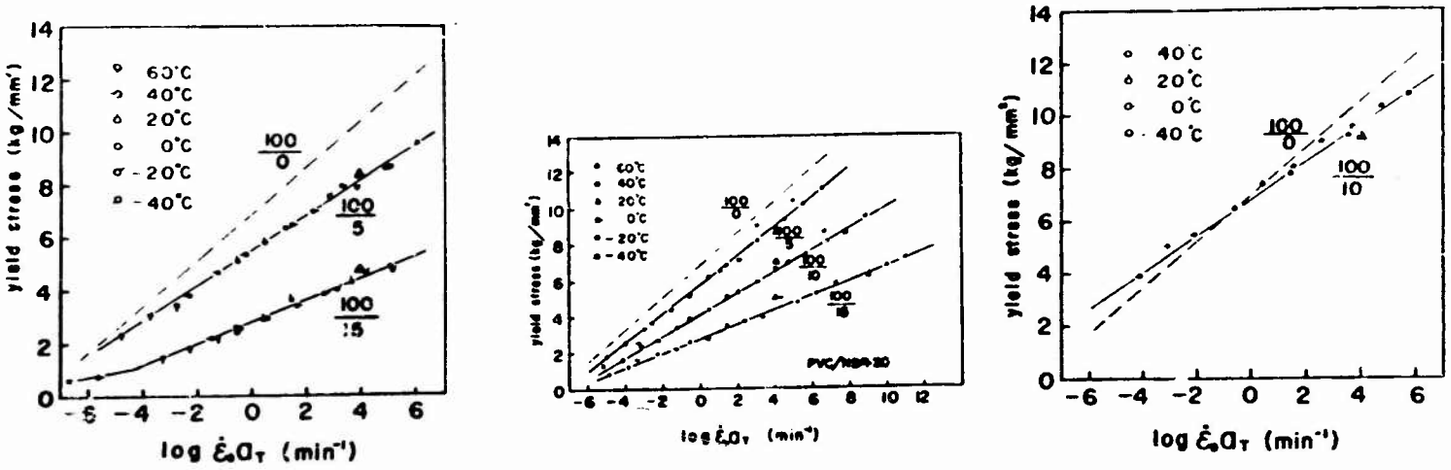

a) PVC/PBD BLENDS (INCOMPATIBLE SYSTEM)

b) PVC/NBR-20 BLENDS (SEMI-COMPATIBLE SYSTEM)

c) PVC/NBR-40 BLENDS (COMPATIBLE SYSTEM)

FIGURE 63. COMPOSITE CURVES OF YIELD STRESS FOR THREE LEVELS OF COMPATIBILITY SYSTEM (IMASAWA AND MATSUO, REF. 53).

polystyrene. These are shawn in Figure 64. The results shawn in Figure 59 to Figure 64 are typically observed in dealing with the plastic-rubber twa-phase polymer systems and demonstrate well the effects of a rubber phase on physical properties. Some common phenomena associated with this are:

1) Compatible blend systems do not exhibit the loss modulus peak corresponding to the glass transition temperature of the rubber component, and the loss modulus peak temperature of the compatible blend system decreases proportionately as the rubber content increases (Figure 61-C).

2) The impact value begins to increase at the temperature approximately corresponding to the glass transition temperature of the rubber component and continues to increase with increasing temperature above the glass transition temperature of the rubber component (Figure 59, 60 and 61).

Boyer surveyed the existing theories concerned with the interpretation of the role of the rubber loss peak in the rubber modified materials and the toughening mechanism (45). He listed the following proposals:

1) Schmitt and Keskkula proposed that numerous cracks initiated by rubber particles contribute to the high impact strength.

2) Newman and Strella proposed that the large energy absorption involved in the cold drawing of the matrix results in high toughness.

3) Bucknall and Smith added the refinement that numerous crazes initiated by the rubber particles contribute largely to high impact strength since craze formation absorbs a lot of energy.

4) Kambour believes that the rubber particles initiate numerous crazes while at the same time preventing any craze from developing into a catastrophic crack. The evidence may be seen in Figure 60 which exhibits that by increasing the adhesive forces between components the impact strength increases.

5) Bucknall and Street have shown the temperature dependence of impact energy absarptian which changes in about the same manner as the total extent of craze formatian daes in the vicinity of the fracture.

Matsuo, Ueda, and Konda have also attempted to explain the phenamena that the Charpy impact strength increases as the temperature increases above the glass transition temperatures of the rubber components from a standpaint of craze formation contribution an high impact strength (52). In their argument they first showed that a Charpy impact strength (I) was expressed by the following equation in terms of the temperatu e (T) above the glass transition temperature of the rubber component:

$$I = A \exp\left(-\frac{B}{T}\right), \quad T \geq Tg \tag{36}$$

where A and B are constants.
Then they stated that the impact fracturing process of these systems might involve some activation process since the above equation had the same form as the Arrhenius equation. They further stated that in their previous work they had discussed that the stress-crazing was the main energy dissipation mechanism of plastic-rubber

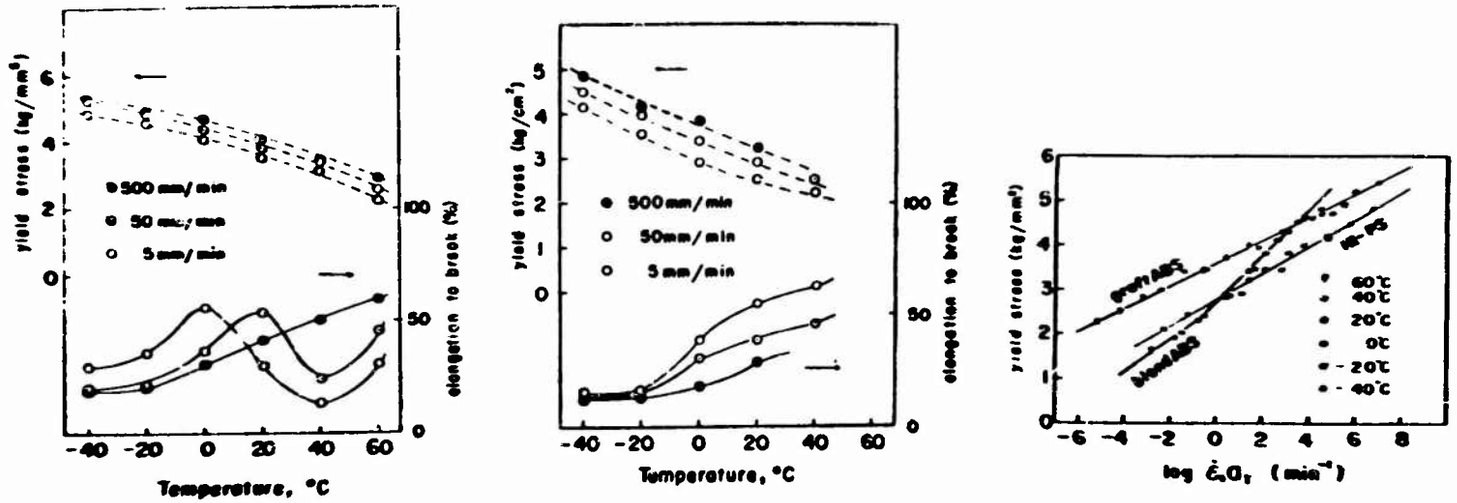

a) GRAFT-ABS

b) COMMERCIAL HIGH-IMPACT POLYSTYRENE

c) GRAFT- AND BLEND-ABS, AND HIGH-IMPACT POLY-STYRENE

FIGURE 64. TEMPERATURE DEPENDENCES OF YIELD STRESS AND ELONGATION-TO-BREAK AND COMPOSITE CURVES OF YIELD STRESS FOR GRAFT- AND BLEND-ABS AND HIGH-IMPACT POLYSTYRENE (REF. 53).

systems. Thus they combined these two points and stated that the B value in the above equation corresponds to the activation energy of the crazing process.

Up to this point the discussion of the impact strength of the plastic-rubber two-phase polymer is based on the data of the notched Charpy impact tests and dynamic viscoelastic measurements. Nielsen (54), however, emphasized that the Izod and Charpy tests use a standard specimen which gives results that cannot be compared with specimens of other dimensions. The data therefore have no absolute physical significance. He further wrote that these tests do not measure the true energy required to fracture the specimen, since they measure the energy to permanently deform the moterial ond the energy to throw the broken ends of the specimen in addition to the energy to initiate and propagate the crack through the specimen. In an effort to find a better testing method to relate part performance ta material properties, simulated abuse tests such as the folling dart have been developed. Nielsen (54) wrote that this type of test generally correlates much better with field tests and practical experience than does the pendulum type, and it also can measure just the energy which forms a crack rather than the total energy which completely fractures the specimen. However, the dart drop type test has some disadvantages such as narrow range of test speeds, lack of sensitivity, large material and man-power requirements, and inability to measure stress and strain. In order to over-come these disadvantages Furno, Webb, and Cook developed an instrumental puncture test in which a specimen was clamped between two plates with a one inch diameter test surface exposed and a plunger, a 1/4 inch steel rod with a spherical end, is forced through the center of the exposed test area at the desired speed (55). The puncture speed they used was 1 to 11,000 inches per minute and the load-head travel curve incorporated with reference pulse of known frequency was recorded on an oscilloscope. Analysis of these curves revealed that a distinct pattern exists on the maximum load versus test speed plots. This is demonstrated in Figure 65 where the results of two ABS plastics — Cycolac Brand Polymer Grade T and Cycolon Brand Polymer Grade AM — and high impact polystyrene are shown.

Malpass (56) utilized the same instrumented puncture test described above and studied the room-temperature impact behavior of a wide range of commerical ABS copolymers and other thermoplostics. He found that up to velocities of more than 1,000 inches per minute the resistance to puncture of ABS polymers and the majority of blends containing ABS is related to deformation velocity by an exponential function. At higher velocities the puncture strength increases rapidly with the logarithm of test velocity. Contrary to the study by Furno, Webb and Cook, no definite critical velocities have been found in Malposs' experiment. Nevertheless, some indications of critical velocity at higher test speeds was indicated beyond the upper limit of the testing range. Concerning the puncture strength of ABS resin, Malpass speculates that the exponential puncture strength behavior of ABS polymers and the majority of blends containing ABS up to the test speeds of more than 1,000 in/min may conform to an activated cold flow process in the same manner that the Eyring theory of flow is applicable to describe the yield stress of rubber-modified polystyrene as a function of strain rate and temperature. Malpass in this study also carried out the high speed tensile test and the notched Izod impact test for ABS polymers and PVC/ABS blends. His results of ABS polymers are shown in Table 16. He commented on these results that the good correlation between notched Izod ond tensile fracture energy shows that change in strain rate does not disturb the general pattern of impact energy behavior with respect to ABS composition. He

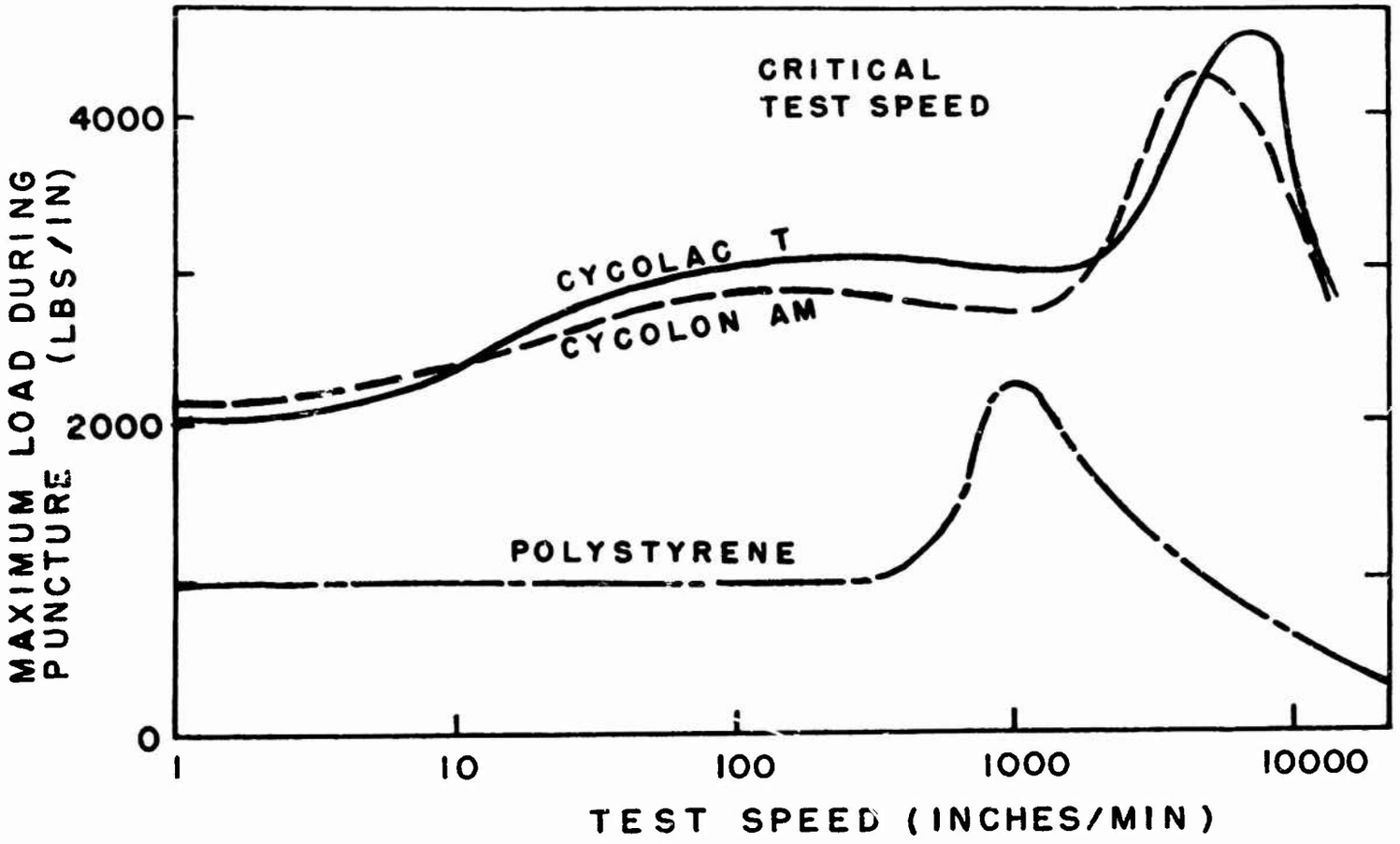

FIGURE 65. LOAD-TEST SPEED CURVES FOR TWO ABS PLASTICS AND POLYSTYRENE (FURNO, WEBB, AND COOK, REF. 55).

Table 16. Comparison of PSAN and ABS Tensile Puncture and Notched Izod Impact Properties (Ref. 56)

Polymer	Diene,%	Tensile strength,psi		Apparent shear strength,psi	
		0.2 in./min.	12,000 in./min.	0.2 in./min.	12,000 in./min.
PSAN*	0	11,300	10,400	1,600	1,376
ABS I	15	6,300	9,940	3,600	9,700
ABS II	20	5,900	8,800	3,200	8,500
ABS III	30	4,800	8,500	2,400	7,400
ABS IV	50	1,600	3,000	900	4,900

*PSAN: Styrene-acrylonitrile Copolymer

Polymer	Tensile Fracture Energy at 12,000 in./min., ft.-lb./in.^{2}	Puncture Energy at 12,000 in./min., ft.-lb./in.^{2}	Notched Izod Impact Energy, ft.-lb./in. notch
PSAN	25	7	0.5
ABS I	84	94	3.1
ABS II	149	88	5.1
ABS III	154	78	7.5
ABS IV	-	61	6.6

further stated that this good correlation indicates the tensile character of the notched Izod test as applied to ABS polymers. Malpass noted the difference between high speed puncture energy and notched Izod impact energy might be attributed to a combination of two factors —— higher strain rate and severe stress concentration due to a notch —— and the complex multiaxial loading condition of the puncture test. Figure 66 constructed by Furno, Webb, and Cook (55) shows graphically the relative test speeds employed in various laboratory mechanical tests.

So far the general behaviors of plastic-rubber two-phase polymers under different testing methods have been reviewed by taking high impact polystyrene, ABS, and PVC/NBR blends as examples. The mechanical properties of acrylic multipolymers will be discussed from this point on. The commerical acrylic multipolymer (XT polymer) was developed about seven years ago, but sufficient data characterizing material structure and viscoelastic properties is not available. The available data are reviewed here. The XT polymer is produced in four different grades: XT-500, XT-375, XT-250, and XT-150. The typical properties of XT polymers are shown in Table 17.

Lewis, Roylance and Thomas (57) at the Army Materials and Mechanics Research Center, Watertown, Massachusetts have studied mechanical properties, ballistic resistance, and puncture performance of acrylic multipolymer with seven different rubber content levels in an effort to develop transparent high ballistic resistant and non-spallation material. The results of their tests of tensile modulus and yield stress of these materials measured by a standard Instron test at an elongation rate of 7 percent/minute are shown in Figure 67. The ballistic resistance of these same materials against 17 grain, 22 caliber, fragment simulation is shown in Figure 68. These results indicate that the maximum ballistic resistance occurs at 10 percent rubber content at the lowest areal density (0.093 inches thick); however, as the thickness increases to 0.156 inches, the materials containing 10 percent or more rubber show the same ballistic resistance, and at the highest areal density (0.250 inches thick) the maximum ballistic resistance occurs at 13 percent instead of 10 percent. They comment that this shift of the optimum ballistic energy absorption to higher rubber contents appears to be caused by the increasing rate of loading. In addition to the ballistic test Lewis, Roylance and Thomas (57) performed the puncture tests of which results are shown in Figure 69. Their results show that at low puncture rates (20 inches per minute) the material with 10 percent rubber content exhibits the optimum work to puncture, but at higher rates (11,700 inches per minute) the materials with 13 percent and 16 percent rubber exhibit higher work than 10 percent.

With this background, the fracture behavior of acrylic multipolymers will be discussed next.

B. Experimental Studies of Crack Propagation in Acrylic Multipolymers

In the previous section the effects of chemical structure and composition in plastic-rubber two-phase systems on the dynamic viscoelastic measurement was reviewed. In addition, mechanical properties such as impact strength, yield stress and elongation at break were reviewed. Various impact tests such as Charpy, Izod and sheet puncture tests were discussed. These various testing methods give contradictory trends for impact strength measured as a function, for example, of rubber

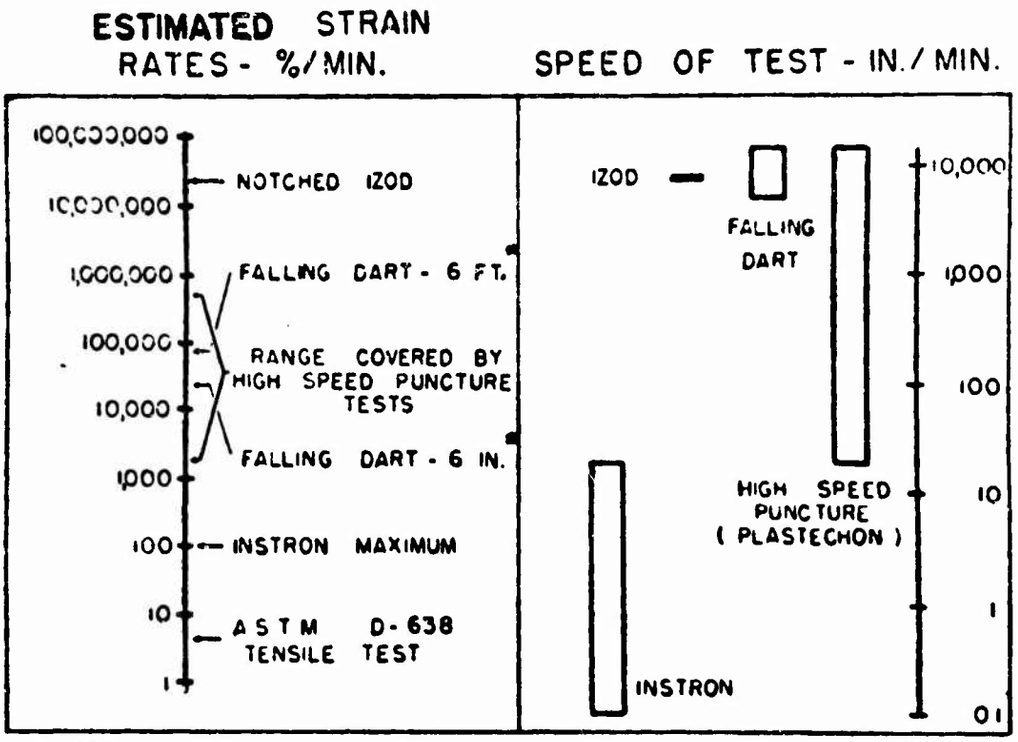

ASTERISKS IN GRAPH INDICATE AVERAGE STRAIN RATE

FIGURE 66. RELATIVE TEST SPEEDS EMPLOYED IN VARIOUS LABORATORY MECHANICAL TESTS (FURNO, WEBB, AND COOK, REF.55).

TABLE 17.

TYPICAL PROPERTIES OF XT-POLYMERS (REF. 51)

PROPERTY	ASTM METHOD	XT-500	XT-375	XT-250	XT-150
Notched					
Izod impact strength (ft. lb./in. of notch)	D-256-56				
1/4 in. bar					
73°F		3.0	2.0	1.0	0.7
32°F		2.3		0.9	0.7
-40°F		1.6	1.2	0.9	0.7
Tensile strength (psi)	D-638-60T	6000	7000	8000	9000
Tensile elongation (%)	D-638-60T				
at yield		3.6	3.6	3.6	4.0
at break		40	28	15	12
Flexural strength (psi)	D-790-59T	9500	11000	13000	16500
Flexural modulus (psi)	D-790-59T	300000	350000	400000	460000
Rockwell hardness	D-785-60T	R108 M24	R114 M45	R119 M68	R120 M73
Deflection temperature (°F) at 264 psi	D-648-56	193	194	195	198
Light transmission (%)	D-307-44	87	87	87	87
Haze (%)	D-1003-52	9	9	8	6
Specific gravity	D-792	1.09	1.10	1.12	1.14

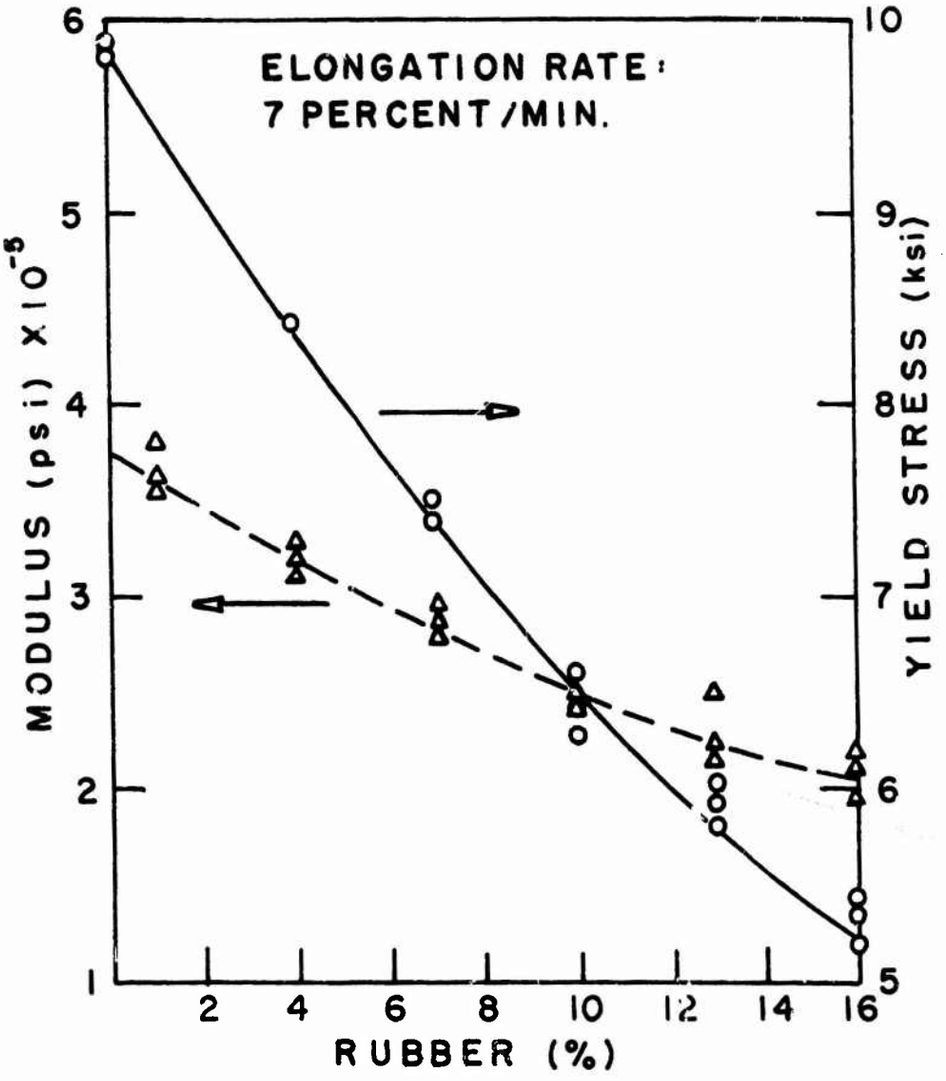

FIGURE 67. TENSILE MODULUS AND YIELD STRESS OF RUBBUR MODIFIED POLY(METHYL METHACRYLATE) (LEWIS, ROYLANCE, AND THOMAS, REF. 57).

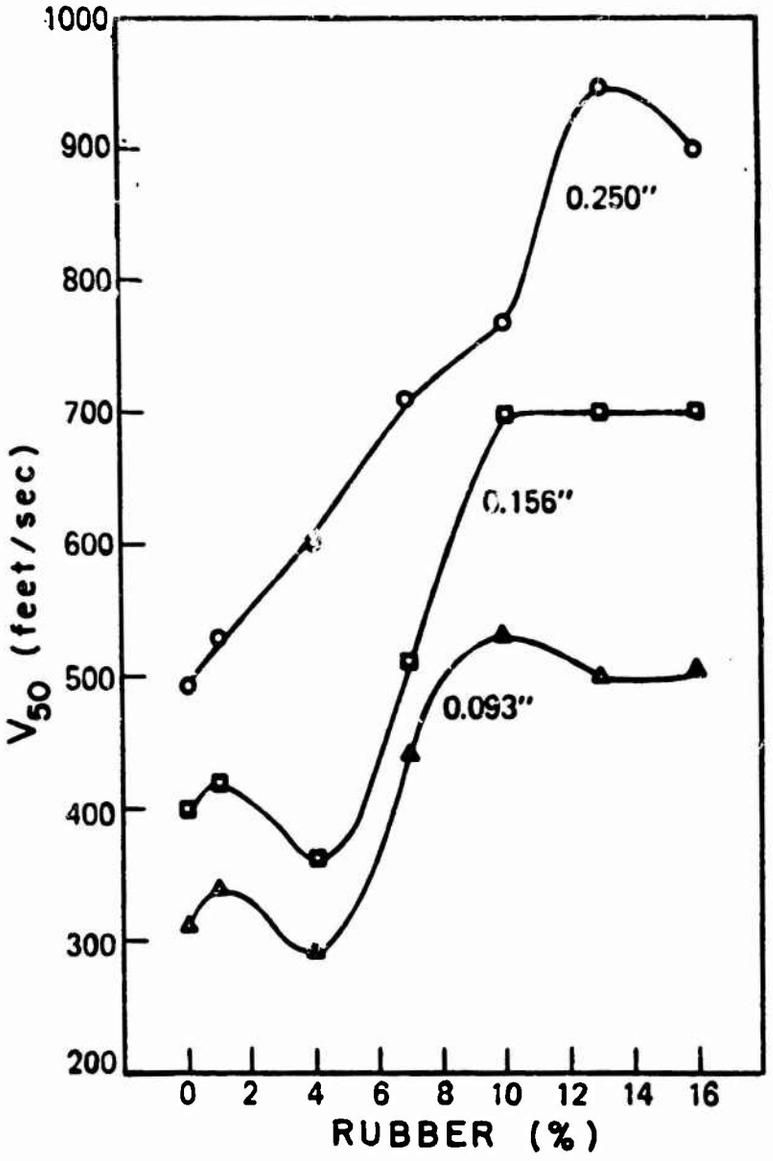

FIGURE 68. V_{50} BALLISTIC LIMIT OF RUBBER-MODIFIED POLY(METHYL METHACRYLATE) AS A FUNCTION OF RUBBER CONTENT FOR 17-GRAIN-22 CALIBER FRAGMENT SIMULATORS (REF. 57).

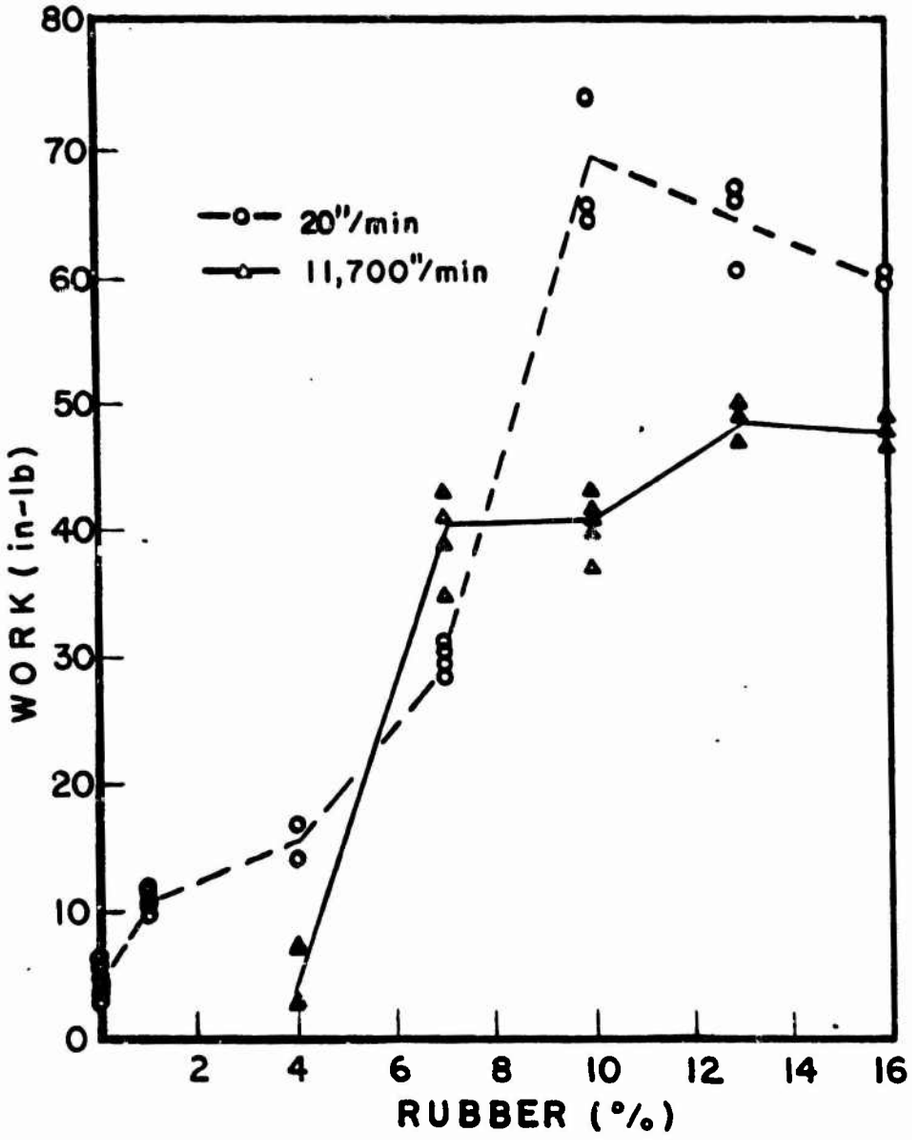

FIGURE 69. WORK TO PUNCTURE AT LOW (20"/min) AND HIGH (11,700"/min) RATES AS A FUNCTION OF RUBBER CONTENT (REF. 57).

content. As demonstrated in Table 16, tensile fracture energy and notched Izod impact energy increase as the rubber percentage increases however, puncture energy decreases as the rubber percentage increases. Since the purpose of a rubber modified acrylic is to imprave the impact properties of the acrylic phase, it is important nat anly to find the structure and camposition af plastic-rubber two-phase systems which maximize the impact and fracture strength, but also to establish praper testing methods. Fracture surface wark measurements far acrylic multipalymers have been made in the study in arder to increase the existing knawledge concerning the fracture behaviar af these systems and to attempt ta find correlations among variaus testing methods.

By using sandwich tapered double contilever beam cleavage specimens the fracture surface work was determined as a function of crack velacity for two grades af commercial acrylic multipolymers (XT-500 and XT-375) and for acrylic multi-palymers with seven different rubber cam.nt levels (rubber contents 0, 1, 4, 7, 10, 13 and 16 percent). All materials were abtained in injection malded plate form (10in x 10in x 0.1in). In additian, XT-500 palymer was obtained in extruded sheet form of different thicknesses (0.10in and 0.06in). All injection malded plates were faund to have high residual stresses. The fallawing annealing process was therefore applied to the material in order ta eliminate residual stresses:

1) The plates were subjected ta 100°C temperature far 10 hours.
2) Then the temperature was lawered ta raom temperature at a cooling rate af 5°C per 10 minutes.

After the annealing pracess a 1/8 inch thick Plexiglas plate was glued an each side with acrylic adhesive (PS-30*), thus creating a sandwich specimen structure. The adhesive was cured at a temperature af 50°C under 50 psi pressure for four hours. Then side graaves and initial crack were machined with a specially designed side groove cutting machine which was discussed in Chapter II. While cutting the grooves, water saluble ail (J-coal+ #230) was used with a ratio af 10 parts af water to one part oil and sprayed with campressed air in order ta eliminate heat generation in the cutting area. Immediately after machining the side grooves and initial crack, specimens were washed tharoughly with water to remove the water saluble oil. Excess water was remaved with compressed air.

The next step in the specimen preparatian was machining the cantour of the tapered double cantilever beam specimen and the twa loading pin hales. After this, eight silver canductive paint lines were drawn at half inch intervals for crack velacity measurements in the high speed testing. Specimen testing was done in an Instran testing machine at law crasshead rates (0.02 to 5 inches per minute) and in a serva-contralled hydraulic high speed loading machine at high crasshead rates (10 to 7,000 inches per minute). In law speed tests crack tip positions were visually abserved and marked an the laad-displacement chart from which crack velacities were calculated. In high speed tests conductive paint lines generated voltage drops when the crack passed and brake each line, and from the records of voltage draps versus

* Trade name; Cadillac Plastics and Chemical Company

+ Trade name; Johnsan Wax Campany

time, crack velocities were obtained. From the load deflection records and crack tip position, the experimental compliance change was calculated and used to determine the fracture surface work. The fracture surface work thus obtained was plotted on the graph against crack velocities. These procedures are explained in detail in Chapter III.

Figure 70 shows the experimental results of fracture surface work versus crack velocity for two grades of commercial acrylic multipolymers (XT-500 and XT-375). These results are also tabulated in Table 18. The XT-500 polymer has two peaks on the curve of fracture surface work versus crack velocity within the experimental crack velocity range (from 10^{-4} to 10^{-2} meters/sec). XT-375 shows one peak in this crack velocity range; however, the trend of the curve of fracture surface work versus crack velocity suggests that there may be another peak at a crack velocity lower than those used in this experiment. The fracture surface work behavior at crack velocities below 10^{-1} meters/sec is much different for the XT-500 and XT-375 materials. However, in the crack velocity range above 10^{-1} meters/sec, the values of fracture surface work for XT-500 and XT-375 are nearly identical to one another. The major material composition difference between XT-500 and XT-375 is apparently the rubber concentration; therefore, it can be concluded that the effect of rubber concentration appears very predominantly in the crack velocity range below 10^{-1} meters/sec but not above 10^{-1} meters/sec. Furthermore, it is proposed that the peak of the fracture surface work versus crack velocity curve for XT-375 at approximately 10^{-3} meters/sec corresponds to the one for XT-500 at 1.5×10^{-2} meters/sec. The peak for XT-500 at the crack velocity of 2.2×10^{-2} meters/sec may correspond to one for XT-375 at a velocity less than those used in these studies. Some of the load-deflection curves and fracture surface photographs for XT-500 and XT-375 are shown in Figures 71, 72, 73 for XT-500 and 74, 75, 76 for XT-375. On the fracture surface stress-whitening phenomena were observed for both XT-500 and XT-375 in the entire measured crack velocity range. Fracture surface roughness is, however, quite dependent upon crack velocity. As shown in Figures 71, 72 for XT-500 and 74, 75 for XT-375, fracture surface roughness caused by pulled out material is seen when the crack velocity is low. When the crack velocity exceeds 10^{-1} meters/sec, the fracture surface becomes mirror smooth as shown in Figure 73 and 76.

In order to study specifically the effects of rubber concentration on fracture behavior of acrylic multipolymers, materials with seven different rubber content levels were tested. This material was obtained from the U.S. Army Materials and Mechanics Research Center. The fracture surface work results for these materials are shown in Figure 77, and tabulated in Table 19. Figure 77 suggests that the effects of rubber concentration on fracture surface work can be compared on the basis of the magnitude and position of the peaks on the curve of fracture surface work versus crack velocity. Acrylic multipolymers with rubber concentrations of 1, 4 and 7 percent exhibit a peak in fracture surface work at a crack velocity of approximately 10^{-4} meters/sec. At higher crack velocities, the fracture surface work for these materials decreases with increasing crack velocity. For the material with 7 percent rubber, the fracture surface work starts to increase again at 10^{-1} meters/sec. The same behavior is expected to occur in materials with 1 and 4 percent rubber, although the velocity at which the second increase in fracture surface work occurs may be different.

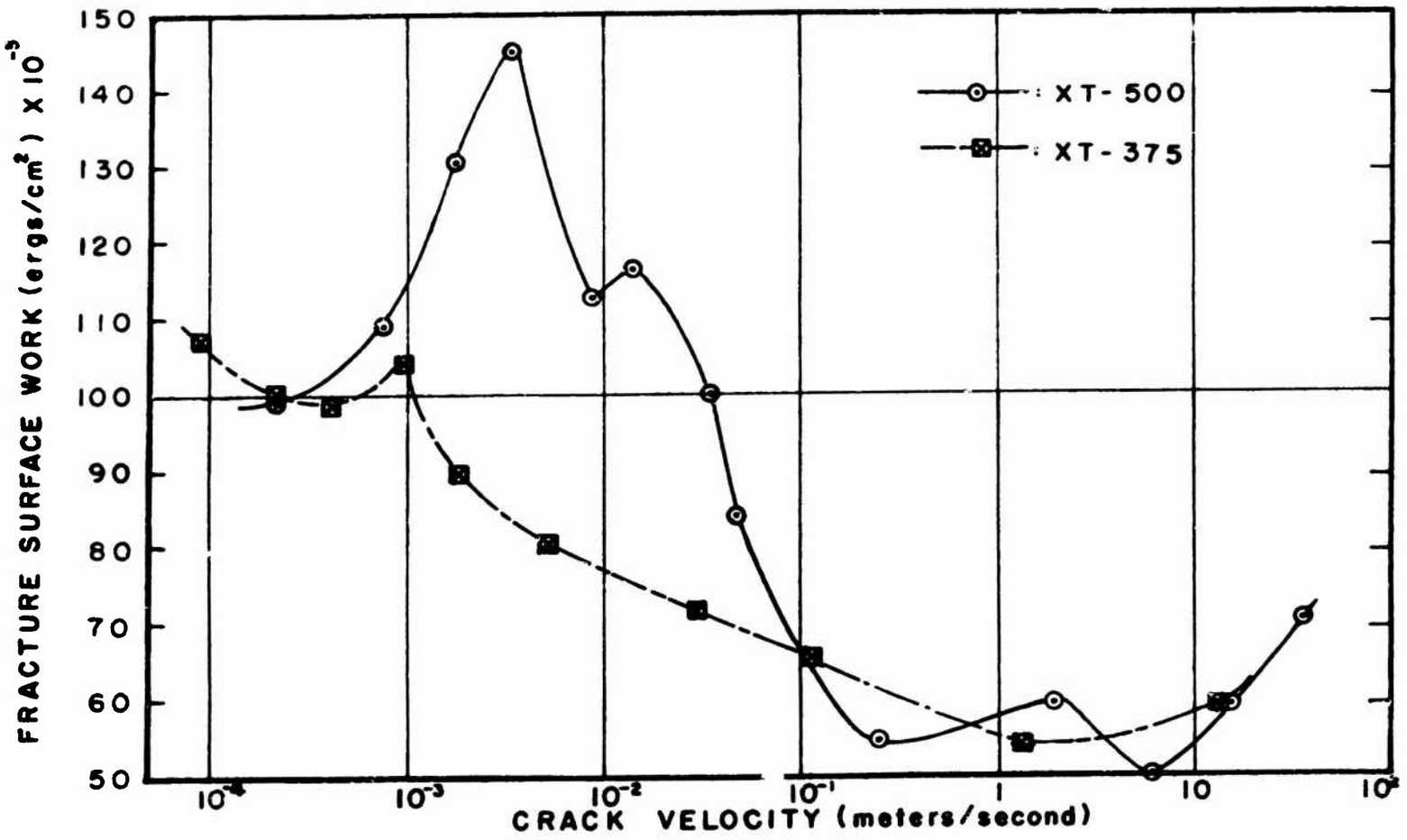

FIGURE 70. FRACTURE SURFACE WORK FOR XT-POLYMERS.

Table 18. Experimental Results of Fracture Surface Work and Crack Velocities for XT-500 and XT-375

Material	Cross Head Rate (inches/min)	Crack Velocity (meters/sec)	Fracture Surface Work (ergs/cm^2)
XT-500	0.1	2.12×10^{-4}	98.4×10^5
	0.5	7.56×10^{-4}	108.5×10^5
	1.0	1.69×10^{-3}	130.5×10^5
	2.0	3.18×10^{-3}	143.5×10^5
	5.0	8.77×10^{-3}	112.8×10^5
	10.0	1.41×10^{-2}	116.5×10^5
	20.0	3.63×10^{-2}	100.0×10^5
	30.0	4.61×10^{-2}	83.5×10^5
	94.8	2.54×10^{-1}	54.6×10^5
	300	8.24×10^{-1}	54.6×10^5
	621	1.89	60.3×10^5
	1560	6.06	50.0×10^5
	3450	10.7	60.2×10^5
	7560	37.8	74.2×10^5
XT-375	0.05	9.10×10^{-5}	107.2×10^5
	0.1	2.00×10^{-4}	101.9×10^5
	0.2	4.15×10^{-4}	98.0×10^5
	0.5	9.85×10^{-4}	103.9×10^5
	1.0	1.75×10^{-3}	89.8×10^5
	2.0	5.16×10^{-3}	80.9×10^5
	9.8	3.03×10^{-2}	73.6×10^5

Table 18 (Continued)

Material	Cross Head Rate (inches/min)	Crack Velocity (meters/sec)	Fracture Surface Work ($ergs/cm^2$)
XT-375	49.6	1.23×10^{-1}	$65.-\times 10^5$
	500	1.46	59.6×10^5
	5143	9.7	62.9×10^5
	10800	29.9	56.2×10^5

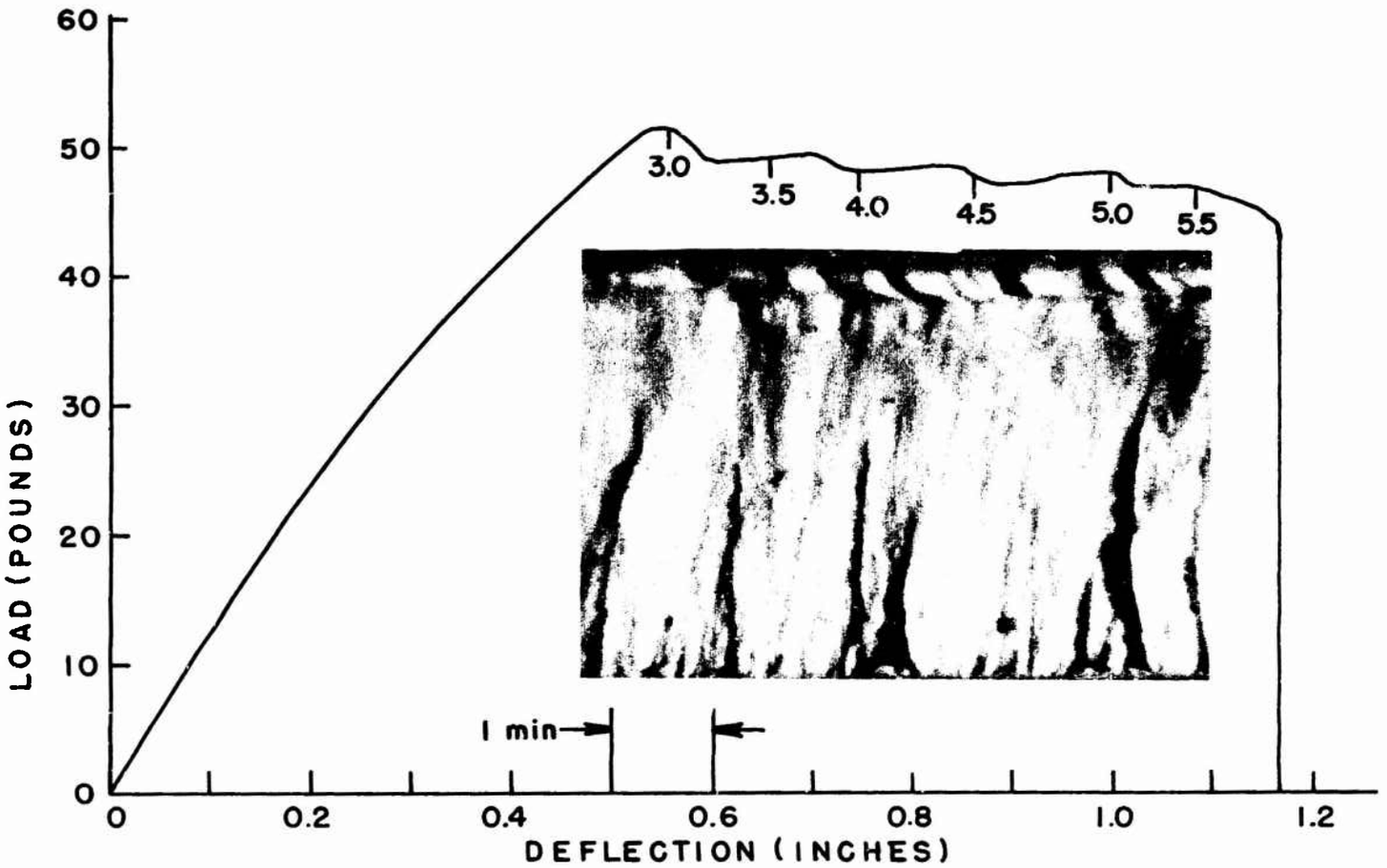

FIGURE 71. LOAD-DEFLECTION CURVE AND FRACTURE SURFACE OF XT-500 TESTED AT CROSSHEAD RATE OF 0.1 IN/MIN.

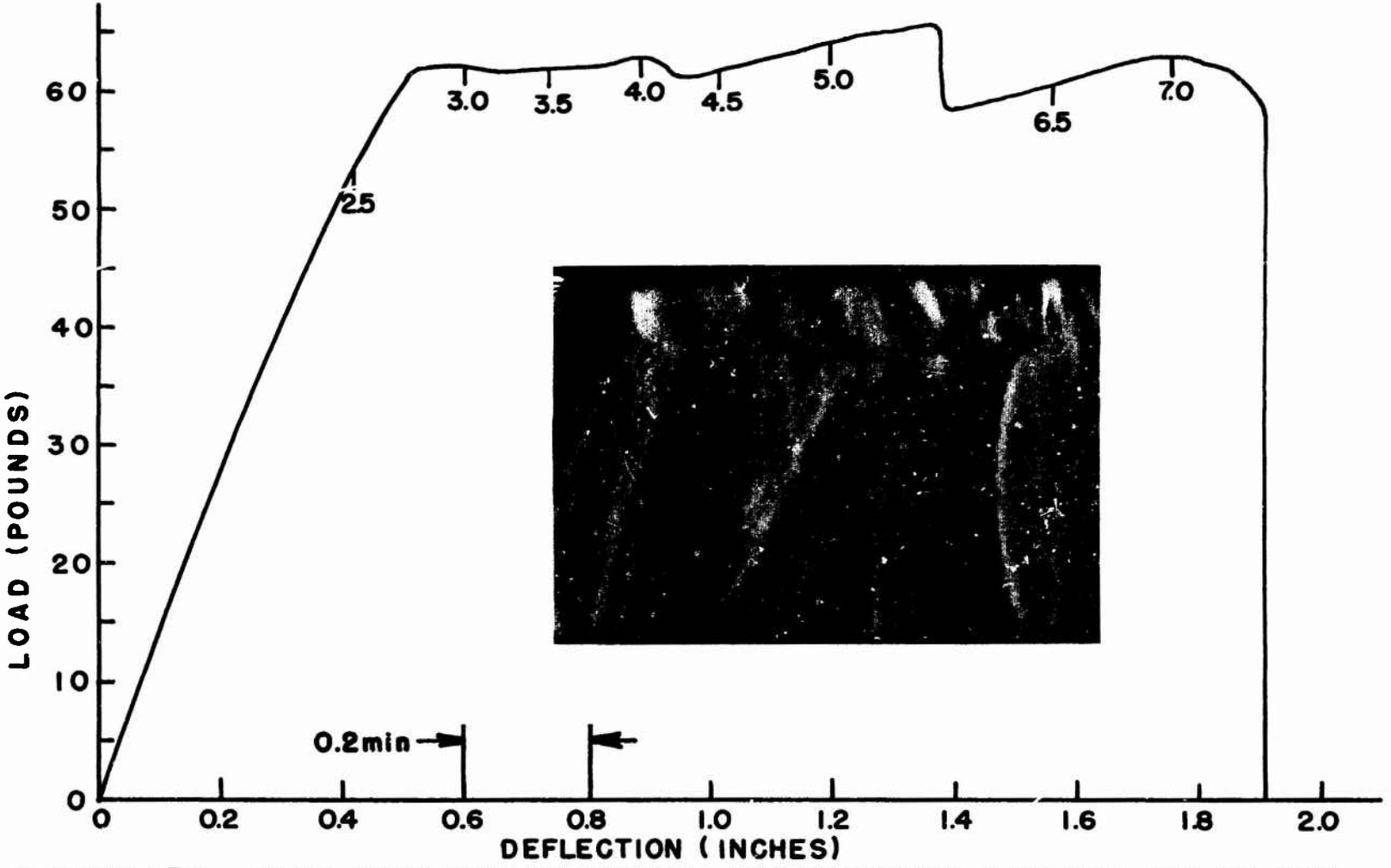

FIGURE 72. LOAD-DEFLECTION CURVE AND FRACTURE SURFACE OF XT-500 TESTED AT CROSSHEAD RATE OF 2 IN/MIN.

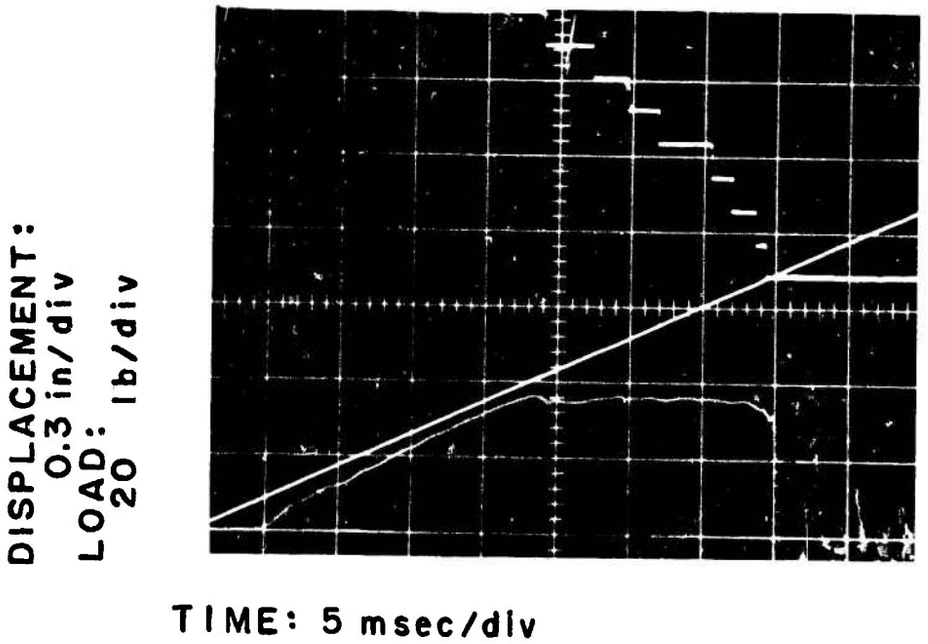

FIGURE 73. LOAD, DEFLECTION, CRACK TIP POSITION RECORD AND FRACTURE SURFACE OF XT-500 TESTED AT CROSSHEAD RATE OF 1560 in/min.

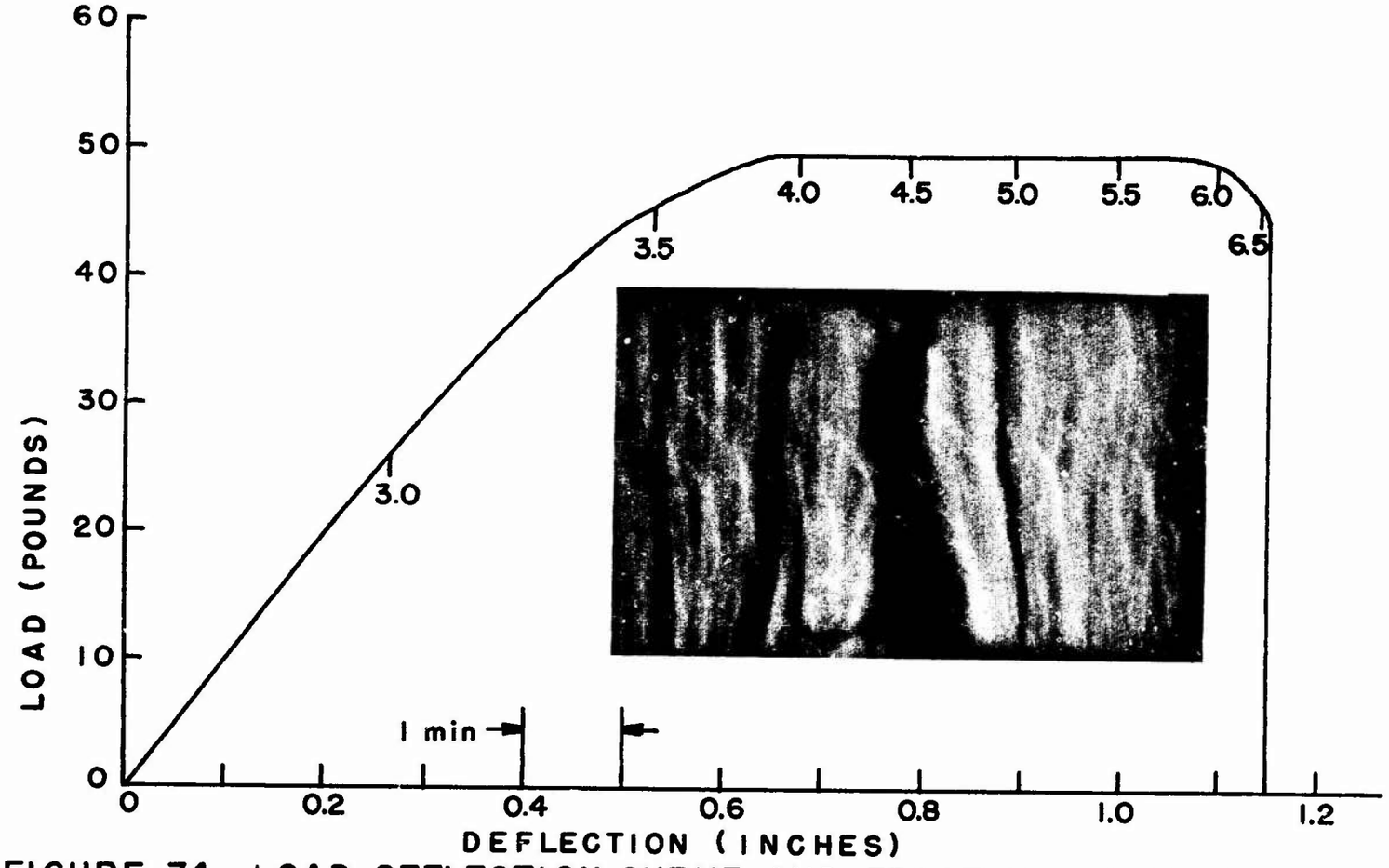

FIGURE 74. LOAD-DEFLECTION CURVE AND FRACTURE SURFACE OF XT-375 TESTED AT CROSSHEAD RATE OF 0.1 IN/MIN.

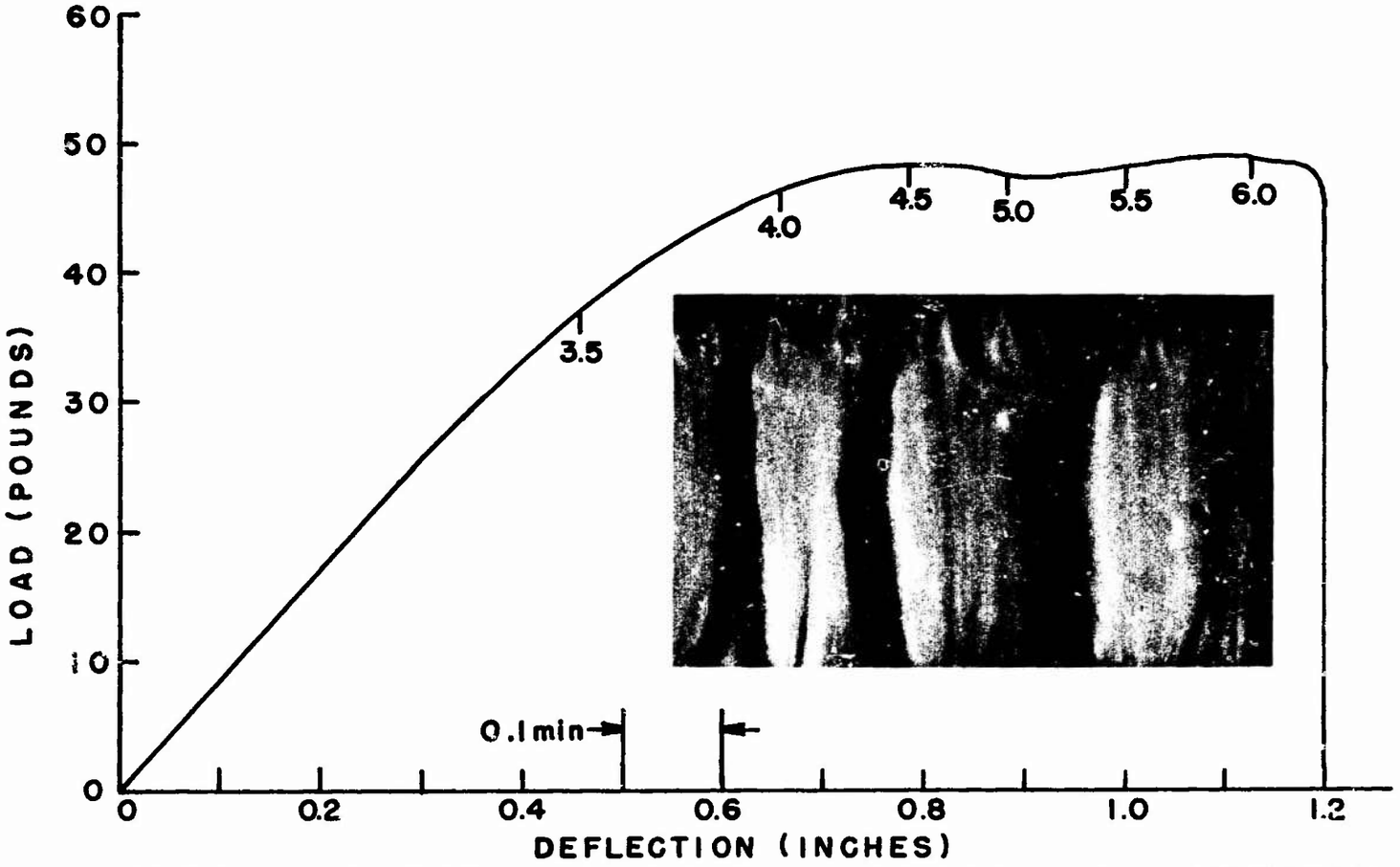

FIGURE 75. LOAD-DEFLECTION CURVE AND FRACTURE SURFACE OF XT-375 TESTED AT CROSSHEAD RATE OF 1 IN/MIN.

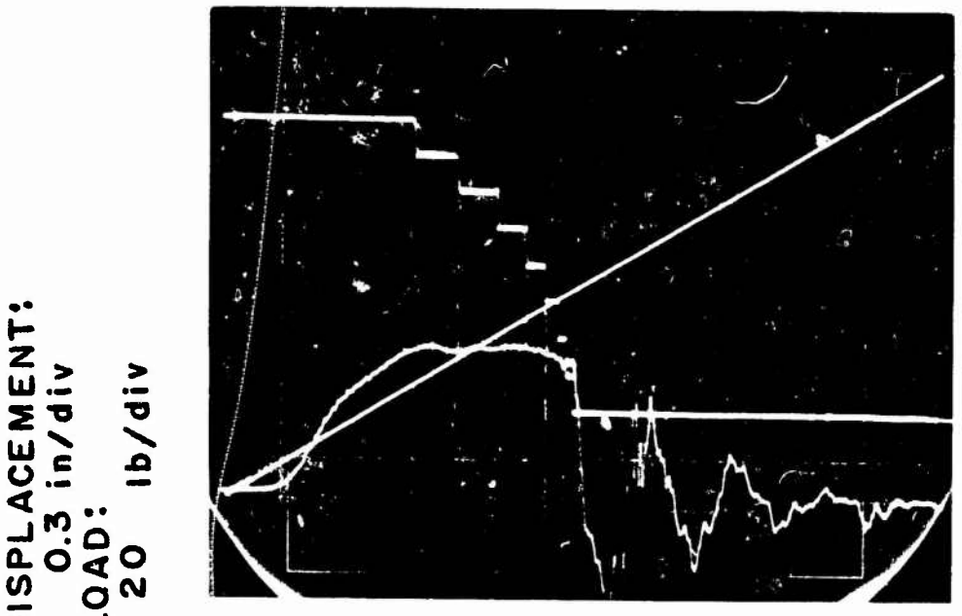

CRACK VELOCITY: 9.7 meters/sec

FIGURE 76. LOAD, DEFLECTION, CRACK TIP POSITION RECORD AND FRACTURE SURFACE OF XT-375 TESTED AT CROSSHEAD RATE OF 5143 in/min.

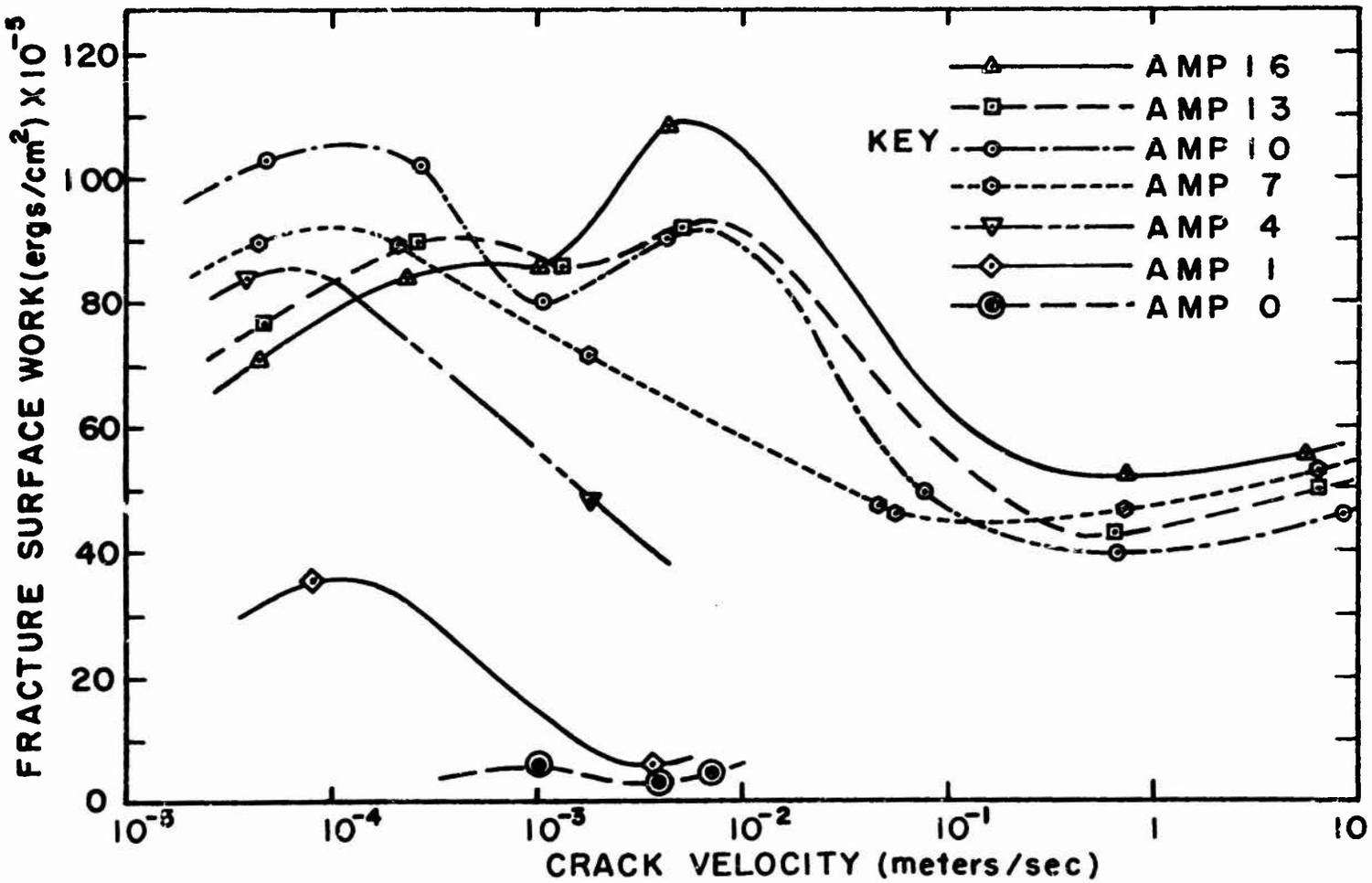

FIGURE 77 FRACTURE SURFACE WORK VERSUS CRACK VELOCITY FOR ACRYLIC MULTIPOLYMERS

Table 19. Experimental Results of Fracture Surface Work and Crack Ve ocities for Acrylic Multipolymers with Seven Different Rubber Content Levels

Material	Cross Head Rate (inches/min)	Crack Velocity (meters/sec)	Fracture Surface Work (ergs/cm^2)
AMP0	0.2	1.09×10^{-3}	5.19×10^{5}
	0.5	4.00×10^{-3}	2.73×10^{5}
	1.0	7.26×10^{-3}	4.04×10^{5}
AMP1	0.02	8.02×10^{-5}	35.0×10^{5}
	0.5	3.53×10^{-3}	5.45×10^{5}
AMP4	0.02	3.72×10^{-5}	89.0×10^{5}
	0.5	1.75×10^{-3}	48.2×10^{5}
AMP7	0.02	4.29×10^{-5}	89.0×10^{5}
	0.1	2.07×10^{-4}	88.7×10^{5}
	0.5	1.77×10^{-3}	71.5×10^{5}
	2.0	--	58.8×10^{5}
	19.8	4.73×10^{-2}	47.0×10^{5}
	19.8	5.59×10^{-2}	45.5×10^{5}
	196	7.30×10^{-1}	46.8×10^{5}
	2130	6.44	53.0×10^{5}
AMP10	0.02	4.60×10^{-5}	103×10^{5}
	0.1	2.49×10^{-4}	102×10^{5}
	0.5	1.05×10^{-3}	79.5×10^{5}
	2.0	4.95×10^{-3}	91.3×10^{5}

Table 19 (Continued)

Material	Cross Head Rate inches/min	Crack Velocity meters/sec	Fracture Surface Work ergs/cm^2
AMP 10	19.8	7.42×10^{-2}	49.0×10^5
	196	6.67×10^{-1}	40.2×10^5
	2130	8.35	45.4×10^5
AMP13	0.02	4.41×10^{-5}	77.3×10^5
	0.1	2.47×10^{-4}	90.8×10^5
	0.5	1.21×10^{-3}	85.8×10^5
	2.0	4.18×10^{-3}	90.8×10^5
	196	6.35×10^{-1}	42.6×10^5
	2130	6.20	50.4×10^5
AMP16	0.02	4.34×10^{-5}	71.2×10^5
	0.1	2.23×10^{-4}	94.0×10^5
	0.5	1.01×10^{-3}	85.2×10^5
	2.0	4.23×10^{-3}	107.5×10^5
	196	7.48×10^{-1}	51.9×10^5
	2130	5.76	54.1×10^5

The acrylic multipalymer with 10 percent rubber exhibits two peaks in fracture surface work: one at 10^{-4} meters/sec (similar to materials with 1, 4 and 7 percent rubber) and another at approximately 6×10^{-3} meters/sec crack velocity. Above the crack velocity of 6×10^{-3} meters/sec the fracture surface work decreases as the crack velocity increases up to 6×10^{-1} meters/sec. Thereafter, fracture surface work increases again slightly (similar to material with 7 percent rubber).

The acrylic multipalymers with 13 and 16 percent rubber exhibit diminishing peaks (also called shoulders) at approximately 3×10^{-4} meters/sec crack velocity. The magnitude of peak height for the material with 16 percent rubber is smaller than that for the material with 13 percent rubber. These materials also have secondary peaks in fracture surface work at approximately 6×10^{-3} meters/sec crack velocity (similar to material with 10 percent rubber). The magnitude of the peak for the material with 16 percent rubber is much larger than that far the material with 13 percent rubber. Above the crack velocity of 6×10^{-3} meters/sec, fracture surface wark of materials with 13 and 16 percent rubber decreases as the crack velocity increases up to 6×10^{-1} meters/sec; thereafter, fracture surface work increases again slightly (similar to materials with 7 and 10 percent rubber).

From these observations, it can be said that fracture surface work of acrylic multipolymers appears to increase as the rubber percentage increases from 1 to 10 in the crack velocity range up to 10^{-4} meters/sec. In materials with rubber content greater than 10 percent an opposite trend appears. For those with rubber contents of 13 and 16 percent, Figure 77 shows that fracture surface work decreases as the rubber percentage increases above 10 percent. In the crack velocity range between 10^{-4} and 10^{-3} meters/sec, fracture surface work versus crack velocity curves cross each other without showing a definite order. In the crack velocity range between 10^{-3} and 10^{-1} meters/sec, the order in the locations of the fracture surface work curves is the same as that of the rubber percentage. In other words, the higher the rubber percentage, the higher the value of fracture surface work. This suggests that the secondary peaks on the curves of fracture surface work and crack velocity may be related salely to the rubber phase contribution to the fracture surface work. In the crack velocity range above approximately 6×10^{-1} meters/sec, the fracture surface work of acrylic multipolymers with 7, 10, 13 and 16 percent rubber appear to increase at the same rate. The fracture surface work in this crack velocity range is greatest far the 16 percent rubber material, followed by the 7, 13 and 10 percent materials. The effects of rubber concentrotion on fracture surface work at various crack velocities, are shown in Figure 78. The values of fracture surface work at three crack velocities (5×10^{-5}, 5×10^{-3} and 6 meters/sec) are replotted from Figure 77.

At this point it is of interest to compare the trend in fracture surface work behavior of acrylic multipolymers with the trends observed by other testing methods such as the notched Izod impact tests, puncture tests, and ballistic tests. The results of the notched Izod impact tesrs are shown in Figure 79. The ballistic resistance results and puncture energy results are shown in Figures 68 and 69 respectively in Section A of this chapter. First, the results of the notched Izod impact test show that the material with 7 percent rubber exhibits higher impact resistance than the materials with 10 and 13 percent rubber. The same trend is seen in the results of fracture surface work at the crack velocity of 6 meters/sec shown in Figure 78. The trends seen in the puncture results at low (20 in/min) and high (11,700 in/min) rates

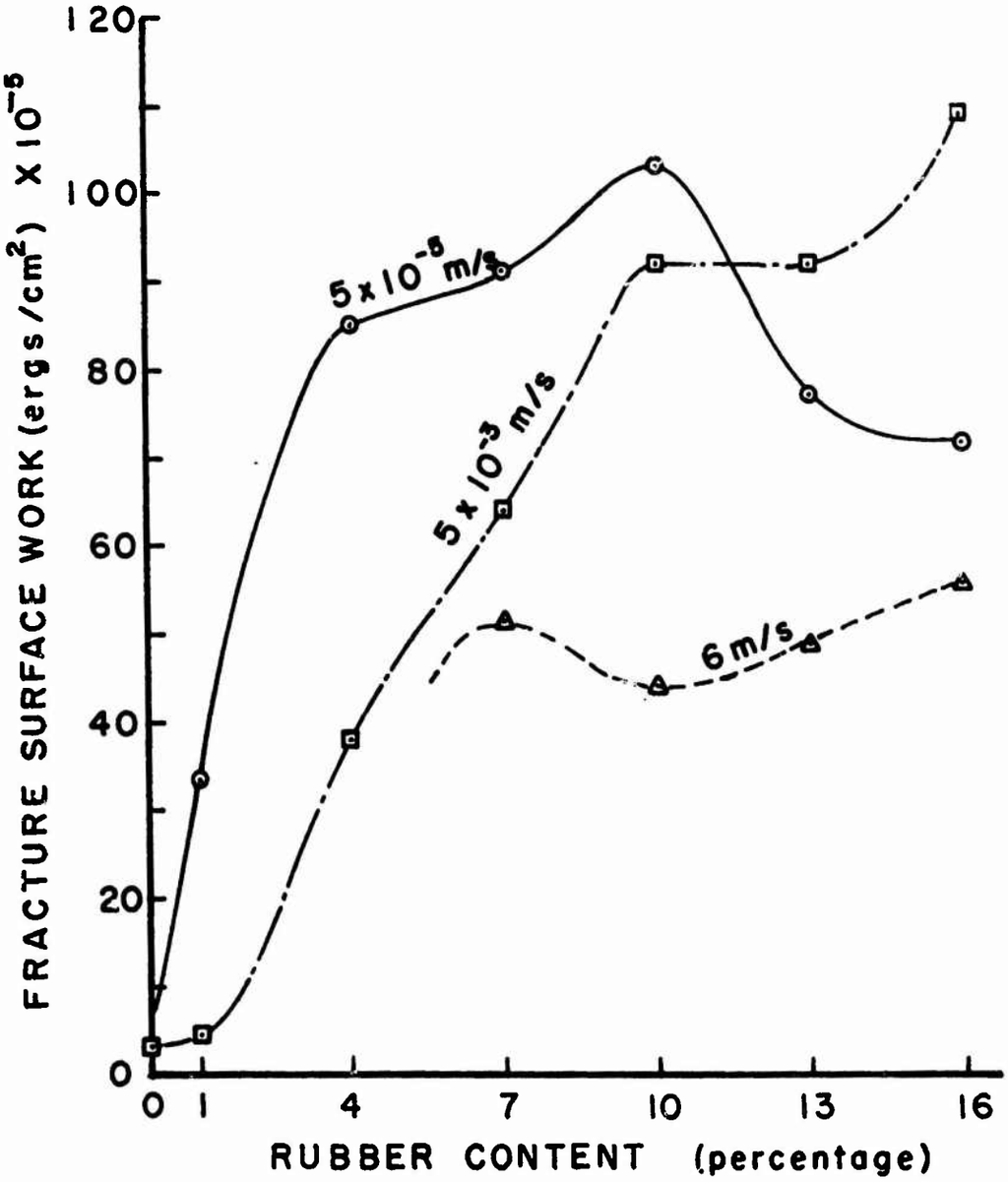

FIGURE 78. FRACTURE SURFACE WORK OF ACRYLIC MULTIPOLYMERS AT THREE DIFFERENT CRACK VELOCITIES.

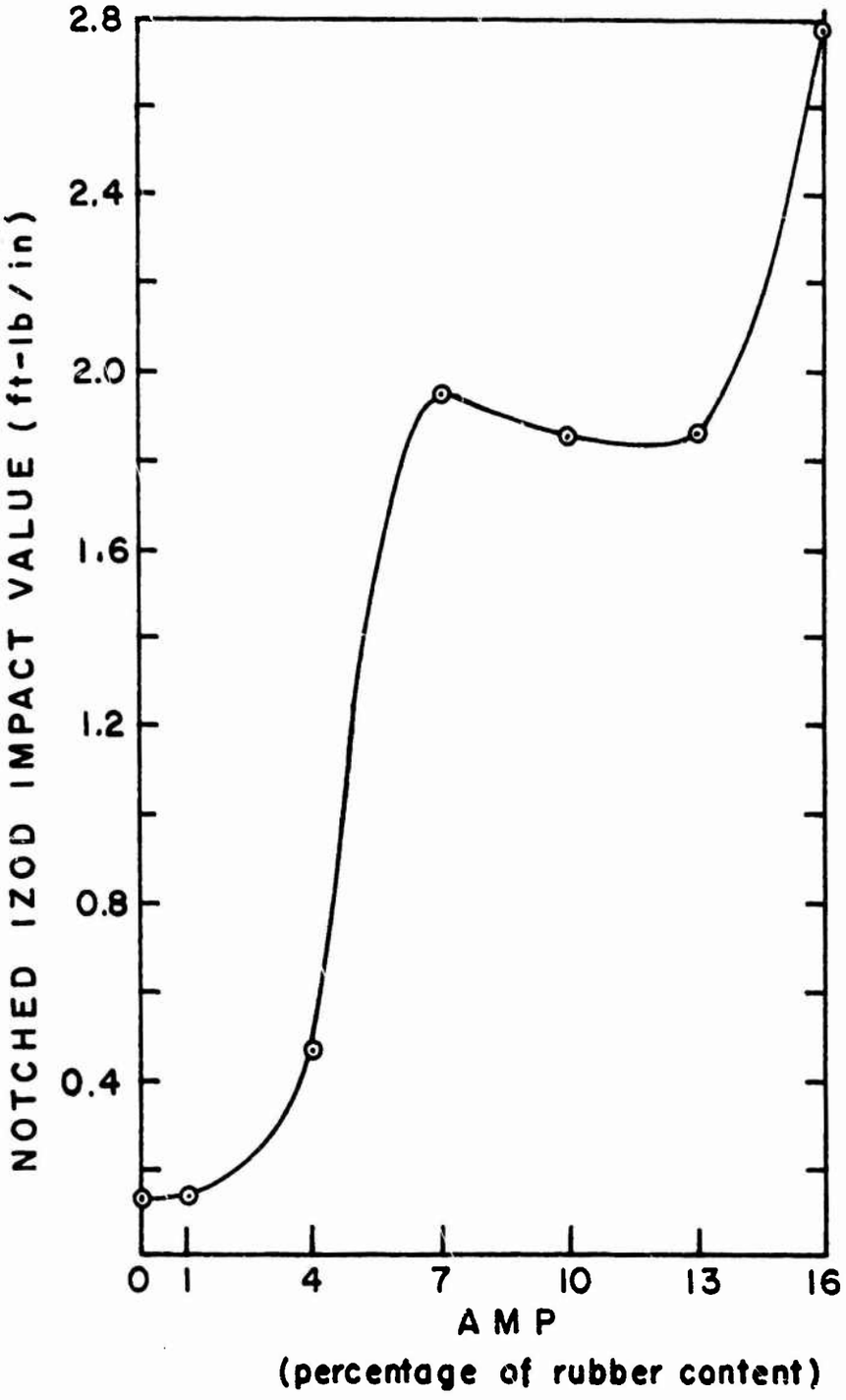

FIGURE 79. NOTCHED IZOD IMPACT STRENGTH FOR VARIOUS RUBBER CONTENTS.

shown in Figure 69 have some similarity to the results of fracture surface work shown in Figure 78. By selecting proper crack velocities in Figure 78 one may be able to find the fracture surface work curves whose trends match closely the results of the puncture tests. The rates involved in the ballistic tests are considered to be quite high; therefore, fracture surface work results at crack velocities higher than those this study may be necessary for comparison.

The effects of rubber modification on fracture behavior can be best demonstrated by the fracture surface photographs of materials with 0, 1 and 4 percent rubber in Figures 80, 81 and 82. The fracture surface of the material with 0 percent rubber obtained at the crack velocity of 4.0×10^{-3} meters/sec shows a relatively smooth and colored appearance with no trace of stress whitening. The fracture surface appearance of the same material in the area where the crack jumped with high velocity shows hackle markings. In the case of material with 1 percent rubber, stress whitening phenomena are observed on the fracture surface where the crack propagated with the velocity of 8.02×10^{-5} meters/sec. When the crack velocity is increased to 3.53×10^{-3} meters/sec, the amount of stress whitening lessens to a trace as shown in Figure 81-b. The fracture surface appearance at higher velocities shows the same hackle markings as observed in the material containing no rubber under fast crack propagation conditions. This indicates that the effects of 1 percent rubber on fracture behavior are observed only in slow crack propagation. At higher crack velocities no effects are observed resulting from the inclusion of one percent rubber in acrylic multipolymers. When the amount of rubber in the specimen is increased to 4 percent, the fracture surface becomes rough and shows stress whitening at a low crack speed (3.72×10^{-5} meters/sec); the surface is smooth but stress whitened at 1.75×10^{-3} meters/sec; and the surface shows slight texturing and diminished stress whitening at higher crack velocities as shown in Figure 82. The materials containing more than 7 percent rubber exhibit stress whitening over the entire range of crack velocities (up to 10 meters/sec). The disappearance of stress whitening at certain crack velocities for the materials containing low percentages of rubber provides an important key to understanding of the relations between fracture process and molecular relaxation mechanisms.

CRACK VELOCITY

4.00×10^{-3} meters/sec

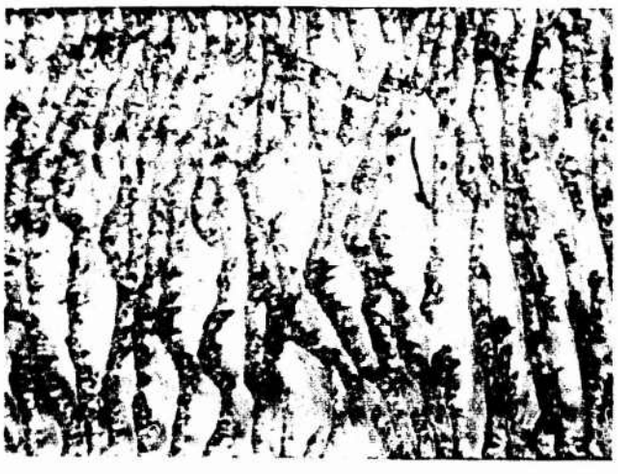

FAST CRACK PROPAGATION AFTER INSTABILITY

FIGURE 80. FRACTURE SURFACES OF AMP 0 AT DIFFERENT CRACK VELOCITIES.

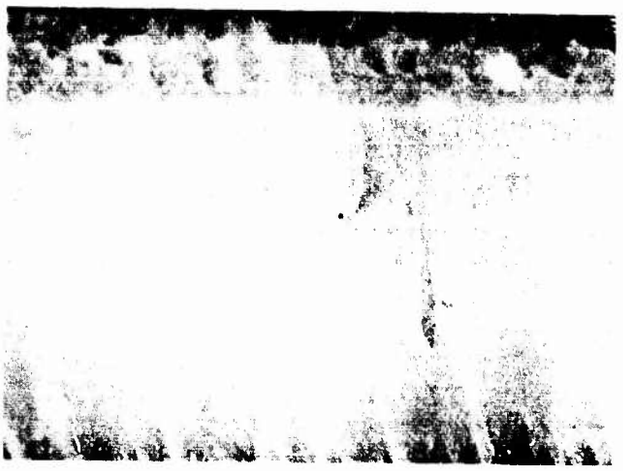

CRACK VELOCITY
8.02×10^{-5}
meters/sec

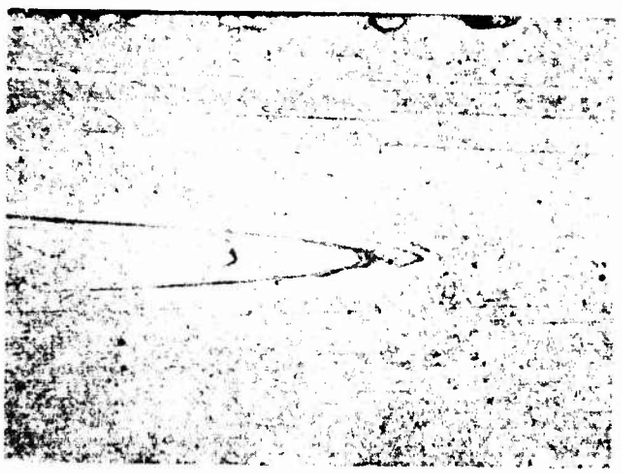

CRACK VELOCITY
3.53×10^{-3}
meters/sec

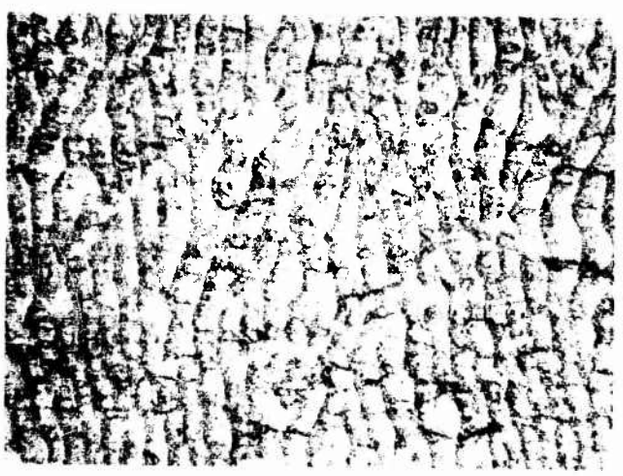

FAST CRACK
PROPAGATION
AFTER INSTABILITY

FIGURE 81. FRACTURE SURFACES OF AMP I
AT DIFFERENT CRACK VELOCITIES.

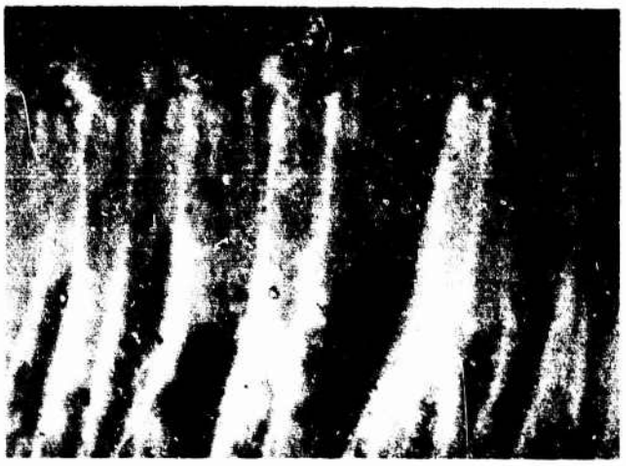

CRACK VELOCITY
3.72×10^{-5}
meters/sec

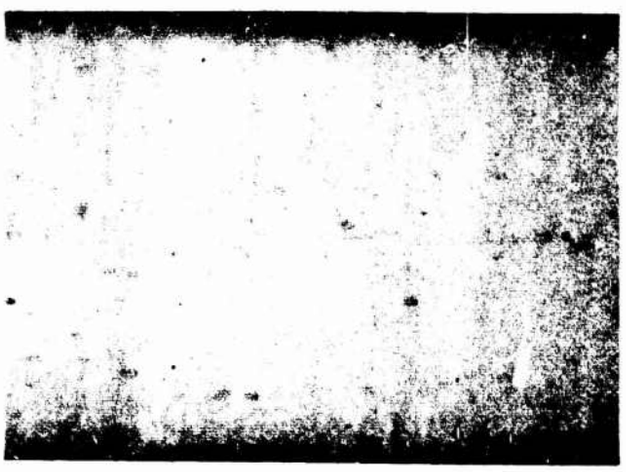

CRACK VELOCITY
1.75×10^{-3}
meters/sec

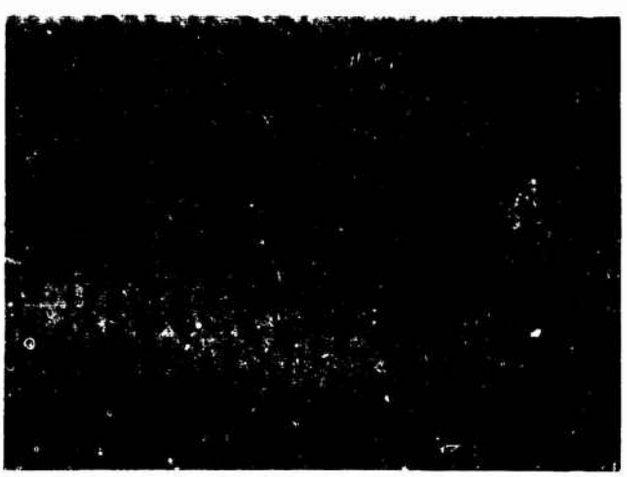

FAST CRACK
PROPAGATION
AFTER INSTABILITY

FIGURE 82. FRACTURE SURFACES OF AMP 4
AT DIFFERENT CRACK VELOCITIES.

CHAPTER VI

CRACK PROPAGATION THEORIES IN POLYMERIC MATERIALS

Fast growing applications of polymeric materials have made it necessary to systematically and thoroughly characterize their mechanical behavior. Furthermore, extensive efforts have been made to correlate the mechanical properties to molecular structure in order to better understand the properties of polymeric materials and collect sufficient data to design new materials from a molecular point of view. Fracture studies of polymeric materials have been subject to the same efforts. However, fractures are ultimate responses of materials, and despite a great deal of effort to characterize the fracture behavior of polymeric materials there is yet insufficient understanding of their fracture or crack propagation behavior.

In the life of a crack there are three distinct stages: initiation, propagation, and arrest (in some cases). Thorough understanding of each stage is of vital importance. The study of crack propagation is of particularly great importance since rapid unstable crack propagation often causes catastrophic failure without warning or opportunity to reduce the load. In this chapter the fracture propagation behavior of polymeric materials is considered mainly on the basis of energy considerations.

Major difficulties are involved in analyzing the fracture propagation in polymeric materials. Namely, there are three conflicting factors which influence crack propagation behavior. These factors are geometry, rate-sensitive fracture resistance, and the contribution of the material's structure and properties to this rate sensitivity of fracture resistance. The first two factors are in the fracture mechanics' domain, and the last factor is in the domain of the material's structure. The material properties' contribution to the rate-sensitivity of fracture resistance is the least studied and developed factor. In this chapter the rate-sensitivity will be considered based on the fundamental viscoelastic parameters, and the effects of viscoelastic parameters on the crack propagation behavior will also be discussed.

Since the fracture propagation in polymeric materials will be examined on the basis of energy considerations, brief comments on the energy balance theories will be made here. (A detailed review may be found in Chapter I). The Griffith energy criterion for fracture of brittle materials has been modified and expanded to include the localized plastic deformation at a crack tip (Orowan (19) and Irwin (58)) and also has been applied as a criterion for the tearing of rubber (Rivlin and Thomas (59)). Erdogen (60) stated in the discussion of crack propagation problems that in these energy balance fracture theories the rate of change of dissipative energy with respect to fracture area, variously called surface free energy, tear energy, fracture energy, fracture toughness, or critical crack extension force, plays an important role and is considered to be an intrinsic property of the material. As reviewed in Chapter I the Griffith criterion has also been successfully applied to polymers by numerous workers, and the fracture surface work has been obtained under various conditions. For example, the fracture surface work of polymers was studied as a function of molecular parameters, as well as of temperature and crack velocity (see Chapter I). From the accumulated results of these investigations it has been recognized that the fracture surface work of polymeric materials is greatly influenced by not only molecular parameters but also

by temperature and strain rate (or crack velocity), just as are viscoelastic parameters. In other words, the fracture surface work of polymeric materials is not an inherent property but may be a viscoelastic parameter. Therefore, in order to fully understand the fracture behavior of polymeric materials and to be able to establish the relationship between molecular parameters and material fracture resistance it is necessary to take a different approach in the treatment of fracture surface work. The approach taken here is to treat the fracture surface work as a function of viscoelastic parameters, and by characterizing the effects of both temperature and crack velocity (strain rate) on the fracture surface work, we attempt to establish the effect of viscoelastic parameters and their contributions to the fracture process of polymeric materials.

In studying experimentally the effects of temperature and crack velocity on the fracture surface work, three factors (specimen geometry, crack instability due to rate-sensitive fracture resistance, and material contribution to this rate-sensitivity of fracture resistance) make experimentation and the analysis of obtained data quite complicated. First, the difficulties caused by specimen geometry and rate-sensitive fracture resistance in obtaining the fracture surface work over a wide range of temperature and crack velocities will be discussed from the point of view of fracture mechanics. The rate-sensitivity can be classified into three categories: rate-insensitivity, positive rate-sensitivity, and negative rate-sensitivity (39). This is illustrated schematically on a graph of crack velocity versus fracture toughness (or fracture surface work, or rate of energy dissipation) in crack extension (Figure 83).

Rate-insensitive fracture toughness means that the fracture resistance or fracture surface work is independent of crack velocity. In this case the energy dissipation per unit crack extension is directly related to the fracture surface geometry. In other words, fracture surface work increases with increasing surface roughness. Furthermore, the crack velocity can be obtained from the thermodynamic equilibrium equation of the body:

$$\frac{dW}{dt} = \frac{dU}{dt} + \frac{dT}{dt} + \frac{dD}{dt} \tag{37}$$

where W is the work done by the external loads

U is the recoverable stored strain energy

T is the kinetic energy

and D is the dissipative energy as fracture surface work. If the crack width is constant, then the rate of dissipative energy is given by the following relation:

$$\frac{dD}{dt} = 2\gamma \cdot \omega v \tag{38}$$

where γ is the rate-insensitive fracture surface work,

ω is the crack width,

and v is the crack velocity.

Therefore, the crack velocity is obtained by

$$v = \frac{1}{2\gamma\omega}\left[\frac{dW}{dt} - \frac{dU}{dt} - \frac{dT}{dt}\right] \tag{39}$$

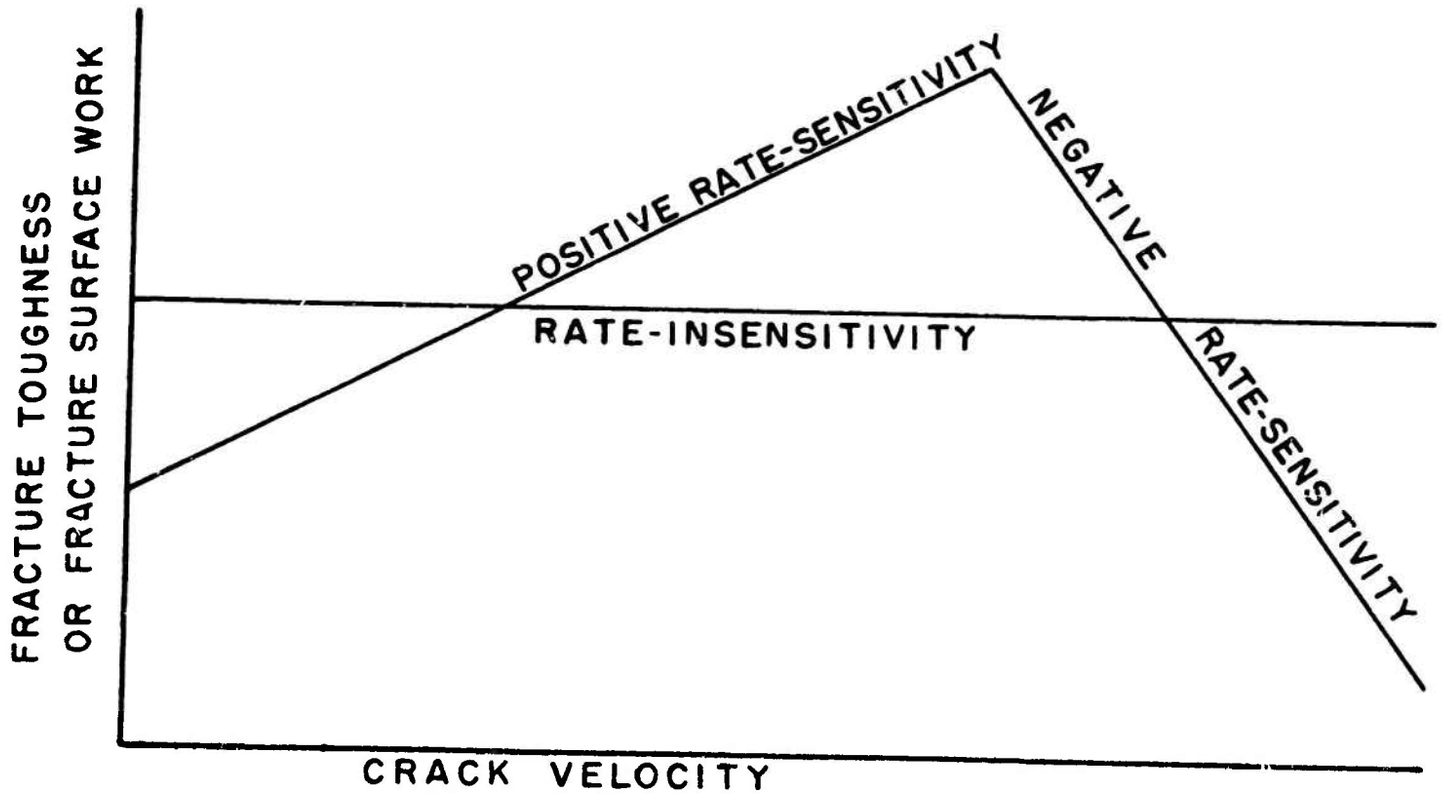

FIGURE 83. SCHEMATIC ILLUSTRATION OF RATE-SENSITIVE FRACTURE RESISTANCE.

The rate-insensitive fracture toughness may be found in ideally brittle materials such as crystalline brittle solids and rate-independent glasses.

In ordinary polymers and metals the fracture surface work or fracture toughness is found to be rate-sensitive. The fracture surface work versus crack velocity results shown in Figure 47 in Chapter IV are one example.

Positive rate-sensitive fracture surface work means that the fracture surface work or fracture resistance increases as the crack velocity increases as shown in Figure 83. The materials with positive rate-sensitive fracture surface work exhibit stable crack propagation, provided that the increase in rate of crack extension force remains less than that of fracture surface work, and acceleration of the crack can be achieved only by increasing the crack extension force. Negative rate-sensitivity of fracture surface work occurs when the material shows decreasing fracture resistance as the crack velocity increases. In this case crack extension tends to be unstable and the crack exhibits self-acceleration. As in the case of poly(methyl methacrylate), other materials often exhibit positive and negative rate-sensitive fracture resistance. This change in rate-sensitivity of fracture surface work, together with the effects of geometry, causes major instability problems in crack extension and makes experimentation in studying the crack velocity effects on fracture surface work difficult. The possible causes of change from positive rate-sensitivity to negative rate-sensitivity of fracture surface work will be discussed later on the basis of fundamental viscoelastic parameters. Here the effects of specimen geometry will be discussed.

The effect of specimen geometry can be simply stated as the variation of crack extension force in terms of crack length. In order to illustrate the crack extension force dependence on the specimen geometry, a rectangular specimen of finite width with a center crack under constant applied tensile load or deflection is considered. Bluhm (61) calculated the crack extension force for the above example utilizing the equation:

$$G = \left(\frac{\sigma^2 W}{E}\right) \tan\left(\frac{\pi \ell}{2W}\right) \qquad (40)$$

where σ is the gross stress

W is the plate width

E is the Young's modulus

and ℓ is the crack length.

He showed the resulting energy release rate as a family of curves with gross stress and deflection as the distinguishing parameter in Figure 84. In the figure, R represents the critical crack extension force which is the material's resistance to crack propagation. Bluhm considered three cases of the material's fracture resistance: rate-insensitive resistance, negative rate-sensitive case, and resistance change due to fracture mode change. First, the rate-insensitive resistance case and the negative rate-sensitive case are considered together. Let ℓ_3 be the initial crack length. As the stress is increased from zero, the crack extension force increases along the line A-B-C in Figure 84. When the stress is less than σ_3, the crack extension force is smaller than the critical crack extension force or fracture resistance of the material and thus the crack does not propagate. When the stress increases beyond point C,

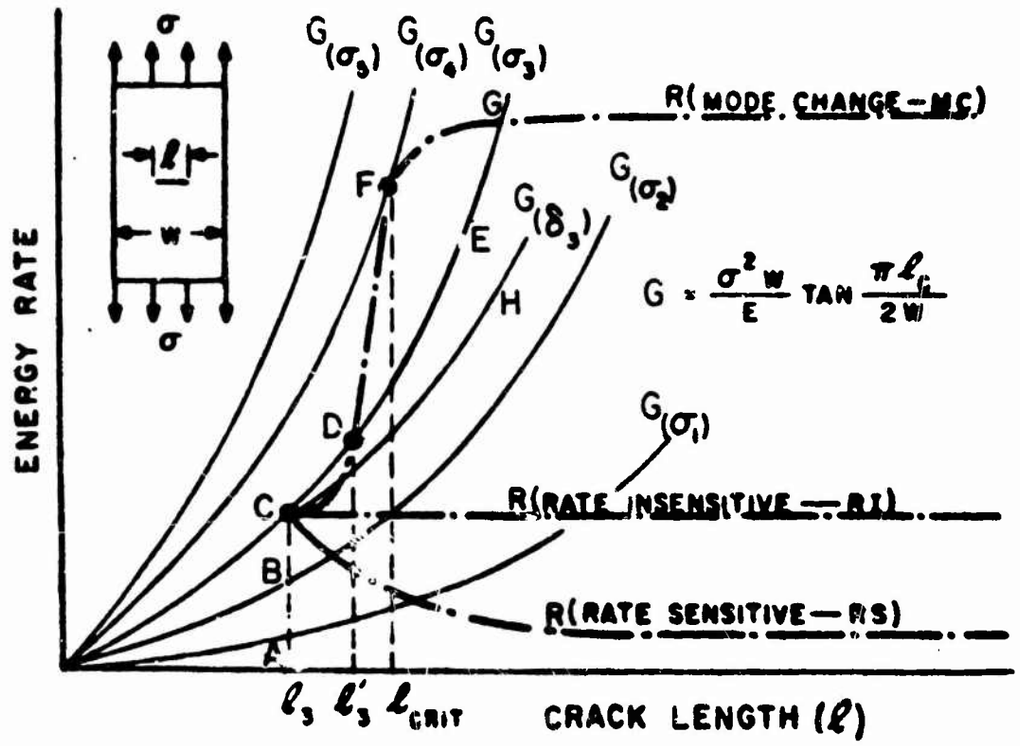

NOTE: 1) σ_3 — CRITICAL STRESS CORRESPONDING TO ℓ_3

2) δ_3 — CRITICAL DEFLECTION CORRESPONDING TO ℓ_3

3) $\sigma_5 > \sigma_4 > \sigma_3 > \sigma_2 > \sigma_1$

FIGURE 84. ENERGY RELATIONS IN A FINITE WIDTH PLATE IN TENSION CONTAINING A CENTER CRACK (BLUHM, REF.61).

the crack extension force becomes higher than the critical crack extension force of the material, and crack extension occurs. If the stress is kept constant, then Eq. (40) predicts that the crack extension force, G, will increase monotonically as the crack length increases. This is demonstrated by a curve C-D-E. In the case of rate-insensitive materials, the fracture resistance remains constant with respect to crack length and crack velocity. Therefore, once the crack starts to move, the difference between the crack extension force and the fracture resistance increases rapidly. For this reason, the crack accelerates faster and faster. The negative rate-sensitive material exhibits a more unstable situation since as soon as the crack starts to move the fracture resistance, R, decreases. The crack, therefore, accelerates much faster than in the case of a rate-insensitive material. In both the rate-insensitive and the negative rate-sensitive materials fracture is catastrophic.

Next, the case in which the fracture resistance, R, increases due to fracture mode change shown in Figure 84 or due to positive rate-sensitivity of materials is considered. If the fracture mode changes, the fracture resistance changes along the curve C-D-F-G. While the crack extension from ℓ_3 is small the crack will propagate since the crack extension force is higher than the fracture resistance. Contrary to the cases of the rate-insensitive and the negative rate-sensitive materials, the fracture resistance, R, increases as the crack extends. When the crack length reaches ℓ_3', the fracture resistance equals the crack extension force, and the crack will be arrested. Thereafter higher stress is necessary to extend the crack since the rate of increase of fracture resistance is higher than that of the crack extension force. In the area between D and F crack propagation is very stable. At point F in Figure 84, the crack extension force equals the fracture resistance again, and after this point the rate of increase of the crack extension force becomes larger than that of the fracture resistance. Thus the crack starts to propagate rapidly again. Positive rate-sensitive materials also exhibit stable crack propagation. Materials such as poly(methyl methacrylate), which have positive rate-sensitivity up to a certain crack velocity and then change to negative rate-sensitivity after passing this crack velocity, exhibit slow stable crack propagation prior to catastrophic fracture. In order to study the behavior of the fracture resistance or the fracture surface work in terms of the crack velocity, it is necessary to create relatively stable crack propagation without regard to the crack velocity. For this reason, the type of specimen geometry just discussed is not suitable because the rate of increase of the crack extension force in terms of crack length is too rapid and always leads to catastrophic failure.

By the above example we have shown that the specimen geometry and the material fracture resistance interact with each other to influence the fracture propagation. It has been seen that the crack extension force variation with crack length is dependent upon the specimen geometry. In order to study the effect of crack velocity on fracture resistance or the fracture surface work, one has to separate the interaction of the instability due to the crack extension force variation from the instability caused by the change in the fracture resistance. If one can design a specimen so that due to its geometry the crack extension force is not a function of the crack length, it is possible to study the fracture resistance or the fracture surface work of the material in terms of the crack velocity. This can be demonstrated by utilizing Irwin's definitions (79) of the crack extension force:

$$G = \frac{f^2}{2w} \cdot \frac{dC}{d\ell} \tag{8}$$

where f is the applied load

w is the crack width

C is the compliance ($C = \frac{\text{deflection}}{\text{applied load}}$)

and ℓ is the crack length.

Mostovoy, Crosley, and Ripling (24) first reported a double cantilever beam cleavage specimen designed such that $dC/d\ell$ would be a constant in Eq. (8). The crack extension force of a specimen with a constant $dC/d\ell$, by design, is independent of the crack length and dependent on only the applied load, the crack width, and a design factor of constant $dC/d\ell$. In other words, this type of specimen exhibits constant crack extension force without regard to crack length, provided that the load and the crack width remain constant. In the work of Mostovoy, Crosley and Ripling, a tapered double cantilever beam cleavage specimen was designed by setting $dC/d\ell$ constant. In the work associated with this report a tapered double cantilever beam cleavage specimen based on a slight modification of their design and a newly developed sandwich tapered double cantilever beam cleavage specimen are used. The design procedure has already been discussed in detail in Chapter III.

With the design of a tapered cleavage specimen the crack extension force of a specimen is independent of the crack length under constant applied load and thus the instability in crack extension due to specimen geometry can be eliminated; however, another type of instability due to rate-sensitivity change from positive to negative may occur. This problem will be discussed together with the two different experimental measurement techniques: load-controlled testing and deflection-controlled testing. In the case of the load-controlled testing method, the prescribed constant load is applied to the specimen. The crack extension force is determined by this constant load as shown in Eq. (8). In the crack velocity range where a material shows positive rate-sensitive fracture resistance, the crack propagates at the velocity where the crack extension force balances the material's fracture resistance. Increasing the load increases the crack velocity. This method is very useful in studying the effects of crack velocity on the fracture surface work up to the crack velocity at which the rate sensitivity of fracture resistance changes from positive to negative; however, with this method it is not possible to measure the fracture surface work in terms of crack velocity above the instability point since the load can not be reduced rapidly enough after instability occurs.

Another testing method is the deflection-control method. In this case the specimen is deformed at a predetermined rate. Here the case in which the deflection of a tapered double cantilever beam cleavage specimen is increased at a constant rate will be analyzed. The crack extension force is given by Eq. (8)

$$G = \frac{f^2}{2w} \frac{dC}{d\ell} \tag{8}$$

In this equation the load f is given by the total deflection of the beams, δ, and the compliance of the specimen, C, as follows:

$$f = \frac{\delta}{C} \tag{41}$$

The deflection is increasing at a constant rate; therefore, the deflection is given by the following equation as a function of time:

$$\delta = at \tag{42}$$

where a is a constant.

By design of the tapered specimen, $dC/d\ell$ is constant; therefore, the compliance is given by the following equation:

$$C = \frac{dC}{d\ell} \cdot \ell + b \tag{43}$$

where b is a constant.

The constant b ideally should be zero if the specimen contour follows the calculated curve (Figure 21 in Chapter III) up to the point of zero crack length. However, in an actual specimen some material is added to allow for loading pin holes as shown in Figure 24. Beacuse of this deviation from the calculated curve for specimen contour, b is not zero and takes negative value as shown in Figure 29. By substituting Eqs. (42) and (43) into Eq. (41), we obtain

$$f = \frac{at}{\frac{dC}{d\ell}\ \ell + b} \tag{44}$$

By substituting Eq. (44) into Eq. (8), we have

$$G = \frac{a^2}{2\omega \cdot \frac{dC}{d\ell}} \left(\frac{t}{\ell + \frac{b}{\frac{dC}{d\ell}}} \right)^2 \tag{45}$$

This equation suggests that the crack extension force for a tapered cleavage specimen subjected to a constant rate of deflection increase is a function of experimental time and the crack length. In order to maintain constant crack extension force, Eq. (45) suggests that the terms $(t/\ell + \frac{b}{\frac{dC}{d\ell}})$ has to be constant.

Therefore

$$\frac{t}{\ell + \frac{b}{\frac{dC}{d\ell}}} = K \tag{46}$$

where K is constant.

From Eq. (46), we have

$$\ell = \frac{1}{K}t - \frac{b}{\frac{dC}{d\ell}} \qquad (47)$$

Eq. (47) indicates that in order to maintain constant crack extension force the crack length has to be a linear function of time (i.e. constant crack velocity $v = d\ell/dt = 1/K$). In the crack velocity range at which the fracture surface work has positive rate-sensitivity, the crack will propagate with a constant velocity at which the crack extension force will balance the material's fracture resistance. The crack velocity at the balance point depends on the rate of deflection as shown in Eq. (45). When the crack velocity exceeds the instability point where the rate-sensitivity of fracture surface work changes from positive to negative, the crack extension force exceeds the material's fracture resistance. Then the crack will accelerate or jump in order to lower the crack extension force by increasing the crack length as indicated in Eq. (45), thus seeking a new balancing point between the crack extension force and the material's fracture resistance. If the negative rate-sensitivity continues, the crack will keep accelerating. However, if the rate-sensitivity of fracture surface work changes from negative to positive at a higher crack velocity, the material's fracture resistance again becomes larger than the crack extension force after the crack has jumped. At this point, since the rate of deflection is low, the only way to increase the crack extension force is for the crack to slow down and/or to arrest itself; thus the crack is at rest until the crack extension force increases as a result of the time, t, (or deflection $\delta = at$) in Eq. (45) increasing. This type of crack propagation is called a stick-slip mode and is observed when the fracture rate-sensitivity of the material changes from positive to negative in a low crack velocity range and then from negative to positive in a higher velocity range. Of course the deflection rate should be such as to produce a crack with a velocity in the negative rate-sensitivity region. In order to create stable crack propagation in the positive fracture rate-sensitivity region which may exist in the higher crack velocity range, equation (45) indicates that a high rate of deflection, a, should be selected. One can then counterbalance a high rate of crack propagation [small value of $\{t/(\ell + \frac{b}{dC/d\ell})\}$] and create conditions in which the magnitude of the crack extension force is raised and balances the fracture resistance at high speed crack extension.

Thus, the deflection controlled testing method has the advantage of making the measurement of the fracture surface work over a wide range of crack velocities more accessible. In this study the deflection-controlled testing method is employed, and with the modified tapered and newly developed sandwich tapered double cantilever beam cleavage specimens, the fracture surface work behavior of poly(methyl methacrylate), polystyrene, and acrylic multipolymers is studied over a wide range of crack velocities. In addition to the effects of crack velocity, temperature effects on the fracture surface work of poly(methyl methacrylate) and polystryrene have also been studied. The results are shown in Figures 47, 52, and 54 in Chapter IV, and in Figures 70 and 77 in Chapter V. From these results it is evident that the fracture surface work is greatly influenced by both crack velocity and temperature; furthermore, all materials studied in this work exhibit positive and negative rate sensitivity fracture surface work. In this section, by analyzing the fracture surface work dependence on the crack velocities and temperature, an attempt is made to explain the mechanism of the fracture process and rate-sensitivity based on the fundamental

viscoelastic behavior of polymers. Some of the existing data and observations will be discussed from this point of view.

In order to study the effects of temperature and crack velocity on fracture surface work and the fracture process, various iso-(fracture surface work) values are selected for poly(methyl methacrylate) as shown from Figure 85 (replot of Figure 47 and 52 in Chapter IV), and the crack velocities and temperatures corresponding to each iso-(fracture surface work) value are determined. From these values an Arrhenius plot of crack velocity versus the reciprocal of testing temperature (^{o}K) is constructed. This is shown in Figure 86 in which some examples of the corresponding points in Figure 85 and Figure 86 are marked by letters from A to Q. Figure 86 indicates that in the temperature range between 62°C and 22°C the crack velocity values from each iso-(fracture surface work) fall on a straight line (for example, the lines C-D-E, H-I-J, and M-N-P). There exists a striking consistency in slope among different iso-(fracture surface work) values in this temperature range. In the case of the fracture surface work value of 2.30×10^5 ergs/cm^2, the crack velocity value at -20°C (marked by L) falls on the same straight line established in the temperature range between 62°C and 22°C (shown by the line M-N-P). In the temperature range between -20°C and -30°C, the crack velocity values for each iso-(fracture surface work) value form lines which have different slopes from those in the temperature range between 62°C and 22°C (for example, the line A-B). The extension of the straight line for the fracture surface work of 2.52×10^5 ergs/cm^2 in the temperature range between -30°C and -20°C (the line A-B) passes through the point F which was obtained in the higher crack velocity range for crack propagation between 2.54 and 19.3 m/sec at room temperature and corresponds to 2.52×10^5 ergs/cm^2 fracture surface work. The slope of the line which passes through the points for a fracture surface work of 2.44×10^5 ergs/cm^2 at 22°C (the point K) and at -20°C (the point G) is very close to that of the line (A-B-F) for 2.52×10^5 ergs/cm^2. The slope of lines for different iso-(fracture surface work) values in the temperature range between 22°C and -22°C are not consistent with each other (for example, the lines B-C, G-H, and L-M). From these results it seems that two distinct slopes exist in this graph. Considering fracture of polymeric materials as a rate process, one can obtain the apparent activation energies from these two slopes by utilizing an Arrhenius equation:

$$v = Ae^{-E/RT} \tag{48-a}$$

or

$$\ell n\, v = \ell n A - \frac{E}{RT} \tag{48-b}$$

where v is the crack velocity

A is a constant

E is the apparent activation energy

R is the Boltzmann constant (1.98 cal/$^{o}K \cdot$mol)

and T is the temperature in Kelvin degrees.

Table 20 shows data used to calculate the apparent activation energy and its values.

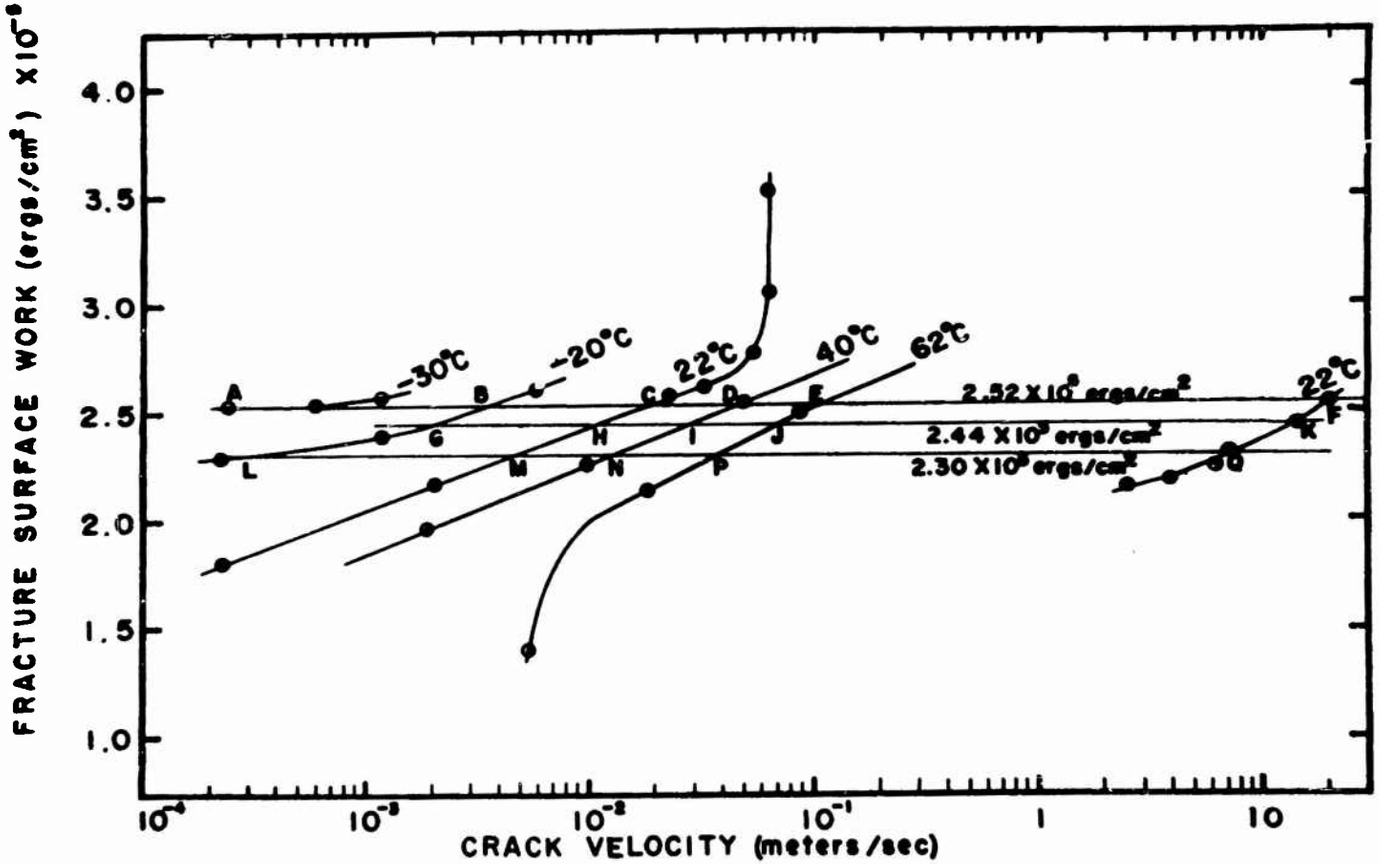

FIGURE 85. FRACTURE SURFACE WORK VERSUS CRACK VELOCITY AT DIFFERENT TEMPERATURES FOR POLY(METHYL METHACRYLATE).

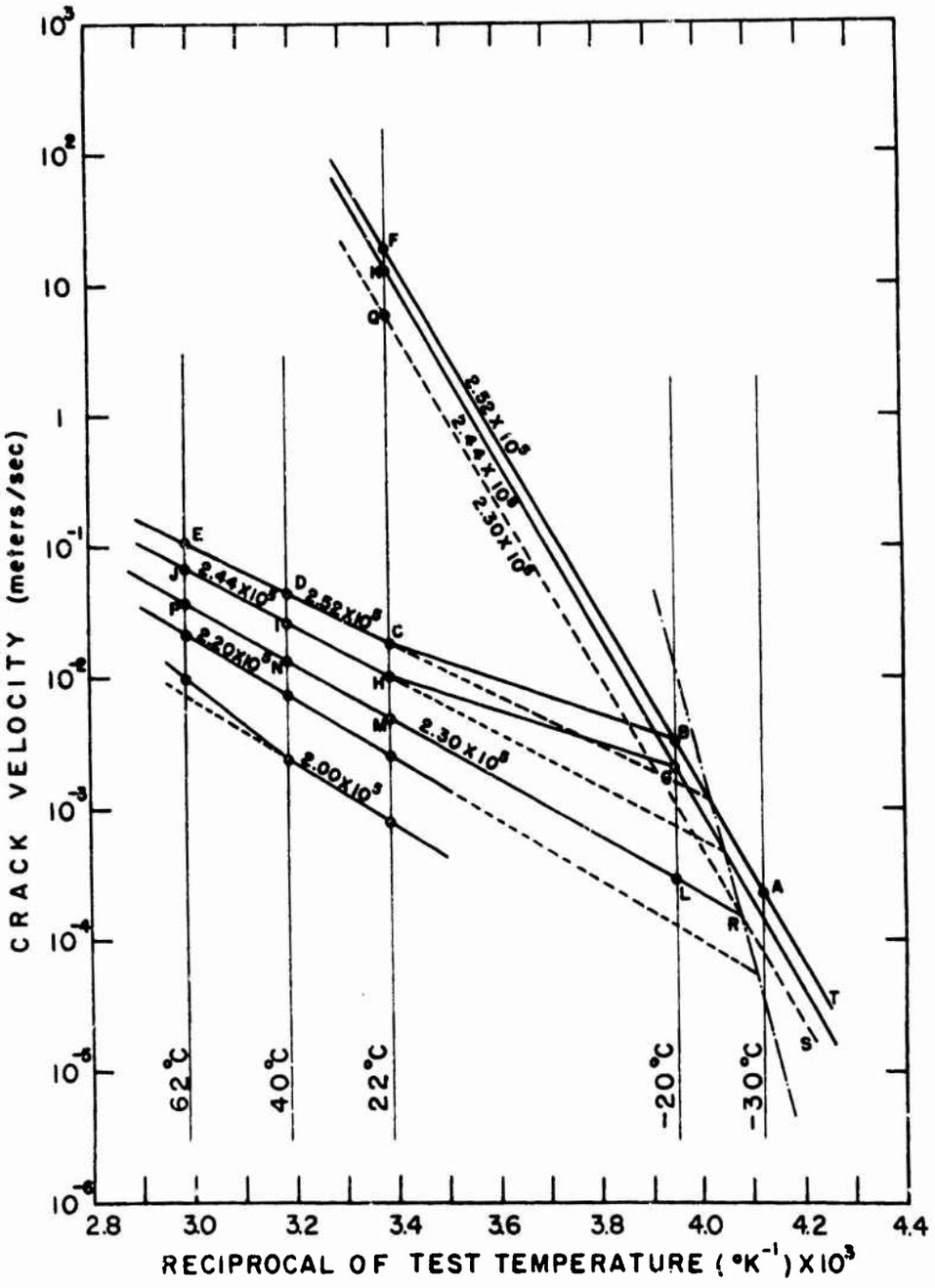

FIGURE 86. CRACK VELOCITY VERSUS RECIPROCAL OF TEST TEMPERATURE FOR VARIOUS ISO-(FRACTURE SURFACE WORK) VALUES.

Table 20. Apparent Activation Energies of Two Fracture Processes for Poly(methyl methacrylate)

Fracture Surface Work (erg/cm^2)	Temperature (^oC)	Reciprocal Absolute Temperature ($1/^oK$)	Crack Velocity (m/s)	Apparent Activation Energy (kcal/mol.)
2.52×10^5	62	2.99×10^{-3}	1.09×10^{-1}	
	40	3.19×10^{-3}	4.50×10^{-2}	8.8
	22	3.39×10^{-3}	1.65×10^{-2}	
2.30×10^5	62	2.99×10^{-3}	3.75×10^{-2}	
	40	3.19×10^{-3}	1.30×10^{-2}	9.8
	22	3.39×10^{-3}	4.80×10^{-3}	
	-20	3.95×10^{-3}	2.95×10^{-4}	
2.52×10^5	22	3.39×10^{-3}	19.0	
	-20	3.95×10^{-3}	3.30×10^{-3}	30.6
	-30	4.12×10^{-3}	2.38×10^{-4}	

Table 20. (Continued)

Fracture Surface Work (erg/cm^2)	Temperature (^oC)	Reciprocal Absolute Temperature ($1/^oK$)	Crack Velocity (m/s)	Apparent Activation Energy (kcal/mol.)
2.44×10^5	22	3.39×10^{-3}	14.3	31.3
	-20	3.95×10^{-3}	2.0×10^{-3}	

The apparent activation energy values obtained here for fracture processes in poly(methyl methacrylate) bear a striking resemblance to the values obtained by Boyer (45) from the data of Maxwell and Harrington, who studied the energy required to break a poly(methyl methacrylate) tensile specimen (see Chapter IV, first section). Boyer obtained the apparent activation energy of 8.5 kcal/mol for the α-process and 34 kcal/mol for the β-process. In this study we have obtained apparent activation energies that average 9.3 kcal/mol and 31 kcal/mol as shown in Table 20. This indicates that the fracture process at and above room temperature in the low crack velocity region may be strongly influenced by the α-process, and the fracture process at low temperature or in the high crack velocity region may be influenced by the β-process. The apparent activation energy values for the α-process, 8.5 kcal/mol obtained by Boyer and 9.3 kcal/mol obtained in this study, are very small when compared with the value of 81 kcal/mol obtained by Roetling who studied the yield stress behavior of poly(methyl methacrylate) from 30° to 90°C over six decades of rate; however, Boyer (45) explained that the low apparent activation energy values are consistent with the findings of McLoughlin and Tobolsky of a low, consistent value until the glass transition temperature is approached, whereupon it rises rapidly.

In view of the supposition that the fracture process of polymeric materials is strongly influenced by the α- or β-processes depending on the temperature and crack velocity conditions, an attempt to explain the fracture phenomena in polymers will be made here. Some comments concerning the α- and β-processes of poly(methyl methacrylate) may be found in Chapter IV, first section, but these may be recapitulated at this point. The α-process is associated with the glass transition temperature and the molecular motion related to the α-process is considered to be the main chain motion. Roetling (62) noted that the molecular motion in the α-process probably involves a rotation of molecular segments about an axis perpendicular to the longitudinal axis of the molecule. The α- to β-process transition occurs below the glass transition temperature. The β-process of poly(methyl methacrylate) is initiated in the vicinity of the β-transition temperature and may be associated with the motion of the carbomethoxy side chains. A conflicting theory cited by Roetling (62) concerns Havriliak's conclusion based on infra-red measurements plus dielectric studies that the β-process could not be due to a side-chain rotation relative to the main chain but is probably due to either a twisting or rotation of the segments of the main chain about its longitudinal axis. Moreover, Roetling stated that side-chain rotation may be more nearly associated with the α-process and may occur at a bend in the chain.

Based on the observation that the temperature coefficient of crazing for poly(methyl methacrylate) and polystyrene agree rather well with apparent activation energies for the respective β-processes, Boyer (45) speculates that crazing may be associated with the β-process. He further speculates that there may be two β-processes, one involving side chain motion, the other involving motion about the main chain, and that the latter motion may permit the cold flow needed to form craze material. Havriliak's findings, quoted by Roetling, seem to give some support to Boyer's speculation.

The schematic diagram showing the typical relationship between crack velocity and temperature for two iso-(fracture surface work) values is drawn in Figure 87 in order to demonstrate the effects of molecular relaxation processes on fracture propagation. First, the effects of temperature are discussed. When the fracture surface work is 2.30×10^{-5} ergs/cm^2 or less, the fracture mechanism is the α-process in the

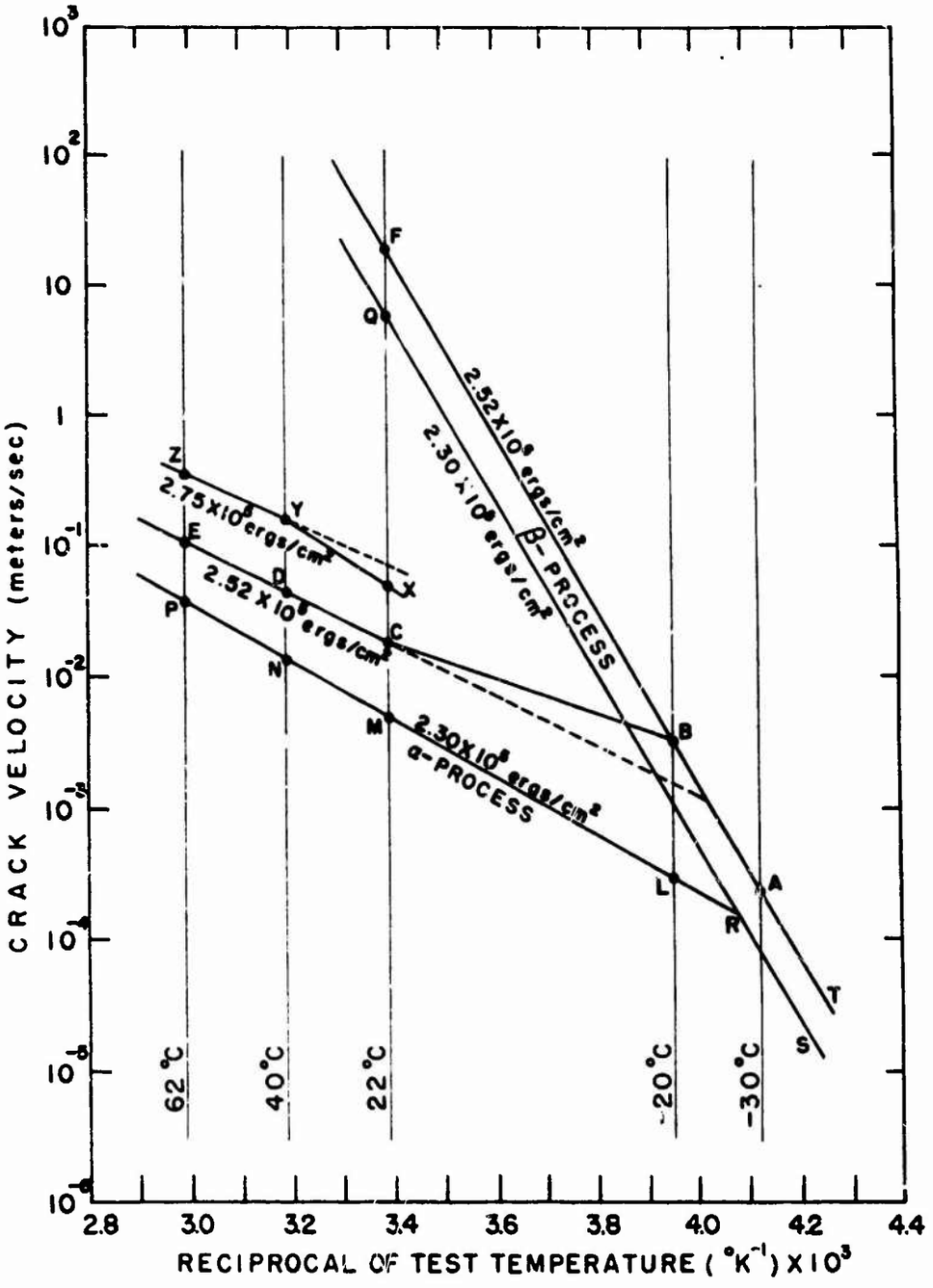

FIGURE 87. CRACK VELOCITY VERSUS RECIPROCAL OF TEST TEMPERATURE FOR ISO-(FRACTURE SURFACE WORK) VALUES OF 2.30×10^5 AND 2.52×10^5 ergs/cm^2.

temperature range between 62°C and -30°C (as indicated by the line P-N-M-L-Q). Below -30°C, the fracture mechanism changes from the α-process to the β-process (the line R-S). By forcing the crack to propagate faster, one could obtain fracture with the β-process dominant and the same fracture surface work in the temperature range above -30°C as shown in Figure 87 by the line Q-R. When the fracture surface work level is 2.52×10^5 ergs/cm^2, the fracture process is dominated by the α-process in the temperature range above 22°C (the line C-D-E). However, unlike the example of fracture surface work at 2.30×10^5 ergs/cm^2, the fracture process between the temperature range 22°C and -20°C is anomalous (the line B-C). At this stage there are no experimental data indicating the relationship between the fracture surface work and crack velocities in the temperature range between 22°C and -20°C. By obtaining the necessary data in the temperature range between 22°C and -20°C, it may be possible to eliminate this anomaly concerning the fracture process. When the temperature is below -20°C, the fracture process is dominated by the β-process (the line B-A-T). Again by forcing the crack to propagate faster, we can obtain fracture in which the β-process is dominant in the temperature range above -20°C (the line B-F).

The effects of crack velocity on the fracture process can be discussed utilizing the data obtained at room temperature. These data are shown in Figure 47 in Chapter IV, second section. In the low crack velocity range between 2.29×10^{-4} and about 3.4×10^{-2} m/sec, the fracture process is dominated by the α-process as indicated in Figure 87. The fracture surface work increases from 1.80×10^5 to about 2.65×10^5 ergs/cm^2 as the crack velocity increases from 2.29×10^{-4} to 3.4×10^{-2} m/sec. In the crack velocity range between about 3.4×10^{-2} and 6.5×10^{-2} m/sec, the fracture surface work increases sharply and an instability in the crack propagation follows. In order to study this phenomenon, the fracture surface work versus crack velocity curves for 40°C and 62°C in Figure 85 are extrapolated to obtain the crack velocity values at the fracture surface work of 2.75×10^5 ergs/cm^2 (see Figure 85). These values are plotted in Figure 87, and are called Y and Z. The crack velocity value at the fracture surface work of 2.75×10^5 ergs/cm^2 at room temperature is also plotted and called X in Figure 87. The slope of the line passing through the two points Y and Z is equal to that of the lines C-D-E and P-N-M-L, which indicates that the line Y-Z represents the α-process, the point X has to be on the extended line of Y-Z; however, the point X is not on the extended line Y-Z. The point X falls on the high crack velocity side. This may indicate that the fracture process at the point X is a mixture of the α- and β- processes. Therefore, in the crack velocity range between 3.4×10^{-2} and 6.5×10^{-2} m/sec, the fracture process may be a mixture of the α- and β-processes. In the higher crack velocity range between about 2.5 and 20 m/sec, the fracture process is dominated by the β-process. In Figure 47 in Chapter IV, second section, the fracture surface work versus crack velocity curve shows a discontinuity at the crack velocity of 6.5×10^{-2} m/sec. This discontinuity may be caused by the fracture process change from the α-process to the β-process.

So far we have discussed how the α- and β-processes are related to the fracture process at different temperatures and crack velocities. Next, the characteristics of fracture surfaces of poly(methyl methacrylate) in the α- and β-process ranges will be examined. The fracture surface photographs corresponding to the α-process are shown in Figures 38, 39, 47 and 48 in Chapter IV, second section. The fracture surface photographs corresponding to the β-process are shown in Figures 42, 43, 44, 50, 51 in Chapter IV, second section. The fracture surface appearance corresponding

to the possible mixture of the α- and the β-process is shown in Figure 41 and 42 (Chapter IV, second section). The fracture surface appearance in the α-process indicates that considerable molecular movement takes place near the crack tip in the fracture process. A distinctive pink and green coloration indicates the presence of uniformly oriented molecular layers on the fracture surface. This gives evidence that considerable molecular motion should exist in the fracture process. The α-process permits this molecular motion in the solid polymer. As reviewed earlier in this chapter, the molecular motion in the α-process may involve a rotation of molecular segments about an axis perpendicular to the longitudinal axis of the molecule. Characteristics of the fracture surface appearance in the β-process condition can be divided into two groups: one with complex subsurface craze-like features, and the other with a relatively smooth surface and a small amount of craze-like structure. The first group appears at low crack velocities running at low temperatures. The second group occurs at higher crack velocities at room temperature. The existence of complex subsurface craze-like features on the fracture surfaces for β-process fracture can be explained by the supposition reviewed earlier in this chapter that crazing may be associated with the β-process. The other type of fracture appearance with a relatively smooth surface and a small amount of craze-like structure may be due to the β-process in which crazing is almost entirely suppressed because of a higher strain rate. In the crack velocity range close to the discontinuity in the curve of fracture surface work versus crack velocity, the fracture surface appearance in Figures 41 and 43 in Chapter IV, second section, indicates a mixture of the dominant α-process (considerable molecular flow as indicated by distinctive coloration) and the β-process (subsurface craze structure). The discontinuity in the curve of fracture surface work versus crack velocity can be explained by the supposition that at the crack velocity corresponding to the discontinuity point the fracture process changes from the possible mixture of the dominant α- and β-process to the β-process. The fracture surface work of the β-process corresponding to the crack velocity at and above the discontinuity point is very small; thus in fracture propagation in poly(methyl methacrylate) the instability occurs. The fracture processes around the discontinuity point in the curve of crack velocity versus fracture surface work is schematically drawn in Figure 88.

We have developed the supposition that the α- and β- processes influence the fracture process and have demonstrated how the α- and β- processes occur and depend upon the crack velocity and temperature, based on the data obtained from poly(methyl methacrylate). Next, we will apply this supposition to some of the existing observations to see whether this supposition explains other fracture phenomena. Broutman and Kobayashi (5) reported that poly(methyl methacrylate) tested at -196°C shows an extremely rough fracture surface in the small area where the crack initiates and becomes unstable. In this area the crack velocity is very low and the temperature is also low (-196°C). From Figure 87 it is evident that the fracture process in this rough surface area at -196°C corresponds to the β-process. The β-process at a low crack velocity can be related to crazing as discussed earlier in this chapter. Thus, the observed phenomena of rough surface and high fracture surface work may be explained by the supposition that the fracture process is dominated by the β-process. Broutman and Kobayashi also reported that at -196°C after the crack initiates it develops a smooth surface region in which fast crack propagation takes place. Here fracture surface appearance is colorless and parabolic markings have been observed. In this fast crack propagation region the fracture process may be dominated by the γ-process. This may explain the existence of a second discontinuity in the curve of fracture

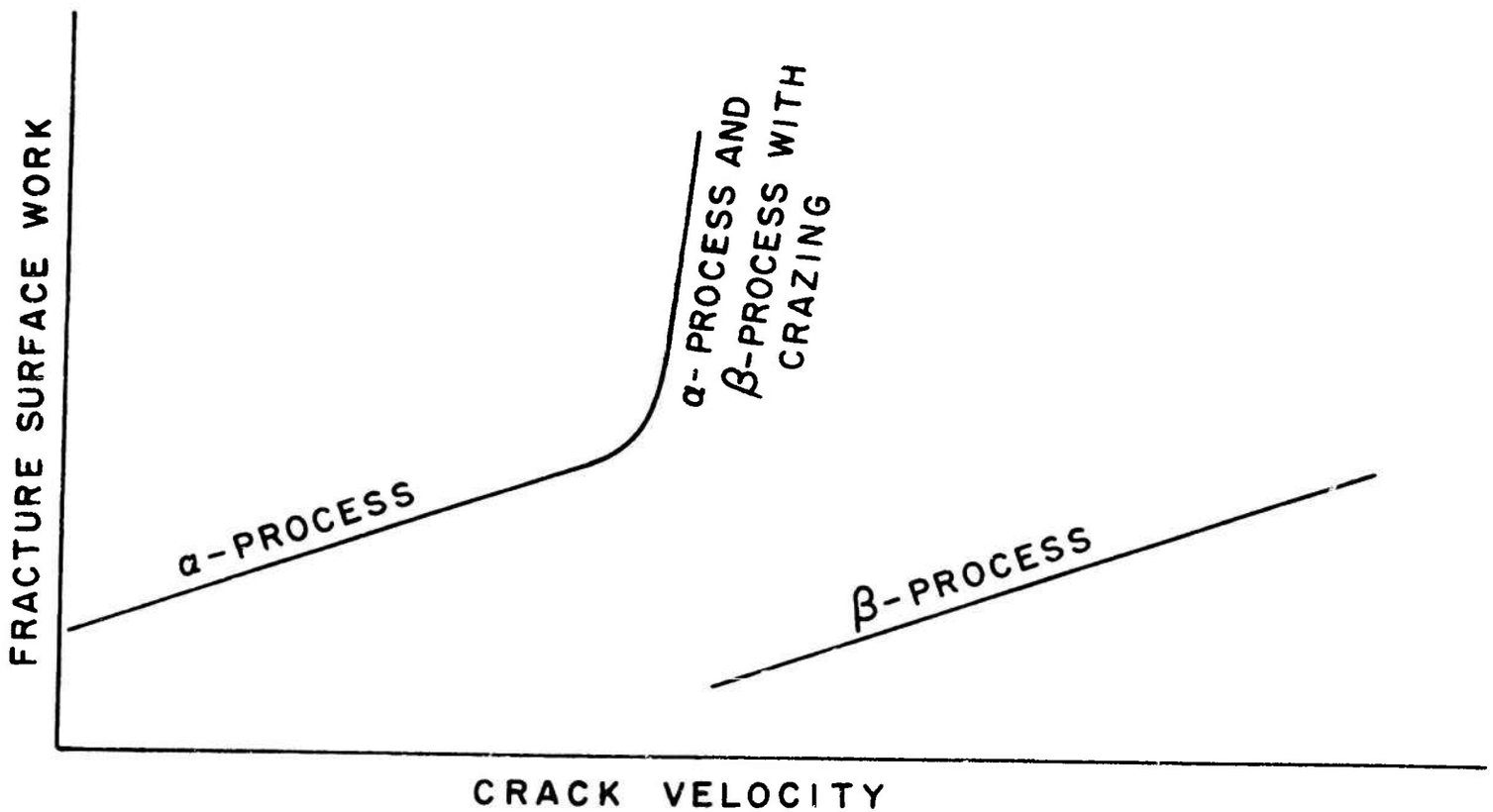

FIGURE 88. SCHEMATIC ILLUSTRATION OF FRACTURE SURFACE WORK VERSUS CRACK VELOCITY CURVE IN TERMS OF α- AND β- PROCESSES.

surface work and crack velocity in Figure 47 in Chapter IV, second section. The appearance of the fracture surface obtained at room temperature above this second discontinuity at a crack velocity of about 20 meters per second shows similar parabolic markings as seen in Figure 45, Chapter IV, second section.

Broutman (63) studied crack propagation in polystyrene in the temperature range between -29°C and 50°C. He reported that in the temperature range between -29°C and 40°C the crack propagation mode is continuous tearing, and that the fracture surfaces have a fine cracked and silvery appearance. The exact crack velocities in these tests are not reported, but a low crack velocity of approximately 1.3×10^{-3} m/sec is indicated. Broutman further reported that the crack propagation mode changes from continuous to discontinuous as the temperature is increased above 50°C and that the fracture surfaces have a finely cracked but non-silvery appearance. In Chapter IV, second section, we have reported that at room temperature continuous crack propagation with a mirror smooth and colored fracture surface appearance is obtained in the crack velocity range between 8.1×10^{-5} and 2.9×10^{-4} m/sec. These fracture phenomena of polystyrene can also be explained by the supposition developed in this chapter that the fracture process is controlled by the α- and β-processes. First, the differences in the β-transition behavior of poly(methyl methacrylate) and polystyrene will be investigated. In order to study the differences, the frequency-temperature locations of the β-relaxation in poly(methyl methacrylate) and polystyrene are plotted in Figure 89 based on the figures shown in Anelastic and Dielectric Effects in Polymeric Solids by McCrum et al. (48). It should be noted here that the lines in this figure have the same significance as the β-process lines in Figure 87 which show the relationship between crack velocities and temperature. Figure 89 shows that the β-relaxation line for polystyrene is located in a much lower frequency region than that for poly(methyl methacrylate). This indicates that the fracture process of polystyrene changes from the α-process to the β-process at a much higher temperature and in a much lower crack velocity range than for poly(methyl methacrylate). In the case of poly(methyl methacrylate), the discontinuity in the curve of fracture surface work versus crack velocity occurs at the crack velocity of 6.5×10^{-2} m/sec when tested at room temperature as shown in Figure 47 (Chapter IV, second section). In the case of polystyrene, Figure 54 in Chapter IV, second section, indicates that the discontinuity in the curve of fracture surface work versus crack velocity occurs at the crack velocity of 2.9×10^{-4} m/sec at room temperature. As calculated at the end of Chapter IV, second section, the crack velocity at this discontinuity point in polystyrene is a factor of 224 lower than that in poly(methyl methacrylate). Figure 89 shows that the β-relaxation frequency at room temperature (22°C) for polystyrene (4.46×10^{-3} cycle/sec) is also a factor of 224 lower than that for poly(methyl methacrylate) (1 cycle/sec). This agreement confirms the suggested explanation that the α- to β-process change may cause the discontinuity on the curve of the fracture surface work and crack velocity. Thus it is evident that at room temperature the fracture process in the crack velocity range between 8.1×10^{-5} and 2.9×10^{-4} m/sec is controlled by the α-process or a mixture of the dominant α-process and β-process. Furthermore, at room temperature the fracture process in the crack velocity range above 2.9×10^{-4} m/sec is dominated by the β-process. Therefore, it is apparent that in Broutman's study on crack propagation in polystyrene in the temperature range between -29°C and 40°C (cited earlier in this chapter) the observed continuous tearing fracture process with a fine cracked and silvery fracture surface appearance is dominated by the β-process. Furthermore, Broutman's observation that the crack propagation mode changes from continuous to discontinuous as the temperature is

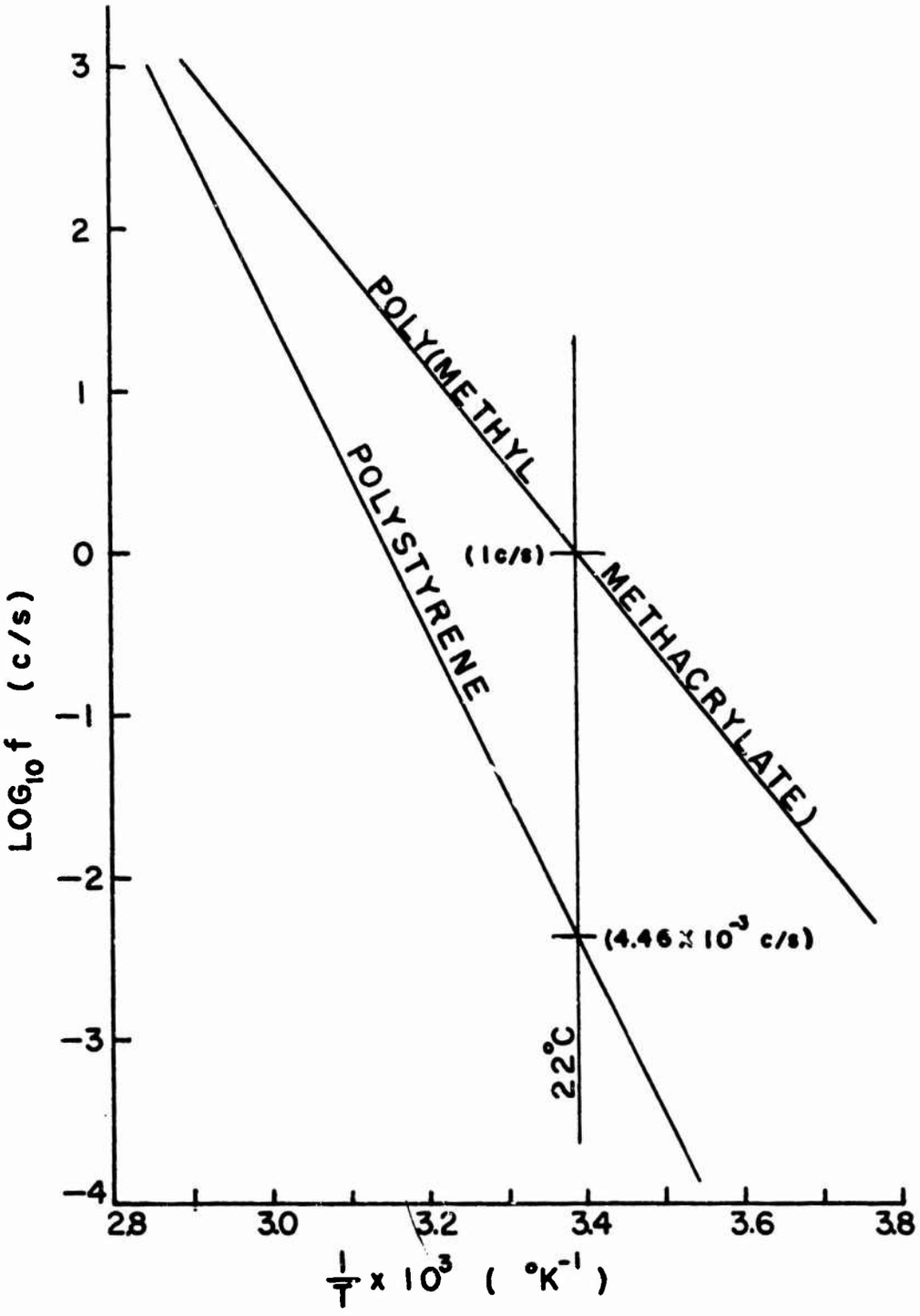

FIGURE 89. β-TRANSITION PEAK BEHAVIOR OF POLY(METHYL METHACRYLATE) AND POLYSTYRENE.

increased above 50°C indicates that at this higher temperature range the process change from α to β starts to take place and results in a discontinuous crack propagation mode. Thus it has been shown that the fracture phenomena of polystyrene can also be explained by the supposition developed in this chapter.

In the case of acrylic multipolymers which are plastic-rubber two phase polymers, it is known that a transition temperature due to rubber particles exists in addition to transitions of the matrix polymers. The existence of a transition temperature due to rubber particles suggests that another type of process should be considered as the fracture process in addition to the α- and β- process based on the matrix polymer. In Figures 70 and 77, the fracture surface work of commercial acrylic multipolymers (XT-500 and XT-375) and experimental acrylic multipolymers with seven different rubber content levels is plotted as a function of crack velocity. These figures indicate that two peaks exist in the curves of fracture surface work versus crack velocity. The peak at higher crack velocity may correspond to the β-processes due to rubber particles as shown in the study of acrylic multipolymers with seven different rubber content levels. Unfortunately at this state we do not have exact transition temperature measurements for these acrylic multipolymers; therefore, we cannot apply the fracture process supposition to these materials. In addition to the measurement of transition temperatures, it is necessary to study the effects of temperature on the fracture surface work. After establishing the simultaneous effects of temperature and crack velocities on the fracture surface work and transition temperatures, it is possible to analyze the precise fracture process of acrylic multipolymers. This is currently in progress.

CHAPTER VII

PROPERTIES OF COLD ROLLED CRYSTALLINE POLYCARBONATE

A. Survey of Crystallization Methods

Although amorphous polycarbonates are of great interest industrially, their crystallization has not yet been investigated extensively. The reasons for this are that the amorphous polycarbonates have already numerous applications due to their high impact strength and are difficult to crystallize thermally. However, by studying crystallization of polycarbonates and its influence on the mechanical properties, one may be able to expand the usefulness of polycarbonates as structural materials. The ability of crystallizable polymers to crystallize depends considerably on molecular chain-flexibility. Polycarbonates have rigid and extended chain structures; therefore, they are difficult to transfer from an amorphous to a crystalline structure. In this section some of the methods for inducing crystallinity will be discussed.

The methods of inducing crystallinity which have been reported in the polymer literature can be classified as follows:

1) thermal crystallization

2) partial swelling by solvents, by crystallizing liquids, or by solvent vapors

E. Turska, et al. (64) studied the influence of molecular weight on the crystallization kinetics of polycarbonates. They crystallized polycarbonates of different molecular weights at 190 + 1 degree centigrade in a thermostat filled with silicone oil after degassing for 24 hours at 140 - 150 degrees centigrade under vacuum (0.1 mm Hg). Figure 90 shows the results on three polymer samples, two of which have molecular weights (viscosity average) close to 31,000 and one approximately 67,600. The samples of higher molecular weight have a considerably lower rate of crystallization and a resulting smaller crystalline content at the end of the process. It was characteristic of all the polymers investigated that crystallization did not occur before an induction period of about 170 hours at 190 degrees centigrade.

Kämpf (65) reported that the first sign of spherulite development on the surface of a specimen was recognized after eight days at 180 degrees centigrade and that after eight days of annealing under nitrogen at 190 degrees centigrade full development of a spherulite structure was obtained. Figure 91 shows the results obtained by Turska, et al. (64) from three polymer samples, one of which has MW =32,050 and the two others MW = 51,300. The latter two are the same polymer; however, one was first dissolved at 280 degrees centigrade for one hour and then precipitated. The results show that the sample which was dissolved exhibits a shorter period of induction and a higher final degree of crystallinity. This indicates that the dissolving treatment has a strong influence on the final results. Turska, et al. Table 64 summarized their results as follows in table 21:

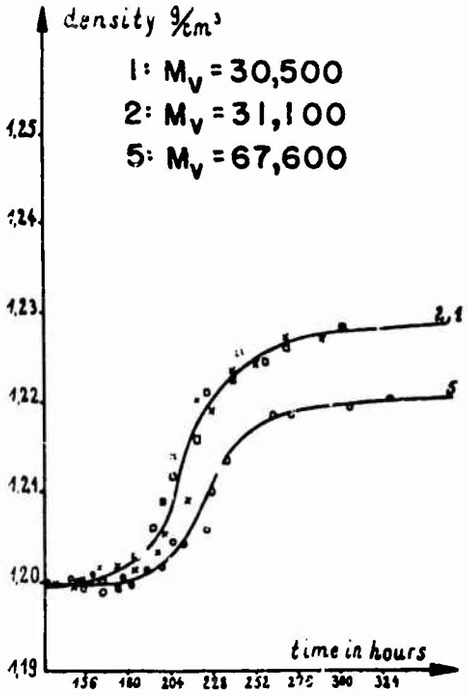

FIGURE 90. CRYSTALLIZATION KINETICS OF DIFFERENT MOLECULAR WEIGHT POLYCARBONATES (REF. 64).

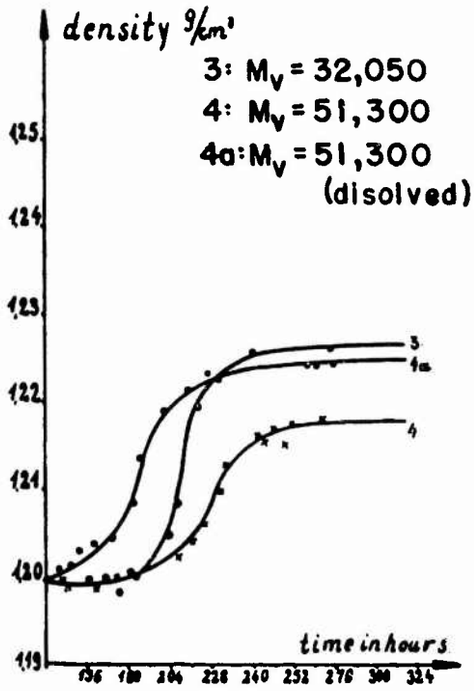

FIGURE 91. CRYSTALLIZATION KINETICS OF DIFFERENT MOLECULAR WEIGHT POLYCARBONATES (REF. 64).

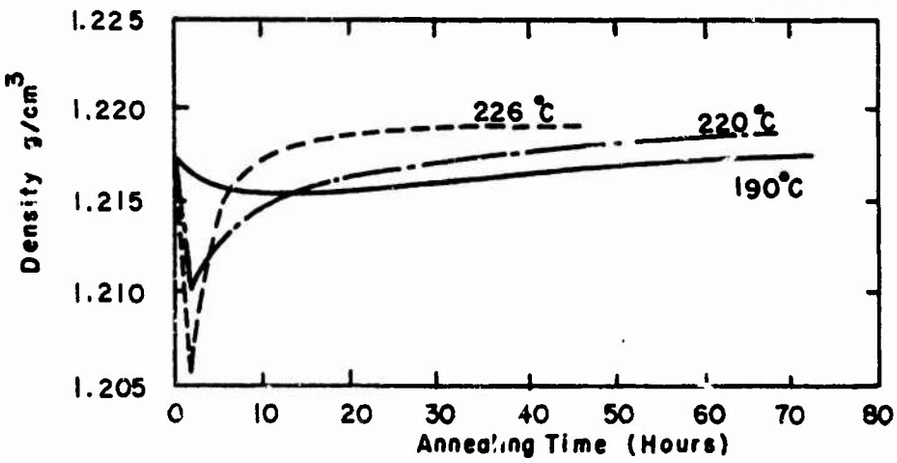

FIGURE 92. ISOTHERMAL ANNEALING TEMPERATURE EFFECT AND RECRYSTALLIZATION ON CRYSTALLIZED POLYCARBONATE (REF. 66).

TABLE 21.

EFFECT OF MOLECULAR WEIGHT ON
CRYSTALLIZATION OF POLYCARBONATES (REF. 64)

Sample	Intrinsic Viscosity	Viscosity Average Moleculat Weight	Annealing Hours	Degree of Crystallinity %
1	0.528	30,500	210	27
2	0.536	31,100	210	28
3	0.549	32,050	216	28.5
4	0.805	51,300	234	20
4a	0.805	51,300	192	26
5	1.019	67,600	228	18.5

Mercier, et al.(66) studied the isothermal annealing temperature effect and recrystallization on crystallized polycarbonates. They annealed samples at three different temperatures: 190, 220 and 226 degrees centigrade. The results are shown in Figure 92. They explain their results by assuming that two opposing processes intervene when one subjects crystallized polymers to an annealing process at a temperature between the crystallization temperature and the temperature of maximum fusion. It first produces rapid fusion of crystallites. The crystallites liquify at a temperature below the temperature of maximum fusion. Upon examination of Figure 92, one notices that a large amount of fusion begins rapidly at the annealing temperature; therefore, when annealed at 190 degrees centigrade, the minimum degree of crystallinity (20%) is measured after one hour. The minimum degree of crystallinity is 12% after one hour at 220 degrees centigrade and 8.5% after the same elapsed time at 226 degrees centigrade. Above 226 degrees centigrade one obtains complete fusion of crystallites despite the fact that this temperature can be 29 degrees centigrade below the point of maximum fusion of polycarbonates which is 265 degrees centigrade. In the second stage of the annealing phenomenon, the density of the polymer increases. It slowly produces recrystallization. The crystallites remaining after fusion act as nuclei.

Mercier (67) also investigated crystallization induced through partial swelling by a solvent vapor and by a crystallizing liquid vapor. The crystallizing liquids are liquids in which polymers are insoluble but do crystallize. Acetone, ethyl acetate, and tetrachlorethylene are crystallizing liquids for polycarbonates. The vapor induced crystallization of polycarbonates has advantages over the thermal crystallization. Specifically, thermal crystallization is not only time consuming but can result in thermal degradation of the material. Any trace of dust on the surface of the sample results in bubbles, and polymers crystallized by this method are usually of poor quality. Vapor-induced crystallization can be carried out at room temperature providing that the swelling agent has a sufficient vapor pressure at the temperature of crystallization.

Mercier pointed out that some complication arises in determining the absolute density of the polymer in the case of liquid and vapor-induced crystallization because it is impossible to remove all of the solvent absorbed by the polymer during crystallization. They carried out preliminary tests to determine how the density of the polymer was affected by residual solvents. Their results are shown in Table 22.

TABLE 22

EFFECT OF RESIDUAL SOLVENT ON DENSITY OF CRYSTALLINE POLYCARBONATE (REF. 67)

Solvent of Crystallization	Time of Drying	Residual Solvent (%)	Apparent Polymer Density
CH_2Cl_2	3 hrs.	21.3	1.259
	29 hrs.	13.8	1.251
	1 wk.	10.0	1.240
CH_2Cl_2	1-1/2 hrs.	26.0	1.259
	24 hrs.	14.8	1.253
	1 wk.	10.2	1.241
Acetone	1 hr.	17.1	1.270
	5 hrs.	14.2	1.267
	24 hrs.	10.6	1.265
	1 wk.	6.8	1.248
Acetone	1 hr.	17.6	1.271
	5 hrs.	13.7	1.267
	24 hrs.	10.4	1.263
	1 wk.	6.6	1.247

They solved this problem by annealing the crystallized polymer at a temperature higher than the glass transition temperature of the amorphous polymer (165 degrees centigrade for 17 hours). They claim that less than 0.5% of solvent remained absorbed in the polymer, and that it did not greatly distort density measurements.

After these initial studies, Mercier, et al., studied the crystallization of polycarbonate induced by vapor of two liquids: methylene chloride, which is classified as one of the best solvents for polycarbonates and has a high vapor pressure at room temperature (35 cm. Hg at 20 degrees centigrade), and acetone, which is classified as a weak precipitant but is known as a crystallizing agent for polycarbonates. Acetone has a lower vapor pressure (14 cm. Hg at 20 degrees centigrade). Figure 93

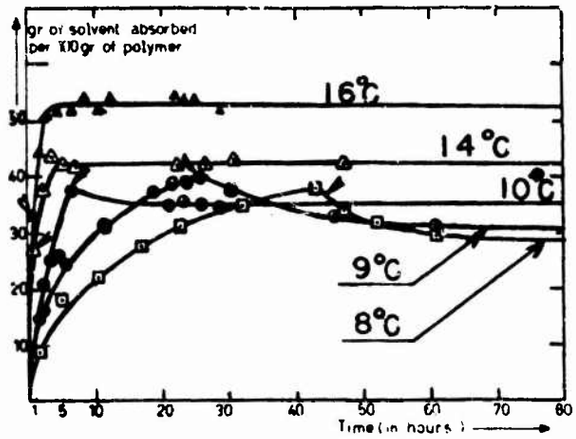

FIGURE 93. METHYLENE CHLORIDE ABSORPTION CURVES AT DIFFERENT TEMPERATURES (REF. 67)

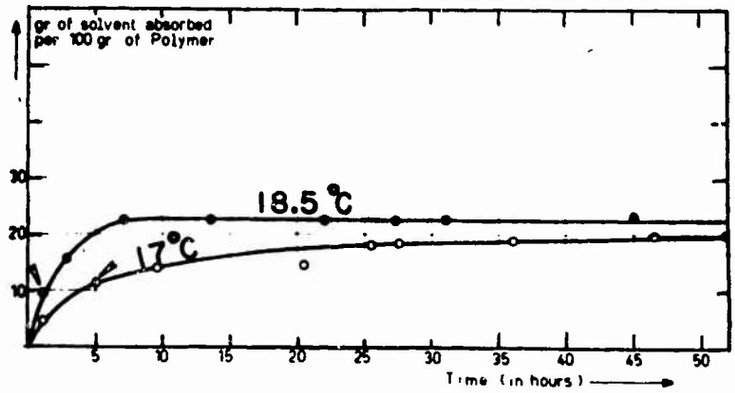

FIGURE 94. ACETONE ABSORPTION CURVES AT TWO DIFFERENT TEMPERATURES (REF. 67)

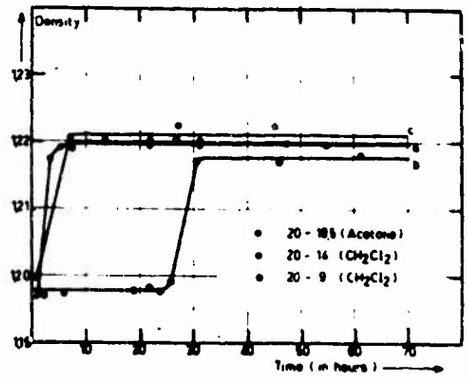

FIGURE 95. DENSITY CHANGE WITH TIME (REF. 67)

shows the absorption (in gms per 100 gms of polymer) of methylene chloride during the crystallization and the influence of the temperature, i.e., of the vapor pressure, of the crystallizing liquids. The temperature of the samples for the experiments was 20 degrees centigrade. From the results one can say that absorption takes place during the first stage of exposure and then remains steady, reaching equilibrium when the temperature of the crystallizing liquid is above 10 degrees centigrade. When the temperature of the liquid is below 10 degrees centigrade, the shape of the absorption isotherm changes. The absorption reaches a maximum, then a desorption phase occurs and, finally, an equilibrium is reached. In Figure 94 the results for the crystallization induced by acetone vapors are shown. The degree of absorption in this system is much lower than with methylene chloride.

Figure 95 shows the variation of density, i.e., crystallinity, with time for the following three cases: methylene chloride (14 degrees centigrade), methylene chloride (9 degrees centigrade) and acetone (18.5 degrees centigrade). The specimen temperature is maintained at 20 degrees centigrade. These results indicate that with sufficient vapor pressure (the solvent temperature is above 10 degrees centigrade in the case of methylene chloride) crystallization taken place very rapidly in a narrow front accompanying absorption. If the vapor pressure is lowered, absorption is less rapid and almost reaches an equilibrium before crystallization starts. This provides a more homogeneous process. This figure also indicates that acetone is more powerful in inducing the crystallization of polycarbonates, despite the fact that methylene chloride is the best solvent for polycarbonates.

B. Experimental Crystallization Procedure

Thermal Method. Plates (8" x 10") of both Lexan* and Merlon+ polycarbonate (extruded sheets), in thickness ranging from 1/16" to 1/4", were heat treated to induce crystallinity. The first experiments were conducted in an air circulating oven. An additional series of experiments was conducted in a vacuum oven under both vacuum conditions and under a nitrogen atmosphere.

A suitable rate and duration of heating for different sample thickness was determined by trial and error. All of the plates were first annealed below the glass transition temperature to remove residual stress or orientation as a result of prior processing. The temperature was then increased very slowly to 190°C and for a time consistent with the sample thickness. This is the temperature at which crystallization takes place most rapidly and completely.

Sample quantities of a low molecular weight polycarbonate, Merlon M-39-1000 natural, was obtained in pellet form from Mobay Chemical Co. The pellets were dried in an air circulating oven prior to compression molding. The mold (1/8" x 5" x 10") was treated with an air-dried and baked release agent and pre-heated before inserting between the platens of a Wabash Press. The molding procedure consisted of heating the material to 520°F at a pressure of 100 to 200 psi for approximately 10 minutes. An attempt was made to crystallize this material

---

* Registered Trademark, General Electric Co.

\+ Registered Trademark, Mobay Chemical Co.

by the methods described previously for the extruded sheet material. However, here, heat treatment was undertaken in the mold under pressure at 190°C for a period of 8 days.

Acetone Vapor Methods. Initial attempts to produce crystallized plates by submersion in liquid acetone were abandoned due to the loss of low molecular weight material to the liquid.

After careful annealing to remove residual stresses, the weight and dimensions of various thickness plates of Merlon polycarbonate were recorded. The plates were then suspended from a rack by a cloth sling inside a sealed jar containing liquid acetone. The liquid level was not allowed to contact the samples. Upon exposure to the acetone vapor for the required time, the samples were removed from the chamber and air-dried prior to elevated temperature treatment to remove the remaining acetone.

A typical annealing schedule to remove residual stresses for a 3/32" thick plate is given below:

(a) heat in air-circulating oven at 110°C for 12 hours

(b) raise temperature at a rate of 2° - 3°C per hour to 165°C and hold for 5 - 10 hours

(c) lower temperature at a rate of about 10°C per hour to ambient

A typical schedule for the removal of acetone is shown below:

(a) measure weight and dimensions of plate

(b) air-dry at room temperature for 48 hours

(c) dry at 130°C in air-circulating oven for time depending on amount of residual acetone and plate thickness desired

(d) measure final weight and dimensions

The weight and dimensions of the plate were recorded so that the residual acetone content and dimensional changes could be determined.

Density and Degree of Crystallinity. The density of the samples was determined in a density gradient column using an aqueous solution of calcium nitrate as the gradient liquid.

The degree of crystallinity was calculated from the density of the samples on the basis that the contribution of the amorphous and crystalline phase was additive. The crystallinity (C), expressed as a percent is given by:

$$C = \frac{\rho - \rho_a}{\rho_c - \rho_a} \times 100 \qquad (49)$$

where ρ is the density of the sample and the subscripts a and c refer to the amorphous and crystalline phase respectively. The values for the completely amorphous and crystalline material at 23°C were taken from the literature (64),

$$\rho_a = 1.194 \text{ gms/cm}^3 \text{ and } \rho_c = 1.310 \text{ gms/cm}^3$$

Molecular Weight Determination. The molecular weight of samples of polycarbonates was determined from measurements of the viscosity of dilute solutions of the material in methylene chloride*. The molecular weight was calculated from the relationship:

$$[\eta] = K M^{\alpha} \qquad (50)$$

where $[\eta]$ = instrinsic viscosity, dl/gm

$K = 1.11 \times 10^{-4}$ (Refs. 64, 66)

$\alpha = 0.82$ (Refs. 64, 66)

C. Experimental Results

Amorphous Material - Tensile Properties. The tensile characterization of the polycarbonate "as received" material was performed on an Instron Universal Test Machine using a Type 1, ASTM D638 Specimen. The properties are tabulated in Table 23 and a typical stress-strain curve appears in Figure 96.

Molecular Weights. Molecular weights, calculated from equation (50) are shown in Table 24 for commercial sheet materials of different thickness. The constants were taken from the literature (64, 66).

1. Thermally Crystallized Material - Tensile Properties.

In Air-Circulating Oven (0.060" thick plates). The tensile properties are tabulated in Table 25. Specimens identified by the character B were heat treated separately from those identified by the character C. The degree of crystallinity for both groups was 19.8% as determined from density measurements. No difference in the appearance of the plates could be discerned. Both sets were yellow-brown in color. A typical stress-strain curve is shown in Figure 97.

In Nitrogen Atmosphere (0.090" thick plates). Table 26 shows the tensile properties of samples treated in a Nitrogen atmosphere for 21 days at 190°C. These thicker plates displayed a darker brownish color than the thinner plates crystallized in an air-circulating oven for shorter periods of time. The stress-strain curves had the same shape for both treatments.

---

* Determined by ARRO Laboratories, Joliet, Ill.

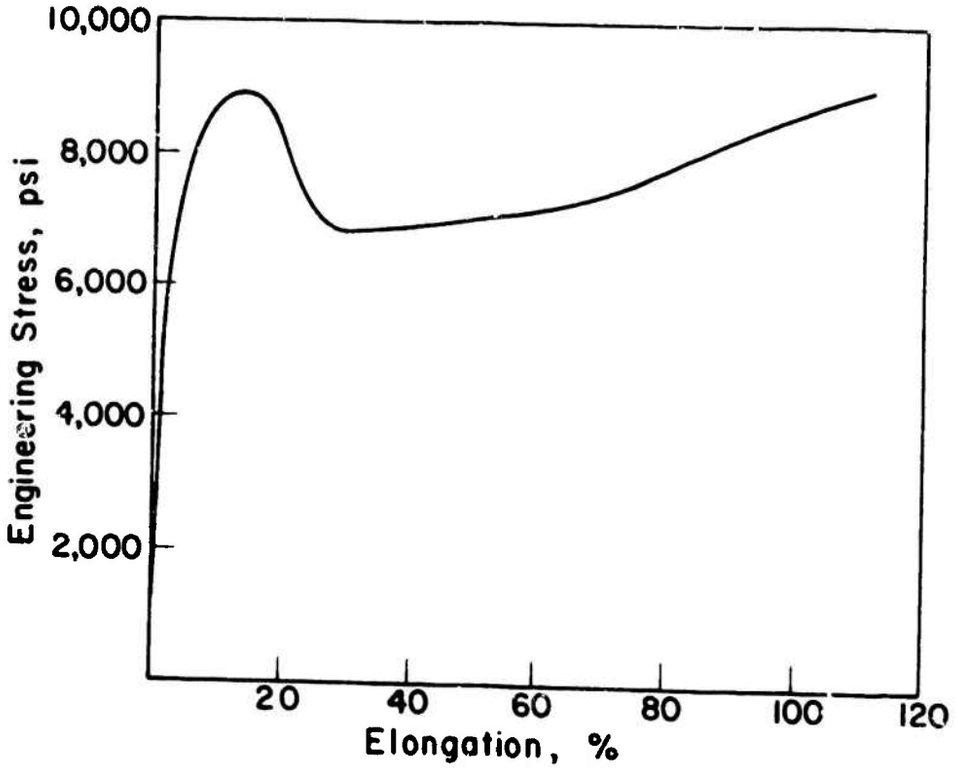

FIGURE 96. TYPICAL STRESS-STRAIN CURVE FOR AMORPHOUS POLYCARBONATE.

Table 23. Tensile Properties of Extruded Polycarbonate (Lexan)

Specimen Number	Width (in)	Thickness (in)	Area (in^2)	Crosshead Speed (in/min)	σ_{max}* (psi)	ε_f** (psi)	E*** (psi)
1	0.540	0.060	0.032	0.50	8,600	--	--
2	0.535	0.060	0.032	0.50	9,000	114	--
3	0.561	0.061	0.034	0.50	9,000	96	--
4	0.526	0.061	0.032	0.50	9,000	110	--
5	0.536	0.060	0.032	0.50	9,000	115	322,000
6	0.522	0.060	0.031	0.50	8,900	112	320,000
				Average	8,900	109	321,000

*Upper yield point

**Direct measurement at fracture for 1" gage length

***E determined using 1" extensometer

Table 24. Viscosity Average Molecular Weights of Polycarbonate Sheets

Sheet Thickness (inches)	ARRO Sample Number	Tradename	$[\eta]$	$\frac{[\eta]}{K}$	$\bar{M}_v^*$
0.060	3529	Lexan	0.700	6310	43,200
0.090	3530	Lexan	0.650	5860	39,600
0.125	3531	Lexan	0.606	5460	36,000
0.250	3532	Merlon	0.628	5660	38,000

$$*\bar{M}_v = \left[\frac{[\eta]}{1.11 \times 10^{-4}}\right]^{1.22}$$

Table 25. Tensile Properties of Crystallized Polycarbonate (1/16" Lexan sheet)*

Specimen Number	Width (in)	Thickness (in)	Area (in^2)	$\sigma_{ult.}$ (psi)	ε_f (%)	E** (psi)
B-1	0.540	0.061	0.033	7,200	2.15	384,000
B-2	0.548	0.061	0.033	7,050	--	--
B-3	0.538	0.062	0.033	7,950	2.36	415,000
B-4	0.542	0.061	0.033	7,300	2.54	320,000
B-5	0.542	0.062	0.034	7,600	2.20	374,000
			Average	7,400	2.31	373,000
C-1	0.542	0.060	0.032	5,900	1.80	373,000
C-2	0.526	0.061	0.032	6,300	1.93	384,000
C-3	0.532	0.061	0.032	5,200	1.53	365,000
C-4	0.532	0.061	0.032	6,050	1.76	373,000
C-5	0.538	0.060	0.032	7,150	2.33	342,000
C-6	0.542	0.060	0.033	7,000	2.34	323,000
C-7	0.538	0.061	0.033	6,050	1.78	358,000
			Average	6,200	1.92	360,000

*elongation rate=0.5 in/min

**E measured using 1" extensometer

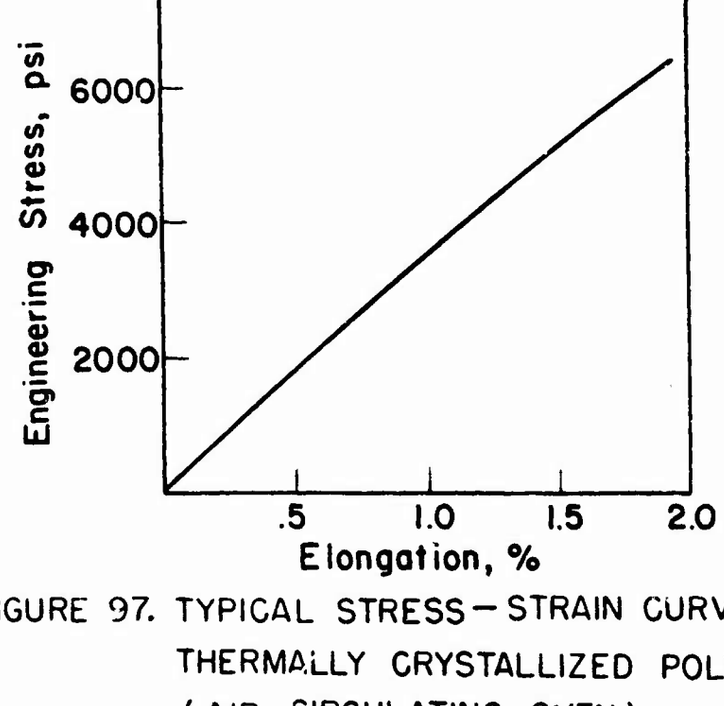

FIGURE 97. TYPICAL STRESS—STRAIN CURVE FOR THERMALLY CRYSTALLIZED POLYCARBONATE (AIR CIRCULATING OVEN).

Table 26. Tensile Properties of Polycarbonate Thermally Crystallized in Nitrogen Gas*

Specimen Number	$\sigma_{ult.}$ (ksi)	ε_f (%)	E (psi x 10^5)
1	5.65	1.59	3.84
2	5.60	1.52	3.87
3	5.75	1.72	3.57
4	6.50	2.17	3.40
5	6.50	2.10	3.65
6	6.35	1.87	4.13
7	5.90	1.69	3.84
Average :	6.04	1.81	3.76

*Plates 0.090 inch thick Lexan--Crystallized at 190°C for 21 days--Crosshead rate for testing 0.05 in/min

2. Acetone Vapor-Induced Crystalline Polycarbonate.

Effect of Acetone. In the case of acetone vapor-induced crystalline polycarbonate it is difficult to remove the acetone completely from the crystallized polycarbonate. Experiments, therefore, were carried out to investigate the effect of the remaining acetone on the modulus, stress-strain behavior, and impact strengths. The results are shown in Figure 98 and Table 27 and will be discussed later. The drying and diffusion process for removal of the acetone from the crystallized plated is discussed in the appendix.

Effect of Cold Rolling on Properties of Crystallized Polycarbonate. Crystallized polycarbonate sheets (Lexan) were cold rolled uniaxially to particular thickness reductions in a laboratory rolling mill. One additional sheet was rolled biaxially to 50% thickness reduction. These rolled sheets were then tested in tension. The tensile properties are shown in Table 28. Figure 99 is a plot of typical stress-strain curves for comparison.

In order to investigate the effect of residual acetone on the mechanical properties of cold rolled crystallized polycarbonate, different sets of polycarbonate sheets (Merlon) which contain different amounts of residual acetone were rolled and tested in bending and tension.

Test results in bending (3 point bending) are shown in Figures 100 and 101, and tensile results are shown in Figures 102 and 103 as well as Table 29. Figures 104 and 105 are photographs indicating the difference of appearance in high acetone content tensile specimens and low acetone content tensile specimens. One interesting difference between high and low residual acetone materials is, as shown in Figures 104 and 105, that stress-whitening appears in high residual acetone material tensile specimens.

In rolling crystallized sheets which contain different amounts of residual acetone one interesting phenomenon was observed. Crystallized sheets which contained residual acetone of 13.15 gms/100 gms of polymer and 10.45 gms/100 of polymer started to show cracking slightly above 30 percent of thickness reduction in rolling; on the other hand, sheets which contained residual acetone of 3.00 gms/100 gms. of polymer and 4.17 gms/100 gms of polymer did not show any sign of cracking even at 56.9 percent thickness reduction in rolling.

D. Discussion

As demonstrated in our experiment and also discussed in the literature, the thermal crystallization method for polycarbonate causes severe material damage by degradation since the material has to be subjected to a high temperature for a long period of time. This is especially so in the case of thicker plates (3/16" - 1/4" thick). The acetone vapor-induced crystallization, however, is carried out at room temperature and does not damage the material. On the other hand, it is very difficult to remove the acetone completely from the material after crystallization, as shown in Figures 110 and 111 in the appendix. It may therefore be necessary to consider the acetone vapor-induced crystallized material as a multi-phase material, that is, a crystalline phase and amorphous phase with absorbed acetone. The actual role of the residual acetone in crystallized polycarbonate is not known, and

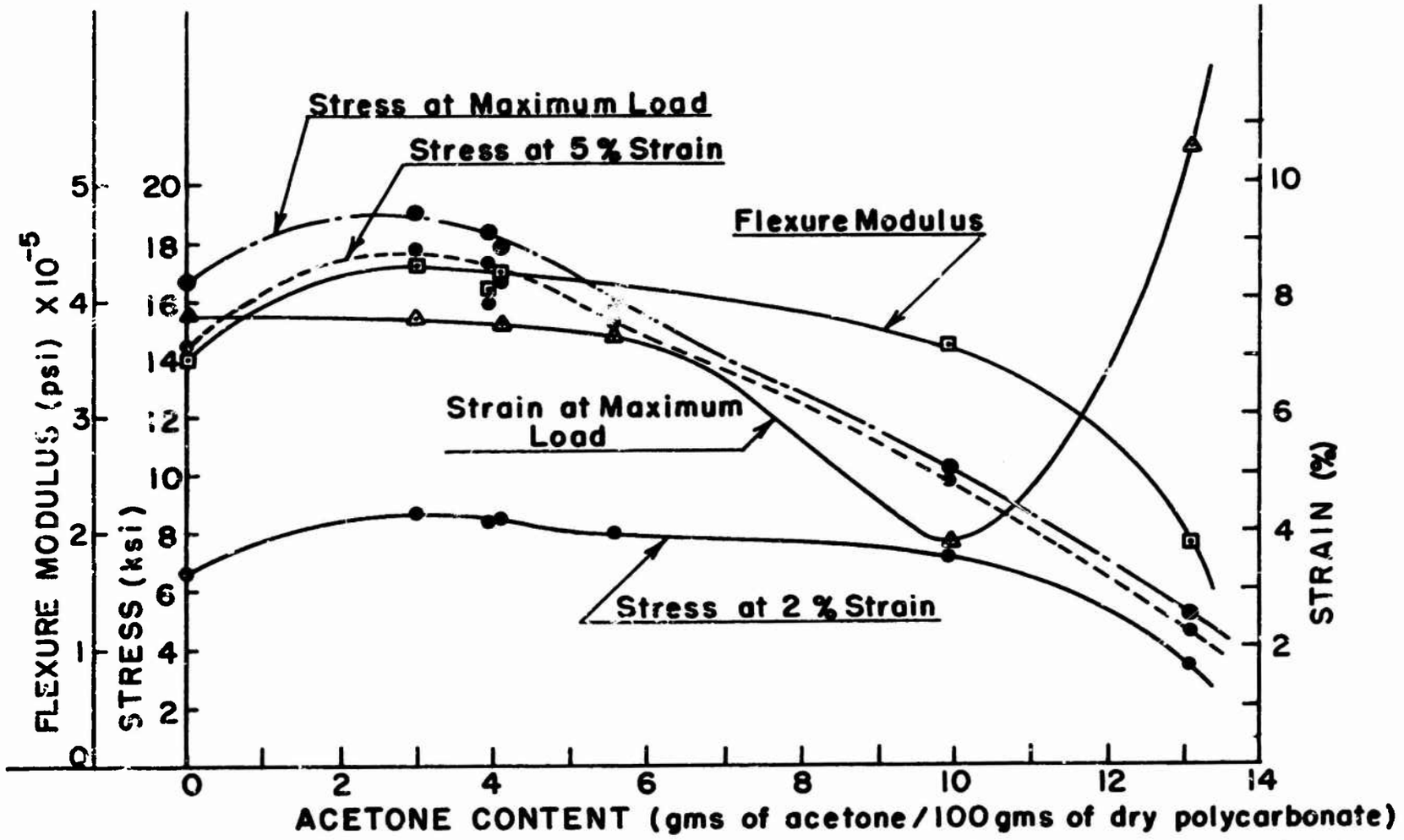

FIGURE 98. EFFECTS OF RESIDUAL ACETONE ON STRESS, STRAIN, AND FLEXURE MODULUS OF POLYCARBONATE.

Table 27. Effect of Remaining Acetone on Mechanical Properties of Crystallized Polycarbonate

Acetone Content (grams/ 100grams dry polycarbonate)	Crosshead rate (in/min)	Flexure Modulus (psi)	Stress at 2% Strain (psi)	Stress at 5% Strain (psi)	Stress at Max. Load (psi)	Strain at Max. Load (%)	Izod Impact $\left(\frac{\text{ft. lb.}}{\text{inch of notch}}\right)$
13.15	0.02	1.75×10^5	--	--	--	--	Too ductile
	0.05	1.88×10^5	3.25×10^3	4.46×10^3	4.90×10^3	10.6	No crack propagation
	0.1	1.89×10^5	--	--	--	--	
	0.05	2.06×10^5	--	--	--	--	
9.98	0.02	3.45×10^5	--	--	--	--	--
	0.05	3.57×10^5	7.18×10^3	9.88×10^3	10.0×10^3	3.86	--
	0.1	3.65×10^5	--	--	--	--	--
	0.5	3.76×10^5	--	--	--	--	--
5.60	0.02	3.98×10^5	8.33×10^3	14.7×10^3	15.3×10^3	8.06	--
	0.1	3.46×10^5	7.95×10^3	15.1×10^3	15.5×10^3	7.39	0.296
	0.5	3.91×10^5	8.47×10^3	15.9×10^3	16.3×10^3	6.45	--
3.97	0.02	4.05×10^5	8.33×10^3	16.5×10^3	17.0×10^3	8.27	--
	0.1	4.09×10^5	8.47×10^3	17.2×10^3	18.4×10^3	7.95	0.447
	0.5	4.09×10^5	8.60×10^3	17.5×10^3	18.9×10^3	7.47	--

Table 27. (Continued)

Acetone Content (grams/ 100 grams dry polycarbonate)	Crosshead rate (in/min)	Flexure Modulus (psi)	Stress at 2% Strain (psi)	Stress at 5% Strain (psi)	Stress at Max. Load (psi)	Strain at Max. Load (%)	Izod Impact $\left(\frac{\text{ft.lb.}}{\text{inch of notch}}\right)$
4.12	0.1	4.235×10^5	8.49×10^3	16.86×10^3	17.70×10^3	7.62	--
3.00	0.1	4.303×10^5	8.61×10^3	17.56×10^3	19.06×10^3	7.70	--
Amorphous Annealed							
0	0.1	3.47×10^5	6.61×10^3	14.4×10^3	16.7×10^5	7.47	--

Table 28. Properties of Rolled Crystallized Polycarbonate (Lexan)

Specimen Number	Area (in^2)	Modulus of Elasticity E(psi x 10^5)	σ_o 2% Offset Yield Stress (ksi)	Fracture Stress (ksi)
25-1-0-1*	0.0272	4.36	6.56	10.3
2		4.34	6.80	10.3
3		4.70	6.45	10.4
50-1-0-1	0.0176	4.93	6.75	13.5**
2		4.83	7.30	16.9
3		4.95	6.50	15.7
50-1-90-1	0.0088	3.70	--	7.85
50-2-0-1	0.0091	4.35	--	11.1
2		4.17	--	11.2
3		4.05	--	11.2
69-1-0-1	0.0113	4.93	7.0	24.5
2		5.13	7.6	23.8
3		4.87	7.55	24.5
69-1-90-1	0.00568	3.35	--	8.70
2		3.45	--	8.20
Amorphous Properties				
		3.21		8.90

*Number Code: First number = % reduction of thickness
Second number = 1 for uniaxially rolled;
2 for biaxially rolled
Third number = orientation of text specimen with respect to roll direction
Fourth number = specimen number

**Failed at site of flow

Table 28. (Continued)

Specimen Number	Strain to Fracture (%)	Original Thickness (in)	Thickness after Crystal-lization (in)	Final Thickness (in)
25-1-0-1	10.0	0.060	0.074	0.056
2	16.0	0.060	0.074	0.056
3	18.0	0.060	0.074	0.056
50-1-0-1	--	0.060	0.072	0.036
2	50.0	0.060	0.072	0.036
3	49.0	0.060	0.072	0.036
50-1-90-1	145.0	0.060	0.072	0.036
50-2-0-1	98.0	0.060	0.074	0.037
2	97.0	0.060	0.074	0.037
3	100.0	0.060	0.074	0.037
69-1-0-1	26.0	0.060	0.074	0.023
2	25.0	0.060	0.074	0.023
3	25.0	0.060	0.074	0.023
69-1-90-1	165.0	0.060	0.074	0.023
2	150.0	0.060	0.074	0.023
Amorphous Properties				
	109.0			

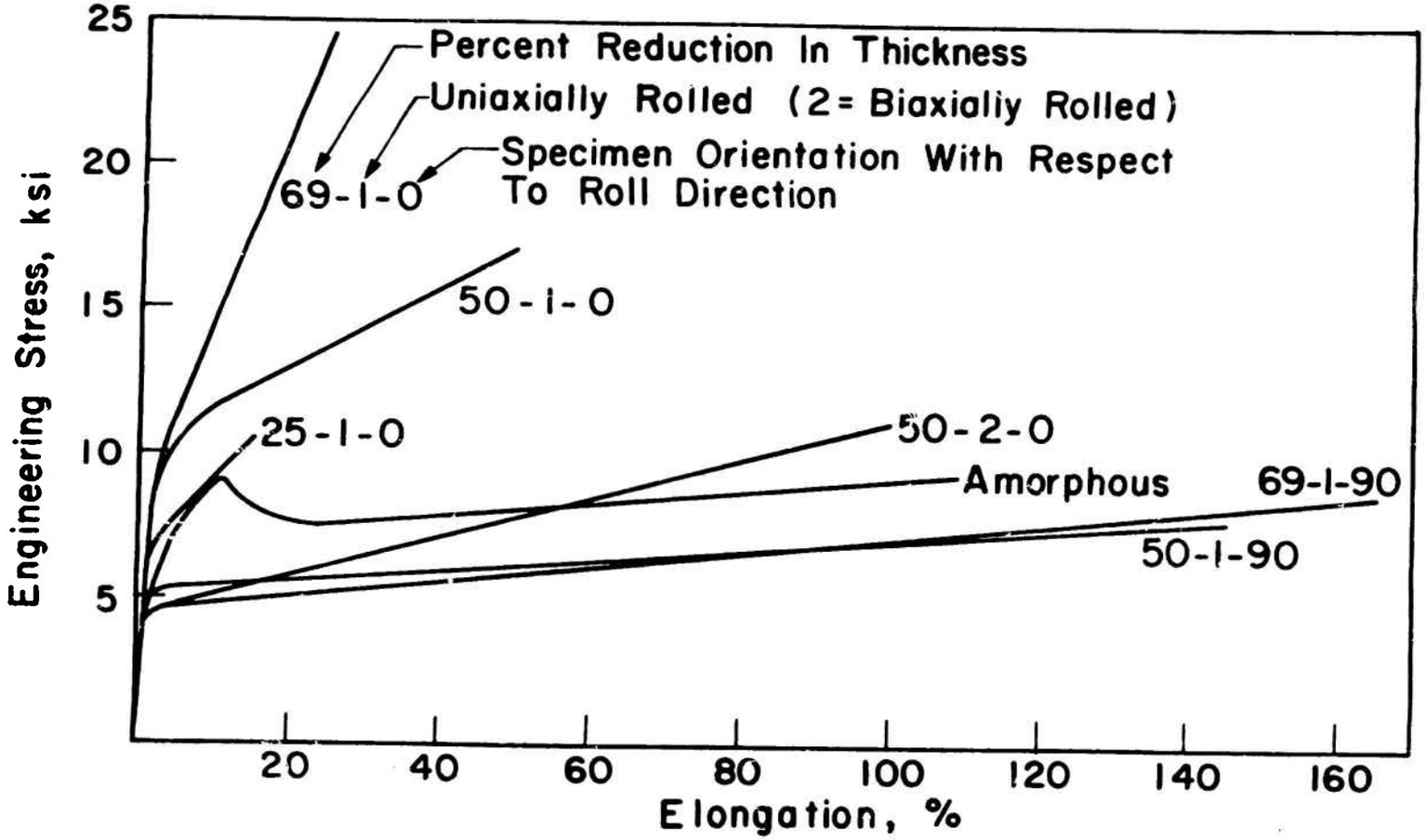

FIGURE 99. COMPARISON OF CRYSTALLIZED AND ROLLED POLY-CARBONATE SHEETS.

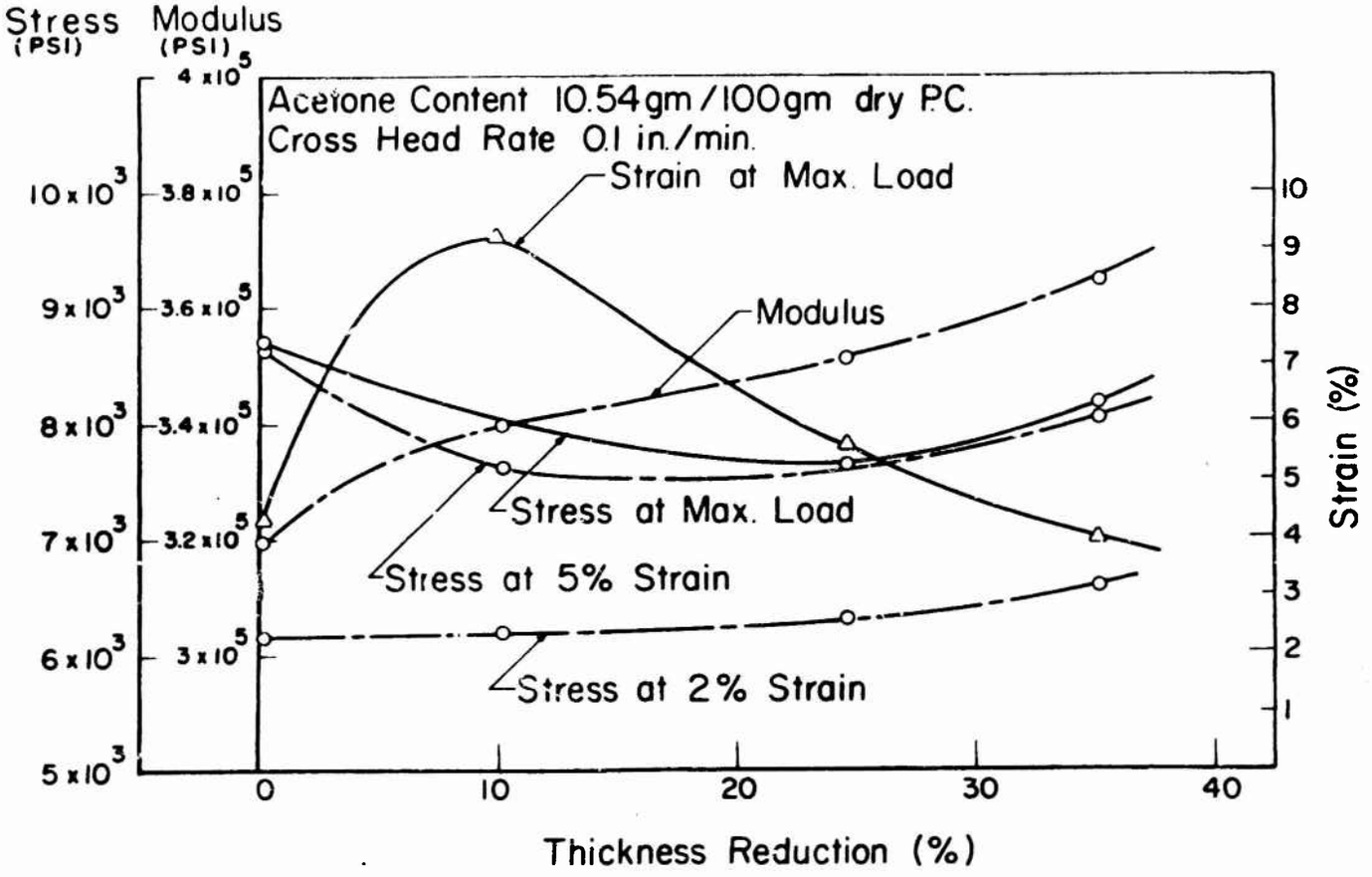

FIGURE 100. EFFECTS OF ROLLING ON STRESS, STRAIN, AND MODULUS OF POLYCARBONATE CONTAINING 10.54 GRAMS OF ACETONE PER 100 GRAMS OF DRY POLYCARBONATE.

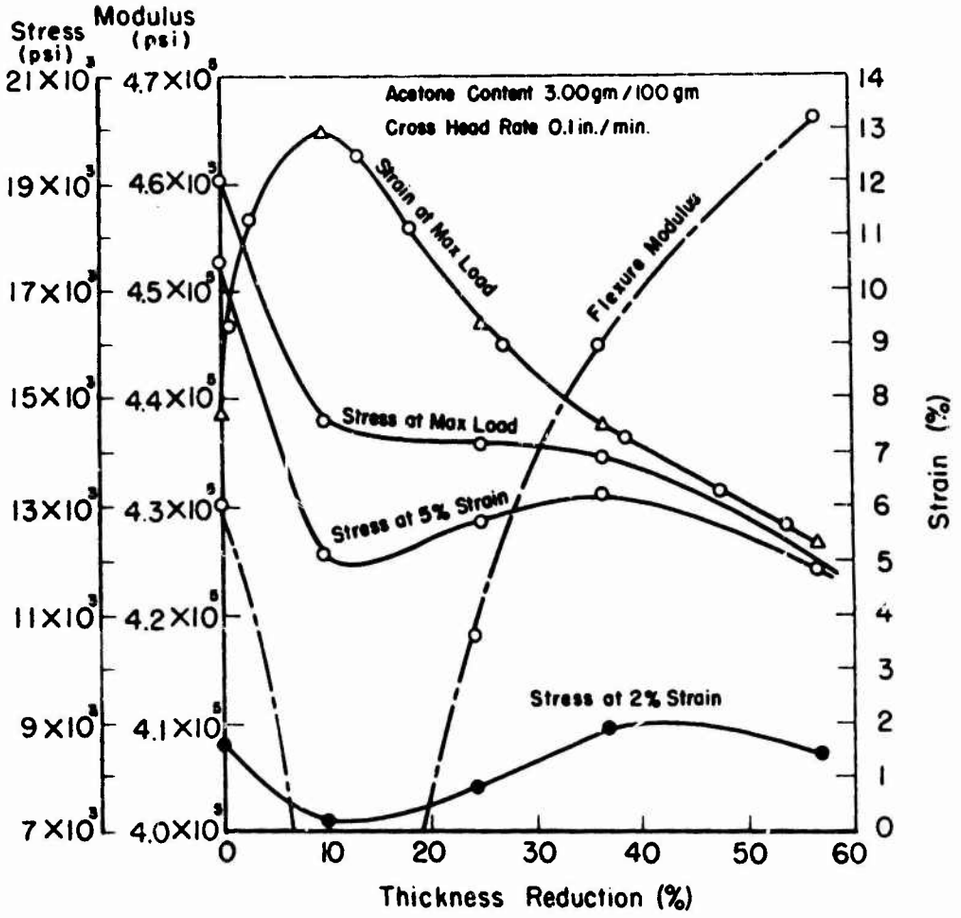

FIGURE 101. EFFECTS OF ROLLING ON STRESS, STRAIN, AND MODULUS OF POLYCARBONATE CONTAINING 3.00 grams OF ACETONE PER 100 grams OF DRY POLYCARBONATE.

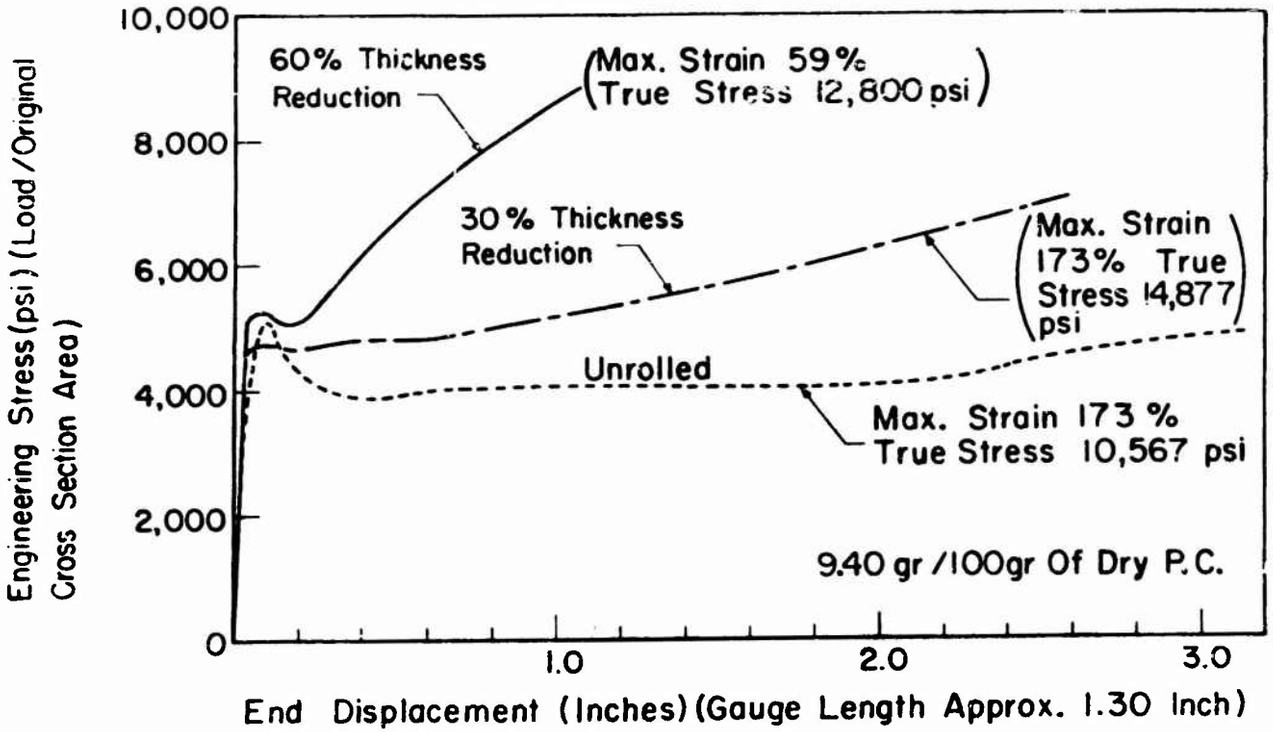

FIGURE 102. STRESS-STRAIN BEHAVIOR OF ROLLED CRYSTALLIZED POLYCARBONATE CONTAINING 9.40 GRAMS OF ACETONE PER 100 GRAMS OF DRY POLYCARBONATE.

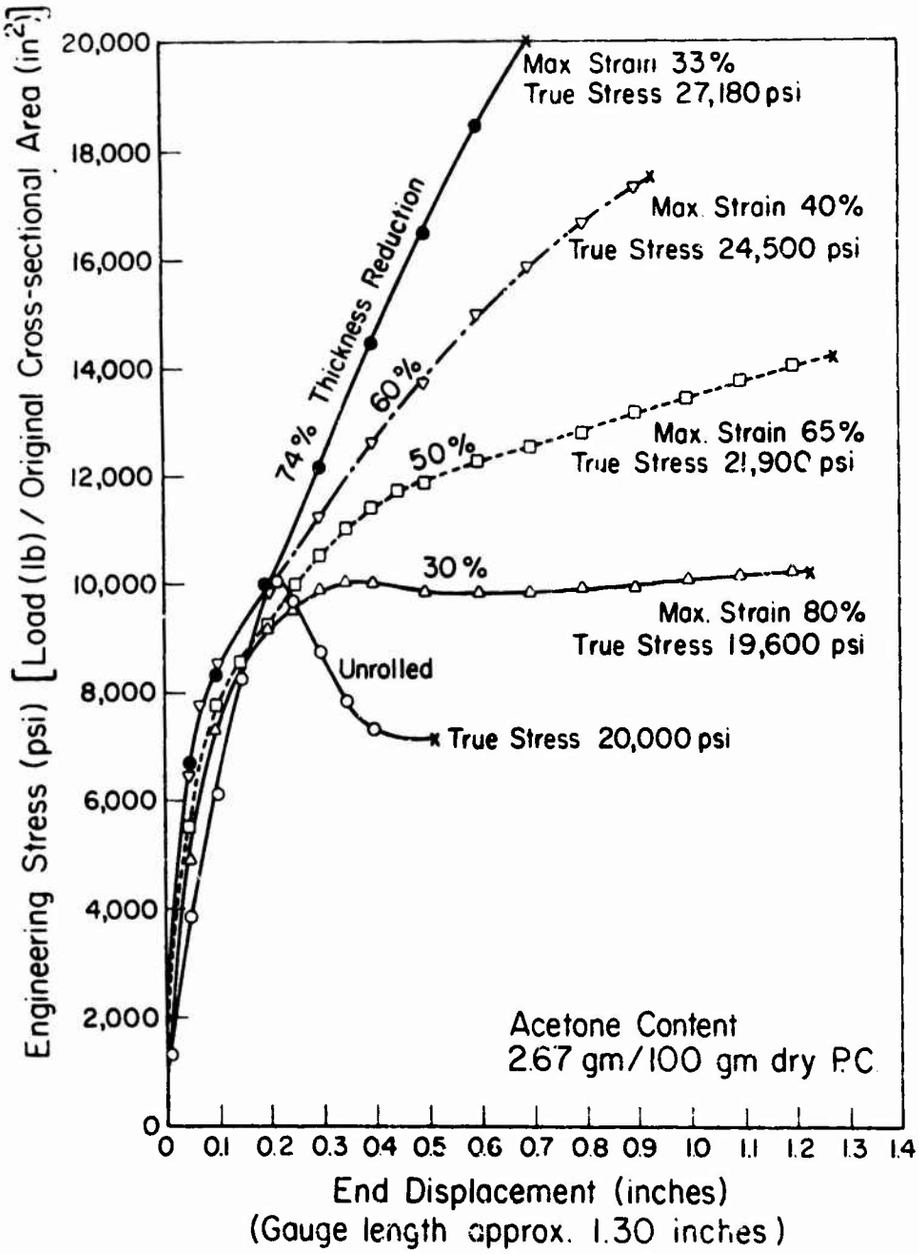

FIGURE 103. STRESS–STRAIN BEHAVIOR OF ROLLED CRYSTALLIZED POLYCARBONATE CONTAINING 2.67 GRAMS OF ACETONE PER 100 GRAMS OF DRY POLYCARBONATE AT DIFFERENT ROLLING THICKNESS REDUCTIONS.

Table 29. Properties of Crystallized and Rolled Polycarbonate (Merlon)

Acetone Content (grams/ 100 grams dry poly-carbonate)	%Reduc-tion of Thick-ness	Initial Cross Sectional Area (in^2)	Final Cross Sectional Area (in^2)	Engineering Stress (psi)	True Stress at Fracture (psi)	Max. Strain
	0	0.0648	0.030	5096 (at yield) 4892 (at fracture)	10,567	173%
9.40	30	0.0291	0.0139	4820 (at yield) 7045 (at fracture)	14,877	143%
	60	0.0163	0.0113	5276 (at yield) 8834 (at fracture)	12,800	59%
	0	0.0868	0.0311	10081 (at yield) 7143 (at fracture)	20,000	--
2.67	30	0.0588	0.0308	10034 (at yield) 10272 (at fracture)	19,610	80%
	50	0.0398	0.0261	14322 (at fracture)	21,900	65%
	60	0.0320	0.0230	17594 (at fracture)	24,500	40%
	74	0.0095	0.0071	20316 (at fracture)	27,183	33%

Cross Head Rate 0.2 in/min

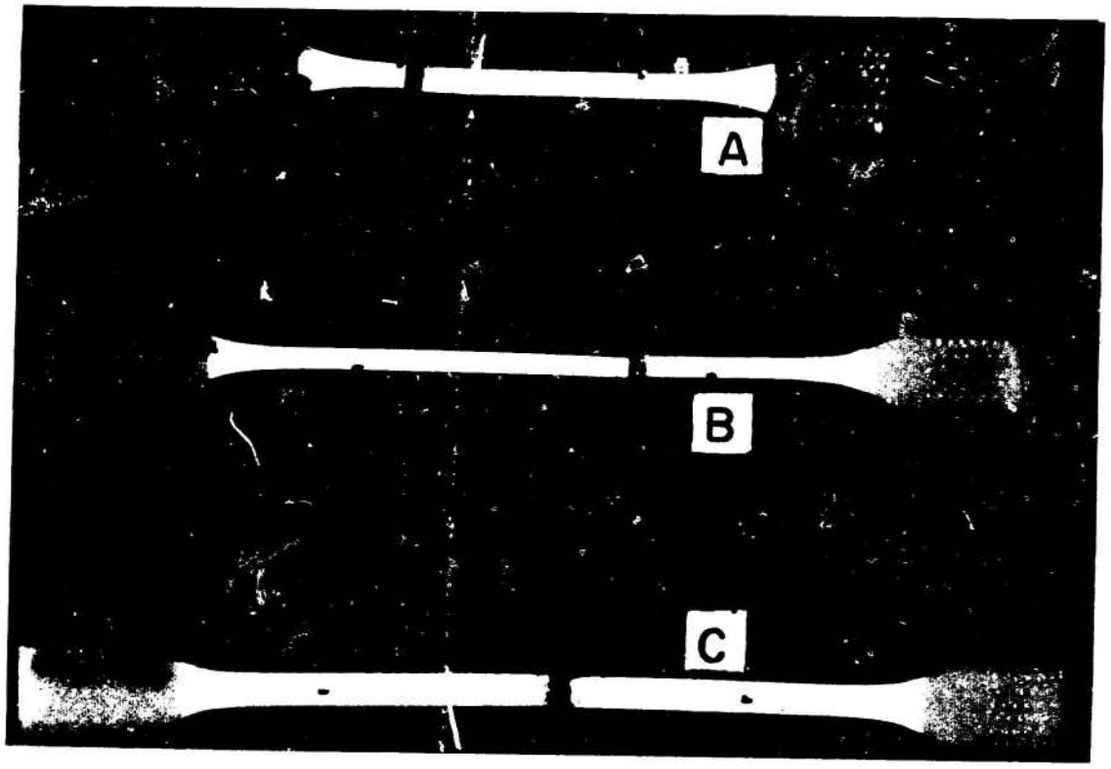

THICKNESS REDUCTION BY ROLLING

A: 60 %

B: 30 %

C: 0 %

FIGURE 104. FRACTURE MODES OF CRYSTALLIZED AND ROLLED SPECIMENS CONTAINING 9.40 GRAMS OF ACETONE PER 100 GRAMS OF DRY POLYCARBONATE.

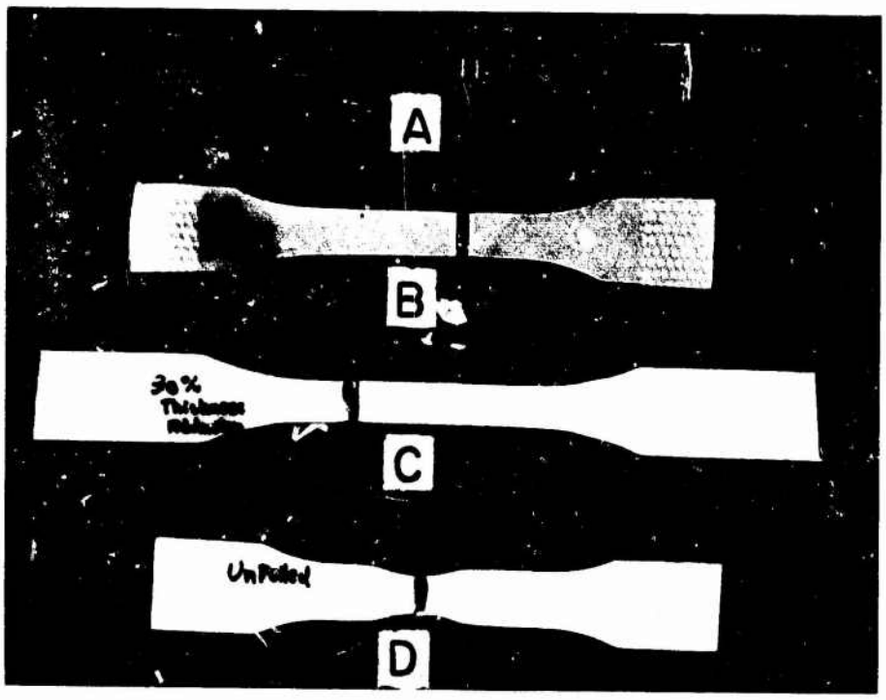

THICKNESS REDUCTION BY ROLLING
A: 74 %, B: 60 %, C: 30 %, AND D: UNROLLED.

FIGURE 105. FRACTURE MODES OF CRYSTALLIZED AND ROLLED SPECIMENS CONTAINING 2.67 GRAMS OF ACETONE PER 100 GRAMS OF DRY POLYCARBONATE.

further study is necessary to define the exact function of residual acetone.

Figure 98 shows the effect of residual acetone on the mechanical properties of the crystallized polycarbonate tested in bending. The equilibrium concentration of acetone at room temperature is about 20 grams of acetone per 100 grams of dry annealed polycarbonate. As the concentration of acetone decreases from this point, the flexure modulus increases very rapidly until the concentration of acetone decreases to 10 grams of acetone in 100 grams of dry polycarbonate. Below this concentration the rate of increase of the flexure modulus becomes much less. The flexure modulus of amorphous polycarbonate is $3.2 - 3.4 \times 10^5$ psi. The modulus of crystallized polycarbonate with 3 percent of acetone concentration is, therefore, increased about 30 percent. Figures 102 and 103 show the load-deflection curves in tension of crystallized polycarbonate with 9.40 and 7.67 percent acetone concentration respectively. From these curves one can see that the crystallized polycarbonate with high acetone concentration shows necking and its propagation is accompanied by stress-whitening shown in Figure 104. On the other hand, crystallized polycarbonate with low acetone concentration shows necking without propagation. No stress-whitening is observed in the area of the neck. This is shown in Figure 105.

The neck phenomenon is also influenced by rolling. The effect of cold rolling on some of the properties of amorphous polycarbonate was reported earlier (5). It was found that cold drawing can be eliminated by a rolling reduction of 30% or more. Crystallized polycarbonate also exhibits the disappearance of necking when rolled 30% or more for the case of sheets with low residual acetone content, however, high acetone content crystallized material exhibits necking even up to 60 percent thickness reduction by cold rolling.

In summary, the amorphous unrolled material exhibits the phenomena of necking and neck growth; however, the crystallized unrolled material exhibits necking but no stable growth. Rolled amorphous material and rolled crystalline material show similar load-deflection curves, but large differences appear on the true stresses and true strains. Crystallization raises the value of true stresses and true strains extensively.

Appendix: Diffusion Process in Acetone Vapor-Induced Crystallization of Polycarbonate

Acetone vapor-induced crystallization is a direct result of diffusion of acetone molecules and the resulting swelling caused by the acetone in the polycarbonate. In this appendix acetone vapor-induced crystallization and related problems such as cracking of specimens during the crystallization process are studied in relation to the diffusion process.

Diffusion in polymers has been studied by many researchers, and two limiting cases of diffusion have been established. One of them is called Fickian diffusion, which satisfies the following of Fick's equations:

$$D\nabla^2 C = \frac{\partial C}{\partial t} \quad \text{or} \quad \nabla [D(C)\, \nabla C] = \frac{\partial C}{\partial t} \tag{51}$$

where C is concentration, D is a constant diffusion coefficient, and D(C) is a concentration-dependent diffusion coefficient. Some of the characteristics of Fickian diffusion are summarized as follows by H. Fujita in his chapter "Diffusion in Polymers" and referred to by Hopfenberg, Holly and Stannett (69):

1. Initial weight increase is proportional to the square root of time.
2. A smooth and continuous concentration profile exists through the thickness of the sample.
3. The concentration becomes uniform across the film at long times.

Fickian diffusion is observed in the case of the diffusion of organic penetrants above the glass transition temperature of a polymer.

The other type of limiting case for diffusion has been observed in glassy polymers and is designated as "Case II" by T. Alfrey, Jr., et al. (70). Its characteristic phenomena are summarized as follows:

1. A sharp advancing boundary separates the inner glassy core of essentially zero penetrant concentration from the outer swollen, rubbery shell.
2. The swollen gel is essentially in an equilibrium state of swelling.
3. The boundary between swollen gel and glassy core advances at constant velocity.
4. The "initial weight" increase is directly proportional to time; whereas Fickian diffusion shows that the initial weight increase is proportional to the square root of time.

The above diffusion processes do not assume any phase change of the materials; however, the diffusion process of acetone in polycarbonate involves a phase change of material: the amorphous polycarbonate swells in contact with acetone vapor and partially crystallizes in the swollen gel. With this in mind, the diffusion of acetone vapor-induced crystallization of polycarbonate is studied.

Figures 106 and 107 show the relations between the weight of absorbed acetone in 100 grams of dry amorphous annealed polycarbonate versus sorption time plotted with a linear scale (Figure 106) and with a log-log scale (Figure 107). Two different sorption temperatures were used and in both cases the specimen and acetone were held at the same temperature, 23°C and 40°C.

Figure 108-1 shows photographs of a series of cross-sections of two plates at 23°C and 40°C at different times and indicating sharp advancing boundaries between the swollen shells and the glassy core of zero concentration. From these pictures, the variables of thickness reduction of the center glassy core and total thickness increase in time are measured. This is shown in Figure 109.

Figure 110 shows the rate of removal of acetone (desorption) from partially crystallized swollen polycarbonate at temperatures of 24°C and 100°C.

Figure 111 is a replotting of the results in Figure 110 on a log-log scale.

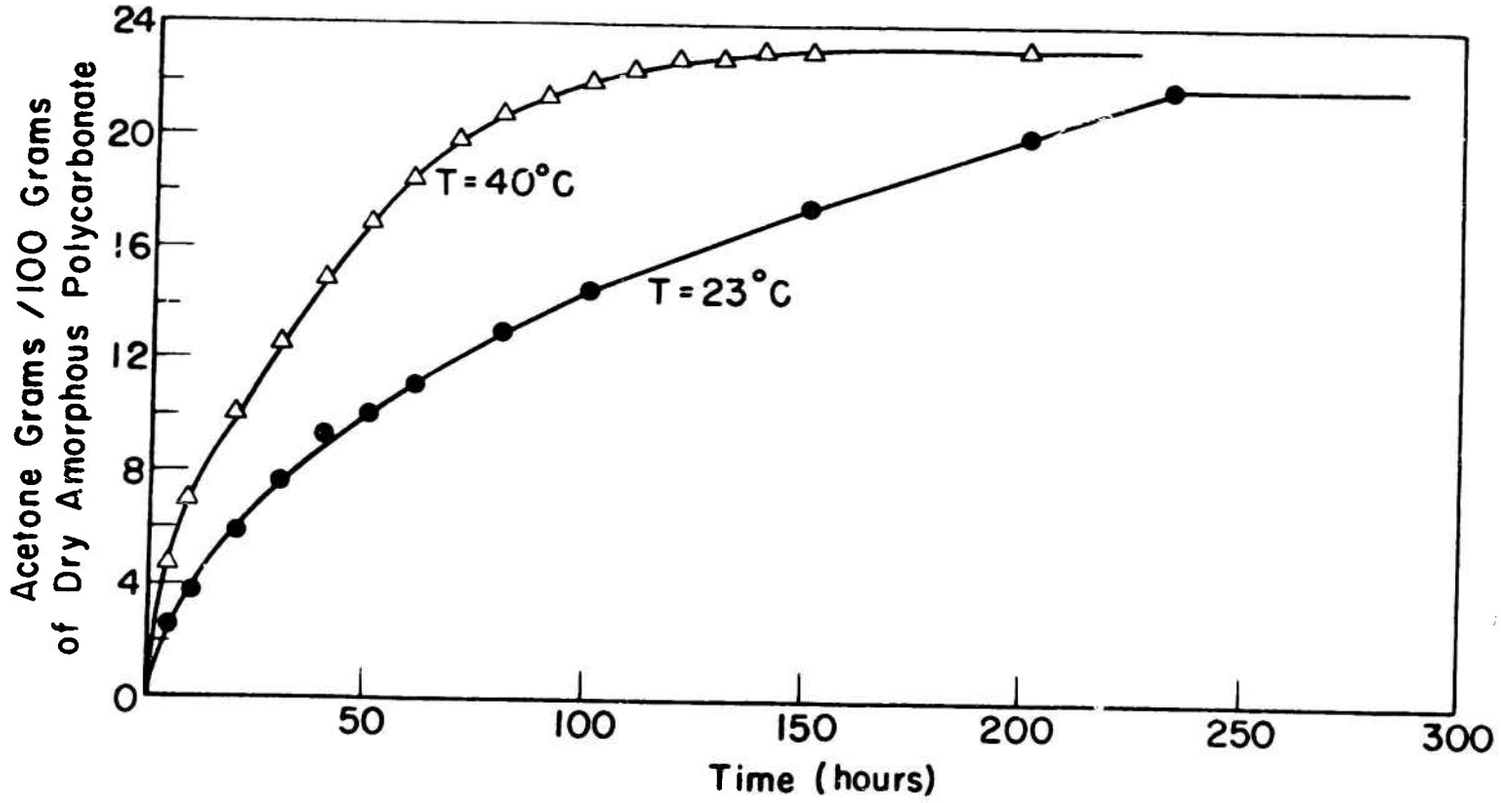

FIGURE 106. ACETONE CONTENT VERSUS SORPTION TIME.

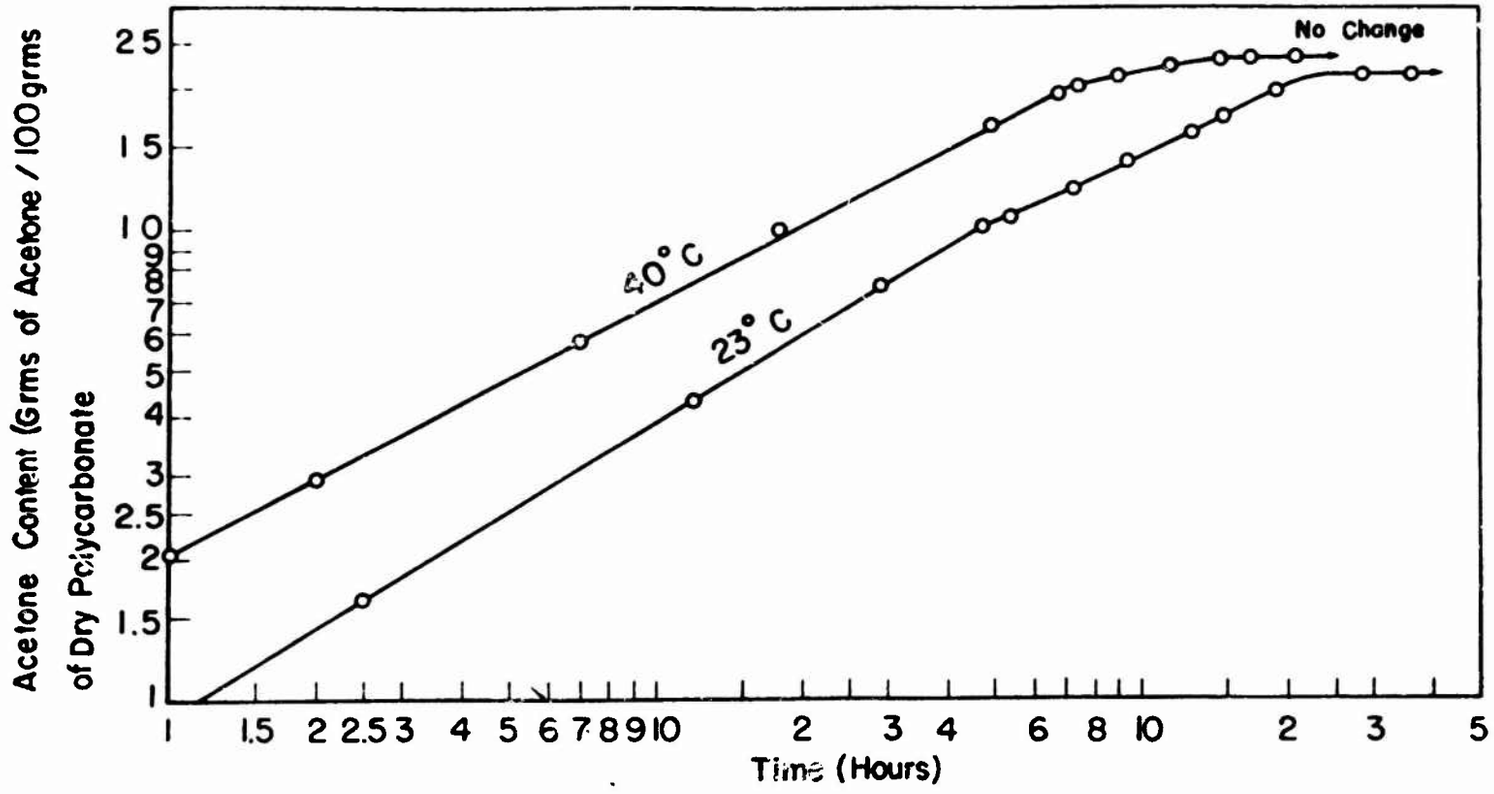

FIGURE 107. ACETONE CONTENT VERSUS SORPTION TIME.

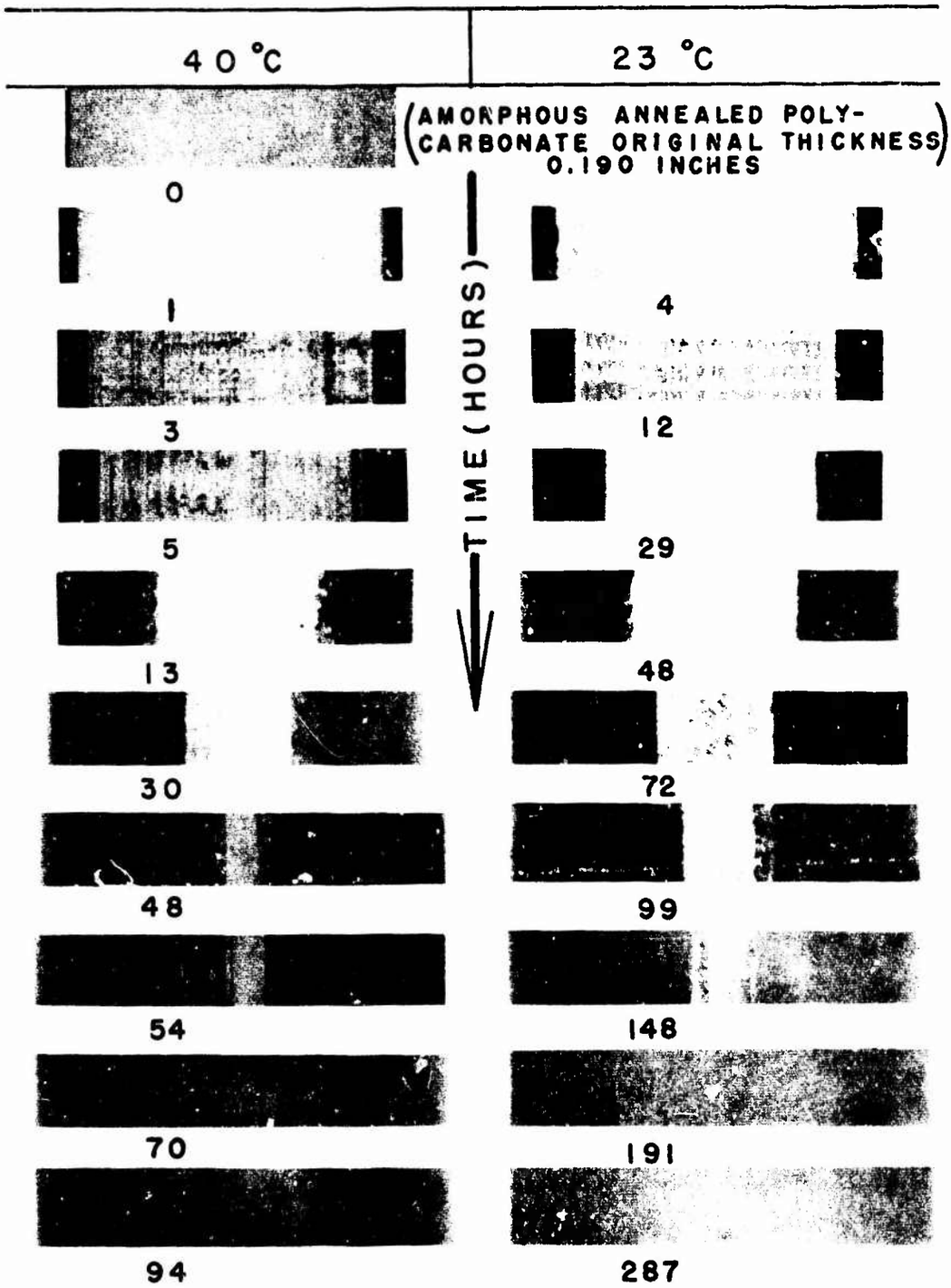

FIGURE 108-1. CROSS-SECTIONS OF SPECIMENS CRYSTALLIZING AT 23°C AND 40°C SHOWING SHARP ADVANCING BOUNDARIES BETWEEN SWOLLEN SHELLS AND GLASSY CORE OF ZERO ACETONE CONCENTRATION (MAG. 11X).

FIGURE 108-2. DETAILED VIEW OF CROSS-SECTION SHOWING TWO ADVANCING BOUNDARIES (MAG. 100 X).

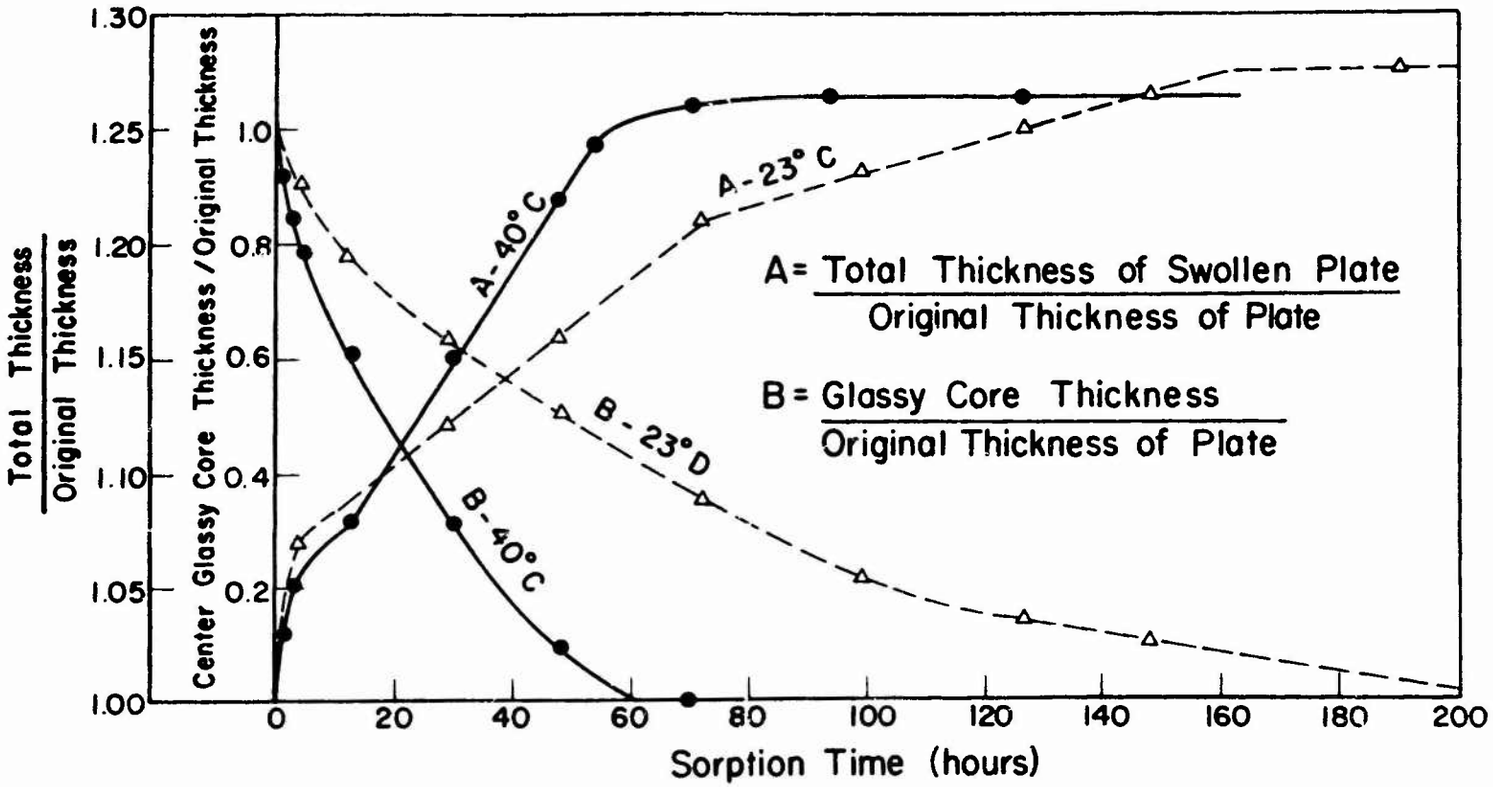

FIGURE 109. RATIOS OF TOTAL THICKNESS OF SWOLLEN PLATE AND GLASSY CORE THICKNESS TO ORIGINAL THICKNESS OF PLATE VERSUS SORPTION TIME.

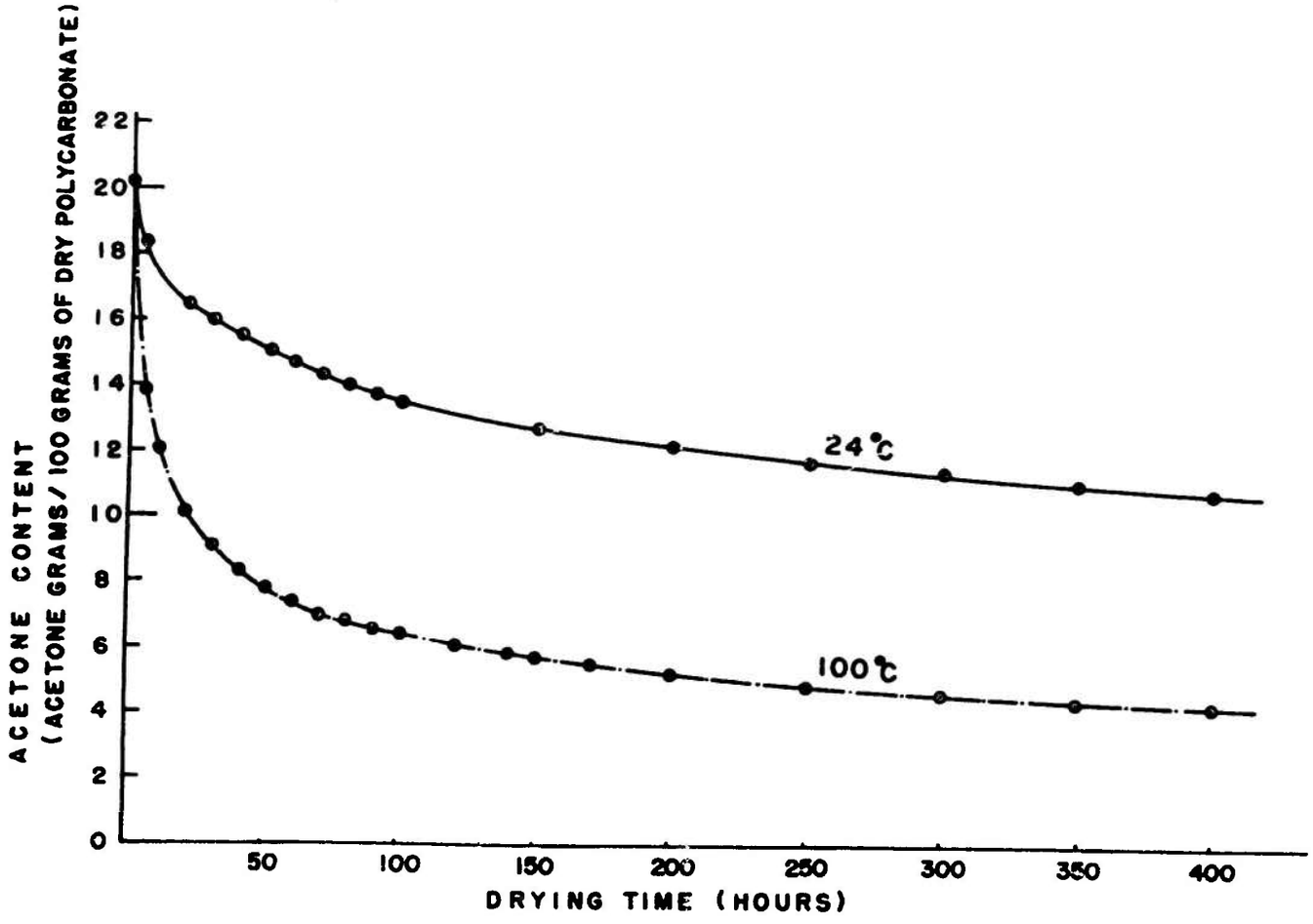

FIGURE 110. RATE OF REMOVAL OF ACETONE FROM CRYSTALLIZED SWOLLEN POLYCARBONATE AT 24°C AND 100°C.

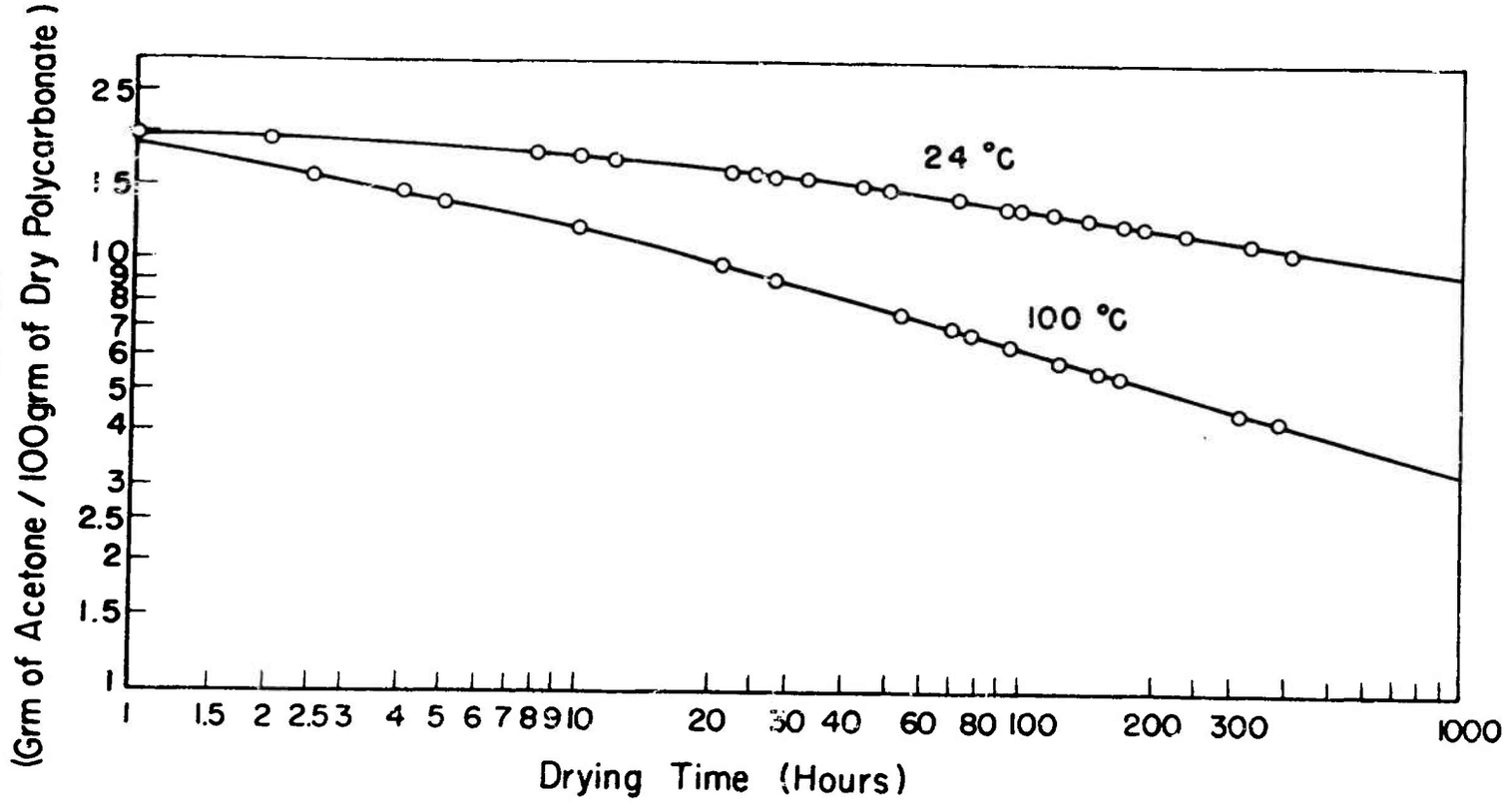

FIGURE III. ACETONE CONTENT VERSUS TIME IN DRYING PROCESS.

From Figure 106, it is noticed that the weight increase is not proportional to time at both 23°C and 40°C. Figure 109 shows that the velocity of the advancing boundary between the swollen shell and glassy core is not constant at both 23°C and 40°C. The diffusion process of acetone vapor-induced crystallization, therefore, is not the "Case II" type diffusion. "Case II" diffusion requires that the boundary between swollen gel and glassy core advance at constant velocity, and the initial weight gain is directly proportional to time. Figure 107, which is a replotting of the results in Figure 106, shows the linear relationship between the logarithm of weight increase and the logarithm of time up to about 45 hours at 23°C and about 65 hours at 40°C. In order to examine the relationship between weight increase and time, the empirical relationship of $\Delta W = Kt^n$ is employed (ΔW is the weight gain, K is a constant, t is time). From the curves in Figure 107, one can obtain n as follows:

$$n = 0.626 \text{ at } 23^\circ C \text{ and } n = 0.543 \text{ at } 40^\circ C$$

These results imply that although the sorption temperatures are far below the glass transition temperature of polycarbonate (150°C), the diffusion process is close to a Fickian diffusion. Ideal Fickian diffusion requires n to be 0.5. As mentioned earlier, however, the diffusion process of acetone vapor-induced crystallization involves a phase change, that is, from an amorphous state to a partially crystallized state in the swollen shell. Therefore, it is possible that the diffusion coefficient is not only a function of concentration but a function of the time to change the amorphous state to a partially crystallized state (crystallization rate). Some of the photographs in Figure 108-2 show that there may actually exist two advancing boundaries. The first boundary may be the one which divides the glassy amorphous state having no penetrant concentration from the amorphous swollen state. The second boundary may be the one between the amorphous swollen state and the partially crystallized state. Further study is necessary to clarify this phenomenon.

From Figure 109 one can obtain the thickness increase of a swollen shell. The following calculation was made to construct Figure 112.

$$\frac{A - 1}{1 - B} \times 100 = \text{percentage thickness increase of swollen shell}$$

From Figure 112, one notices there is a considerable volume expansion in the swollen shell; however, the plate dimension parallel to the neutral plane of the plate did not change because of the constraint imposed by the glassy core. As volume expands, therefore, the shearing stresses builds up in the boundary between the swollen shells and the glassy core. Thus, the swollen shells are under compression, and the glassy core is under tension. Alfrey, et al. indicated in their paper (70) that stresses caused by swelling are high enough to crack specimens. In our experiment, however, we did not observe any cracking of samples in the process of swelling, but we did observe cracking of the plate in the drying process after the completion of crystallization. This phenomenon was especially severe in the case of extruded and unannealed plates. It is believed that this is due to the combination of swelling stresses and residual stresses (compression stress at the outside faces of the plate and tensile stress in the

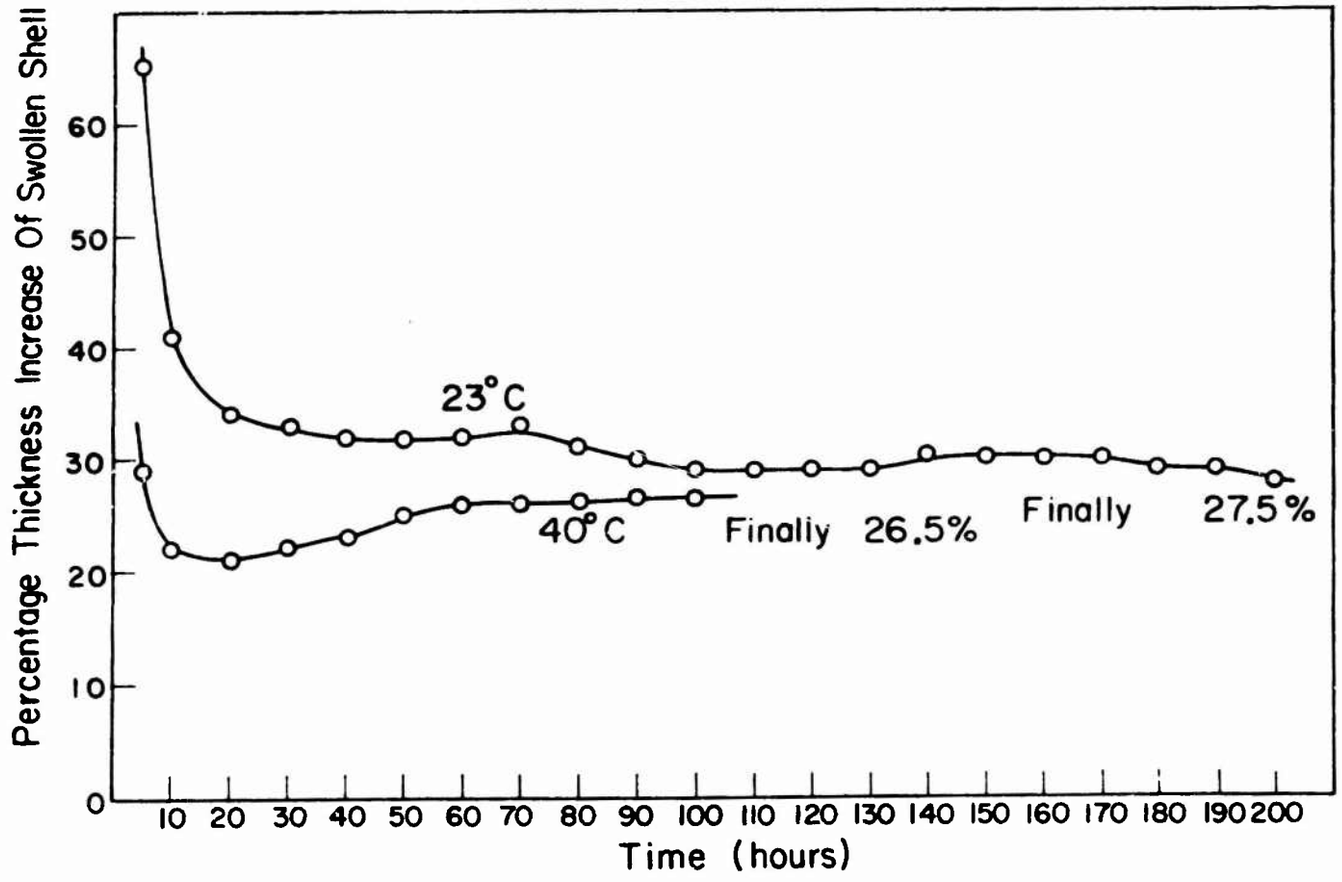

FIGURE 112. PERCENTAGE THICKNESS INCREASE OF SWOLLEN SHELL VERSUS TIME.

interior) in the extruded unannealed sheet. The reason that cracking of the samples did not occur in the process of swelling but did occur in the drying process can be explained by the study of residual acetone effects on modulus and stress-strain behavior. When the amount of residual acetone is high, the modulus of the swollen material is very low; however, in the drying process the modulus quickly increases as the acetone content is reduced. Thus, the compression stress in the swollen shell and tensile stress in the glassy core increase enough to crack the material. Figure 113 illustrates the case in which the outer swollen shell buckled due to the compression stress since the glassy core was too thick to break.

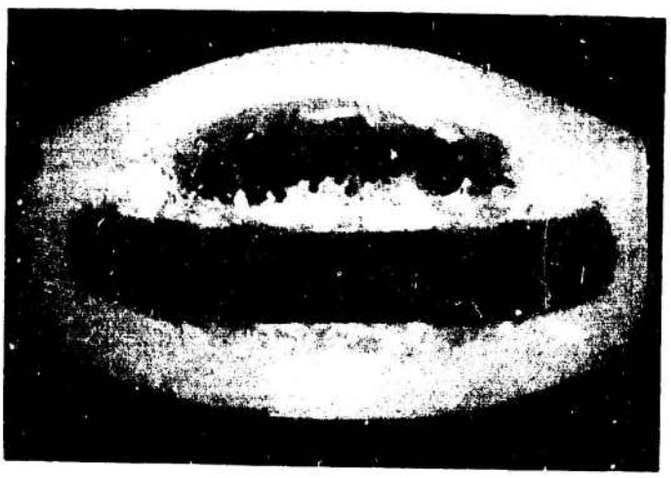

FIGURE 113. CROSS-SECTIONAL VIEW OF BUCKLED OUTER CRYSTALLIZED SHELL IN DRYING PROCESS.

CHAPTER VIII

TOUGHNESS OF COLD ROLLED AMORPHOUS POLYMERS

A. Procedures

Cold rolling, a process wherein a polymer sheet is reduced in thickness in a conventional rolling mill at room temperature, produces marked structural and physical property changes in polymeric materials. The deformation process that takes place in cold rolling is complex and depends on the rolling conditions such as roll diameter, roll speed, reduction per pass, rolling temperature and also on the material that is being rolled.

In this study cold rolling was performed on a laboratory 2 roll mill having 10 inch diameter rolls at a roll speed of 50 ft/min. The reduction in thickness per pass depended upon the material type but in general the sheet thickness was reduced 0.003 to 0.005 inches per pass.

Although the rolling was performed at room temperature, a temperature increase occurred in the material during the rolling process as a result of the irreversible deformation. Initially, when the roll gap setting was large and the deformation of the material was within the elastic limit, no permanent reduction in thickness was recorded due to the total spring back of the material with little or no temperature rise of the specimen. In certain cases an increase in sheet thickness was observed at this stage of cold rolling. This may be due to the release of locked-in deformations which were present in the virgin extruded sheets. A marked increase in sheet temperature was observed as soon as a permanent reduction in sheet thickness was recorded. In the case of 0.245 inch thick polycarbonate sheets, for example, the roll gap setting at which a permanent reduction in sheet thickness occurred was 0.210 inches.

To study the effect of cold rolling on the impact strength, sheets of ABS, PVC, Noryl (Polyphenylene Oxide), XT (rubber modified acrylic) and polycarbonate were uniaxially cold rolled to various percent roll reductions and Izod-impact strengths determined. In some cases, the Izod-impact strength was determined at 45 and 90 degrees to the roll directions.

B. Results and Discussion

The variation in impact strength for cold rolled ABS (Monsanto Chemical Co.) is shown in Fig. 114 for specimens oriented at 0, 45 and 90 degrees to the roll direction. In the 0 and 45 degree directions the impact strength, at first, increases gradually with percent roll reduction. A maximum value is reached and then the impact strength drops off gradually at higher values of percent roll reduction. The maximum value of impact strength is obtained at 30 percent roll reduction and is about 9 ft lb/in which is approximately twice that of the virgin material. For specimens at 45°, the maximum value is obtained at about 40 percent roll reduction and is about 7.5 ft lb/in. In the 90 degree direction the impact strength shows a

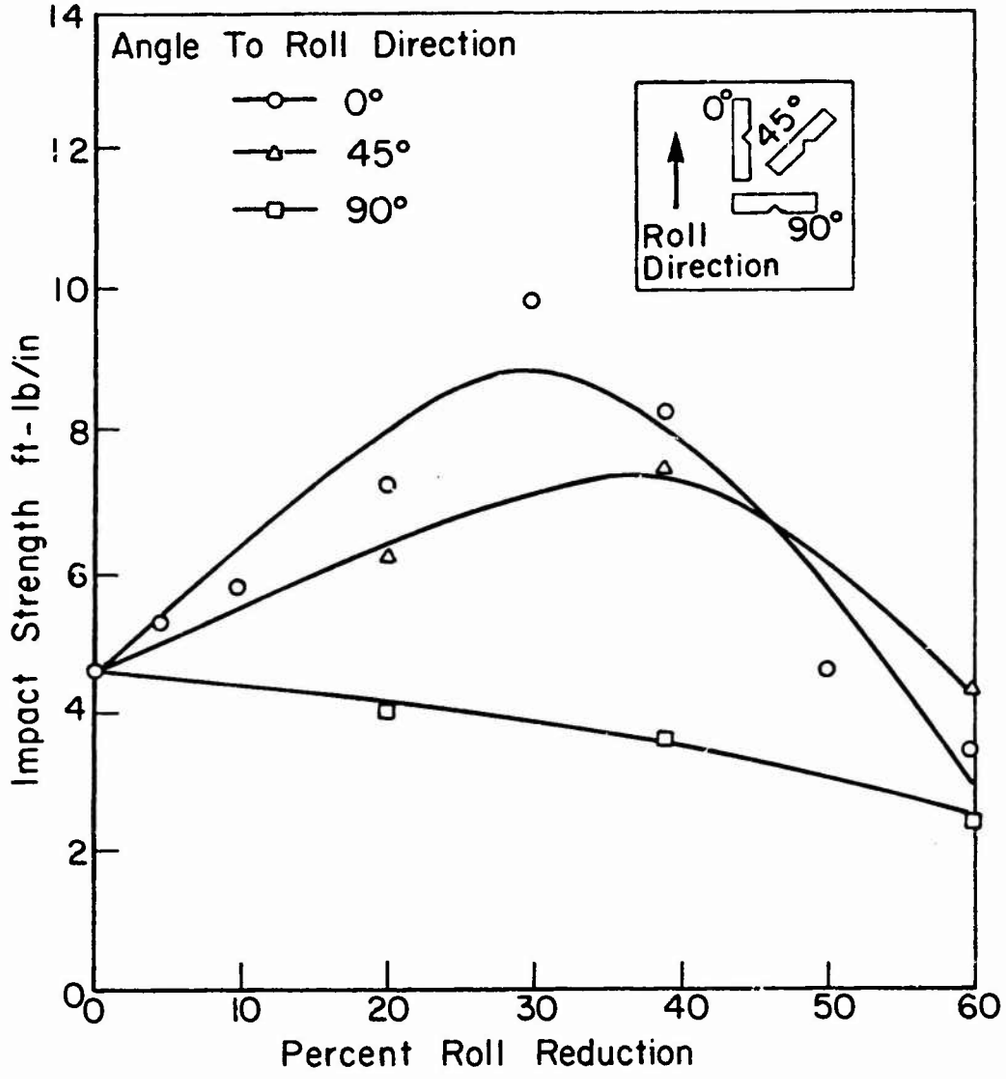

FIGURE 114. VARIATION OF IZOD IMPACT STRENGTH WITH PERCENT ROLL REDUCTION FOR ABS (ORIGINAL SHEET THICKNESS 0.250 INCHES).

steady decrease with percent roll reduction. In Fig. 115 is shown the results for another ABS polymer (Cycolac MS, Marbon Chemical Co.) with smaller original sheet thickness, 1/8" compared to 1/4". A maximum impact strength of nearly 9 ft lb/in was achieved at approximately 25% roll reduction corresponding to a 350% increase.

The results for the XT polymer (American Cyanamid Co., XT 500) having an original sheet thickness of 0.110 inches are shown in Fig. 116. It can be seen that only a modest increase in impact strength occurred.

The variation in impact strength with percent roll reduction for a PVC polymer (General Tire and Rubber Co.) having an original sheet thickness of 0.141 inches is shown in Fig. 117. At a very low roll reduction of about 2% a large increase in impact strength to 15 ft lb/in from 2.7 ft lb/in is observed. The maximum of 30 ft lb/in is achieved at approximately 35% roll reduction.

The results for Noryl are shown in Fig. 118. Up to 30 percent roll reduction the increase is modest. There is a large increase of impact strength between 30 and 40 percent roll reduction reaching a value of about 9 ft lb/in at 40 percent roll reduction. The virgin material, machined down to a thickness corresponding to 40 percent roll reduction, is found to have the same impact strength as the unrolled material indicating that the observed increase in impact strength was not due to "the thickness transition effect" which will be discussed below.

The results for cold rolled polycarbonate are summarized in Figs. 119 to 126. The impact strengths of virgin sheet materials are shown plotted in Fig. 119 as a function of sheet thickness and it can be seen that a transition with thickness occurs between 0.125 inches and 0.180 inches. The impact strength reduces from 19 ft lb/in to approximately 3 ft lb/in. Thus, if a sheet with an original thickness of 0.128 inches is rolled, only a modest increase in impact strength occurs as shown in Fig. 120. Also shown in Fig. 120 are impact strengths of specimens taken at 45 and 90 degrees to the roll direction.

However, for sheets greater than 0.128 inches in thickness, which have low impact strength values in the as-extruded state, a large improvement in impact strength values is achieved after a few percent roll reduction. In Fig. 121 the data for 0.186 inch thick sheets are summarized. A maximum in impact strength occurs at 2 percent roll reduction. At higher roll reductions the impact strength is decreased and at 50 percent reduction the impact strength is reduced to approximately the unrolled value.

The results for rolled sheets having original thicknesses of 0.245 inch, 0.382 inch, 0.540 inch and 0.645 inch are summarized in Figs. 122 through 125 respectively. For 0.245 inch thick sheet, as shown in Fig. 122, the impact strength values in all the three directions are increased to about 19 ft lb/in from 3 ft lb/in at a very low roll reduction of 3.5 percent. In all cases (for all starting sheet thicknesses) the maximum impact strength achieved is about 19 ft lb/in regardless of the unrolled sheet thickness and the percent roll reduction at which the maximum value occurs. The percent roll reduction at which a large increase in impact strength values occurs increases with the unrolled sheet thickness and is plotted

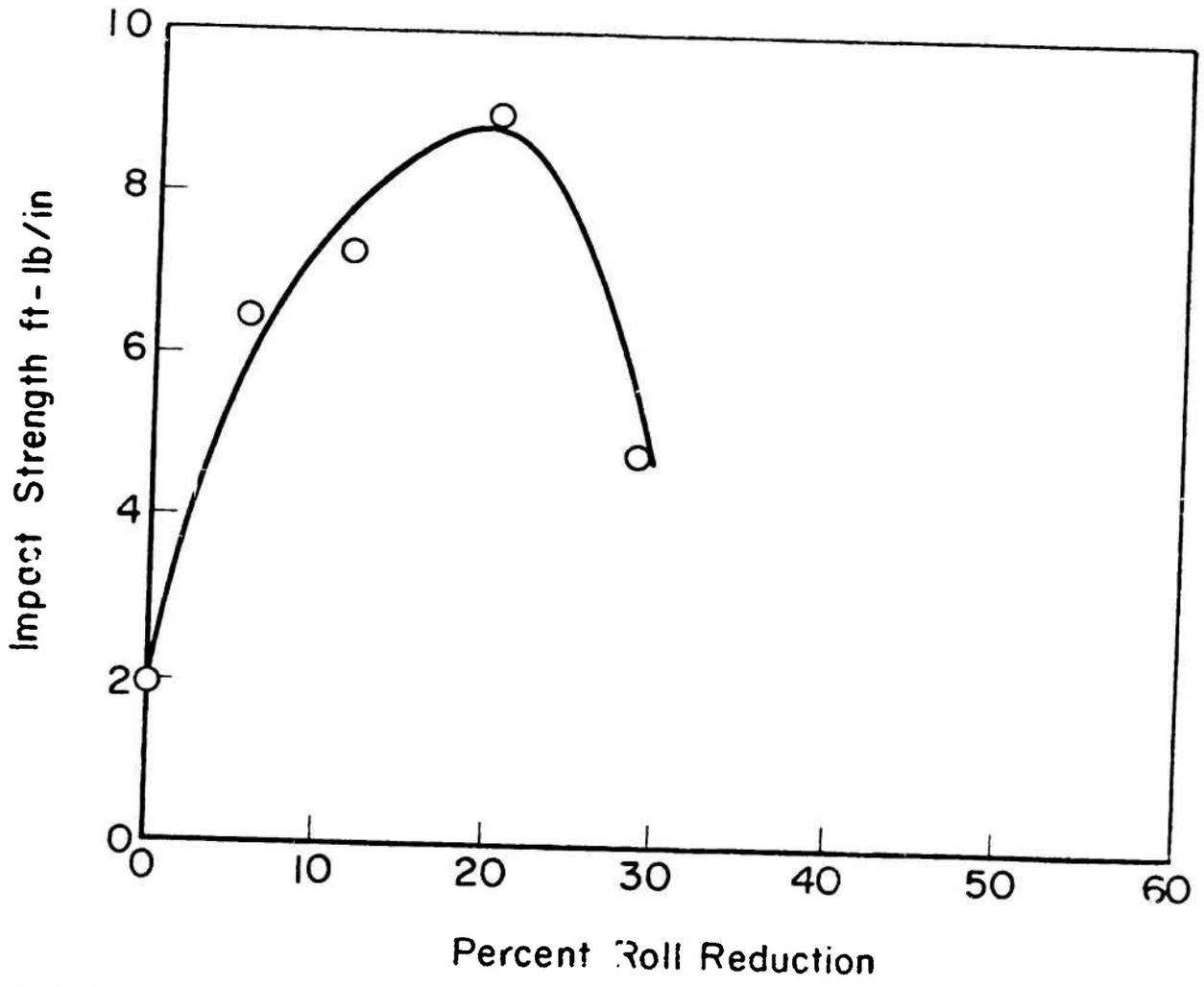

FIGURE 115. VARIATION OF IZOD IMPACT STRENGTH WITH PERCENT ROLL REDUCTION FOR ABS (ORIGINAL SHEET THICKNESS 0.125 INCHES).

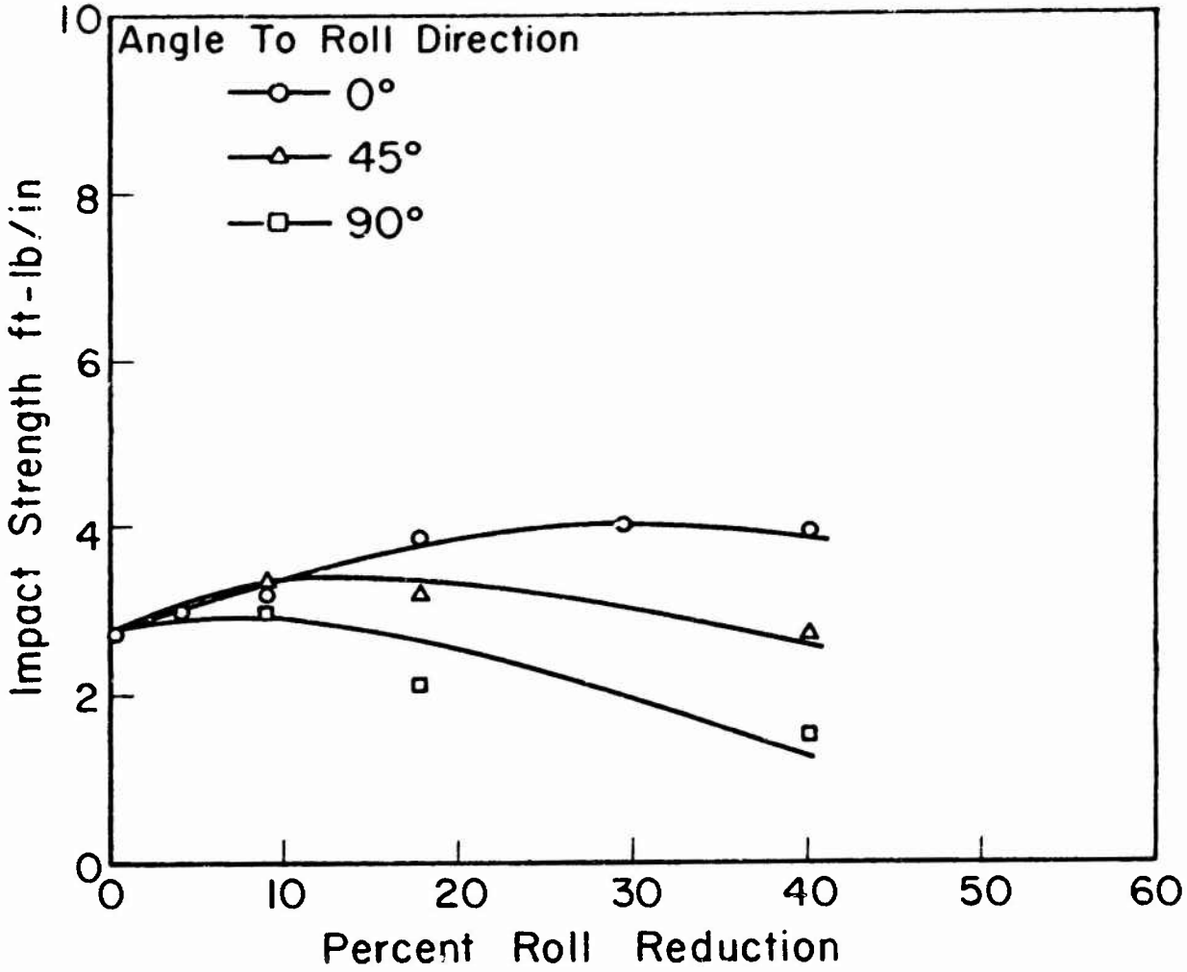

FIGURE 116. VARIATION OF IZOD IMPACT STRENGTH WITH PERCENT ROLL REDUCTION FOR XT (ORIGINAL SHEET THICKNESS = 0.110 INCHES).

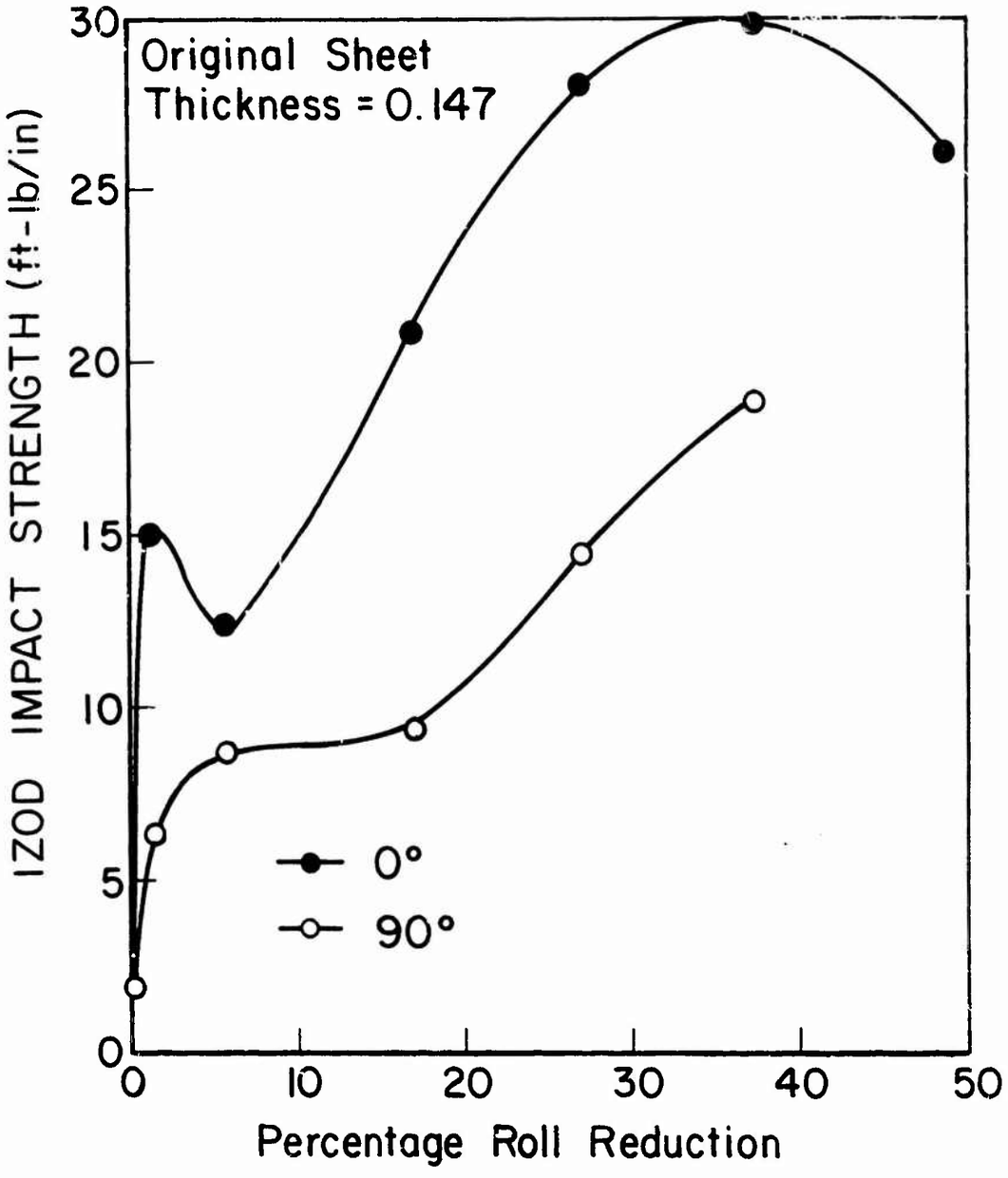

FIGURE 117. IZOD IMPACT STRENGTH OF ROLLED PVC.

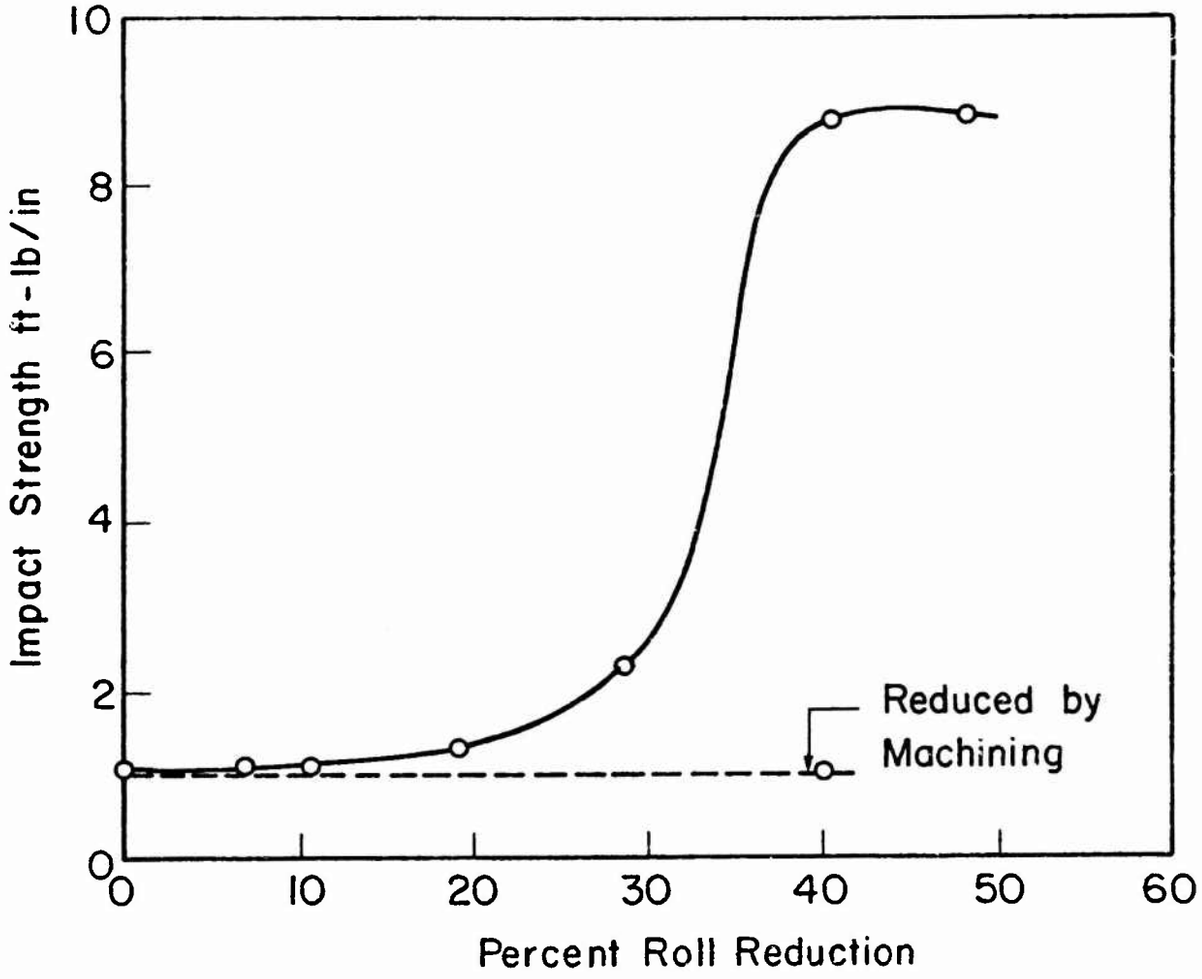

FIGURE 118. VARIATION OF IZOD IMPACT STRENGTH WITH PERCENT ROLL REDUCTION FOR NORYL (ORIGINAL SHEET THICKNESS 0.187 INCHES).

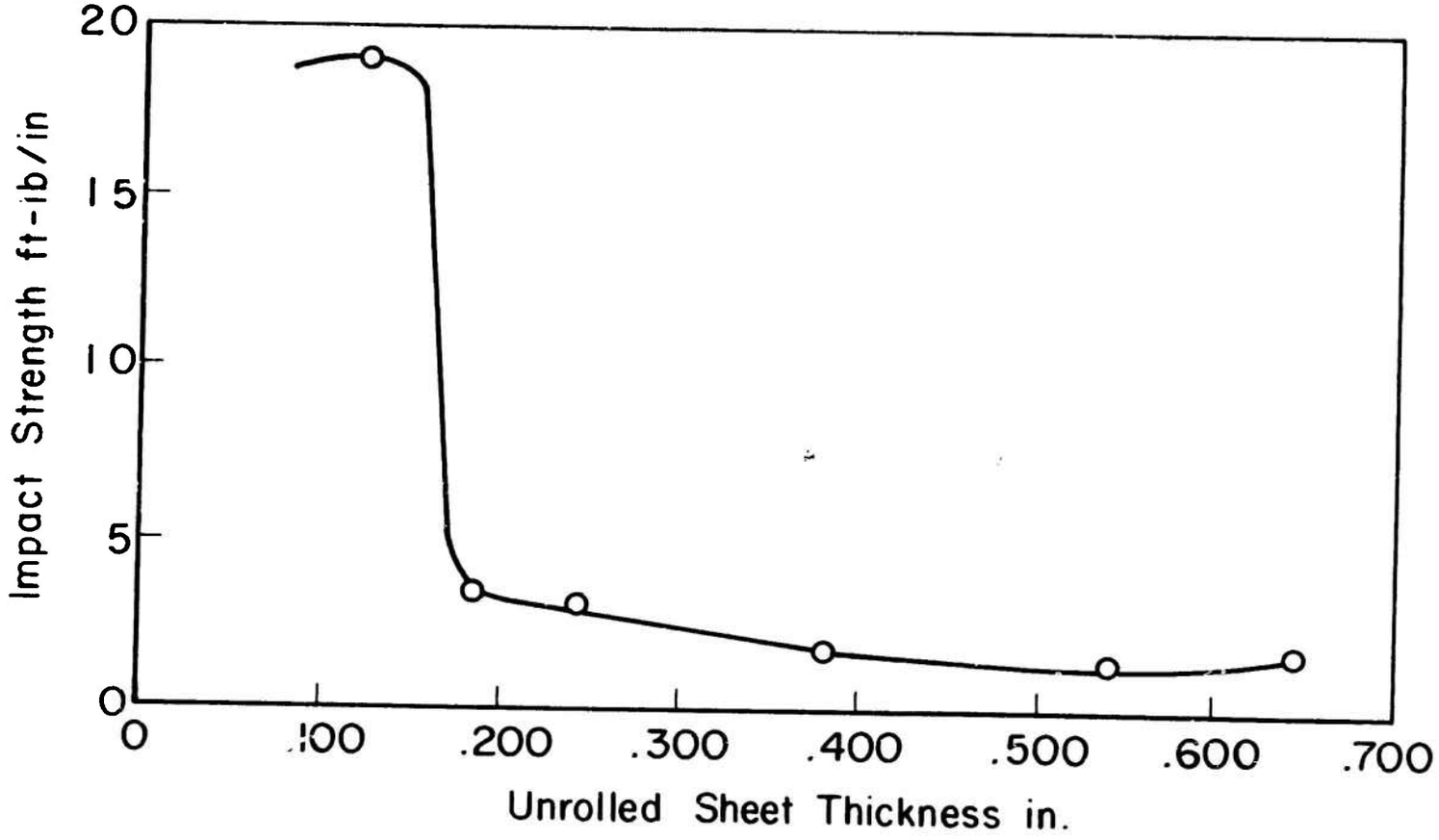

FIGURE 119. VARIATION OF IZOD IMPACT STRENGTH WITH SHEET THICKNESS FOR UNROLLED POLYCARBONATE.

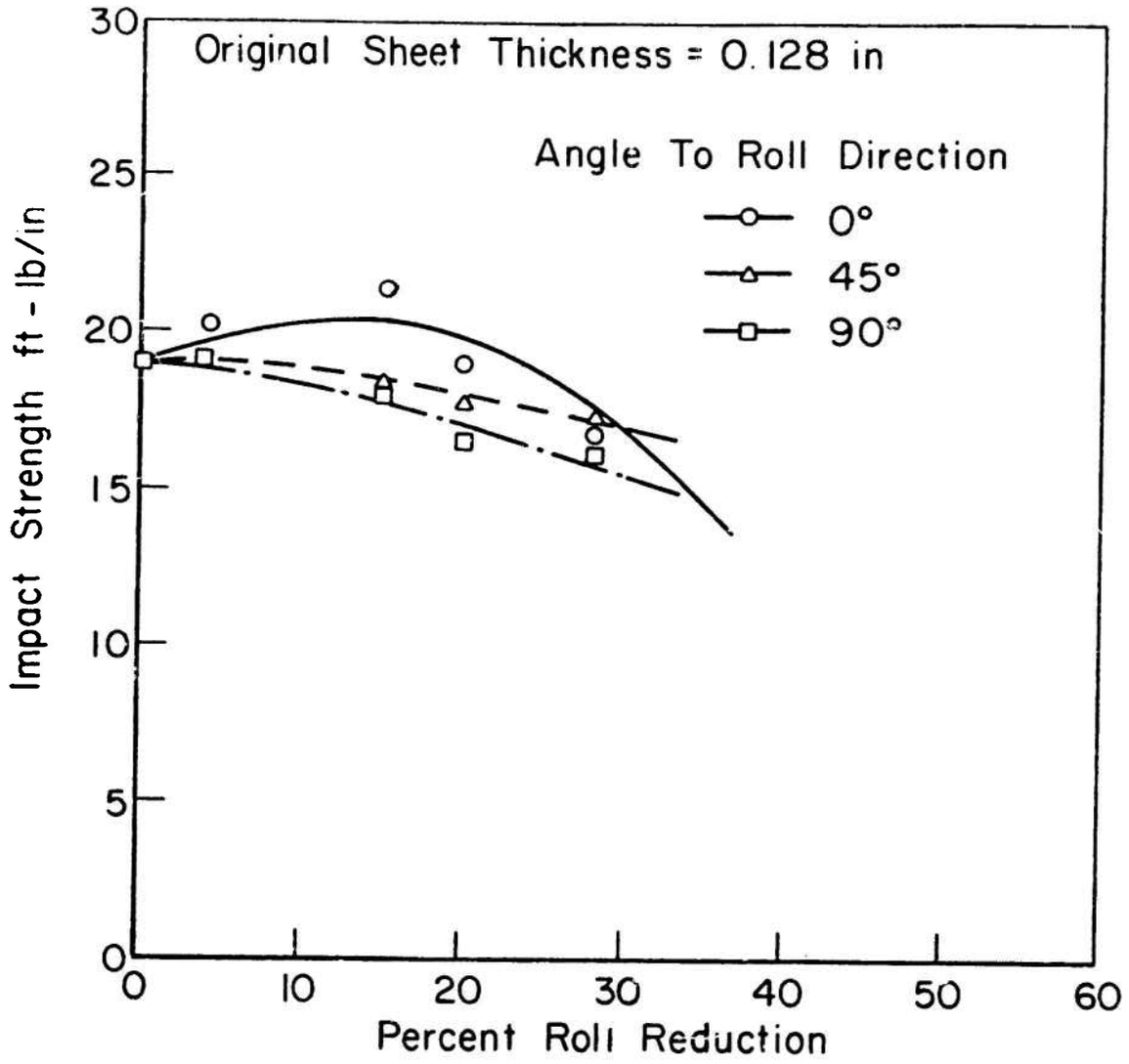

FIGURE 120. VARIATION OF IZOD IMPACT STRENGTH WITH PERCENT ROLL REDUCTION FOR POLYCARBONATE (ORIGINAL SHEET THICKNESS = 0.128 INCHES).

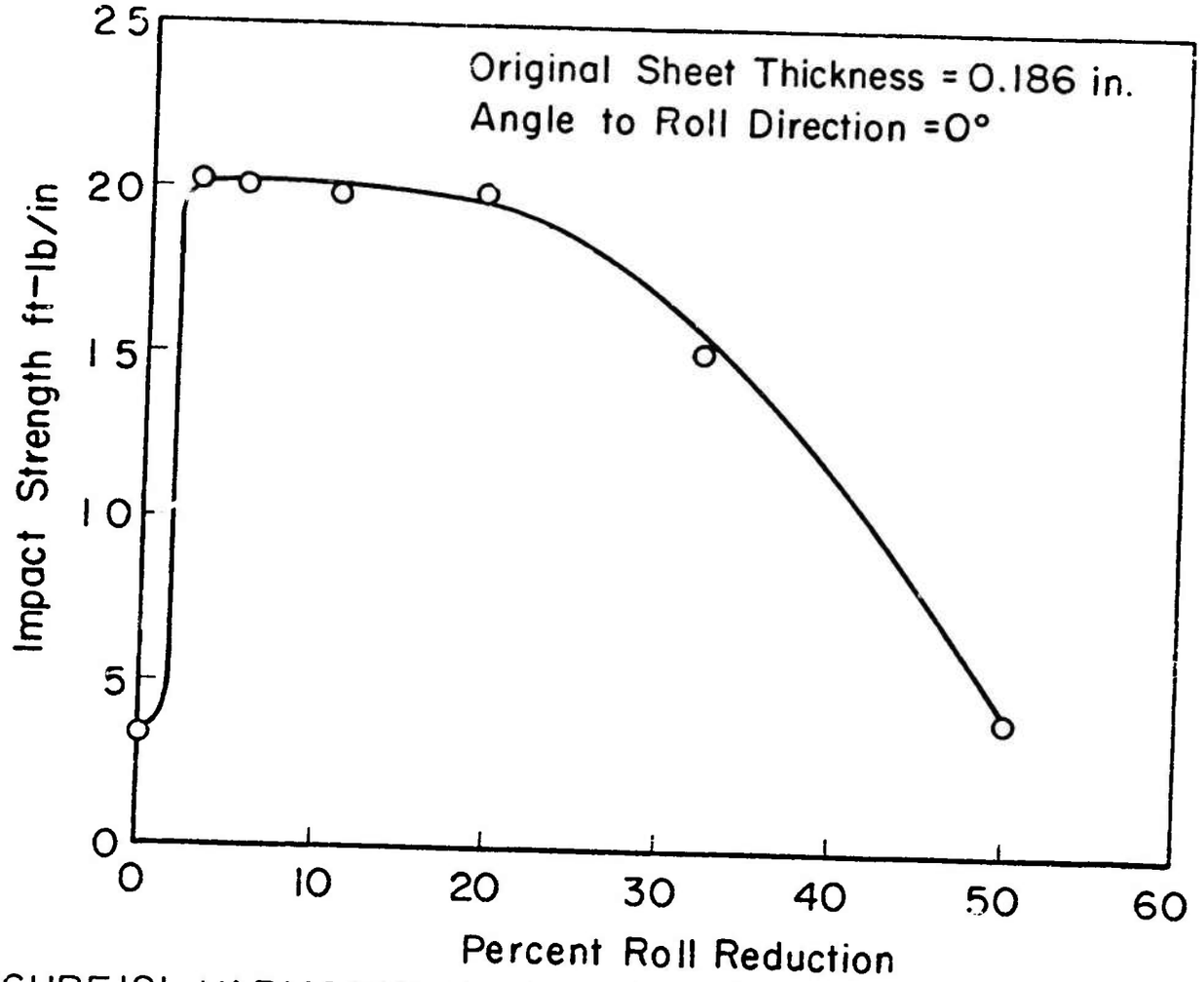

FIGURE 121. VARIATION OF IZOD IMPACT STRENGTH WITH PERCENT ROLL REDUCTION FOR POLYCARBONATE (ORIGINAL SHEET THICKNESS =0.186).

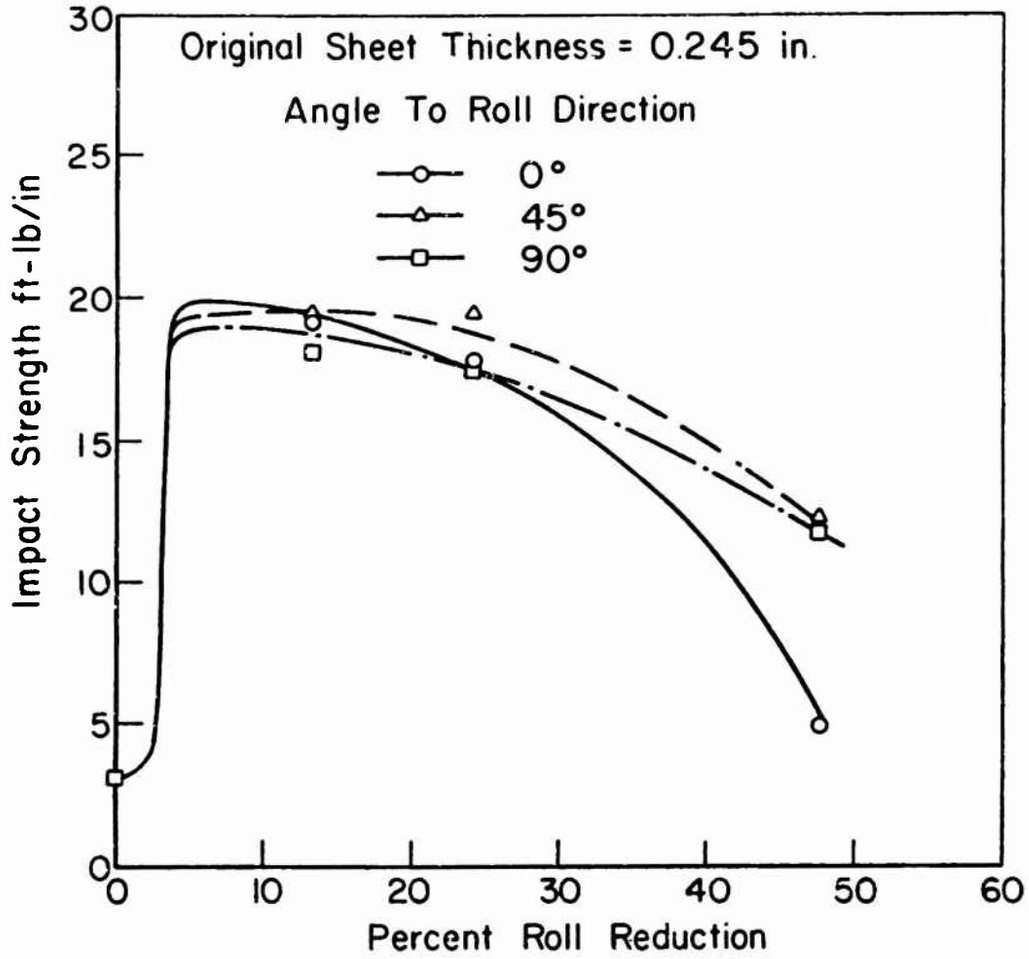

FIGURE 122. VARIATION OF IZOD IMPACT STRENGTH WITH PERCENT ROLL REDUCTION FOR POLYCARBONATE (ORIGINAL SHEET THICKNESS = 0.245 INCHES).

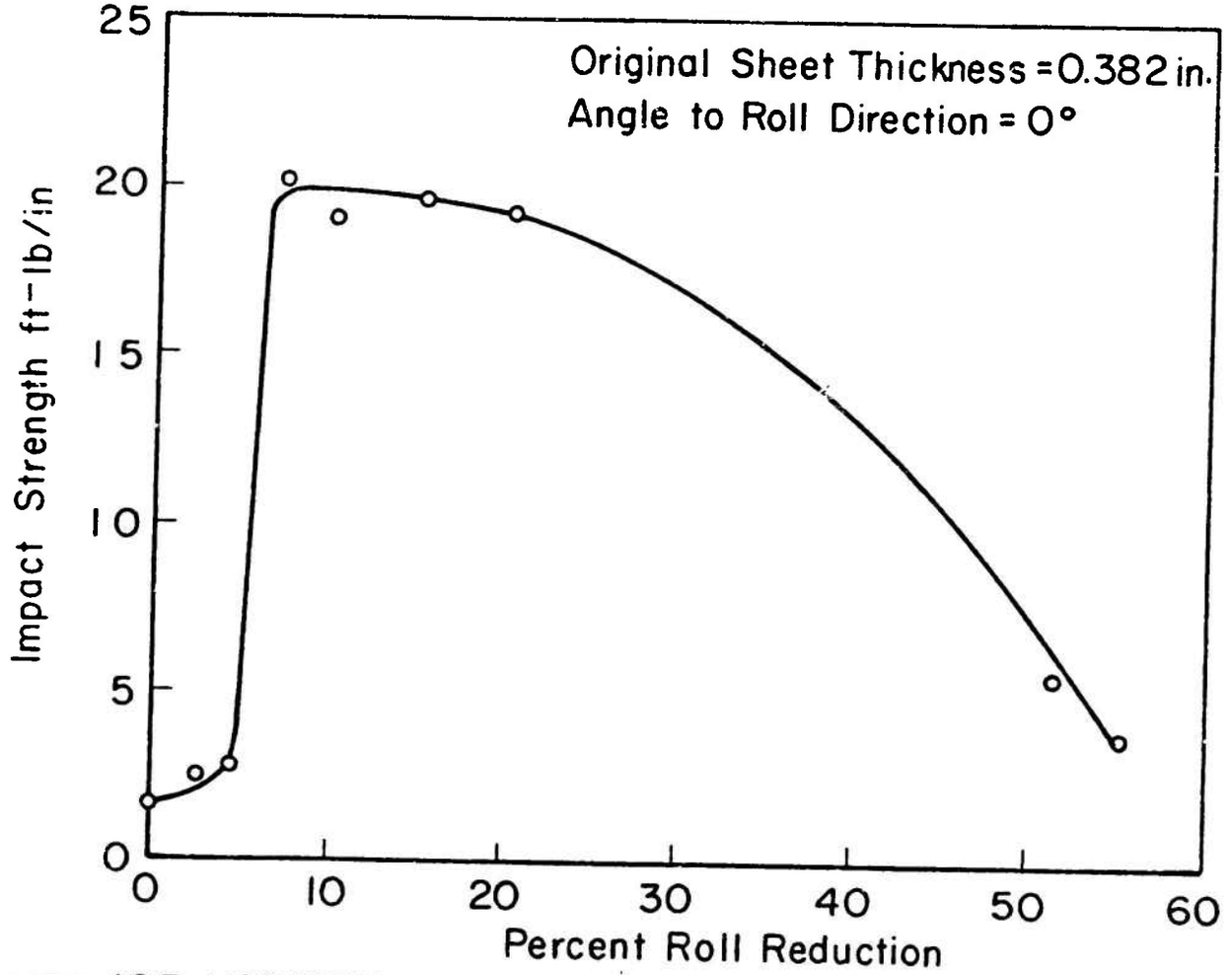

FIGURE 123. VARIATION OF IZOD IMPACT STRENGTH WITH PERCENT ROLL REDUCTION FOR POLYCARBONATE (ORIGINAL SHEET THICKNESS = 0.382 INCHES).

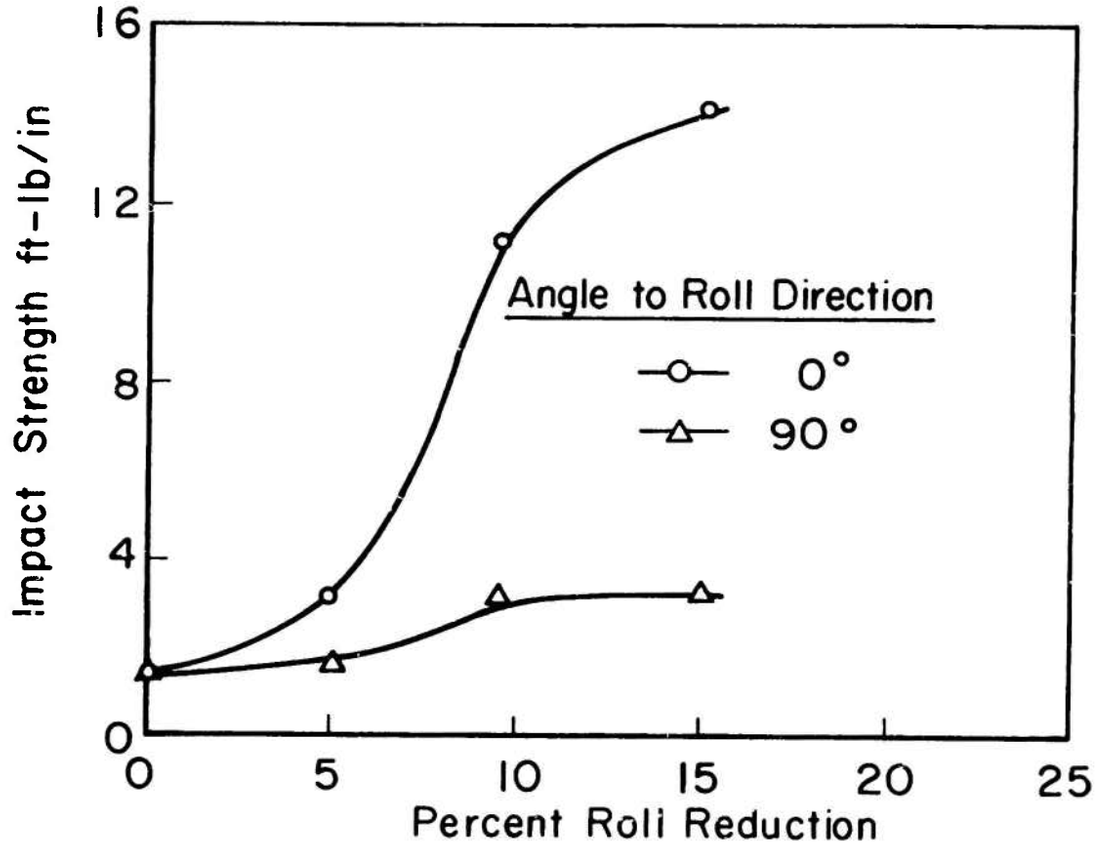

FIGURE 124. VARIATION OF IZOD IMPACT STRENGTH WITH PERCENT ROLL REDUCTION FOR POLYCARBONATE (ORIGINAL SHEET THICKNESS = 0.540 INCHES).

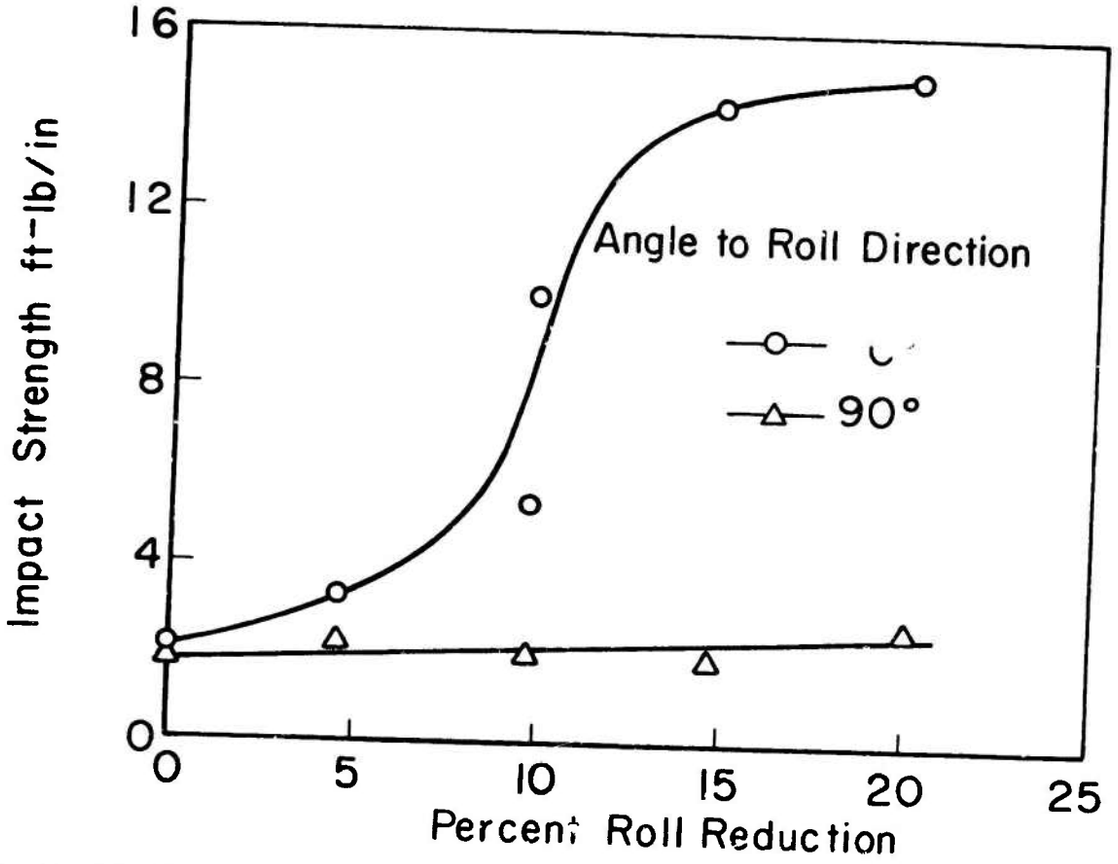

FIGURE 125. VARIATION OF IZOD IMPACT STRENGTH WITH PERCENT ROLL REDUCTION FOR POLYCARBONATE (ORIGINAL SHEET THICKNESS = 0.645 INCHES).

in Fig. 126. This increase in transition thickness may be a result of differences in sheet orientation since the same rolling mill and conditions were used with these sheets widely varying in thickness.

The variation of density of cold rolled polycarbonate sheets of 0.128 inch, 0.187 inch and 0.245 inch with percent roll reduction is shown in Fig. 127. A density gradient column using water and calcium nitrate solutions was used for accurate measurements of density. A rapid rise in density occurs during the initial 10 percent roll reduction followed by a more gradual increase in density up to 60 percent roll reduction. A large decrease in volume due to the closing up of microvoids during the initial stages of cold rolling gives rise to the rapid rise in density. The impact strength variation of rolled polycarbonate sheets is plotted as a function of density in Fig. 128.

The large increase in impact strength achieved by modest percent roll reductions of 2 to 5 percent in the cases of 0.187 inch and 0.245 inch thick sheets and the loss of impact strength values at higher roll reductions leads one to question the effect of the orientation of molecules. The effect is generally thought to be the mechanism causing improvement of impact strength for hot stretched materials where large amounts of stretching occur.

To better understand the mechanisms involved other investigations were conducted. For example, polycarbonate sheets 0.187 inches thick were compressed between parallel plates to various final thicknesses. The compression was carried out with and without a silicone lubricant. The compressed sheets showed higher impact strength values. The results are summarized in Table 30. It is seen that an increase in the impact strength, very similar to that which occurs in cold rolling, can be achieved by simple compression.

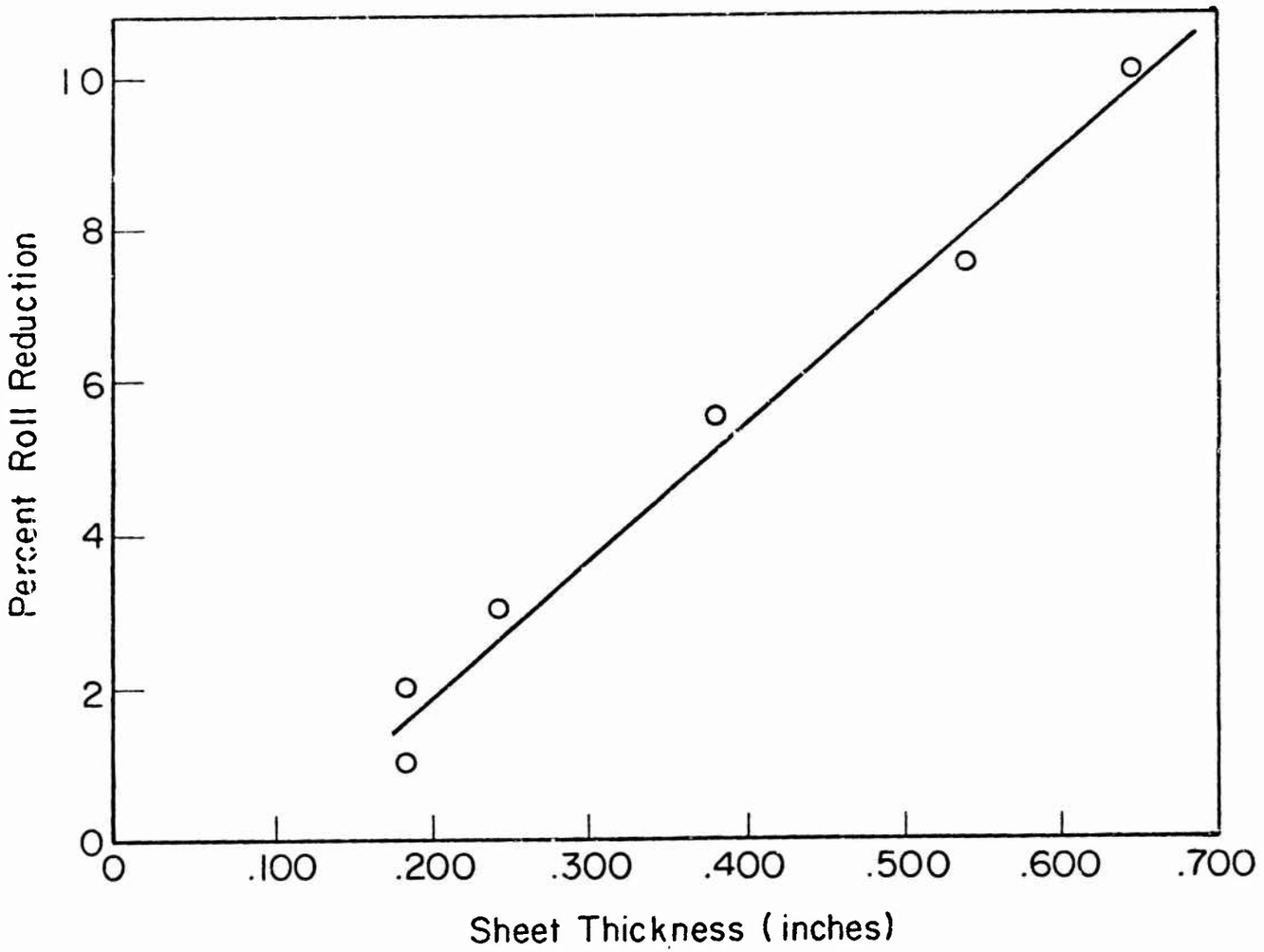

FIGURE 126. ORIGINAL SHEET THICKNESS VS. PERCENT ROLL REDUCTION AT WHICH SUDDEN INCREASE IN IMPACT VALUE OCCURS IN POLYCARBONATE.

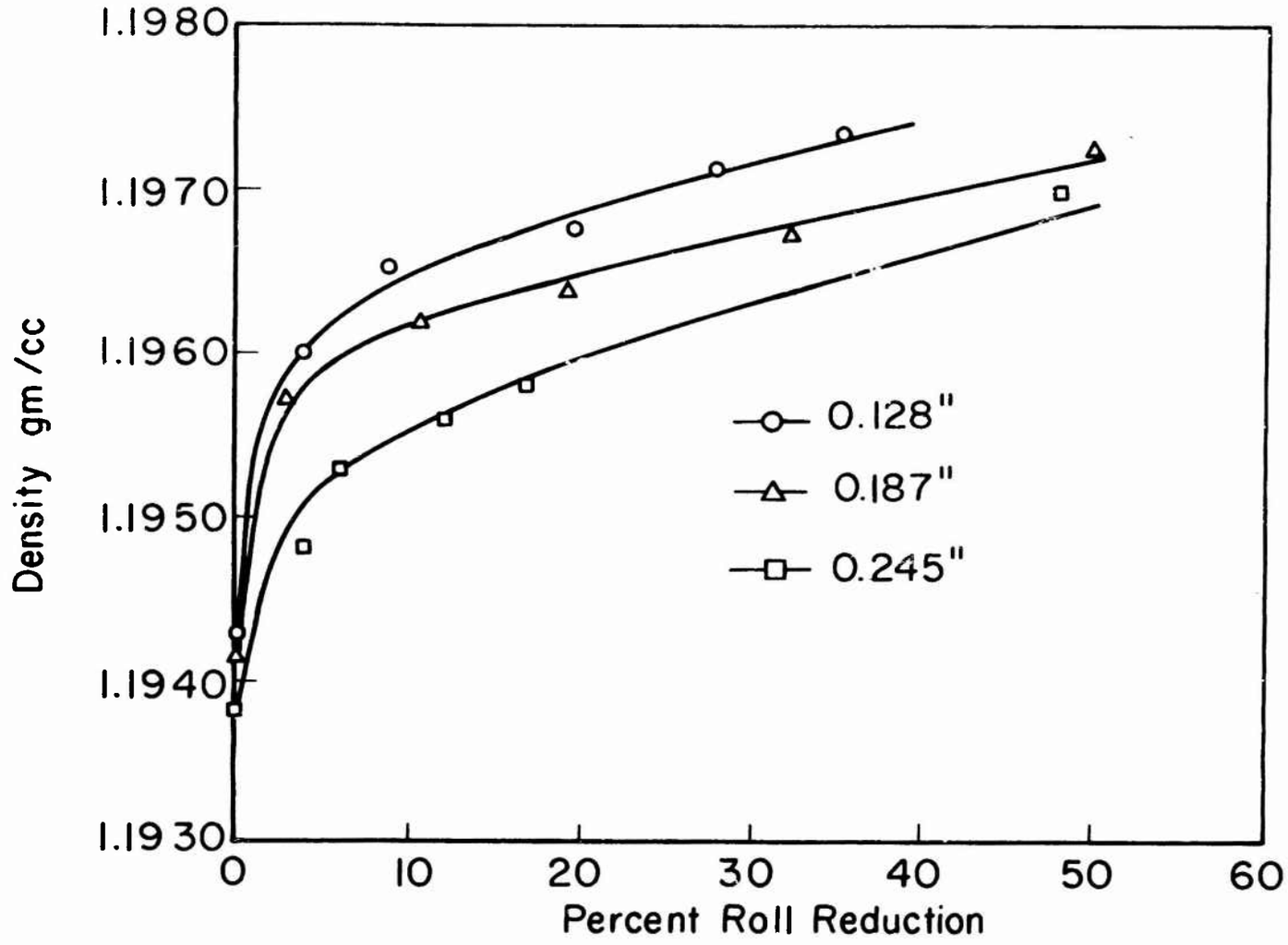

FIGURE 127. VARIATION OF DENSITY WITH PERCENT ROLL REDUCTION FOR POLYCARBONATE.

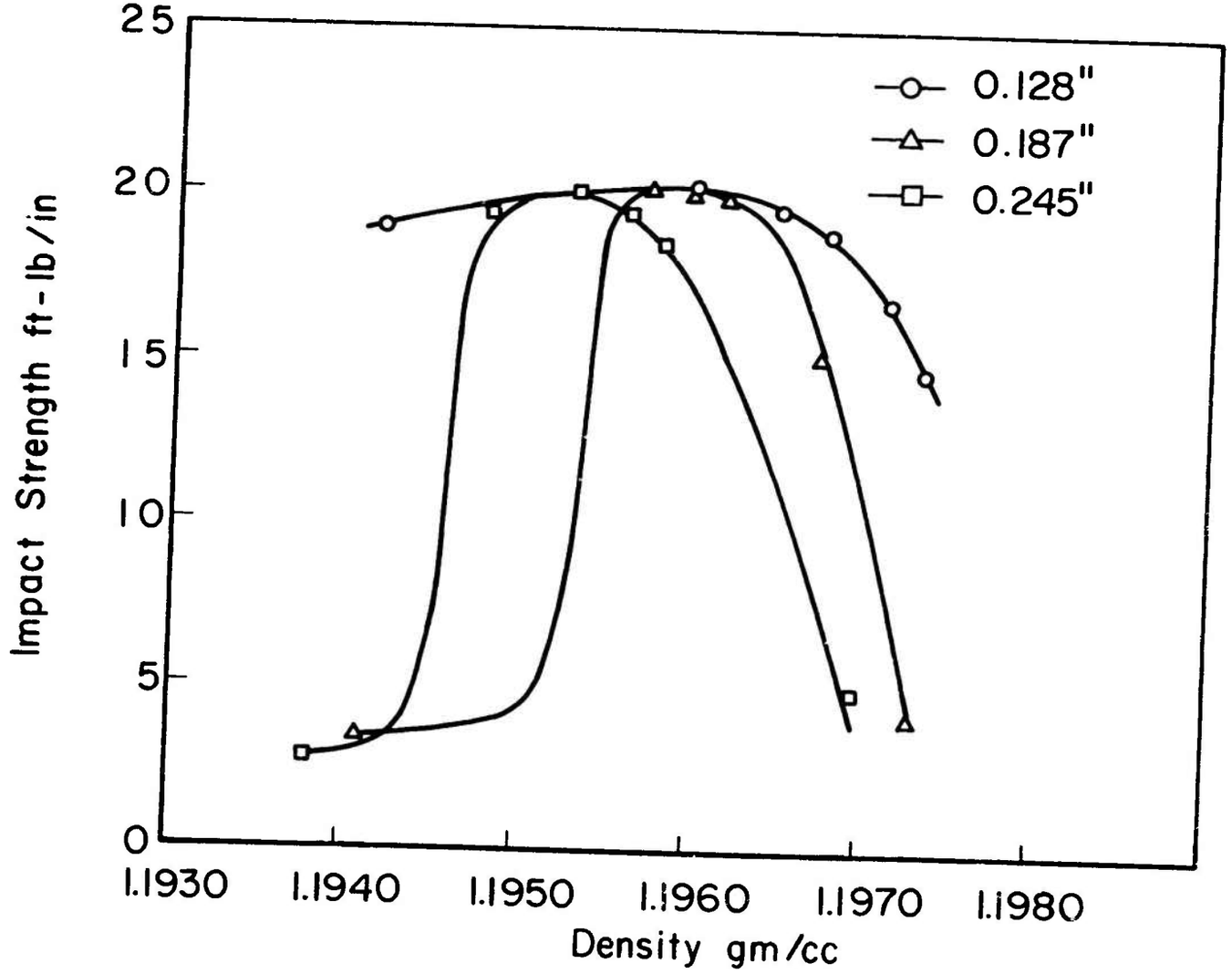

FIGURE 128. VARIATION OF IZOD IMPACT STRENGTH WITH DENSITY FOR POLYCARBONATE.

TABLE 30

Impact Strengths (Notched Izod) for Pressed Polycarbonate Sheets*

% Reduction in Thickness	% Elongation Width	% Elongation Length	Izod Impact Strength ft. lb./in.
4.054	5.424	1.362	17.71
4.595	6.294	1.203	17.76
2.973	4.804	0.608	17.68
	With Silicone Lubricant		
3.514	2.832	2.373	19.07
3.784	2.812	2.288	18.96

*Original Specimen Dimensions = 2.495" x 0.570" x 0.185"

Original Impact Strength = 1.350 ft lb/in

CHAPTER IX

FRACTURE TOUGHNESS OF COLD ROLLED RUBBER MODIFIED ACRYLICS BY 3 POINT BEND TEST

The fracture surface work of the rubber modified acrylics was determined using a 3 point notched bend specimen. The specimen configuration was developed to give a smooth load deflection curve and also to enable an accurate measurement of the fracture area. The specimen dimensions are as shown in Fig. 129. The loading rate was selected to give a smooth and slow crack extension giving a load deflection curve similar to that shown in Fig. 130a. The loading rates which gave rise to catastrophic crack extension, indicated by a load deflection curve as shown in Fig. 130b were avoided. A cross head rate of 0.2 in/min was found to give the desired load deflection curve.

On the typical load deflection curve shown in Fig. 130a, the distinct load-drop portion b to c occurs when the crack front reaches the 0.5t diameter hole. The test is stopped after c at some point d. The fracture surface area, corresponding to the fracture work given by the shaded area o a b c o on the load deflection plot, is twice the triangular area below the 0.5t diameter hole. Thus,

$$\text{Fracture surface work} = \gamma_{eff} = \frac{W}{2a} \quad \text{ergs/cm}^2$$

where W = fracture work corresponding to area o a b c o in ergs and 2a = area of fracture surface in cm^2.

The fracture surface was magnified under a microscope and the area was calculated from the measured dimensions. For thin sheets, to improve the ridigity, specimens were prepared as sandwich specimens using plexiglas sheets as the outer faces as shown in Fig. 131.

Rubber modified acrylic sheets, 0.252 inches thick, were cold rolled uniaxially to 10 and 30 percent roll reduction. Sheets with rubber content lower than 4 % were found to develop cracks when cold rolled. The fracture surface work was determined for specimens cut at 0 and 90 degrees to the roll direction. The fracture surface work was also determined for unrolled 0.097 inches thick rubber modified acrylic sheets. The results are shown in Fig. 132. Notched Izod impact strengths of the above sheets are shown in Fig. 133.

For the unrolled sheet, the variation of the fracture surface work values with rubber content is seen to be quite similar to that of the notched Izod impact strength values.

In the three point bend test, the apparent average crack velocity for the unrolled sheets was found to be between 0.85×10^{-3} meters/sec and 1.30×10^{-3} meters/sec. It is interesting to note that the variation of fracture surface work with rubber content of the unrolled sheet as obtained by three point bend test when compared with the results of cleavage tests shown in Fig. 77, is found to be similar to the curve corresponding to a crack velocity of 5.0×10^{-3} meters/sec.

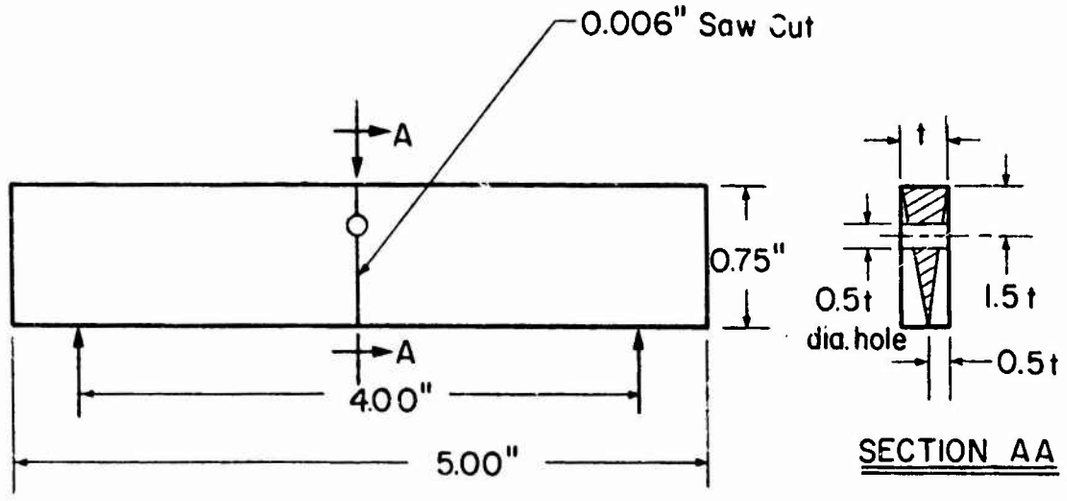

FIGURE 129. THREE POINT NOTCHED BEND SPECIMEN.

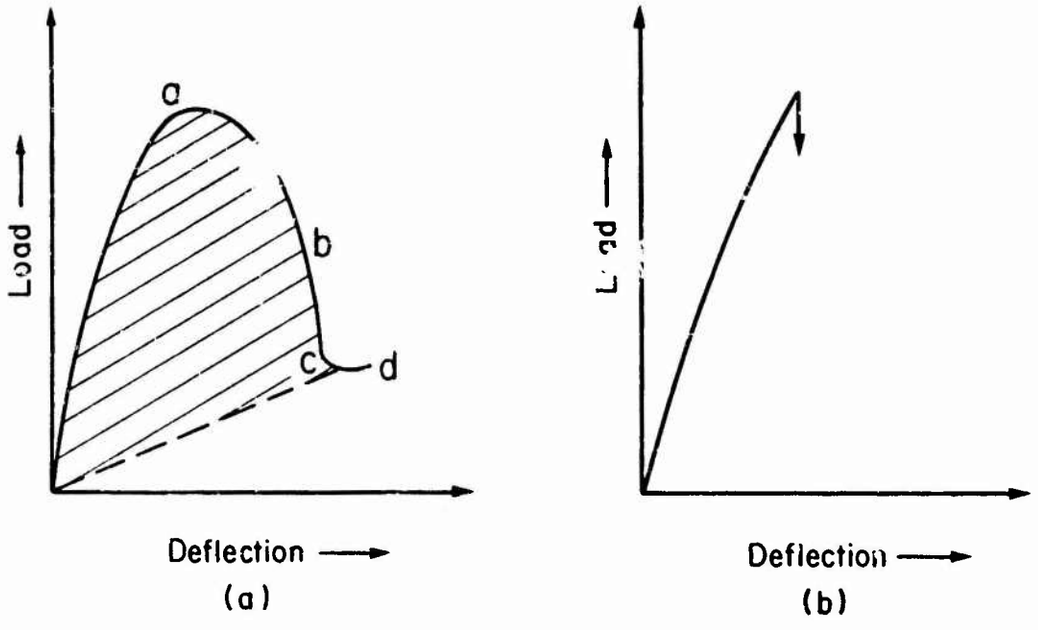

FIGURE 130. LOAD-DEFLECTION CURVES OBTAINED IN THREE POINT BEND TEST.

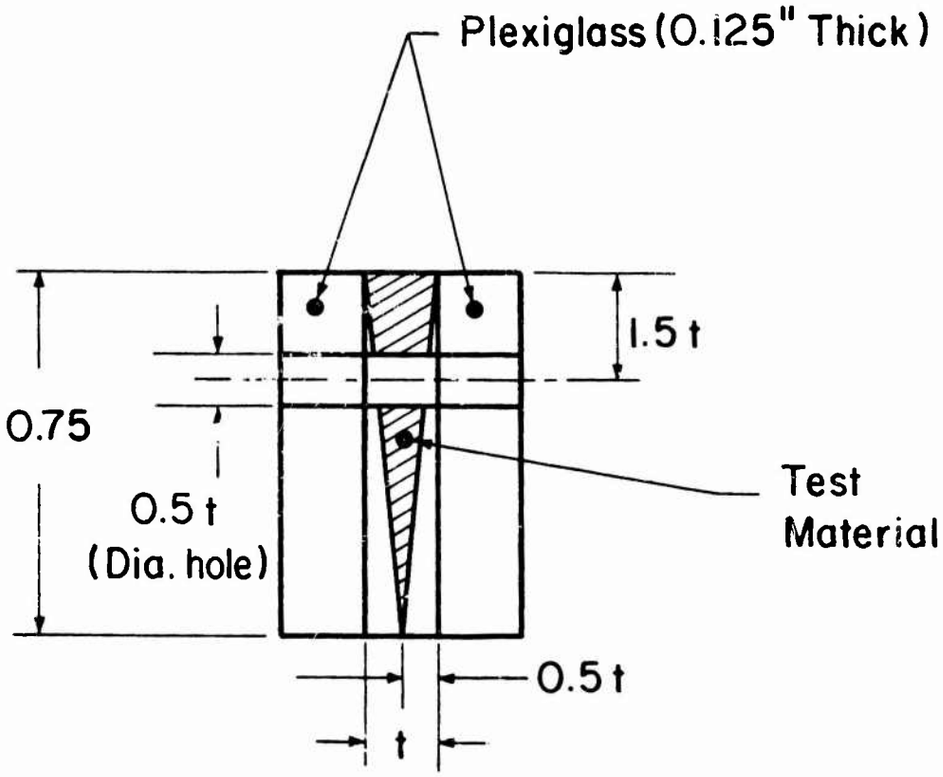

FIGURE 131. CROSS SECTION OF A THREE POINT BEND SANDWICH SPECIMEN.

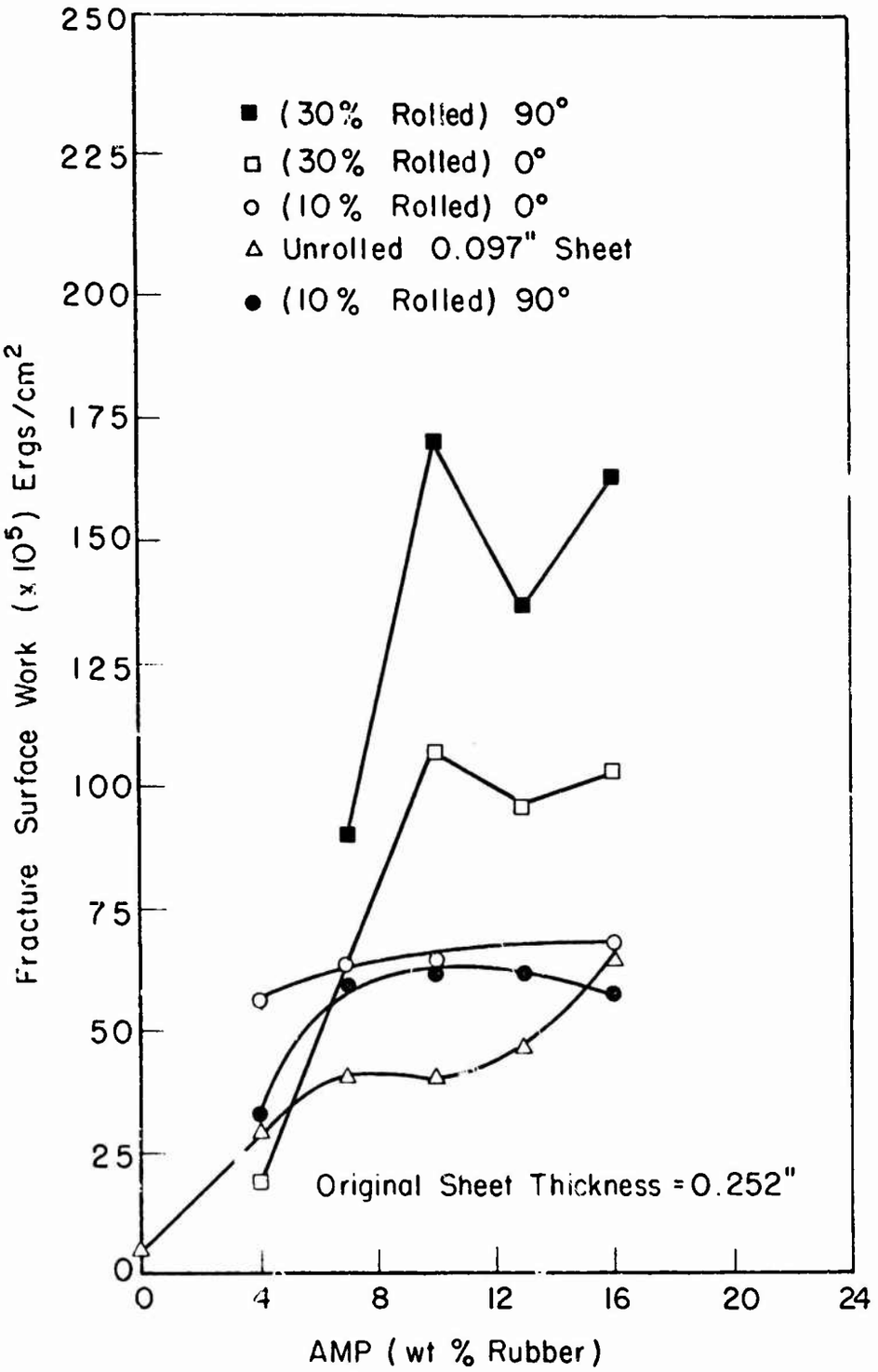

FIGURE 132. FRACTURE SURFACE WORK OF ROLLED ACRYLIC MULTIPOLYMERS BY THREE POINT BEND TEST.

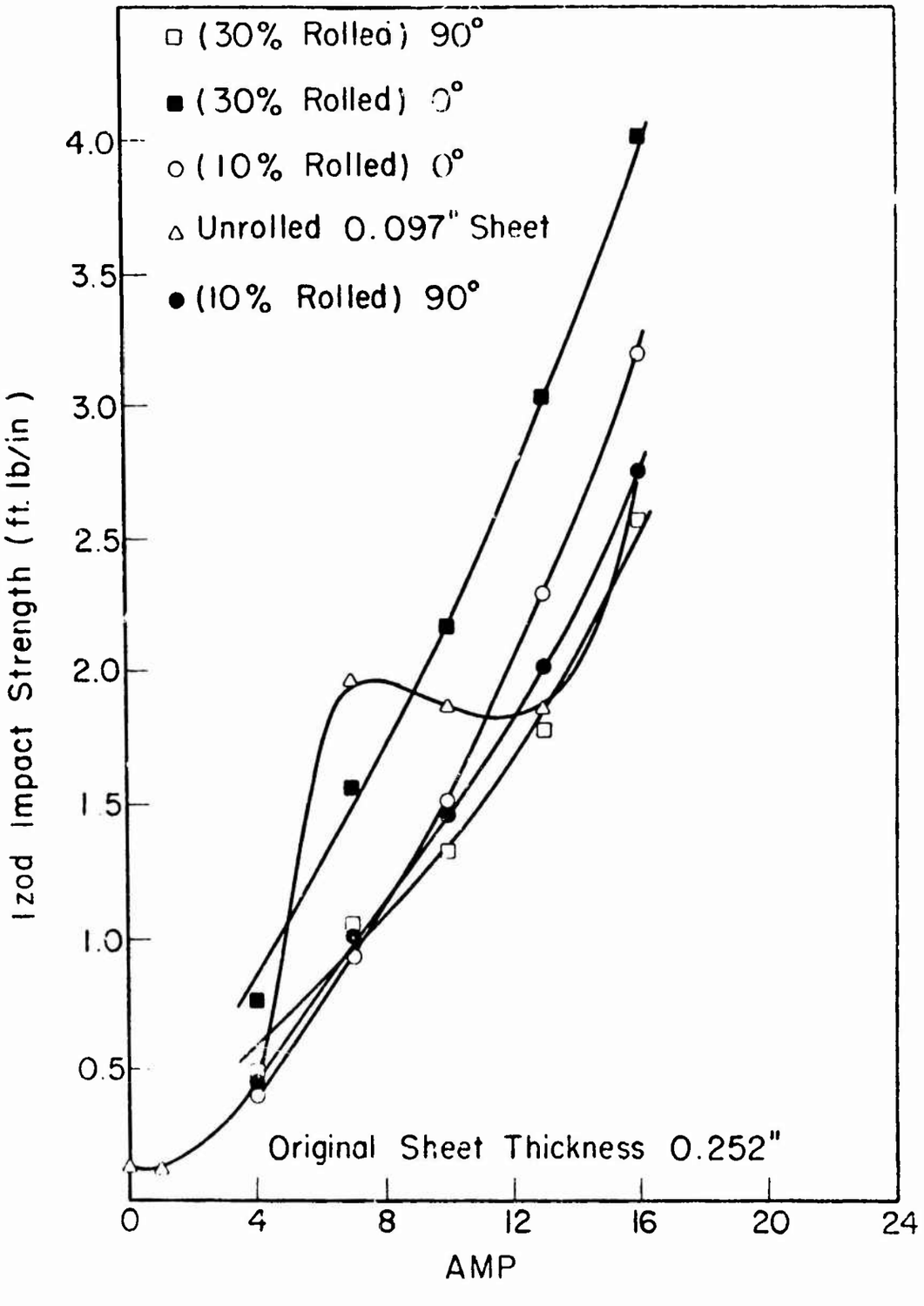

FIGURE 133. IZOD IMPACT STRENGTH OF ROLLED ACRYLIC MULTIPOLYMERS.

The fracture surface work, in general, increases with the degree of cold rolling. The degree of enhancement is higher at higher rubber content.

For sheets with a rubber content higher than 10% , the notched Izod impact strength is increased with degree of cold rolling. The enhancement is more in the direction of rolling than in the perpendicular direction. In sheets with a rubber content below 7 percent, cold rolling is found to decrease the impact strength. At lower rubber contents the change in impact strength with cold rolling is not appreciable.

CHAPTER X

MICROMECHANICS STUDIES OF RUBBER-REINFORCED GLASSY POLYMERS

A. Introduction

Many investigations have been performed to study the toughness and mechanisms of toughness enhancement in rubber modified glassy polymers such as ABS or rubber modified acrylic polymers (71-79). These polymers represent an unusual class of composites since most composites consist of a rigid inclusion surrounded by a more ductile or less hard matrix. In this case, a rubbery particle is filling a harder or more rigid matrix. Since the modulus of elasticity of the rubber is much less than that of the glassy polymer matrix and Poisson's ratio is greater than that of the matrix, the modified polymer will have a decreasing modulus and increasing Poisson's ratio as rubber filler content is increased. Of course the most significant benefit is that the toughness of the relatively brittle matrix polymer (e.g. styrene-acrylonitrile) can be greatly increased. The tensile strength of the matrix is reduced but the ultimate elongation is increased as the rubber content is increased. The end result is a compromise and a moderately hard material is produced with good impact strength as a result of the rubber reinforcement.

The mechanism of the toughness enhancement and energy absorption capability of this material is believed related to internal crazing of the matrix throughout the volume caused by stress concentrations around the finely dispersed rubber particles (72, 74, 75, 77). This crazing also manifests itself in the familiar stress whitening of rubber modified polymers. Since it is believed that stress intensifications around the particles are responsible for the crazing or cold drawing of the matrix adjacent to the rubber particles, it would be desirable to analyze for the internal stresses around the rubber particles. A finite element stress analysis method is presented in this paper for calculation of these internal stresses. Matonis (78,79) has calculated the stresses surrounding a single inclusion in an infinite medium and has reported on the stresses at the interface and in the matrix. He was particularly interested in the effect of the interface or more properly the interphase between spherical filler and matrix and the effect of interphase properties on stresses around the inclusion.

The finite element technique used in this study is not limited to the analysis of a single inclusion in an infinite matrix but can be utilized to analyze multi-inclusion problems and results are presented here for rubber (filler) contents as high as 50 percent. In addition to determining internal stresses for various filler volume fractions and filler properties, the composite modulus of elasticity, Poisson's ratio and critical stress for stress whitening or yield point can be determined.

B. Finite Element Method

The finite element method discussed in detail elsewhere (80,81) has been employed here as a numerical stress analysis technique to analyze for the internal stresses in a rubber sphere filled composite material. A computer program for axisymmetric solids (solids of revolution) was used and a Univac 1108 computer

generated the data.

The finite element method reduces the continuous structure or medium to a system of discrete elements. In the finite element approximation of axisymmetric solids, the continuous structure or medium is replaced by a system of axisymmetric elements, which are interconnected at nodal circles. It has been assumed that the rubber reinforced polymer (assumed to possess symmetry) could be approximated by a unit cell as shown in Fig. 134 which when rotated 360° around axis AD produces a hemisphere embedded within a cylinder. The interparticle spacing is equal to $2(r_1 - r_2)$ where r_1 and r_2 are shown in Fig. 134. The volume percent of filler particles (radius = r_2) can be altered by changing the ratio r_2/r_1 (note AB = BC = CD = AD in Fig. 134) and the volume percent filler can be calculated from r_2 and r_1. It should be noted that this axisymmetric representation of the rubber filled polymer only approximates the real packing and structure of the composite. These axisymmetric cells (Fig. 134) do not constitute an actual repetitive unit but are related in their dimensions to the interparticle spacing. A three-dimensional computer program without restrictions (e.g., using tetrahedral elements) would have to be used to truly model a particulate composite.

The finite elements used for the case $r_2/r_1 = 0.36$ ($V_f = 3.03\%$) are shown in Fig. 135. The radial and tangential stresses as well as the principal stresses and their directions are determined for each element. The analysis leading to the determination of these stresses begins with the assumption for the displacement field within each element:

$$u_r(r, z) = b_1 + b_2 r + b_3 z$$

$$u_z(r, z) = b_4 + b_5 r + b_6 z$$

This linear displacement field assures continuity between elements, since "lines which are initially straight, remain straight in their displaced position". Based on this assumption and using equilibrium equations for the elements, and the relations of continuity between elements, it is possible to determine u_r, u_z for each nodal circle and the stresses in each element. A computer program written by E. L. Wilson permitted the application of this method to our problem (82).

In order to make the above calculations the following assumptions were made concerning the material:

1. Rubber particles are spherical and of uniform size; packing of particles can be represented by axisymmetric element (Fig. 134).
2. Both filler and matrix materials obey elastic stress-strain relationships.
3. Perfect bonding exists between filler and matrix (continuity of displacements at the interface).

C. Application of the Finite Element Method

The finite element method permits the calculations of the stress and displacement

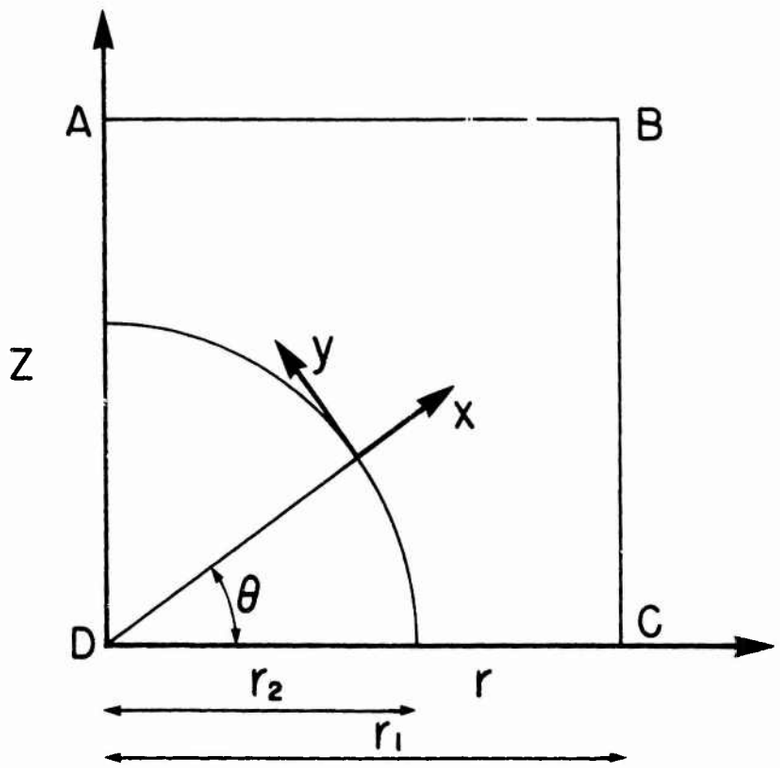

FIGURE 134. AXISYMMETRIC CELL.

distributions in the typical region ABCD (Fig. 135) for certain loading and boundary conditions. It will be assumed here that the composite is stretched by a force in the z direction and that there are no applied tractions in the r direction. By symmetry, on the boundary ABCD

$$\tau_{rz} = \tau_{zr} = 0$$

thus the sides AB and BC remain parallel to their original positions after a displacement due to the force in the z direction while AD and DC remain fixed. Thus, AB and BC will undergo normal displacements and the tractions in the r direction must be zero so that

$$\int_{BC} \sigma_r \, dz = 0$$

where the integral is replaced by a summation in the finite element method.

In order to satisfy the above boundary conditions the following procedure is used (83, 84):

1. Find the stress and displacement distribution (1) such that

   $(u_{z1})_{AB} = 1$ (arbitrarily specified unit displacement).

   $(u_{z1})_{DC} = 0$ (symmetry)

   $(u_{r1})_{BC} = 0$ (specified displacement condition)

   $(u_{r1})_{AD} = 0$ (symmetry)

   $\tau_{rz} = \tau_{zr} = 0$ (on ABCD)

From these boundary conditions, σ_{r1} and σ_{z1} are determined in all elements and displacements u_{r1}, u_{z1} in all nodal circles are determined.

2. Find the stress and displacement distribution (2) such that

   $(u_{z2})_{AB} = 0$ (specified displacement condition)

   $(u_{z2})_{DC} = 0$ (symmetry)

   $(u_{r2})_{AD} = 0$ (symmetry)

   $(u_{r2})_{BC} = 1$ (arbitrarily specified unit displacement)

   $\tau_{rz} = \tau_{zr} = 0$ (on ABCD)

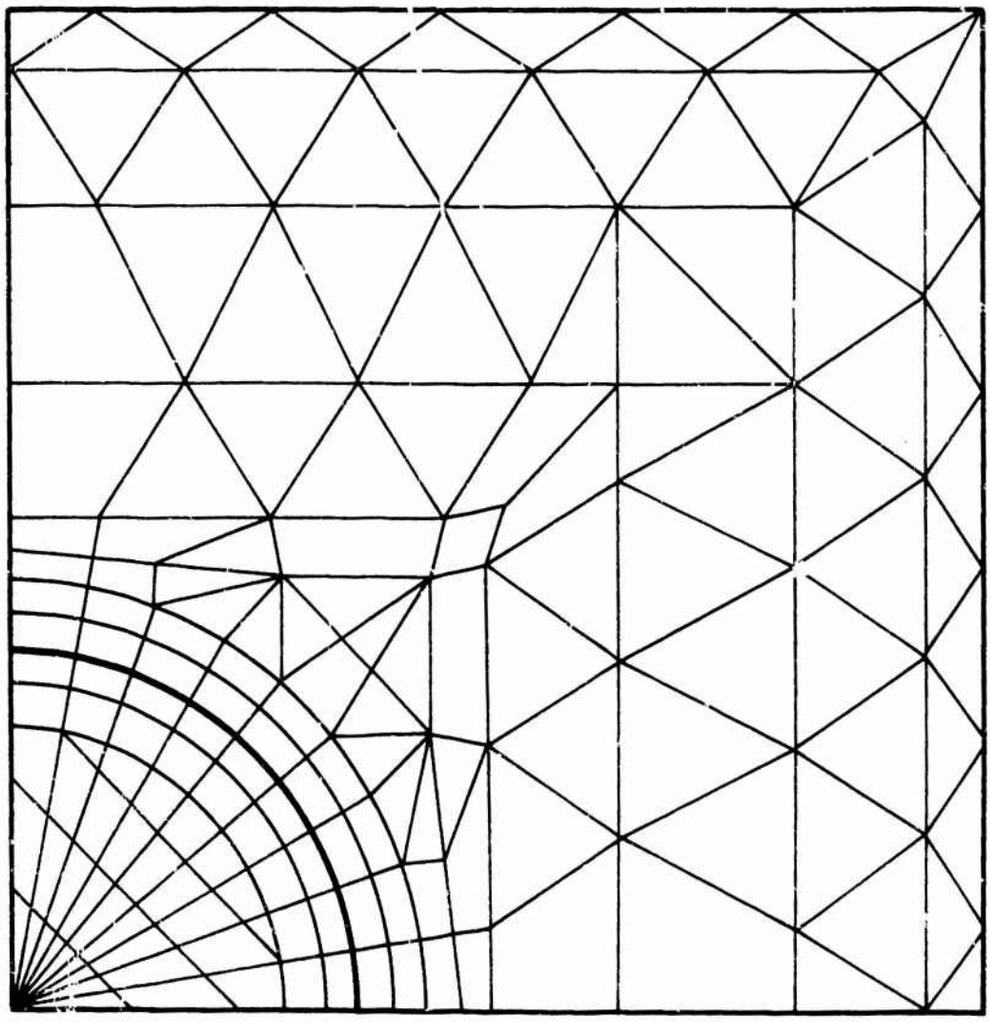

FIGURE 135. FINITE ELEMENTS.

3. The two above stress and displacement distributions are superimposed to obtain

$$\sigma = \sigma_1 + k\,\sigma_2$$

$$u = u_1 + k\,u_2$$

where k is determined such that the net force in the r direction along BC is zero. Thus

$$(F_r)_{BC} = \int_{BC} (\sigma_{r1} + k\,\sigma_{r2})\,dz = |BC|\,(\bar{\sigma}_{r1} + k\,\bar{\sigma}_{r2})_{BC} = 0$$

So $$k = -\left(\frac{\bar{\sigma}_{r1}}{\bar{\sigma}_{r2}}\right)_{BC}$$

The stress on AB is thus

$$(\bar{\sigma}_z)_{AB} = (\bar{\sigma}_{z1})_{AB} - \left(\frac{\bar{\sigma}_{r1}}{\bar{\sigma}_{r2}}\right)_{BC} (\bar{\sigma}_{z2})_{AB}$$

and the displacement is

$$(u_z)_{AB} = (u_{z1})_{AB} - \left(\frac{\bar{\sigma}_{r1}}{\bar{\sigma}_{r2}}\right)_{BC} (u_{z2})_{AB} = (u_{z1})_{AB}$$

since $(u_{z2})_{AB} = 0$.

D. Calculation of Polymer Composite Modulus of Elasticity and Poisson's Ratio

To calculate the stiffness or modulus of elasticity of the rubber modified plastic composite, the average stress on the boundary AB is calculated, or

$$\bar{\sigma}_z = \frac{\int_A \sigma_z\,dA}{A} = (\bar{\sigma}_z)_{AB}$$

Where A is the area of the top of the cylinder in the finite element analysis and the integral is replaced as a summation as follows:

$$\int_A \sigma_z\,dA = 2\pi \int_0^{r_1} \sigma_z\,r\,dr = 2\pi \sum_{i=1}^{n} 1/2\,(r_i^2 - r_{i-1}^2)\,\sigma_z$$

Where r_i and r_{i-1} are the radii to the nodal circles that define the elements on the top of the cylinder, n is the number of such circles, and σ_z is the corresponding normal stress in each element.

The modulus is defined as $E = \frac{\bar{\sigma}_z}{\bar{\epsilon}_z}$

where the strain used is calculated from the specified boundary displacement

$$\bar{\epsilon}_z = \frac{(U_z)_{AB}}{|\overline{BC}|}$$

Poisson's ratio was calculated from the displacements

$$u = u_1 + ku_2$$

From Fig. 134, the displacement of boundary AB is

$$(u_z)_{AB} = (u_{z1})_{AB} + k\,(u_{z2})_{AB}$$

however $(u_{z2})_{AB} = 0$, thus $(u_z)_{AB} = (u_{z1})_{AB}$

Also, the displacement of boundary BC is

$$(u_r)_{BC} = (u_{r1})_{BC} + k\,(u_{r2})_{BC}$$

but $(u_{r1})_{BC} = 0$, thus

$$(u_r)_{BC} = k\,(u_{r2})_{BC}$$

Poisson's ratio can be written as

$$\nu = \frac{|(u_r)_{BC}|\,\overline{AB}}{|(u_z)_{AB}|\,\overline{BC}} = \frac{|k|\,(u_{r2})_{BC}\;\overline{BC}}{(u_{z1})_{AB}\;\overline{AB}}$$

and since $(u_{r2})_{BC} = (u_{z1})_{AB} = 1$

$$\nu = |k|\,\frac{\overline{BC}}{\overline{AB}} = |k| \qquad (\overline{BC} = \overline{AB})$$

E. Calculation of Composite Critical Stress

A composite critical stress can be calculated which might be considered the fracture strength for a brittle composite, the yield point for a ductile composite or in the case here the stress required to initiate internal crazing or cold drawing which manifests itself as stress whitening of the rubber modified composite.

In order to calculate this composite critical stress, it was assumed that the composite would reach this stress as soon as an element of the matric reached a large enough value of stress to cause crazing of the matrix. The spherical inclusion causes large stress concentrations and it is reasonable to expect that the critical condition

will be achieved at the filler-matrix interface where the stresses are large. Since the matrix is subjected to combined stresses (triaxial) a suitable failure or crazing criterion has to be used in order to predict matrix failure or crazing under combined stresses. The Von Mises failure criterion or distortion energy theory was selected which is represented as follows:

$$1/2\,[(\sigma_1 - \sigma_2)^2 + (\sigma_2 - \sigma_3)^2 + (\sigma_3 - \sigma_1)^2] = (\sigma^*)^2$$

where σ_1 σ_2 and σ_3 are principal stresses at the point in question and σ^* is the critical stress in simple unixial tension.

This criterion is then applied by determining which element has the maximum value of distortion energy for the calculated applied stress $\bar{\sigma}_z$ found on boundary AB. This value of distortion energy may not exceed the value needed to fail or craze the matrix materials $(\sigma^*)^2$ and thus the composite critical stress is calculated from

$$S_c = \bar{\sigma}_z \frac{\sigma^*}{(U_{max})^{1/2}}$$

where U_{max} is the maximum value of distortion energy determined for the arbitrary specified displacement which produces the average stress $\bar{\sigma}_z$, and S_c is the composite critical stress.

F. Internal Stresses

The internal triaxial stresses have been calculated throughout the volume (in each element shown in Fig. 135) of rubber modified glassy polymers. The stresses have been calculated for rubber volume contents up to 44 percent. This corresponds to a minimum in interparticle spacing of $.26r_2$ (where r_2 = radius of rubber particle). In addition, the stresses have been investigated assuming various properties for the rubber particle to determine the effect of Poisson's ratio and elastic modulus on these stresses.

For the calculations presented in this paper, the following component properties have been assumed:

Polymer matrix:		E (modulus of elasticity) = 400,000 psi
		ν (Poisson's ratio) = 0.35
rubber filler:	1)	E = 3000 psi
		ν = 0.48
	2)	E = 3000 psi
		ν = 0.35
	3)	E = 3000 psi
		ν = 0.50
	4)	E = 1000 psi
		ν = 0.48

The volume percent filler can be determined from the ratio r_2/r_1 (Fig. 134) by calculating the volume of the hemisphere contained within the cylinder when the cell in Fig. 134 is rotated 360° around axis AD. The following r_2/r_1 ratios and corresponding filler contents were used in this analysis:

r_2/r_1	v_f (%)
.357	3.03
.502	8.45
.615	15.51
.714	24.2
.833	38.4
.870	43.8

The stresses around the interface between the rubber particle and glassy matrix are shown in Figs. 136, 137 and 138. The results shown in these figures are for the rubber filler with E = 3000 psi and $\nu = 0.48$ except when indicated in the figure. The stresses are presented as a ratio, $\sigma/\bar{\sigma}_z$, where $\bar{\sigma}_z$ can be considered the average stress applied to the polymer composite. Thus, the ratio represents the stress concentrations around the rubber particles. The stress system is defined in figure 136. From Fig. 135 it can be seen that there are 9 finite elements around the interface and the calculated stresses are assumed to act at the center of each element. The effect of changing the rubber properties has a very small effect on the internal stresses as shown in Fig. 136 for a change in the Poisson's ratio of the rubber. Figs. 137 and 138 present the interfacial stresses for two additional volume percents of rubber. In all of the cases shown, the radial and tangential stresses at the interface are almost equivalent to the principal stresses and thus the shear stresses (e.g. τ_{xy}) are nearly zero. In Fig. 137, the hydrostatic stress as well as the absolute value of maximum shear stress has been plotted along the interface. The hydrostatic stress is given by:

$$p = \frac{\sigma_1 + \sigma_2 + \sigma_3}{3} \qquad (\sigma_1 > \sigma_2 > \sigma_3 \text{ are principal stresses})$$

and the absolute value of maximum shear stress is

$$\tau_{max} = \frac{\sigma_1 - \sigma_3}{2}$$

The hydrostatic stress produces only volume changes without distortion and as can be seen in Fig. 137, volume expansions occur for $\theta < 50^\circ$ and volume contractions occur for values of $\theta > 50^\circ$. The variation of the stresses at the pole ($\theta = 90^\circ$) and equator ($\theta = 0^\circ$) of a spherical rubber particle are shown in Fig. 139 as a function of rubber filler content. If the curve for one of the tangential stresses at the equator (σ_Y) is extrapolated to $V_f = 0$ percent almost perfect agreement is obtained with the theoretical solution of Goodier (86) for a single inclusion in an infinite matrix.

The decay of stresses away from the interface are shown in Fig. 140. The stresses have been plotted beginning from the interface and continuing along the boundaries AD and CD as shown in Fig. 140. Only the stress normal to the boundary has been plotted. It can be seen that for a low volume percent filler (3%) the normal stress along CD reduces to the average stress, $\bar{\sigma}_z$, at the midpoint between two

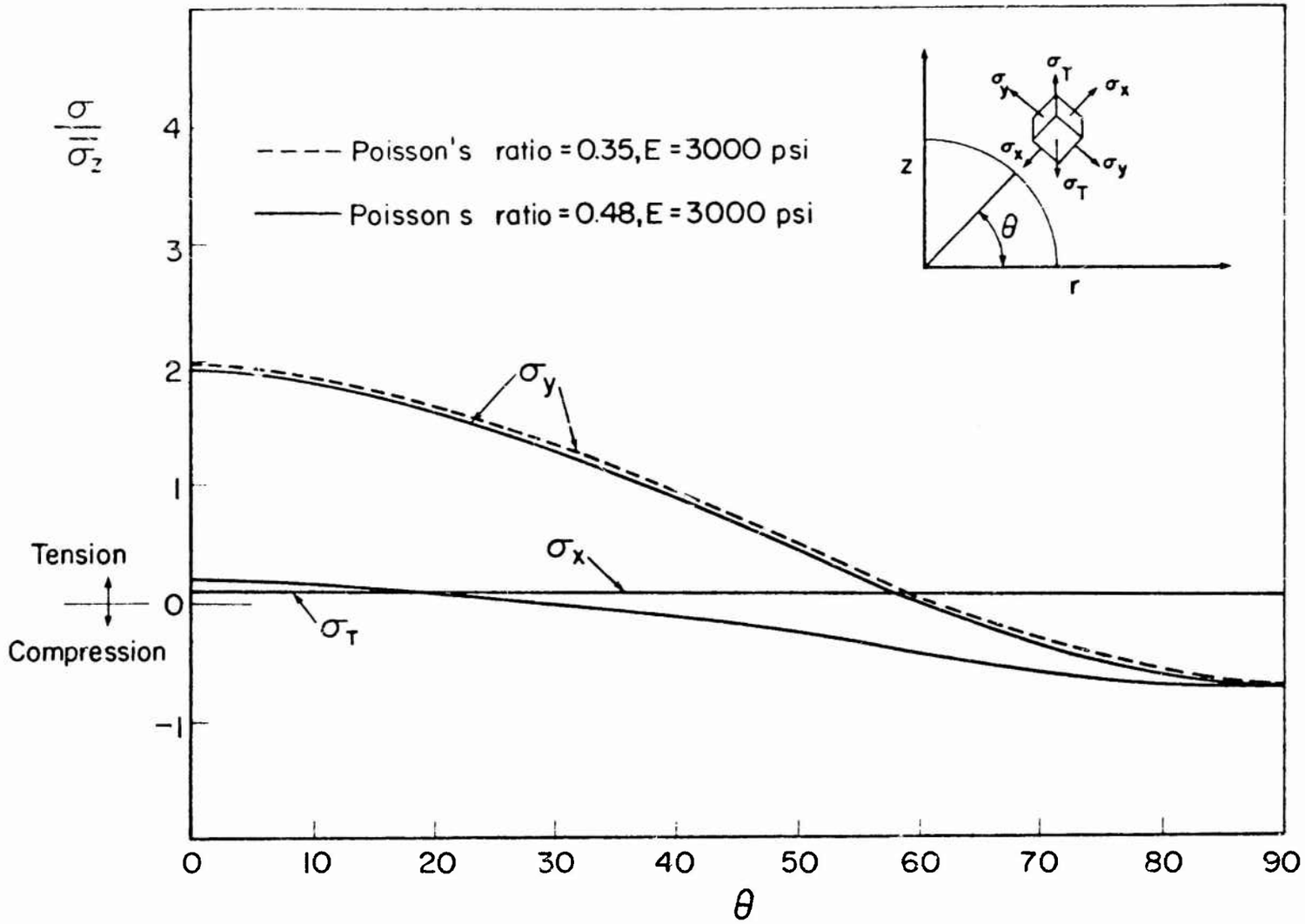

FIGURE 136. INTERFACIAL STRESSES IN A RUBBER MODIFIED POLYMER (V_f = 3.03%).

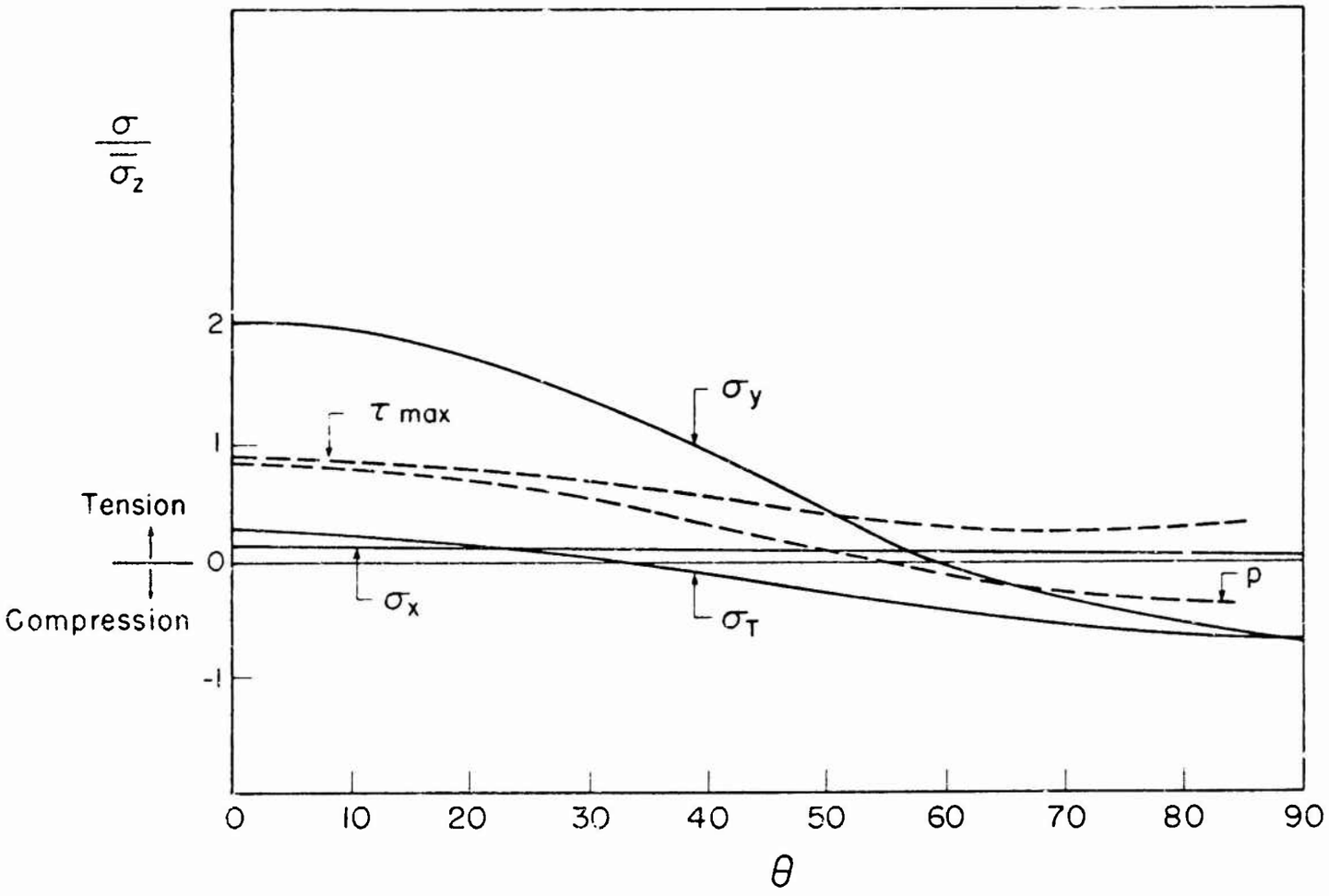

FIGURE 137. INTERFACIAL STRESSES IN A RUBBER MODIFIED POLYMER (V_f=8.45%).

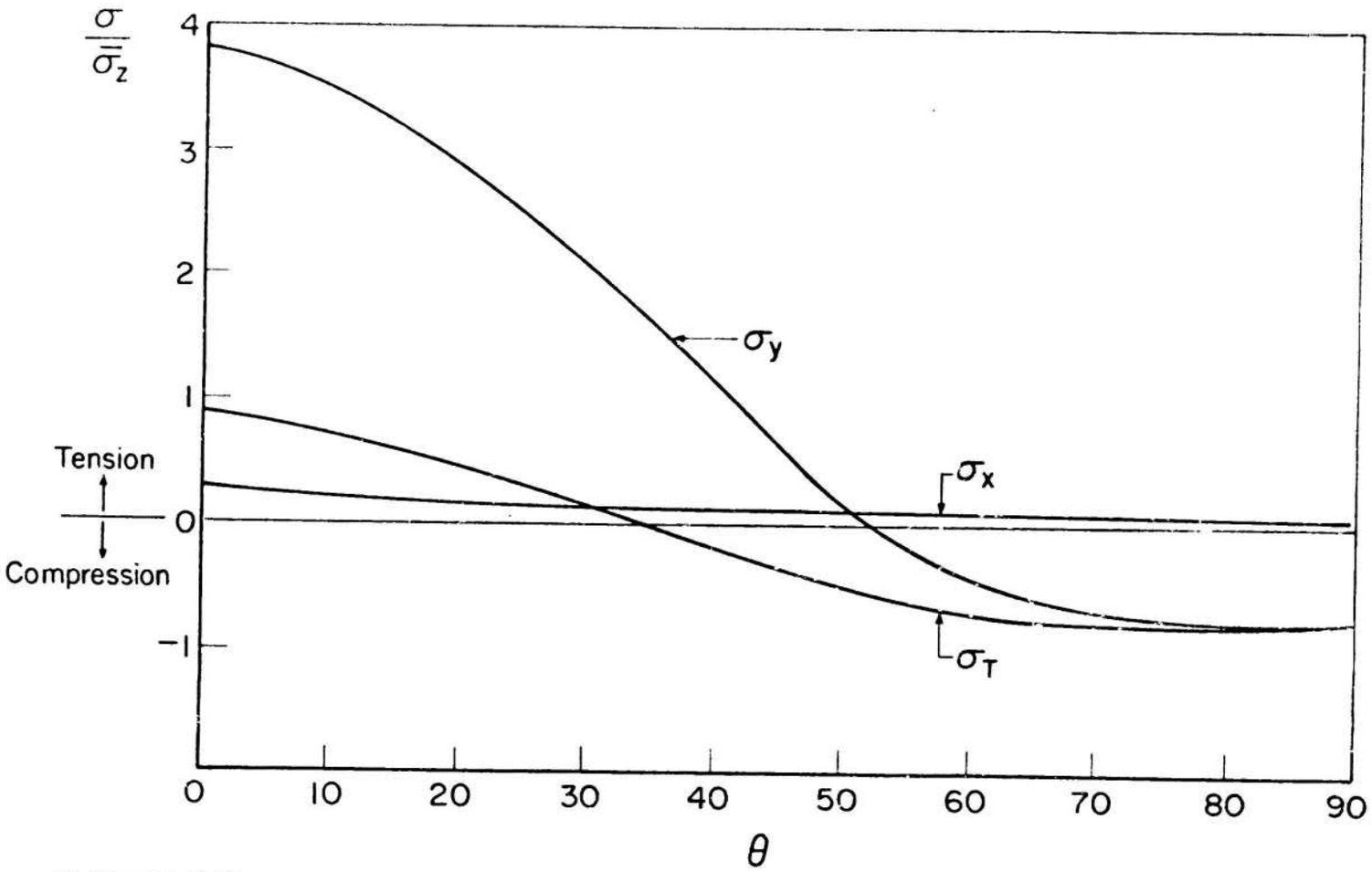

FIGURE 138. INTERFACIAL STRESSES IN A RUBBER MODIFIED POLYMER (V_f = 43.8 %).

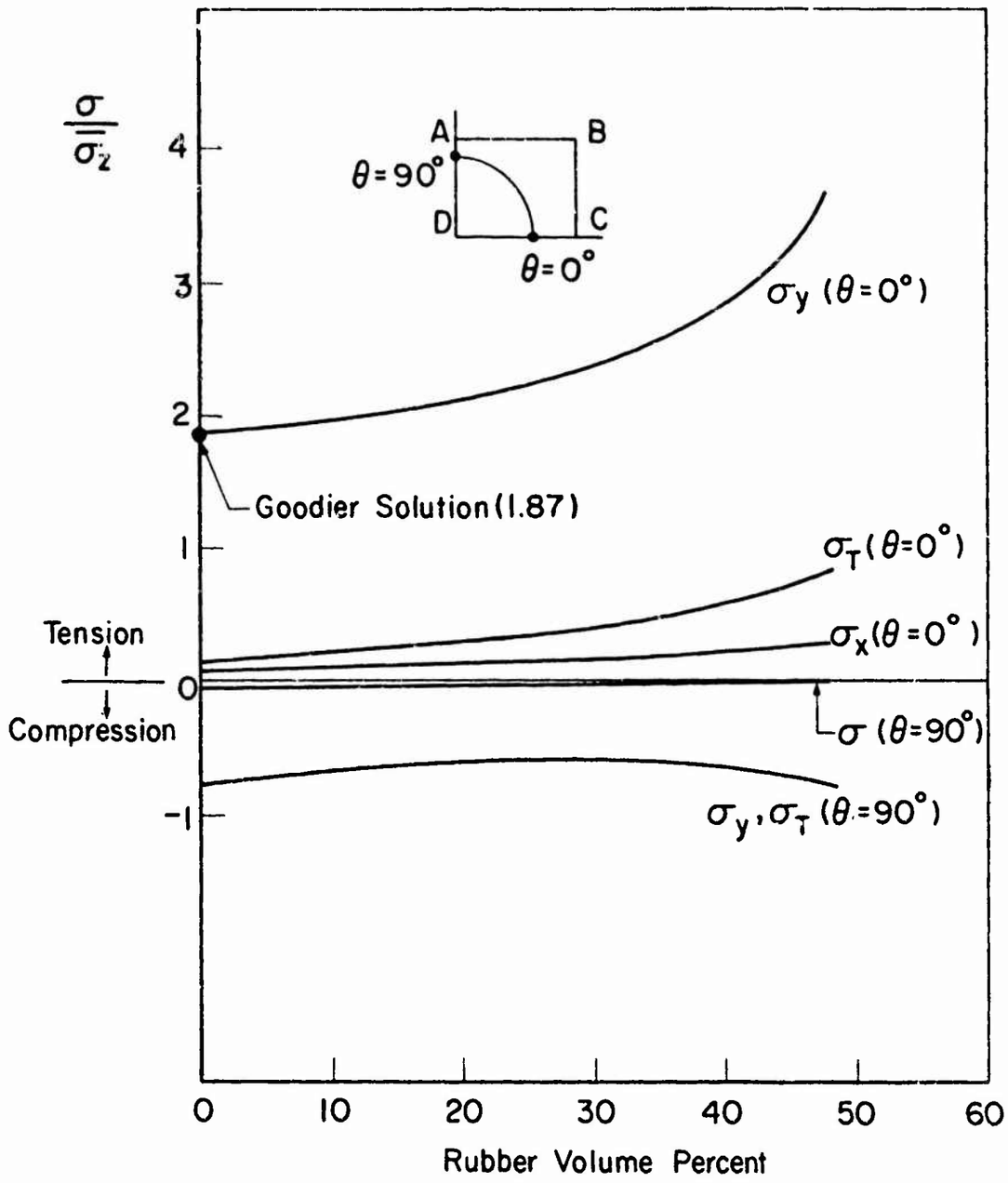

FIGURE 139. VARIATION OF THE STRESSES AT THE POLE AND EQUATOR OF A SPHERICAL RUBBER PARTICLE AS A FUNCTION OF RUBBER CONTENT.

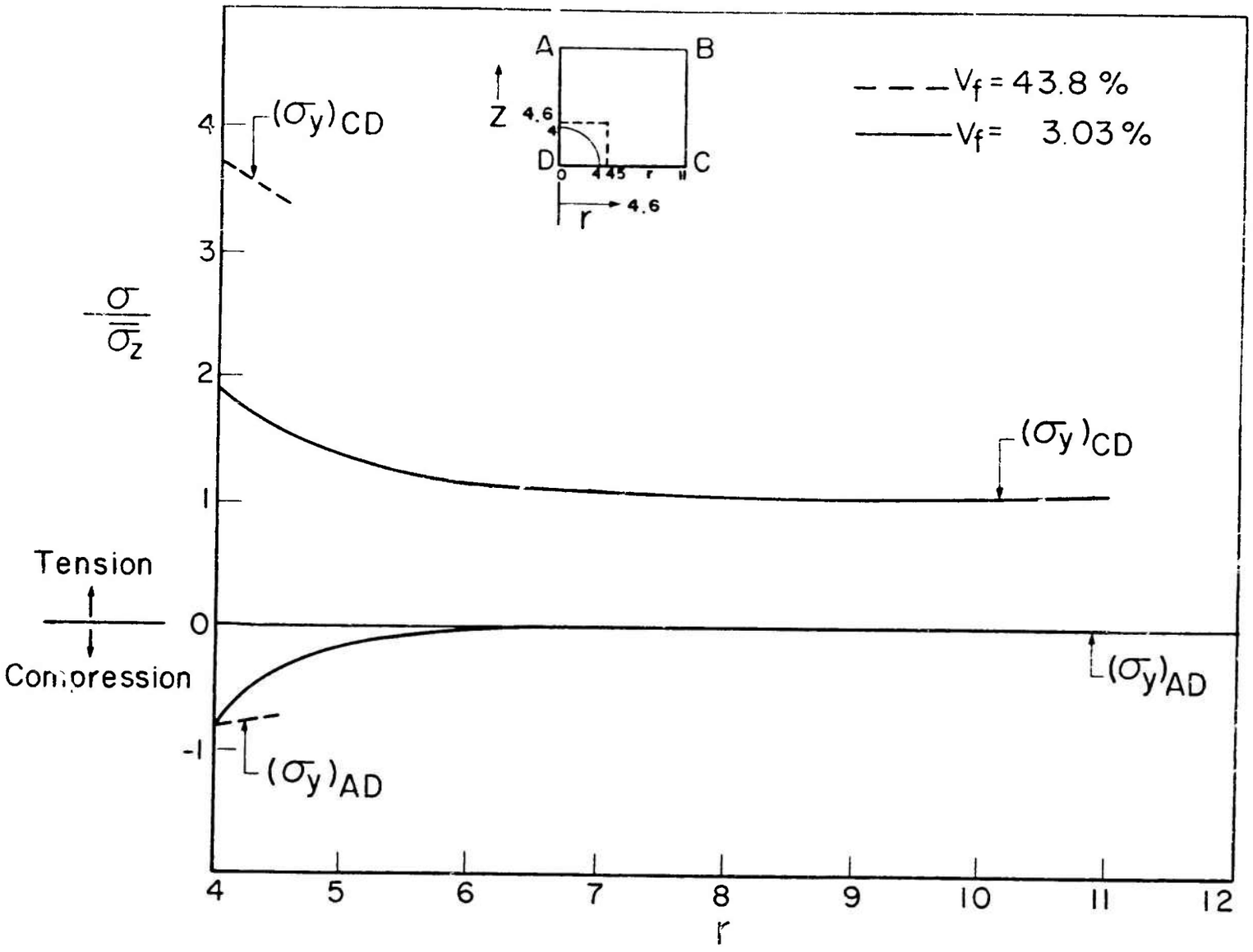

FIGURE 140. DECAY OF STRESSES AWAY FROM THE INTERFACE.

inclusions while the normal stress along AD approaches zero as it should. However, if the results for higher volume percents are plotted as also shown in Fig. 140 the stress concentrations persist even at the midpoint between two inclusions because of the close particle spacing.

G. Elastic Constants

The predicted results for the modulus of elasticity and Poisson's ratio are shown in Fig. 141 and table 31. Both the modulus and poisson's ratio are reduced by the addition of rubber particles. Because of the great difference in modulus of the matrix and filler, the filler acts almost as a void and thus both composite properties are reduced. Experimental data for the modulus of rubber particle modified epoxy resin has been compared to the predicted curve in Fig. 141 for rubber contents up to 10 volume percent. Excellent agreement is obtained (86). It is difficult to find additional data in the literature although Fletcher et al (74) and Schmitt and Keskkula (72) have presented limited modulus data on rubber modified polystyrene. The problem in trying to compare this data to the predicted values of modulus is that the theory used here assumed elastic behavior of the components whereas the actual behavior is viscoelastic. Furthermore, the amount or rate of stress relaxation is dependent upon the rubber content (72) and if the modulus of a series of rubber modified polymers with various rubber contents is determined at the same strain rate the results will not agree with the values predicted by this analysis. This analysis will give an upper bound since it assumes elastic behavior and would probably be accurate for tests performed at high rates of strain where relaxation would be minimized. It can be seen in table 31 that for large changes in the rubber properties only slight changes in the polymer composite properties are produced.

H. Composite Critical Stress

The composite critical stress to initiate crazing or stress whitening is shown in Fig. 142 as a function of volume percent rubber and also summarized in table 31. It has been assumed that this critical stress for the unmodified matrix is 8000 psi. As shown in figure 142 the composite critical stress is reduced with the first addition of rubber. Although crazing may initiate at the low stresses indicated it may not be visible as stress whitening until higher stresses ore reached particularly for the low rubber contents as only a small volume of material is affected. It should be noted that the failure model used here assumes perfect bonding and also assumes that crazing is initiated as soon as the first element reaches a critical stress condition. The first element to reach this condition is on the equator of the spherical particle at the interface.

I. Conclusions

A method has been discussed for calculating internal stresses in rubber modified polymers and for predicting elastic constants as well as a critical stress for onset of crazing. A simple model is used to simulate the structure and behavior of the composite as indicated by the necessary assumptions listed in the paper. However, it is possible to account for interactions between particles which to date has been

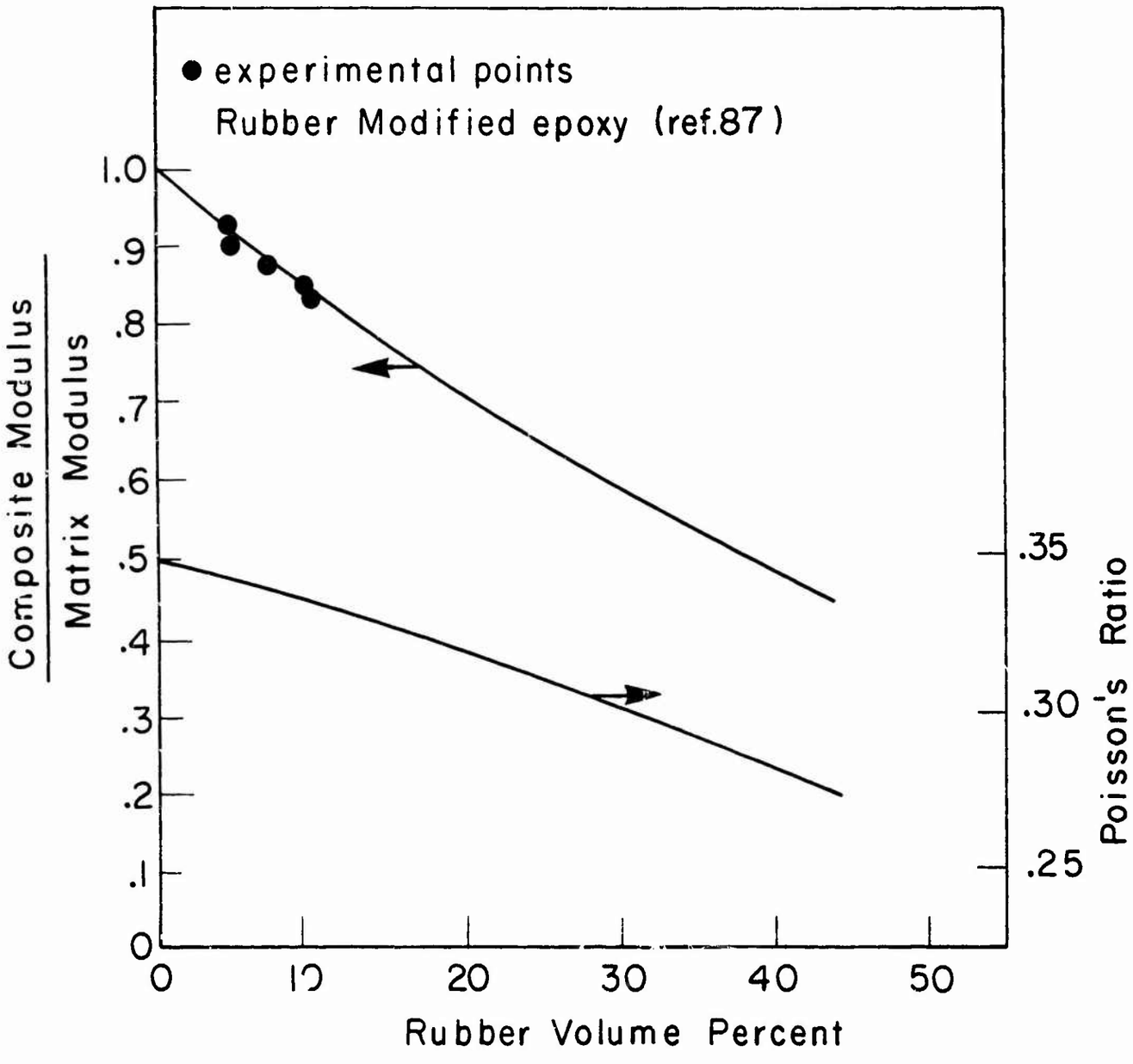

FIGURE 141. PREDICTED MODULUS OF ELASTICITY AND POISSON'S RATIO.

TABLE 31.

SUMMARY OF COMPOSITE PREDICTED PROPERTIES*

Volume Fraction Rubber (%)	Assumed Filler Properties		Predicted Composite Properties		
	E (psi)	ν	E (psi)	ν	σ^* (psi)
3.03	3000	0.48	0.380×10^6	0.346	4610
8.45	3000	0.48	0.347×10^6	0.337	4557
15.50	3000	0.48	0.307×10^6	0.326	4308
24.20	3000	0.48	0.264×10^6	0.311	3928
38.4	3000	0.48	0.200×10^6	0.285	2937
43.8	3000	0.48	0.177×10^6	0.279	2509
15.50	1000	0.48	0.304×10^6	0.319	4191
15.50	3000	0.35	0.304×10^6	0.318	4162
15.50	3000	0.50	0.305×10^6	0.316	4162

* Assumed matrix properties: E = 400,00 psi

ν = 0.35

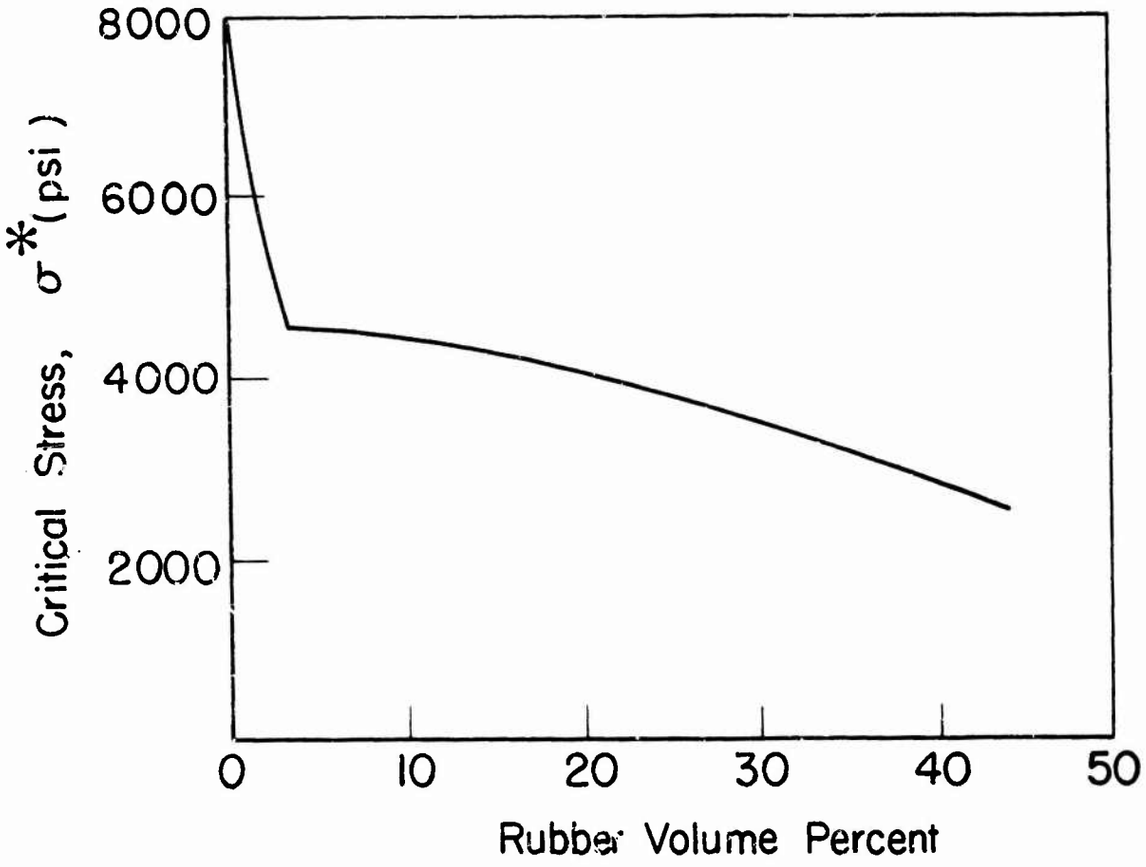

FIGURE 142. CRITICAL STRESS TO INITIATE CRAZING OR STRESS WHITENING.

neglected in other analyses. Further study is being given to the problem to develop a more realistic model by changing from an elastic to an elastic-plastic or viscoelastic matrix. Also modifications in the failure model will be studied.

BIBLIOGRAPHY

1. Griffith, A. A., Phil. Trans. Roy. Soc., A221, 163 (1920).
2. Berry, J. P., SPE Trans., 1, 3 (1961).
3. Berry, J. P., J. Poly. Sci., 2, 4069 (1964).
4. Benbow, J. J., Proc. Phys. Soc., 78 (1961).
5. Broutman, L. J., and Kobayashi, T., "Fracture Studies in Glassy Polymers," Final Report AMMRC CR 69-13, Contract DAAG 17-67-C-0133 (Aug. 1969).
6. Broutman, L. J., and McGarry, F. J , J. Appl. Poly. Sci., 9, 585 (1965).
7. Berry, J. P., J. Poly. Sci., A-1, 993 (1963).
8. "Study of Mechanisms of Armor Penetration Resistance." Contract DA-04-495-AMC-93(R), 30 (Jan. 1964).
9. Broutman, L. J. and McGarry, F. J., J. Appl. Poly. Sci., 9, 609 (1965).
10. Svenson, N. L., Proc. Phys. Soc., 77, 876 (1961).
11. Mueller, H. K., and Knauss, W. G., Trans. of the Soc. of Rheology, 15, 2, 217 (1971).
12. Knauss, W. G., Trans. of the Soc. of Rheology, 13, 3, 291 (1969).
13. "Closed Loop." Magazine published by MTS Systems Corp., 1, 5, 3 (1966).
14. Vincent, P. I., and Gotham, K. V., Nature, 210, 1254 (1966).
15. Cotterell, B., Appl. Mats. Res., 4, 227 (1965).
16. Mostovoy, S., and Ripling, E. J., "Fracture Controlling the Strength of Composites," Final Report for Naval Air Systems Command, Contract NOO 19-67-C-0493, (Feb. 1968).
17. Inglis, C. E., Trans. Inst. Nav. Arch., 55, 219 (1913).
18. Orowan, E., "Fracture and Strength of Solids," Report on Progress in Physics, Physical Society of London, 12, 185 (1949).
19. Orowan, E., Welding J. Res. Suppl., 34, 157s (1955).
20. Irwin, G. R., Kies, J. A., and Smith, H. L., ASTM Proc., 58, 640 (1958).

21. Irwin, G. R., Appl. Mats. Res., 3, 2, 65 (Apr. 1964).

22. Berry, J. P., J. Poly. Sci., 50, 107 (1961 and 50, 331 (1961).

23. Berry, J. P., J. Appl. Phys., 33, 1741 (1962) and 34, 62 (1963).

24. Mostovoy, S., Crosley, P. B., and Ripling, E. J., J. of Mats., 2, 661 (1967).

25. Wolock, I., and Newman, S.B., "Fracture Topography," Fracture Processes in Polymeric Solids, B. Rosen, Ed., Interscience Publishers, New York (1964).

26. Higuchi, M., Rpts. of Res. Inst. for Appl. Mech., Hyushu University, 6, 173 (1958).

27. Berry, J. P., Nature, 185, 91 (1960).

28. Hull, D., J. of Mats. Sci., 5, 357 (1970).

29. Cotterell, B., Int. J. Fracture Mech., 4, 3, 209 (Sept. 1968).

30. Kambour, R.P., J. Poly. Sci., A-2, 4, 17 (1964).

31. Kambour, R. P., J. Poly. Sci., A, 3, 1713 (1965).

32. Van den Boogart, A., "Physical Basis of Yield and Fracture", Conference Proceedings, A. C. Strickland, ed., Oxford (Sept. 1968).

33. Murray, J., and Hull, D., J. Poly. Sci., A-2, 8, 583 (1970).

34. Rogers, S., and Mandelkern, L., J. Phys. Chem., 61, 985 (1957).

35. Halden, R. A., and Simha, R., J. Appl. Phys., 39, 3, 1890 (1968).

36. DiBenedetto, A. T., and Trachte, K. L., J. Appl. Poly. Sci., 14, 2249 (1970).

37. Veith, A. G., "Tearing of Rubber," Publication of Instron Engineering Corporation.

38. Smith, T. L., "Strength and Extensibility of Elastomers," Rheology, 5, F. R. Eirich, ed., Academic Press, New York (1969).

39. Williams, J. G., Radon, J. C., and Turner, C. E., Poly. Eng. and Sci., 130 (Apr. 1968).

40. Mullins, J., Trans. I. R.I., 35, 213 (1959).

41. Gilman, J. J., J. Appl. Phys., 31, 2208 (1960).

42. Clausing, D. P. Int. J. Fracture Mech., 5, 211 (1964).

43. Srawley, J.E. and P. Gross. NASA TN D-3820, (Feb. 1967).

44. Turley, S. G. and H. Keskkula, J. of Poly. Sci., C, 14, 69 (1966).

45. Boyer, R. F. Poly. Eng. and Sci., 8, 3 161 (1968).

46. Roetling, J.A. Applied Polymer Symposia, 5, 161, (1968).

47. Zitek, R. and J. Zelinger, J. Appl. Poly. Sci., 14, 1243 (1970).

48. McCrum, N.G., B. E. Read and G. Williams, Anelastic and Dielectric Effects in Polymeric Solids. John Wiley and Sons, Inc., New York (1967).

49. Clark, A. B. J. and G. R. Irwin, Exp. Mech., 321 (June 1970).

50. Modern Plastics Encyclopedia, 44, 1A, 115 (1967).

51. Modern Plastics Encyclopedia, 43, 82 (1966).

52. Matsuo, M., Ueda and Y. Kondo, Poly. Eng. and Sci., 10, 5, 253 (1970).

53. Imawasa, Y. and M. Matsuo, Poly. Eng. and Sci., 10, 5, 261 (1970).

54. Nielsen, L.E. Mechanical Properties of Polymers, Reinhold Publishing Co. New York (1962).

55. Furno, F. J., R. S. Webb and N. P. Cook, J. Appl. Poly. Sci., 8, 101 (1964).

56. Malpass, V. E. Applied Polymer Symposia, 5, 87 (1967).

57. Lewis, R. W., M. E. Eoylance and G. R. Thomas, "Rubber Toughened Acrylic Polymers for Armor Applications", Private communication from Army Materials and Mechanics Research Center, Watertown, Mass.

58. Irwin, G.R. "Fracture", Encyclopedia of Physics, 6, Springer, Berlin (1958).

59. Rivlin, R.S. and A.G. Thomas, J. Poly. Sci., 10, 291 (1953).

60. Erdogan, F "Crack Propagation Theories", Fracture, 2, H. Liebowitz, ed. Academic Press, New York (1971).

61. Bluhm, J. I. "Fracture Arrest", Fracture, 5, H. Liebowitz, ed. Academic Press, New York (1971).

62. Roetling, J. A. Polymer, 6, 311 (1965).

63. Broutman, L J. The Effects of Temperature, Crosslinking and Pre-orientation on the Surface Work of Glassy Polymers. Doctoral Dissertation, M.I.T. (1963).

64. Turska, E., W. Pryzgocki, and M. Maslowski, J. of Poly. Sci., C, 16, 3373 (1968).

65. Kampf, G. Kolloiz-Zeitschrift, 172, 1, 54 (1960).

66. Mercier, J. P., G Groeninckx, and K. B. Goldblum. "Etude du Comportement Viscoelastique du Polycarbonate de Bisphenol-A Crystallise. I. Les Courbes de Madule-Temperature et la Resistance au Choc".

67. Mercier, J. P., G. Groeninckx and M. Lesne, J. of Poly. Sci., C, 16, 2059 (1967).

68. Collier, J. R. and L. M. Neal, Poly. Eng. and Sci., 9, 3 (1969).

69. Hopfenberg, H. B., R. H. Hallig and V. Stannett, Paly. Eng. and Sci., 9, 4, 242 (1969).

70. Alfrey, T., Jr., E. F. Gurnee, and W. G. Lloyd, J. of Poly. Sci., C, 12, 249 (1966).

71. E. H. Merz, G. C. Claver and M. Baer, J. Poly. Sci. 22, 325 (1956).

72. J. A. Schmitt and H. Keskkula, J. Appl. Poly. Sci. 3, 132 (1960).

73. A. J. Staverman, Prac. Royal Soc. 282A, 115 (1964).

74. K. Fletcher, R. N. Haward and J. Mann, Chem. Ind. 1045 (Nov. 6, 1965).

75. R. N. Haward and J. Mann, Proc. Roy. Soc. 282A, 120 (1964).

76. S. Newman and S. Strella, J. Appl. Poly. Sci. 9, 2297 (1965).

77. C. B. Bucknall and R. R. Smith, Polymer 6, 437 (1965).

78. V. A. Matonis and N. C. Small, ibid 9, 90 (1969).

79. V. A. Matonis, ibid 9, 100 (1969).

80. O. C. Zienkiewicz, The Finite Element Method (McGraw Hill Publishing Co. 1967).

81. E. L. Wilson, "Structural Analysis of Axisymmetric Solids", AIAA Journal (Dec. 1965).

82. E. L. Wilson, Structural Engineering Laboratory Report 63-1, Univ. of California, Berkeley, Calif (June 1963).

83. P. E. Chen and J. M. Lin, "Transverse Properties of Fibraus Compasites", Materials Research and Standards (Aug 1969).

84. S. W. Tsai, D. F. Adams, and D. R. Doner, "Effect of Constituent Material Properties on the Strength of Fiber Reinforced Composite Materials", AFML-TR-66-190, Air Force Materials Laboratory, Aug., 1966.

85. J. N. Goodier, J. Appl. Mech., 55-7, 39 (1933).

86. F. J. McGarry and J. N. Sultan, Research Report R69-8, Dept. of Civil Engineering, MIT, Cambridge, Mass. (Feb. 1969).